

CARDIFF UNIVERSITY

Optimisation and enhancement of a liposomal delivery system

by
Peter Yasin Hansal

January 2022

A thesis submitted in partial fulfilment for
the degree of Doctor of Philosophy

Cardiff School of Pharmacy and Pharmaceutical Science
Cardiff University

Abstract

Polymethyl methacrylate (PMMA) bone cement is commonly used for implant fixation in total joint replacement surgery (TJR), for the treatment of end stage arthritis. The use of antibiotic loaded bone cement (ALBC) is well-established in the prevention of post-surgical infections. Currently, elution of antibiotics from ALBCs occurs in a biphasic profile, with a high initial burst release within the first hours of application, followed by release of sub-inhibitory concentrations over long periods of time. Due to the inability of ALBCs to release clinically effective concentrations of antibiotic over an extended time-period, infections are still a major challenge; moreover, sub-inhibitory antibiotic release may increase the potential for antimicrobial resistance. The aim of this study was to develop and test a new bone cement formulation with optimised sustained antibiotic release, whilst maintaining the mechanical properties of the commercial bone cement. A liposomal bone cement delivery system containing gentamicin sulfate was produced and validated. The liposomal bone cement released a lower mass quantity of gentamicin than commercial ALBC; however, it released a higher percentage of its total incorporated gentamicin content compared to the commercial ALBC, whilst maintaining the antimicrobial efficacy and the mechanical properties of the commercial bone cement. Fluorescent labelled liposomes were used to determine that no measurable quantity of lipid was released from the bone cement.

A freeze-dried liposomal formulation was investigated as a means to make the liposomal bone cement a more commercially feasible product. Gentamicin loaded liposomes were freeze-dried and incorporated into bone cement at gentamicin base concentrations of 0.15% w/w - 0.60% w/w of the PMMA bone cement. Whilst these cements showed improved antimicrobial properties, antibiotic release was generally below the limit of detection and mechanical properties were only maintained for the cement containing 0.15% w/w gentamicin. The process was also relatively inefficient, with freeze-drying causing a reduction in lipid and gentamicin content to around half of the initial mass quantities used.

Given the limited functionality of the freeze-dried formulation and the commercial impracticality of the non-freeze-dried liposomal bone cement, alternative bone cement formulations were investigated. ALBC containing different mass quantities of hydrophilic (lactose) and hydrophobic (magnesium stearate) additives at concentrations of 10% w/w - 25% w/w of the PMMA bone cement were prepared. Cement containing lactose, released much higher mass quantities of gentamicin than the commercial ALBC and the magnesium stearate cements, although the magnesium stearate cements had a more gradual drug release profile. All cements containing additives had comparable antimicrobial properties to the commercial ALBC, however, the mechanical properties were only maintained for the 10% w/w lactose cement. Since magnesium stearate cements had a more extended drug-release profile, magnesium stearate was used to dry particle coat gentamicin sulfate using different mixing methods of varying shear (tumble mixer, pestle and mortar, ball mill). All bone cements made from dry powder coated gentamicin sulfate, released a similar mass of gentamicin, which was significantly lower than the gentamicin dose released in the commercial ALBC. Antimicrobial activity was maintained, and mechanical properties were comparable to the commercial ALBC.

This research has shown that incorporating liposomal antibiotic formulations in bone cements, in a manner that is commercially feasible, is extremely challenging. Whilst the use of liposomes can improve the drug release profile, the manufacturing process can result in significant loss of the active ingredient. Dry particle coating of gentamicin, using small mass quantities of magnesium stearate, could be used as an alternative approach to modify the drug release profile from bone cement, however, further investigation is required to optimise parameters such as mixing method, particle size and type of guest particle, and to establish the potential impact of this approach on toxicity and cement longevity.

Acknowledgements

I express my sincerest and genuine gratitude to my supervisors: Prof James C Birchall, Dr Wayne N Ayre and Dr Sion A Coulman for their invaluable guidance and support during my PhD; without them, this would have been a different journey. I cannot thank them enough for everything that they have done for me.

A special thanks to Dr Lleucu Davies for all her help and support when I started my PhD. I also thank Mrs Wendy Davies for her help and kindness during my time here.

I would like to thank those who have helped me with instrumentation and technical advice, across the various disciplines: Dr Sarah Bamford, Mrs Denise Barrow, Mr Nick Corps, Mrs Rebecca Cummings, Dr Maria Dul, Dr Matthew Ivory, Mrs Emma Jones, Dr Ketan Patel, Dr Fabrizio Pertusati, Mr Andy Robertson, Mrs Wendy Rowe, Dr Chris Thomas, and Dr Tom Williams.

I also thank Versus Arthritis for funding my project.

I would like to express my love and gratitude to my parents, Mr and Mrs Hansal.

Contents

| | | |
|--------|--|----|
| 1 | Introduction | 28 |
| 1.1 | Indications for total joint replacements | 28 |
| 1.2 | Total joint replacement | 30 |
| 1.2.1 | Cemented and uncemented approach in TJR | 31 |
| 1.3 | Biomaterials..... | 32 |
| 1.3.1 | Biocompatibility | 33 |
| 1.4 | Bone cement | 33 |
| 1.4.1 | PMMA polymerisation | 35 |
| 1.4.2 | The use of bone cement in surgery | 37 |
| 1.5 | Revision Surgery | 38 |
| 1.6 | Prosthetic joint infections (PJI)..... | 40 |
| 1.6.1 | Microorganisms in PJI..... | 40 |
| 1.7 | Prophylaxis in joint replacement surgery..... | 41 |
| 1.7.1 | Antibiotic resistance | 42 |
| 1.8 | Gentamicin sulfate..... | 42 |
| 1.8.1 | Antibiotic loaded bone cement (ALBC)..... | 44 |
| 1.8.2 | Characterisation of gentamicin..... | 44 |
| 1.9 | Effect of antibiotic on mechanical properties..... | 46 |
| 1.10 | Drug release of antibiotics in bone cement | 46 |
| 1.11 | Nanotechnology and nanoparticles..... | 47 |
| 1.12 | Nano-formulations in antibiotic loaded cements..... | 47 |
| 1.12.1 | Carbon nanotubes (CNT) | 48 |
| 1.12.2 | Mesoporous silica nanoparticles (MSN) | 49 |
| 1.12.3 | Hydroxyapatite (HAP): $\text{Ca}_{10}(\text{PO}_4)_6(\text{OH})_2$ | 50 |
| 1.12.4 | Halloysite nanotubes (HNT) | 50 |
| 1.12.5 | Chitosan nanoparticles (CS)..... | 51 |
| 1.12.6 | Silver nanoparticles (AgNP) | 52 |

| | |
|--|----|
| 1.12.7 Liposomes..... | 53 |
| 1.13 Liposomal cement | 62 |
| 1.13.1 Pluronic..... | 63 |
| 1.14 Current status of liposomal bone cements..... | 64 |
| 1.14.1 Disinfectant bone and dental filler materials comprising liposomes | 64 |
| 1.14.2 Liposomal bone cement containing amphotericin | 65 |
| 1.15 Scope of thesis..... | 66 |
| 2 General Methods..... | 67 |
| 2.1 Cement and liposome preparation..... | 67 |
| 2.1.1 PMMA bone cement preparation..... | 67 |
| 2.1.2 Liposome preparation | 67 |
| 2.1.3 Liposome pellet preparation | 68 |
| 2.1.4 Release of antibiotic and lipids from cement discs | 68 |
| 2.2 Particle size and zeta potential of liposomes | 69 |
| 2.3 Contact angle measurement..... | 69 |
| 2.4 Mechanical testing..... | 70 |
| 2.4.1 Compressive strength | 70 |
| 2.4.2 Bending modulus | 70 |
| 2.4.3 Bending strength..... | 71 |
| 2.5 Stewart assay (determination of phospholipid content)..... | 71 |
| 2.6 Extraction of lipids in solution using the Bligh and Dyer method | 73 |
| 2.7 Liquid chromatography–mass spectrometry (LC–MS) analysis of gentamicin..... | 73 |
| 2.7.1 Method 1 (Thermo Spectra System P4000) | 73 |
| 2.7.2 Method 2 (Bruker Amazon SL)..... | 74 |
| 2.8 Analysis of lipids using fluorescence spectrophotometry | 74 |
| 2.8.1 Development and validation of method for analysis of fluorescent lipids in methanol..... | 74 |
| 2.8.2 Analysis of fluorescent lipids in chloroform..... | 75 |
| 2.9 Antimicrobial testing methods..... | 76 |

| | |
|--|----|
| 2.9.1 Sterilisation of glassware and media | 76 |
| 2.9.2 Quantitative suspension test | 77 |
| 2.9.3 Analysis of biofilm formation..... | 78 |
| 2.10 Scanning electron microscopy | 78 |
| 2.11 Statistical analysis | 78 |
| 3 Validation and characterisation of the liposomal delivery system..... | 79 |
| 3.1 Introduction..... | 79 |
| 3.2 Methods | 80 |
| 3.2.1 Materials | 80 |
| 3.2.2 Liposome preparation | 81 |
| 3.2.3 Cement preparation | 81 |
| 3.2.4 Zeta potential and particle size..... | 81 |
| 3.2.5 Contact angle measurement | 81 |
| 3.2.6 Mechanical testing | 81 |
| 3.2.7 Release of antibiotic and lipids from cement discs | 81 |
| 3.2.8 Stewart assay | 82 |
| 3.2.9 LC-MS..... | 82 |
| 3.2.10 High performance liquid chromatography (HPLC) analysis of lipids..... | 83 |
| 3.2.11 Determination of encapsulation efficiency | 83 |
| 3.2.12 Analysis of lipids using fluorescence spectrophotometry | 83 |
| 3.2.13 Antimicrobial testing | 84 |
| 3.2.14 Scanning electron microscopy..... | 84 |
| 3.2.13 Statistical analysis..... | 84 |
| 3.3 Results | 84 |
| 3.3.1 Zeta potential and particle size of liposomes | 84 |
| 3.3.2 Contact angle measurement | 85 |
| 3.3.3 Mechanical properties | 86 |
| 3.3.4 LC-MS method optimisation (Thermo Spectra System P4000)..... | 89 |
| 3.3.5 Antimicrobial testing | 98 |

| | |
|---|-----|
| 3.3.6 Scanning electron microscopy (SEM) of cement disc surface | 111 |
| 3.3.7 Determination of lipid release from cement | 111 |
| 3.4 Discussion..... | 118 |
| 3.5 Conclusions..... | 126 |
| 4 Developing and evaluating a freeze-dried liposome-gentamicin formulation for use in bone cement | 128 |
| 4.1 Introduction..... | 128 |
| 4.2. Methods..... | 130 |
| 4.2.1 Materials | 130 |
| 4.2.2 Sample preparation..... | 130 |
| 4.2.3 LC-MS..... | 131 |
| 4.2.4 Mechanical testing | 132 |
| 4.2.5 Zeta potential and particle size..... | 132 |
| 4.2.6 Contact angle measurement | 132 |
| 4.2.7 Antimicrobial testing..... | 132 |
| 4.2.8 Scanning electron microscopy..... | 132 |
| 4.2.9 Statistical analysis..... | 132 |
| 4.3 Results | 133 |
| 4.3.1 Gentamicin release from FDL-CEMENT | 133 |
| 4.3.2 Mechanical testing | 134 |
| 4.3.3 Characterising the components of the freeze-dried liposome-gentamicin formulation to be used in cements (FDL) | 137 |
| 4.3.4 Contact angles for cement discs | 139 |
| 4.3.5 Antimicrobial testing..... | 140 |
| 4.3.6 SEM images of cement disc surface | 142 |
| 4.3.7 Measurement of phosphatidylcholine loss during liposome manufacturing processes | 145 |
| 4.4 Discussion..... | 151 |
| 4.5 Conclusions..... | 162 |
| 5 Incorporation of hydrophilic and hydrophobic additives..... | 164 |

| | |
|--|-----|
| 5.1 Introduction..... | 164 |
| 5.2. Methods..... | 167 |
| 5.2.1 Materials | 167 |
| 5.2.2 Cement preparation | 167 |
| 5.2.3 LC-MS to assay gentamicin release from cement discs | 168 |
| 5.2.4 Antimicrobial testing | 168 |
| 5.2.5 Mechanical testing | 168 |
| 5.2.6 Scanning electron microscopy..... | 168 |
| 5.2.7 Analysis of cement discs by micro computed tomography..... | 169 |
| 5.2.8 Contact angle measurement | 171 |
| 5.2.9 Sample weight loss after storage in PBS..... | 171 |
| 5.2.10 Statistical analysis..... | 171 |
| 5.3. Results | 172 |
| 5.4.1 Antibiotic release from Palacos R+G containing different incorporated percentages of lactose and magnesium stearate..... | 172 |
| 5.4.1 Antimicrobial testing | 174 |
| 5.4.1 Mechanical testing | 176 |
| 5.4.1.1 Scanning electron microscopy..... | 180 |
| 5.5 Discussion..... | 195 |
| 5.6 Conclusions..... | 199 |
| 6 Dry particle coating of gentamicin sulfate with magnesium stearate | 200 |
| 6.1 Introduction..... | 200 |
| 6.2 Methods | 203 |
| 6.2.1 Materials | 203 |
| 6.2.2 Cement preparation | 203 |
| 6.2.3 Mixing techniques used for gentamicin sulfate and magnesium stearate | 204 |
| 6.2.4 LC-MS..... | 204 |
| 6.2.5 Compressive strength | 205 |
| 6.2.6 Particle size analysis using laser diffraction..... | 205 |

| | |
|---|-----|
| 6.2.7 Contact angle measurement | 205 |
| 6.2.8 Antimicrobial Testing | 205 |
| 6.2.9 Scanning electron microscopy..... | 206 |
| 6.2.10 Scanning electron microscope using Energy Dispersive X-ray Spectroscopy (SEM-EDX) | 206 |
| 6.2.11 Statistical analysis | 206 |
| 6.3 Results | 206 |
| 6.3.1 Scanning electron microscopy images of gentamicin and magnesium stearate powder blends | 206 |
| 6.3.2 Particle size analysis using laser diffraction..... | 209 |
| 6.3.3 Scanning electron microscope using Energy Dispersive X-ray Spectroscopy (SEM-EDX) to characterise gentamicin and magnesium stearate blend | 211 |
| 6.3.4 Compressive strength | 216 |
| 6.3.5 Contact angles for cement discs | 217 |
| 6.3.6 Antibiotic release from the different cement formulations of Palacos R containing magnesium stearate powder coated gentamicin sulfate | 218 |
| 6.3.7 Antimicrobial testing | 221 |
| 6.3.8 Sample weight loss after storage in PBS..... | 222 |
| 6.3.10 SEM images of cement disc surface | 223 |
| 6.4 Discussion | 230 |
| 6.5 Conclusions | 239 |
| 7 Conclusions and future work | 241 |
| 7.1 Conclusions | 241 |
| 7.2 Future work | 245 |
| References | 248 |

List of Figures

| | |
|--|----|
| Figure 1: X-ray images showing narrowing of the joint space in (A) a healthy knee joint, and (B) a knee joint affected by osteoarthritis (Arthritis of the Knee-OrthoInfo - AAOS, 2012)..... | 29 |
| Figure 2: Schematic diagrams showing the difference in fixation between the implant and bone interface for (A) cemented and (B) uncemented fixations in TKR (www.orthoped.org, 2017)..... | 32 |
| Figure 3: Chemical structures of the polymerisation components (A) PMMA (polymer), (B) MMA (monomer), (C) BPO (initiator) and (D) DMPT (activator)..... | 35 |
| Figure 4: The different steps of the polymerisation process are shown (A-E). Both products shown in (A) and (B) are formed during the initiation step; (A) benzoyl oxide radicals are formed and (B) benzoyl oxide radicals and MMA react, forming a combined product. (C) the polymer chain is lengthened during the propagation step. (D) and (E) are both termination steps; (D) termination by combination and (E) termination by disproportionation..... | 36 |
| Figure 5: List of the five individual components, C1, C1a, C2, C2a and C2b, found in gentamicin sulfate complex (A). The gentamicin components differ in the degree of substitution indicated by R2 and R3 on the 6-position carbon of the purpurosamine unit, and R1 on the nitrogen atom connected to the 6-position carbon (British Pharmacopoeia, 2021). | 43 |
| Figure 6: Structures of (A) single walled nanotubes (SWNT) and (B) multiple walled nanotubes (MWNT) (Aboofazeli 2010) | 48 |
| Figure 7: Diagram showing the structure of MCM-41; the regular hexagonal arrangement and cylindrical mesopores are shown..... | 49 |
| Figure 8: Electron micrograph of halloysite nanotubes SEM image of HNT (Wei et al. 2012). | 51 |
| Figure 9: General chemical structure of a phospholipid molecule, with the three adjacent carbon positions on the glycerol backbone labelled 1,2 and 3 in red. The different moieties are labelled that make up phospholipid molecules are labelled phosphate, glycerol and fatty acid. R1 and R2 represent hydrocarbon chains. R3 represents different molecules such as choline, serine, glycerol, inositol or ethanolamine, that are part of the polar head group..... | 54 |
| Figure 10: Schematic diagram of representation of phospholipids, lipid bilayer and liposome, all in aqueous media. The polar head and non-polar hydrocarbon chains are shown on the phospholipids at the different stages of liposome formation. Note that for the purpose of this illustration, the liposome diagram shows just one bilayer (unilamellar liposome); and the liposome is shown in 2D, when in fact liposomes are 3D objects..... | 57 |

| | |
|---|----|
| Figure 11: Molecular structure of cholesterol with particular emphasis on its hydroxyl group and aliphatic carbon chain..... | 58 |
| Figure 12: Proposed liposome-Pluronic structure, showing the interactions of Pluronic with respect to MMA molecules and the liposome surface; allowing the liposomes to be suspended in MMA (Ayre et al. 2015). | 62 |
| Figure 13: Contact angle measurements for commercial cements Palacos R and Palacos R+G, LCP-CEMENT, commercial R+G cement containing different Pluronics at concentrations ranging from 1 – 10% w/w. (n=3). Asterisks indicate the level of significance (* p<0.05, ** p<0.01, *** p<0.001) | 86 |
| Figure 14: Compressive strength results for Palacos R and Palacos R+G and LCP-CEMENT. Data is presented as mean ± standard deviation (n=5). Asterisks indicate the level of significance (* p<0.05, ** p<0.01, *** p<0.001)..... | 87 |
| Figure 15: Bending modulus results for Palacos R and Palacos R+G and LCP-CEMENT. Data is presented as mean ± standard deviation (n=5). Asterisks indicate the level of significance (* p<0.05, ** p<0.01, *** p<0.001) | 88 |
| Figure 16: Bending strength results for Palacos R and Palacos R+G and LCP-CEMENT. Data is presented as mean ± standard deviation (n=5). Asterisks indicate the level of significance (* p<0.05, ** p<0.01, *** p<0.001)..... | 89 |
| Figure 17: Examples of gentamicin peaks for concentrations of (A) 3 µg/ml (LOQ) and (B) 60 µg/ml (upper quantification limit), showing clear identifiable peaks at retention time of around 7 minutes..... | 90 |
| Figure 18: Calibration curve of gentamicin base by the LC-MS method (Thermo Spectra System P4000) for concentrations ranging from 3 µg/ml (LOQ) to 60 µg/ml (upper quantification limit) (n=3). R2 (>0.99) is deemed acceptable (Pinto et al., 2017) | 91 |
| Figure 19: Chromatograms showing (A) LOQ and (B) LOD, using concentrations of 3 µg/ml (LOQ) and 1 µg/ml (LOD). Signal-to-noise ratios of at least 3 and 10 were deemed acceptable for the limits of detection and quantification respectively (Wang et al., 2019).... | 92 |
| Figure 20: Cumulative drug release of GS (µg) from PMMA bone cement stored in PBS solution (pH 7.4, 37 °C) at different time points (0 to 3240 hours). Error bars indicate standard deviation from the mean of experimental data performed in triplicate (n=3)..... | 93 |
| Figure 21: Cumulative drug release of GS (µg) from PMMA bone cement stored in PBS solution (pH 7.4, 37 °C) from time points 0 to 72 hours. Error bars indicate standard deviation from the mean of experimental data performed in triplicate (n=3)..... | 94 |
| Figure 22: Calibration curve for gentamicin base determination, by LC-MS method (Bruker Amazon SL) for concentrations ranging from 1 µg/ml (LOQ) to 120 µg/ml (upper quantification limit) (n=3). R2 (>0.99) is deemed acceptable (Pinto et al., 2017)..... | 95 |

| | |
|--|-----|
| Figure 23: Cumulative drug release of GS (μg) from PMMA bone cement samples containing different incorporated percentages of Pluronic L31, L43 and L61 all stored in PBS solution (pH 7.4, 37 °C) from time points 0 to 2160 hours. (n=3) | 96 |
| Figure 24: Cumulative drug release of GS (μg) from PMMA bone cement samples containing different incorporated percentages of Pluronic L31, L43 and L61 all stored in PBS (pH 7.4, 37 °C) from time point 0 to 72 hours. (n=3). Note that lines for two sets of data (L31 1% and L61 5%) are indistinguishable from one another at these times points..... | 97 |
| Figure 25: Colony forming units (CFU) for samples after 4 hours contact with <i>S. aureus</i> cultures in TSB at 37 °C (n=3). Asterisks indicate the level of significance with respect to Palacos R+G (* p<0.05, ** p<0.01, *** p<0.001) | 99 |
| Figure 26: Colony forming units (CFU) for 0.01 g GS, 0.01 g and 0.1 g of MMA after 4 hours contact with <i>S. aureus</i> cultures in TSB at 37 °C (n=3) | 100 |
| Figure 27: SEM surface images of Palacos R samples (A) before and (B) after incubation in PBS for one week at 37 °C; sample magnifications are x80, x800 and x2.5k respectively..... | 101 |
| Figure 28: SEM surface images of Palacos R+G samples (A) before and (B) after incubation in PBS for one week at 37 °C; sample magnifications are x80, x800 and x2.5k respectively. Arrows indicate PMMA particles (orange) and pores (blue) | 102 |
| Figure 29: SEM surface images of LCP-CEMENT samples (A) before and (B) after incubation in PBS for one week at 37 °C; sample magnifications are x80, x800 and x2.5k respectively. Arrows indicate PMMA particles (orange) and pores (blue) | 102 |
| Figure 30: SEM surface images of Palacos R+G cement samples containing 1% w/w of Pluronic L31 (A) before and (B) after incubation in PBS for one week at 37 °C; sample magnifications are x80, x800 and x2.5k respectively. Arrows indicate PMMA particles (orange) and pores (blue) | 103 |
| Figure 31: SEM surface images of Palacos R+G cement samples containing 5% w/w of Pluronic L31 (A) before and (B) after incubation in PBS for one week at 37 °C; sample magnifications are x80, x800 and x2.5k respectively. Arrows indicate PMMA particles (orange) and pores (blue) | 104 |
| Figure 32: SEM surface images of Palacos R+G cement samples containing 10% w/w of Pluronic L31 (A) before and (B) after incubation in PBS for one week at 37 °C; sample magnifications are x80, x800 and x2.5k respectively. Arrows indicate PMMA particles (orange) and pores (blue) | 105 |
| Figure 33: SEM surface images of Palacos R+G cement samples containing 1% w/w of Pluronic L43 (A) before and (B) after incubation in PBS for one week at 37 °C; sample magnifications are x80, x800 and x2.5k respectively. Arrows indicate PMMA particles (orange) and pores (blue) | 106 |

| | |
|--|-----|
| Figure 34: SEM surface images of Palacos R+G cement samples containing 5% w/w of Pluronic L43 (A) before and (B) after incubation in PBS for one week at 37 °C; sample magnifications are x80, x800 and x2.5k respectively. Arrows indicate PMMA particles (orange) and pores (blue)..... | 107 |
| Figure 35: SEM surface images of Palacos R+G cement samples containing 10% w/w of Pluronic L43 (A) before and (B) after incubation in PBS for one week at 37 °C; sample magnifications are x80, x800 and x2.5k respectively. Arrows indicate PMMA particles (orange) and pores (blue). | 108 |
| Figure 36: SEM surface images of Palacos R+G cement samples containing 1% w/w of Pluronic L61 (A) before and (B) after incubation in PBS for one week at 37 °C; sample magnifications are x80, x800 and x2.5k respectively. Arrows indicate PMMA particles (orange) and pores (blue) | 109 |
| Figure 37: SEM surface images of Palacos R+G cement samples containing 5% w/w of Pluronic L61 (A) before and (B) after incubation in PBS for one week at 37 °C; sample magnifications are x80, x800 and x2.5k respectively. Arrows indicate PMMA particles (orange) and pores (blue) | 110 |
| Figure 38: SEM surface images of Palacos R+G cement samples containing 10% w/w of Pluronic L61 (A) before and (B) after incubation in PBS for one week at 37 °C; sample magnifications are x80, x800 and x2.5k respectively. Arrows indicate PMMA particles (orange) and pores (blue) | 111 |
| Figure 39: Calibration curve for phosphatidylcholine determination, using the Stewart assay (n=3). R2 (>0.99) is deemed acceptable (Pinto et al., 2017) | 112 |
| Figure 40: Chromatograms obtained from HPLC analysis of phosphatidylcholine in bone cement: (A) 0.5 mg/ml phosphatidylcholine after extraction and, (B) Palacos R cement eluent..... | 113 |
| Figure 41: Emission and excitation wavelengths for 1 µg/ml of 18:1-06:0 NBD PC fluorescent lipid in methanol. The wavelengths were determined as 467 nm (excitation) and 535 nm (emission) | 115 |
| Figure 42: Calibration curve of 18:1-06:0 NBD PC phospholipid in methanol using concentrations from 0.2 µg/m (LOQ) I to 20 µg/ml (upper quantification limit) (n=3). R2 (>0.99) is deemed acceptable (Pinto et al., 2017) | 115 |
| Figure 43: Emission and excitation wavelengths for 5 µg/ml of 18:1-06:0 NBD PC fluorescent lipid in chloroform. The wavelengths were determined as 464 nm (excitation) and 531 nm (emission) | 117 |
| Figure 44: Calibration curve of 18:1-06:0 NBD PC phospholipid in chloroform using concentrations of 0.0005 µg/ml LOQ) to 3 µg/ml (upper quantification limit) (n=3). R2 (>0.99) is deemed acceptable (Pinto et al., 2017) | 117 |

Figure 45: Compressive strength results for Palacos R and Palacos R+G, LCP-CEMENT, FDL-CEMENT015 and FDL-CEMENT030. Data is presented as mean \pm standard deviation (n=5). Asterisks indicate the level of significance (* $p < 0.05$, ** $p < 0.01$, *** $p < 0.001$)135

Figure 46: Bending modulus results for Palacos R and Palacos R+G, LCP-CEMENT, FDL-CEMENT015 and FDL-CEMENT030 (n=5). Data is presented as mean \pm standard deviation (n=5). Asterisks indicate the level of significance (* $p < 0.05$, ** $p < 0.01$, *** $p < 0.001$).....136

Figure 47: Bending strength results for Palacos R and Palacos R+G, LCP-CEMENT, FDL-CEMENT015 and FDL-CEMENT030 (n=5). Data is presented as mean \pm standard deviation (n=5). Asterisks indicate the level of significance (* $p < 0.05$, ** $p < 0.01$, *** $p < 0.001$)137

Figure 48: Contact angles for Palacos R and Palacos R+G, LCP-CEMENT, FDL-CEMENT015, FDL-CEMENT030 and FDL-CEMENT060 (n=3). Data is presented as mean \pm standard deviation (n=3). Asterisks indicate the level of significance (* $p < 0.05$, ** $p < 0.01$, *** $p < 0.001$)140

Figure 49: Colony forming units (CFU) for Palacos R and Palacos R+G, LCP-CEMENT, FDL-CEMENT015, FDL-CEMENT030 and FDL-CEMENT060 (n=3). Data is presented as mean \pm standard deviation (n=3). Asterisks indicate the level of significance with respect to Palacos R+G (* $p < 0.05$, ** $p < 0.01$, *** $p < 0.001$)141

Figure 50: SEM surface images for Palacos R and Palacos R+G, LCP-CEMENT, FDL-CEMENT015, FDL-CEMENT030 and FDL-CEMENT060; (A) before and (B) after incubation in PBS for one week at 37 °C; sample magnifications are x80, x800 and x2.5k respectively. Arrows indicate PMMA particles (orange) and pores (blue)145

Figure 51: SEM images of Whatman Track-Etched Membranes, of pore sizes 100 nm, 200 nm and 400 nm. Images taken show control samples that have not been extruded (A) and membranes after liposome extrusion (B) and (C)147

Figure 52: Amount of lipid measured in mg for both the pellet and supernatant after centrifugation at an average force of 107,000 g at time points of 1.5, 3.0 and 4.5 hours (n=3). Asterisks indicate the level of significance (* $P < 0.05$, ** $P < 0.01$, *** $P < 0.001$)148

Figure 53: Average particle diameter measure for liposomes in both the pellet and supernatant after centrifugation at an average force of 107,000 g at time points of 1.5, 3.0 and 4.5 hours (n=3)149

Figure 54: Amount of lipid measured in mg for both the pellet and supernatant after centrifugation at an average force of 207,000 g at time points of 1.5 and 3.0 hours (n=3). Asterisks indicate the level of significance (* $p < 0.05$, ** $p < 0.01$, *** $p < 0.001$)150

Figure 55: Average particle diameter of measure for liposomes in both the pellet and supernatant after centrifugation at an average force of 207,000 g at 1.5 hours (n=3)151

Figure 56: Chemical structure of magnesium stearate which exists as a salt containing two stearate anion equivalents and one magnesium cation.....166

| | |
|---|-----|
| Figure 57: Chemical structures of A) anhydrous α -lactose B) anhydrous β -lactose and C) α lactose monohydrate..... | 166 |
| Figure 58: Schematic diagram of a cement disc used for characterising changes due to penetration of water from the top surface. Line (A) is where the saw is placed and cut in the direction of line (B) | 169 |
| Figure 59: Schematic diagram of an object with (A) two open pores and (B) one closed pore. Solid matter (C), within the object, is coloured green..... | 170 |
| Figure 60: Cumulative drug release of GS (μg) from Palacos R+G, and Palacos R+G containing 10% w/w and 25 % w/w of magnesium stearate cement discs all stored in PBS solution (pH 7.4, 37 °C) from time point 0 to 1296 hours. (n=3) | 173 |
| Figure 61: Cumulative drug release of GS (μg) from Palacos R+G, Palacos R+G containing 10% w/w and 25% w/w of lactose and Palacos R+G containing 10% w/w and 25% w/w of magnesium stearate cement discs all stored in PBS solution (pH 7.4, 37 °C) from time point 0 to 72 hours. (n=3) | 174 |
| Figure 62: Colony forming units (CFU) for Palacos R, Palacos R+G, and for lactose 10% and 25%, and MgSt 10% and 25% cement discs. Data is presented as mean \pm standard deviation (n=3). Asterisks indicate the level of significance with respect to Palacos R+G (* p<0.05, ** p<0.01, *** p<0.001) | 175 |
| Figure 63: Bending modulus results for commercial cements, Palacos R, Palacos R+G, and cements containing 10% w/w and 25% w/w each of lactose and magnesium stearate. Data is presented as mean \pm standard deviation (n=5). Asterisks indicate the level of significance (* p<0.05, ** p<0.01, *** p<0.001) | 177 |
| Figure 64: Bending strength results for commercial cements, Palacos R, Palacos R+G, and cements containing 10% w/w and 25% w/w lactose and magnesium stearate. Data is presented as mean \pm standard deviation (n=5). Asterisks indicate the level of significance (* P<0.05, ** P<0.01, *** P<0.001) | 178 |
| Figure 65: Compression results for commercial cements, Palacos R, Palacos R+G, and cements containing 10% w/w and 25% w/w lactose and magnesium stearate. Data is presented as mean \pm standard deviation (n=5). Asterisks indicate the level of significance (* p<0.05, ** p<0.01, *** p<0.001) | 179 |
| Figure 66: Contact angles for commercial cements Palacos R, Palacos R+G, and cements containing 10% w/w and 25% w/w lactose and magnesium stearate. Data is presented as mean \pm standard deviation (n=3). Asterisks indicate the level of significance (* p<0.05, ** p<0.01, *** p<0.001) | 180 |
| Figure 67: SEM surface images of Palacos R samples (A) before and (B) after incubation in PBS for one week at 37 °C; sample magnifications are x80, x800 and x2.5k respectively..... | 182 |

Figure 68: SEM surface images of Palacos R+G samples (A) before and (B) after incubation in PBS for one week at 37 °C; sample magnifications are x80, x800 and x2.5k respectively. Arrows indicate PMMA particles (orange) and pores (blue)182

Figure 69: SEM surface images of lactose 10% (A) before and (B) after incubation in PBS for one week at 37 °C; sample magnifications are x80, x800 and x2.5k respectively. Arrows indicate PMMA particles (orange) and pores (blue)183

Figure 70: SEM surface images of lactose 25% (A) before and (B) after incubation in PBS for one week at 37 °C; sample magnifications are x80, x800 and x2.5k respectively. Arrows indicate PMMA particles (orange) and pores (blue)183

Figure 71: SEM surface images of Palacos R+G cement samples containing lactose 80% (A) before and (B) after incubation in PBS for one week at 37 °C; sample magnifications are x80, x800 and x2.5k respectively. Arrows indicate solid matrix (orange), smaller non-pmma particles (green) and pores (blue)184

Figure 72: SEM surface images of Palacos R+G cement samples containing MgSt 10% (A) before and (B) after incubation in PBS for one week at 37 °C; sample magnifications are x80, x800 and x2.5k respectively. Arrows indicate fused PMMA particles (orange), lesser-fused PMMA particles (yellow) and pores (blue)184

Figure 73: SEM surface images of Palacos R+G cement samples containing MgSt 25% (A) before and (B) after incubation in PBS for one week at 37 °C; sample magnifications are x80, x800 and x2.5k respectively. Arrows indicate fused PMMA particles (orange), lesser-fused PMMA particles (yellow) and pores (blue)185

Figure 74: SEM images of inside portion of Palacos R disc cut horizontally (A) before and (B) after incubation in PBS for one week at 37 °C; sample magnifications are x200 and x1k. Arrows indicate pores.....186

Figure 75: SEM images of inside portion of Palacos R+G disc cut horizontally (A) before and (B) after incubation in PBS for one week at 37 °C; sample magnifications are x200 and x1k. Arrows indicate PMMA particles (orange) and pores (blue)186

Figure 76: SEM images of inside portion of Palacos R+G disc containing lactose 10% disc cut horizontally (A) before and (B) after incubation in PBS for one week at 37 °C; sample magnifications are x200 and x1k. Arrows indicate PMMA particles (orange) and pores (blue)187

Figure 77: SEM images of inside portion of Palacos R+G disc containing lactose 25% disc cut horizontally (A) before and (B) after incubation in PBS for one week at 37 °C; sample magnifications are x200 and x1k. Arrows indicate pores.....187

Figure 78: SEM images of inside portion of Palacos R+G disc containing lactose 80% disc cut horizontally (A) before and (B) after incubation in PBS for one week at 37 °C; sample magnifications are x200 and x1k. Arrows indicate solid matrix (orange), smaller non-pmma particles (green) and pores (blue)188

Figure 79: SEM images of inside portion of Palacos R+G disc containing MgSt 10% disc cut horizontally (A) before and (B) after incubation in PBS for one week at 37 °C; sample magnifications are x200 and x1k. Arrows indicate PMMA particles (orange) and pores (blue).....188

Figure 80: SEM images of inside portion of MgSt 25% disc cut horizontally (A) before and (B) after incubation in PBS for one week at 37 °C; sample magnifications are x200 and x1k. Arrows indicate PMMA particles (orange) and pores (blue)189

Figure 81: MicroCT 3D images obtained for control sample disc, Palacos R+G, after incubation in PBS for one week at 37 °C. A) is the top view, B) is the side view, C) is the view of the sample disc cut with the software vertically, halfway through the middle; and D) is the view of the sample disc cut with the software horizontally, halfway through the middle.....191

Figure 82: MicroCT 3D images obtained for sample disc, lactose 25%, after incubation in PBS for one week at 37 °C. A) is the top view, B) is the side view, C) is the view of the sample disc cut with the software vertically, halfway through the middle; and D) is the view of the sample disc cut with the software horizontally, halfway through the middle.....191

Figure 83: MicroCT 3D images obtained for sample disc, lactose 80%, after incubation in PBS for one week at 37 °C. A) is the top view, B) is the side view, C) is the view of the sample disc cut with the software vertically, halfway through the middle; and D) is the view of the sample disc cut with the software horizontally, halfway through the middle.....192

Figure 84: Percentage weight loss for Palacos R, Palacos R+G, Palacos R+G discs containing 10% w/w and 25% w/w of lactose and Palacos R+G discs containing 10% w/w and 25% w/w of magnesium stearate cement discs, after incubation in PBS at 37 °C for one week (n=3). Asterisks indicate the level of significance (* p<0.05, ** p<0.01, *** p<0.001).....193

Figure 85: Percentage weight loss for discs produced from Palacos R+G containing 25% w/w, 50% w/w and 80% w/w of lactose, after incubation in PBS at 37 °C for one week (n=3). Asterisks indicate the level of significance with respect to Palacos R+G (* p<0.05, ** p<0.01, *** p<0.001)194

Figure 86: SEM images of (A) gentamicin sulfate, (B) magnesium stearate and (C) gentamicin sulfate and magnesium stearate 25% w/w preliminary mixture, (D) gentamicin sulfate and magnesium stearate 25% w/w mixture at a high magnification. Sample magnifications are between x1k and x3.7k.....207

Figure 87: SEM images of gentamicin sulfate and magnesium stearate powder blends of concentration 1% w/w, 5% w/w and 10% w/w with respect to gentamicin sulfate, prepared by hexagonal mixing. Sample magnifications are 1.5k.....207

Figure 88: SEM images of gentamicin sulfate and magnesium stearate powder blends of concentration 1% w/w, 5% w/w and 10% w/w with respect to gentamicin sulfate, prepared by manually grinding with a mortar and pestle. Sample magnifications are 1.5k.....208

Figure 89: SEM images of gentamicin sulfate and magnesium stearate powder blends of concentration 1% w/w, 5% w/w and 10% w/w with respect to gentamicin sulfate, prepared by the ball mill technique. Sample magnifications are between x3k and x3.5k.....208

Figure 90: Particle size, D50, measurements (μm) for unprocessed gentamicin sulfate, gentamicin sulfate (ball milled), magnesium stearate, BM, HEX and PM mixtures. BM (ball mill), HEX (hexagonal mixer) and PM (pestle and mortar) indicate particles produced from these mixing methods; 1, 5, and 10 indicate the percentage weight of magnesium stearate added to gentamicin sulfate, prior to mixing. Data is presented as mean \pm standard deviation ($n=3$). Asterisks indicate the level of significance with respect to unprocessed gentamicin sulfate (* $p<0.05$, ** $p<0.01$, *** $p<0.001$)210

Figure 91: Span (no units) showing width of distribution calculated from particle distribution data for unprocessed gentamicin sulfate, gentamicin sulfate (ball milled), magnesium stearate, BM, HEX and PM mixtures. BM (ball mill), HEX (hexagonal mixer) and PM (pestle and mortar) indicate particles produced from these mixing methods; 1, 5, and 10 indicate the percentage weight of magnesium stearate added to gentamicin sulfate, prior to mixing. Data is presented as mean \pm standard deviation ($n=3$)211

Figure 92: Energy-dispersive EDX spectra for gentamicin sulfate, showing detection of elemental carbon, oxygen and sulfur; magnification is shown at x550.....212

Figure 93: Energy-dispersive EDX spectra magnesium stearate, showing detection of elemental carbon, oxygen and sulfur; magnification is shown at x550.....212

Figure 94: Energy-dispersive EDX spectra for gentamicin sulfate and magnesium stearate blends prepared by ball mill technique, hexagonal mixing and mortar and pestle. The red peaks denote the point of interest on the left-hand SEM image, and blue peaks denote the point of interest on the right-hand image; magnification is shown at x550.....216

Figure 95: Energy-dispersive EDX spectra for Palacos R bone cement showing detection of elemental silicon, zirconium and calcium; magnification is shown at x550.....216

Figure 96: Compressive strength results for Palacos R and Palacos R+G, BM1, BM5, BM10, HEX1, HEX5, HEX10, PM1, PM5 and PM10. Data is presented as mean \pm standard deviation ($n=5$). There was no significant difference between any of the sample groups tested.....217

Figure 97: Contact angles for Palacos R and Palacos R+G, BM1, BM5, BM10, HEX1, HEX5, HEX10, PM1, PM5 and PM10 cements. Data is presented as mean \pm standard deviation (n=3). Asterisks indicate the level of significance (* p<0.05, ** p<0.01, *** p<0.001)218

Figure 98: Cumulative drug release of GS (μg) from Palacos R+G, BM1, BM5, BM10, HEX1, HEX5, HEX10, PM1, PM5 and PM10 cement discs all stored in PBS solution (pH 7.4, 37 °C) from time point 0 to 624 hours. (n=3)219

Figure 99: Cumulative drug release of GS (μg) from Palacos R+G, BM1, BM5, BM10, HEX1, HEX5, HEX10, PM1, PM5 and PM10 cement discs all stored in PBS solution (pH 7.4, 37 °C) from time point 0 to 72 hours. (n=3)220

Figure 100: Colony forming units (CFU) for Palacos R and Palacos R and Palacos R+G, BM1, BM5, BM10, HEX1, HEX5, HEX10, PM1, PM5 and PM10. Data is presented as mean \pm standard deviation (n=3). Asterisks indicate the level of significance with respect to Palacos R+G (* p<0.05, ** p<0.01, *** p<0.001)222

Figure 101: Percentage weight loss for commercial cements Palacos R and Palacos R+G and BM1, BM5, BM10, HEX1, HEX5, HEX10, PM1, PM5 and PM10 cements all stored in PBS solution (pH 7.4, 37 °C) for one week and dried. Data is presented as mean \pm standard deviation (n=3). Asterisks indicate the level of significance with respect to Palacos R+G (* p<0.05, ** p<0.01, *** p<0.001)223

Figure 102: SEM surface images for Palacos R and Palacos R+G, BM1, BM5, BM10, HEX1, HEX5, HEX10, PM1, PM5 and PM10 cements (A) before and (B) after incubation in PBS for one week at 37 °C; sample magnifications are x80, x800 and x2.5k respectively. Arrows indicate PMMA particles (orange), lesser-fused particles (yellow) and pores (blue)230

List of Tables

| | |
|---|-----|
| Table 1: Antibiotic laden commercial bone cement constituents included in the powder and liquid components of commercial bone cement, Palacos R+G. | 34 |
| Table 2: Common naturally occurring phospholipids are listed. Phospholipids are denoted by the general chemical structure R, attached to atoms/molecules that make up the polar head groups. Note that atoms/molecules completing the polar head groups shown in this table represent R3 that is attached to the generic phospholipid molecule shown in Figure 9. | 55 |
| Table 3: Different classes of liposome based on size and number of bilayers (Castañeda-Reyes et al., 2020; New, 2003) | 62 |
| Table 4: Scheme for the addition of reagent volumes to each tube: the tube for the blank sample contains only addition of chloroform and ammonium ferrothiocyanate with no addition of the standard solution. The test sample tubes labelled 1-6 contain different volumes of the standard solution with the addition of chloroform and ammonium ferrothiocyanate. | 72 |
| Table 5: Particle size (nm), Polydispersity index (PDI) and zeta potential measurements (mV) for gentamicin loaded liposomes, non-loaded liposomes and non-loaded NBD labelled liposomes. (n=3). Average particle diameter is reported as the intensity average, since a unimodal distribution was observed for all samples. | 85 |
| Table 6: %RSD of the gentamicin peak areas for repeat injections of 5 µg/ml gentamicin (n=6). %RSD of <5% is deemed acceptable (Pinto et al., 2017). | 91 |
| Table 7: Signal-to-noise ratios for validation of method (Thermo Spectra System P4000). LOQ (3 µg/ml) and LOD (1 µg/ml) (n=3). | 92 |
| Table 8: Difference in mass quantity of gentamicin released (µg), between 12 hours and 2160 hours (3 months), for each sample (Palacos R+G, all cements containing Pluronic L31, L43 and L61). | 98 |
| Table 9: Absorbances obtained for LCP-CEMENT eluents at 1, 2 and 5 days, by UV-Vis (n=3). | 112 |
| Table 10: Gentamicin release (µg) at different time-periods (non-cumulative), over a period of 2160 hours (90 days) from a Palacos R+G formulation and FDL-CEMENT samples: FDL-CEMENT015, FDL-CEMENT030 and FDL-CEMENT060 (n=3). | 133 |
| Table 11: Total, cumulative, mass quantity (µg) of gentamicin released at 2160 hours (90 days) from Palacos R+G formulation and FDL-CEMENT samples: FDL-CEMENT015, FDL-CEMENT030 and FDL-CEMENT060 (n=3). | 134 |
| Table 12: Average particle size (nm), zeta potential measurements (mV) and polydispersity index for gentamicin-loaded freeze-dried liposomes measured at 3 days and 12 months after freeze-drying and (n=3). Note that the formulation measured at 3 days is reported as the | |

| | |
|--|-----|
| intensity average particle size and the formulation measured at 12 months is reported as the volume average particle size..... | 138 |
| Table 13: Porosity calculations obtained for samples discs Palacos R+G and Palacos R+G discs containing 25% w/w and 80% w/w of lactose, after incubation in PBS for one week at 37 °C (n=1). | 190 |
| Table 14: Difference in mass quantity of gentamicin released (μg), between 6 hours and 624 hours, for each sample (Palacos R+G, all HEX, BM and PM cements). | 221 |

Abbreviations

| | |
|-------------------|---|
| 2D | Two-dimensional |
| 3D | Three-dimensional |
| AgNP | Silver Nanoparticles |
| ALBC | Antibiotic loaded bone cement |
| ANOVA | Analysis of variance |
| API | Active pharmaceutical ingredient |
| BaSO ₄ | Barium sulfate |
| BP | British Pharmacopoeia |
| BPO | Benzoyl peroxide |
| C | Cholesterol |
| CCD | Charge-coupled device detector |
| CE | Capillary electrophoresis |
| CNT | Carbon Nanotubes |
| CS | Chitosan nanoparticles |
| D ₅₀ | Mass median diameter |
| DLS | Dynamic light scattering |
| DMAEA | 2-dimethylaminoethyl methacrylate |
| DMPT | N,N-dimethyl-p-toluidine |
| DOTAP | 1,2 dioleoyl-3-trimethylammonium-propane |
| DPCC | Dipalmitoylphosphatidylcholine |
| EO | Ethylene oxide unit |
| EDX | Energy-dispersive X-ray spectroscopy |
| EPO | European Patent Office |
| ESI | Electrospray ionization |
| FDA | The United States Food and Drug Administration |
| GC-FID | Gas-chromatography with flame ionisation detector |
| GS | Gentamicin sulfate |
| HAP | Hydroxyapatite |
| HLB | Hydrophilic lipophilic balance |
| HNT | Halloysite Nanotubes |
| HPLC | High Performance Liquid Chromatography |
| HPLC-UV-vis | High-pressure liquid chromatography with a UV-Vis detector |
| ICH | International Council for Harmonisation of Technical Requirements for Pharmaceuticals for Human Use |
| ISO | International Organization for Standardization |
| IUV | Intermediate unilamellar vesicles |
| L31 | Pluronic L31 |
| L43 | Pluronic L41 |
| L61 | Pluronic L61 |
| LC-MS | Liquid chromatography-mass spectroscopy |
| LOD | Limit of detection |
| LOQ | Limit of quantification |
| LUV | Large unilamellar vesicles |
| MgSt | Magnesium stearate |

| | |
|----------------|---|
| MIC | Minimum inhibitory concentration |
| MicroCT | Micro computed tomography |
| MMA | Methacrylate |
| MRI | Magnetic resonance imaging |
| MRSA | Methicillin resistant <i>Staphylococcus aureus</i> |
| MSN | Mesoporous silica nanoparticles |
| MWNT | Multiple walled tubes |
| MLV | Multilamellar vesicles |
| Mw | Molecular weight |
| NBD | Nitrobenzoxadiazole |
| NIST | National Institute of Standards and Technology standard |
| ONS | Office for National Statistics |
| PA | Phosphatidic acid |
| PBP | Penicillin-binding protein |
| PBS | Phosphate buffered saline |
| PC | Phosphatidylcholine |
| PE | Phosphatidylethanolamine |
| PEO | Polyethylene oxide |
| PFTE | Polytetrafluoroethylene |
| PFFPA | Pentafluoropropionic anhydride |
| PG | Phosphatidylglycerol |
| PHT | o-phthaldialdehyde |
| PI | Phosphatidylinositol |
| PJI | Prosthetic joint infection |
| PMMA | Polymethyl methacrylate |
| PO | Propylene oxide unit |
| PPO | Polypropylene oxide |
| PS | Phosphatidylserine |
| PTFE | Polytetrafluoroethylene |
| QCS | Quaternary ammonium chitosan-derivatives |
| RCF | Relative Centrifugal Force |
| RSD | Relative standard deviation |
| Rt | Retention time |
| SA | Stearylamine |
| SD | Standard deviation |
| SEM | Scanning electron microscopy |
| SEM-EDX | Scanning electron microscope using Energy Dispersive X-ray Spectroscopy |
| S/N | Signal-to-noise ratio |
| SWNT | Single walled tubes |
| SUV | Small unilamellar vesicles |
| T _c | Phase transition temperature |
| THR | Total hip replacement |
| TJR | Total joint replacement |
| TKR | Total knee replacement |
| TSB | Tryptone soya broth (TSB) |
| TSC | Tryptone sodium chloride medium |
| UK | United Kingdom |

| | |
|------------------|--|
| USA | United States of America |
| UV | Ultraviolet |
| UV-Vis | Ultraviolet–visible spectroscopy |
| WHO | World Health Organisation |
| WIPO | World Intellectual Property Organization |
| ZrO ₂ | Zirconium dioxide |

Chapter 1

1 Introduction

1.1 Indications for total joint replacements

Total joint replacement surgery (TJR) is performed for people with end-stage arthritis, intractable pain, and stiffness (Al Thaher et al., 2016). In 2019 there were a total of 194,000 TJR surgeries performed in the UK. This number is representative of both total knee replacement (TKR) and total hip replacement (THR) procedures; 92,000 THRs and 102,000 TKRs were performed in the UK (2019 16th Annual Report National Joint Registry for England, Wales, Northern Ireland and the Isle of Man, 2019). TJR is a surgical procedure where parts of a damaged or arthritic joint are removed and replaced with a prosthetic device made from a biomaterial such as plastic, ceramic or metal (Al Thaher et al., 2016; Katti, 2004). The aim of TJR surgery is to replicate normal movement of a healthy joint (Katti, 2004). There are several indications requiring TJRs, which include congenital deformities, osteoarthritis, rheumatoid arthritis and trauma (King & Phillips, 2016; Kremers et al., 2015); however, the primary cause is overwhelmingly due to osteoarthritis (TKR 96%, THR 93%) (King & Phillips, 2016; Kremers et al., 2015).

Osteoarthritis affects 240 million people globally and it is the third most common diagnosis made by doctors in older patients (Neuprez et al., 2020). Around 9 million people seek treatment for osteoarthritis every year in the UK (Conaghan et al., 2015). Osteoarthritis is a complex process that affects different joints in the body (Larsen, 2008); it is referred to as a degenerative joint disease (Larsen, 2008; Petersson & Jacobsson, 2002). Osteoarthritis is characterised by damage to the cartilage and underlying bone (Li et al., 2013). Cartilage damage can be observed by joint space narrowing using either X-ray or magnetic resonance imaging (MRI) techniques (Bager et al., 2019). Joint space narrowing occurs when cartilage is no longer sufficient to keep the bones a normal distance apart (Bager et al., 2019; Matthijssen et al., 2016). Figure 1A shows an X-ray of a healthy knee and Figure 1B shows an arthritic knee. The space shown between both bones by the healthy knee (Figure 1A),

shows healthy cartilage, whereas the X-ray of the arthritic knee (Figure 1B) shows joint space narrowing between the two bones i.e., a loss of healthy cartilage, which will likely result in joint pain, by causing the bones to exert pressure on one another (Bager et al., 2019).

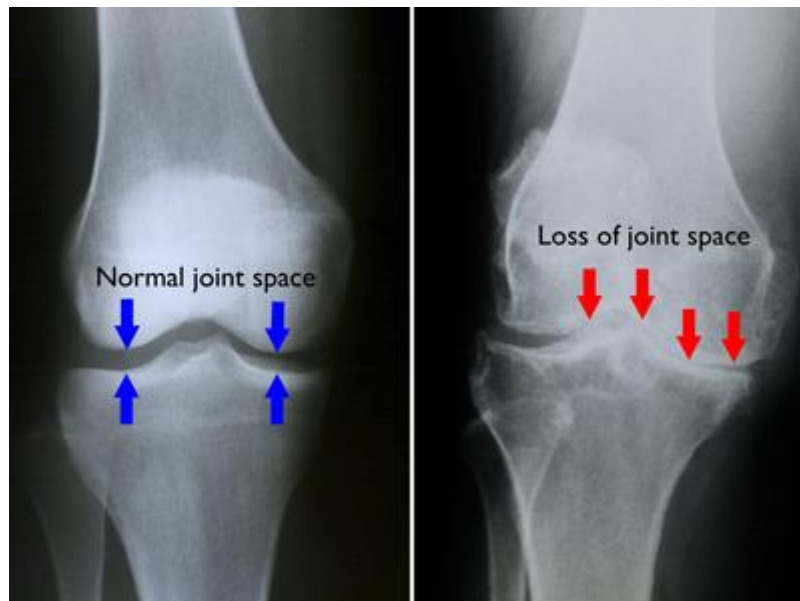


Figure 1: X-ray images showing narrowing of the joint space in (A) a healthy knee joint, and (B) a knee joint affected by osteoarthritis (Arthritis of the Knee-OrthoInfo - AAOS, 2012).

Apart from joint pain, common symptoms of osteoarthritis also include stiffness, limited movement and inflammation (Petersson & Jacobsson, 2002). The most common risk factor for developing osteoarthritis is age (Bayliss et al., 2017; Neuprez et al., 2020; Pereira et al., 2011). The World Health Organisation (WHO) Scientific Group on Rheumatic Diseases has estimated that 10% of the world's over 60 population is affected by osteoarthritis (Pereira et al., 2011). Approximately 85% of patients currently undergoing hip or knee replacements are over 60 years of age (Bayliss et al., 2017). Furthermore, gender appears to have a significant effect on the risk factor with almost twice as many women as men developing osteoarthritis (Glyn-Jones et al., 2015; Neuprez et al., 2020). Other significant risk factors include obesity, injury to joints through impact, poor muscular development and skeletal deformities (Glyn-Jones et al., 2015). Non-surgical methods of treatment include pain relief by analgesic drugs, lifestyle choices such as weight loss, physiotherapy, regular exercise and steroid injections (King & Phillips, 2016). It is estimated that within the next 15 years, the number of people with osteoarthritis will double due to an increase in the over 60s population and an increase in obesity (Conaghan et al., 2015; Neuprez et al., 2020). According to the

Office of National Statistics (ONS), the over 65 years age group will increase from 13 million in 2015 to 17 million by 2035 (Rutherford, 2012). There is also an increasing rise in younger patients having surgeries (Bayliss et al., 2017; Gustke, 2017). These statistics and the current popularity of TJRs provide cause for concern regarding the burden on the National Health Service (Bumpass & Nunley, 2012).

1.2 Total joint replacement

Total joint replacement surgery (TJR) is a surgical procedure where a dysfunctional joint is removed and replaced with a joint prosthesis (Chopra, 2015). A joint prosthesis is a medical device made of ceramic, metal, or plastic, which replicates the original movement prior to injury (King & Phillips, 2016). Most human joints can be replaced, such as wrist, shoulder and ankle joints for example (Chopra, 2015); however, total knee replacement (TKR) and total hip replacement (THR) are the most commonly performed procedures worldwide (Chopra, 2015; King & Phillips, 2016). Total joint replacements are clinically effective as they have been shown to reduce pain, they are fit for purpose, and they improve the quality of life for patients, as well as being cost effective (Bayliss et al., 2017; Bumpass & Nunley, 2012). Total joint replacements represent cost effectiveness by way of the average cost per year of a patient's life after surgery (Dakin et al., 2012). It been shown that on average it costs only £6000 per quality-adjusted year for patients (Dakin et al., 2012). Choosing which implant to use for TJR, i.e. whether TKR or THR is performed, depends on the operating surgeon's own judgement regarding the particular indication for surgery, the patient's anatomy and the surgical team's skillset (King & Phillips, 2016). Fixation of prostheses may be cemented, uncemented or a combination of the cemented and uncemented techniques (hybrid) (King & Phillips, 2016; Onggo et al., 2020).

1.2.1 Cemented and uncemented approach in TJR

Currently, there are two main methods for the fixation of bone to prosthesis: cemented and uncemented (Figure 2); although, a combination of the two is also sometimes used, called hybrid (King & Phillips, 2016; Onggo et al., 2020). In a cemented fixation, the impaired joint is completely removed, and a cavity is made inside the bone. PMMA bone cement is used to fill the cavity and then the implant is placed and positioned in the cavity whilst the cement sets (Al Thaher et al., 2016). The cement acts as a grout to hold the bone and implant together to effectively fill free space between the bone and implant (Jones & Buckle, 2020). The functions of bone cement are primarily to hold the implant against the bone and to transfer mechanical stresses and loads between the implant, particularly as bone cement in hip and knees are subject to high stresses for example forces transferred through the hip are 3 times the body weight when walking and up to 8 times the body weight whilst stumbling (Bergmann et al., 1993); furthermore, bone cements can also provide prophylaxis for post-surgical infections, depending on whether the bone cement used contains antibiotics (Al Thaher et al., 2016).

Uncemented fixations follow a similar procedure except that the implant is placed in direct contact with bone, using a bioactive compound to promote osseointegration (Al Thaher et al., 2016; Łukaszewska-Kuska et al., 2018). The surfaces of the prosthesis surfaces are roughened and treated with a bioactive coating such as hydroxyapatite or tricalcium phosphate to create a porous coating to facilitate bone ingrowth (Prasad et al., 2020; Ranjan et al., 2017). This method uses a 'press-fit' technique which effectively presses the implants onto the bone. Bone ingrowth is therefore required to firmly secure the implant (Horváth et al., 2020; Wilson & Maggs, 2018). In a hybrid fixation, e.g. in TKR, the tibia can be cemented for example, and the femur can be uncemented (Onggo et al., 2020). Figure 2 shows the difference in fixation of a metallic prosthesis and bone; in the cemented procedure (Figure 2A), the two components are attached and separated by bone cement; whereas in the uncemented procedure (Figure 2B) the components are attached without cement and are separated by the bioactive, porous coating. The fixation method used is dependent on the judgement of the operating surgeon either prior or during surgery, with each method providing satisfactory implant fixation (Onggo et al., 2020). In both cemented and uncemented cases, damaged bone is removed from the joints and the bone is shaped to fit the prosthesis. In the UK (2015), 38% of THRs were cemented, 41% were uncemented and 21% were hybrid. However, 94% of TKRs were cemented (King & Phillips, 2016).

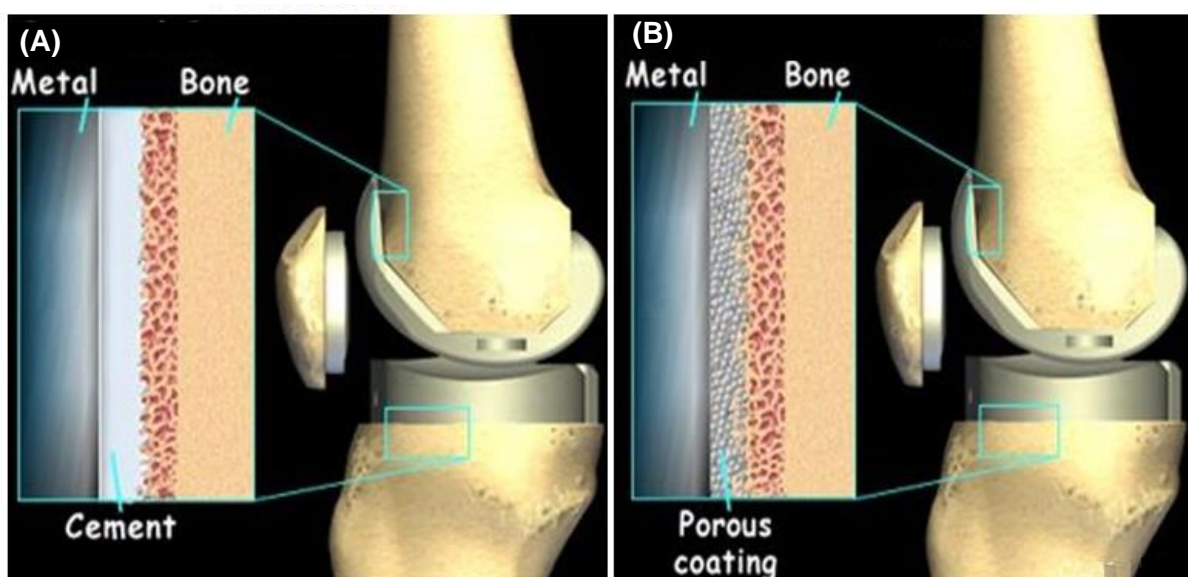


Figure 2: Schematic diagrams showing the difference in fixation between the implant and bone interface for (A) cemented and (B) uncemented fixations in TKR (www.orthoped.org, 2017).

1.3 Biomaterials

A biomaterial is a natural or synthetic material that has been designed for interaction with a biological system, specifically for diagnostic or therapeutic purposes (Sternberg, 2009). IUPAC defines biomaterials as materials which are utilised and are in contact with either microorganisms, living tissues or organisms (Vert et al, 2012). The requirements for biomaterials for use in medical implants are (Sternberg, 2009; Vert et al, 2012):

- Material must have specific mechanical properties suitable for functionality.
- Stability with regards physiological conditions.
- For biodegradable biomaterials, the degradation process must be residue free.
- The material must have a high degree of biocompatibility.
- Reasonably long shelf-life for the application.
- Sterilisable without changes in composition or form.

1.3.1 Biocompatibility

Biocompatibility refers to a material's ability to be biologically compatible with a living system (Delaey et al., 2020); moreover, it should not illicit an adverse local or systemic response with the host tissue. ISO 10993 is a series of standards for evaluating biocompatibility of a given biomaterial or medical device (Morais et al., 2010). There are several definitions for biocompatibility (Mertz, 2013); however, the most widely used definition is “the ability of a material to perform with an appropriate host response in a specific application” (Ratner, 2011).

1.4 Bone cement

Polymethyl methacrylate (PMMA), is widely used as bone cement, and its use in orthopaedics is well documented since the 1950s (Whitehouse & Evans, 2010). PMMA bone cement is considered to be an inert biomaterial (Webb & Spencer, 2007). As already mentioned, bone cement is used to secure artificial joints to bone tissue, acting as a grout. Commercial bone cement is made from two separate components: liquid and a powder component (Table 1) (Haraeus, 2018; Monzón et al., 2019; Whitehouse & Evans, 2010). The powder component usually contains either pre-polymerised PMMA beads or PMMA with the addition of copolymers such as 2-dimethylaminoethyl methacrylate (DMAEA), methacrylic acid and polystyrene, depending on the grade of cement and manufacturer (Monzón et al., 2019); a radiopacifier such as barium sulfate (BaSO_4) or zirconium dioxide (ZrO_2) is used for radiographic identification of the bone cement post-surgery (Hendriks et al., 2004); the polymerisation reaction initiator (benzoyl peroxide, BPO) which reacts with the reaction activator N,N-dimethyl-p-toluidine (DMPT) from the liquid component to form radicals; antibiotics such as gentamicin sulfate amongst possible others; and a dye such as a chlorophyll-copper-complex for visual differentiation from bone (Monzón et al., 2019). The liquid component contains the reaction monomer (methyl methacrylate, MMA); the reaction activator (DMPT); the stabiliser (hydroquinone) which inhibits premature polymerisation; and a dye which is the same chlorophyll-copper-complex as found in the powder component (Monzón et al., 2019). Percentage compositions are provided by the manufacturer (Heraeus Medical GmbH) for Palacos R+G, which contains gentamicin sulfate as an antibiotic (Table 1); however, percentage amounts are not given for hydroquinone nor for the chlorophyll complex dye (Haraeus, 2018). The molecular structures of PMMA, MMA, BPO and DMPT, which are the compounds required for the polymerisation to make PMMA cement

(Whitehouse & Evans, 2010) are shown in Figure 3. Bone cement is available with incorporated antibiotic and it is available without antibiotic (Whitehouse & Evans, 2010). The most commonly used antibiotics in commercial bone cements are gentamicin sulfate, tobramycin and vancomycin as these particular antibiotics have properties that are required for incorporation into bone cement; properties that make an antibiotic suitable for ALBCs include having a broad antibacterial spectrum, low toxicity risk, high water solubility, and they should maintain their antibacterial properties after being mixed with bone cement (Hinarejos et al., 2015). In Europe, gentamicin is the most widely used antibiotic added to commercial bone cement (Dunne et al., 2008).

Table 1: Antibiotic laden commercial bone cement constituents included in the powder and liquid components of commercial bone cement, Palacos R+G.

| Composition of PMMA bone cement | |
|---|--|
| Powder | Liquid |
| <ul style="list-style-type: none"> • Polymer: polymethylmethacrylate (PMMA)/PMMA with copolymer (82%) • Initiator: benzoyl peroxide (BPO) • Radiopacifier: zirconium dioxide (ZrO₂), barium sulfate (BaSO₄) (15%) • Antibiotics* e.g., gentamicin sulfate (2%) • Dye** | <ul style="list-style-type: none"> • Monomer: methyl methacrylate (MMA) (98%) • Activator: N,N-dimethyl-p-toluidine (DMPT) (2%) • Stabilizer: hydroquinone** • Dye** |

* Bone cement is also available without antibiotic.

** The manufacturer lists these components as *other constituents*; no percentage for them is given.

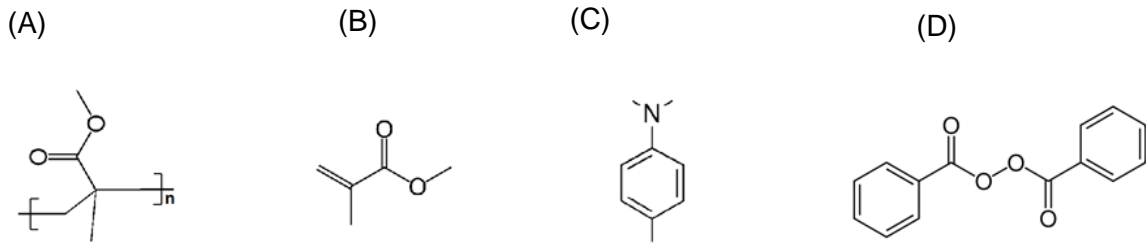


Figure 3: Chemical structures of the polymerisation components (A) PMMA (polymer), (B) MMA (monomer), (C) BPO (initiator) and (D) DMPT (activator).

1.4.1 PMMA polymerisation

PMMA is a synthetic polymer made from the methyl methacrylate monomer (Ali et al., 2015). PMMA bone cement is made by free-radical polymerisation (Monzón et al., 2019; Whitehouse & Evans, 2010). Free-radical polymerisation consists of three steps: initiation, propagation and termination (Cioffi et al., 2001; Whitehouse & Evans, 2010). When mixed together, at room temperature, the initiator and activator react to produce radicals (DMPT in liquid/BPO in powder), initiating the polymerisation reaction (Whitehouse & Evans, 2010). Figure 4 shows the different steps of the free-radical polymerisation reaction:

Initiation: BPO and DMPT react together to form benzoyl oxide radicals (Figure 4A), which add across the monomer polymerisable double bond and combine with the MMA forming a new combined radical (Figure 4B).

Propagation: the combined radical continues to polymerise by adding across double bonds of MMA molecules, effectively making the polymer chain longer (Figure 4C).

Termination: this step occurs by one of two mechanisms either by combination or disproportionation (Hosseinzadeh et al., 2013; Whitehouse & Evans, 2010):

Combination: two growing radical polymers react with each other forming a molecule with a saturated bond (Figure 4D).

Disproportionation: a hydrogen abstraction occurs via hydrogen from one chain end to another, consequently forming two molecules: one with an unsaturated end-group and one with a saturated end-group (Figure 4E).

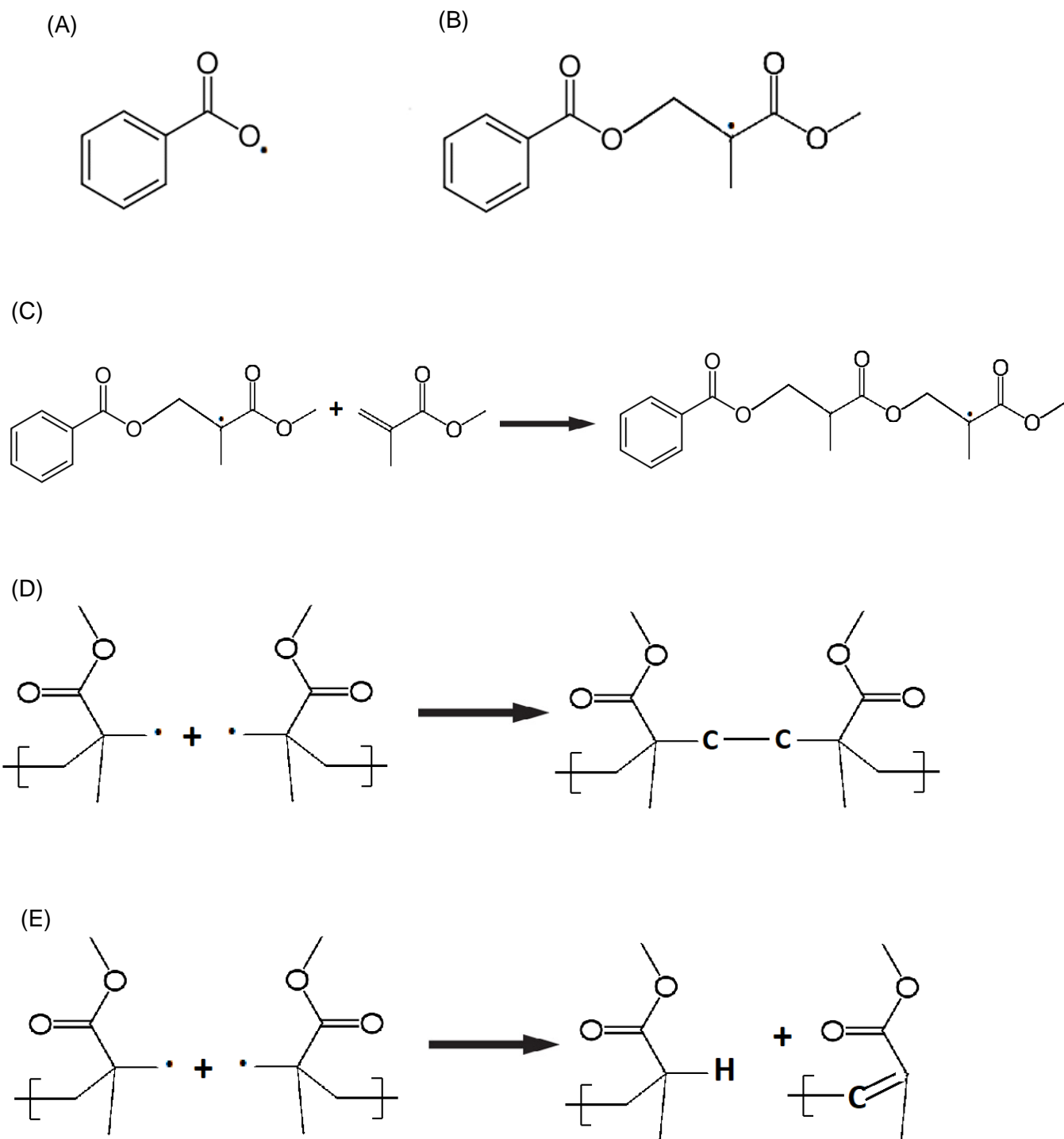


Figure 4: The different steps of the polymerisation process are shown (A-E). Both products shown in (A) and (B) are formed during the initiation step; (A) benzoyl oxide radicals are formed and (B) benzoyl oxide radicals and MMA react, forming a combined product. (C) the polymer chain is lengthened during the propagation step. (D) and (E) are both termination steps; (D) termination by combination and (E) termination by disproportionation.

It is worth noting that this polymerisation reaction is exothermic, since addition of monomer to the growing polymer chain requires that double bonds are converted into single bonds, causing for a gain in enthalpy (Monzón et al., 2019; Schwalm, 2007; Webb et al., 2013). Theoretically, this is a cause for concern as exposure to temperatures above 53 °C may cause bone and tissue damage, which can lead to aseptic loosening (Hasandoost et al., 2020), which is defined as a failure between bond and bone, in the absence of any infection or trauma (Jones & Buckle, 2020; King & Phillips, 2016). *In vitro* polymerisation temperatures exceeding 100 °C have been documented (Monzón et al., 2019; Webb & Spencer, 2007); however, such high temperatures have not been recorded in *in-vivo* studies involving animals, and furthermore, where temperatures have exceeded the 53 °C threshold, no adverse effects were observed (Monzón et al., 2019). Although high temperatures have been observed, temperatures of 40-47 °C are most commonly measured (Ranjan et al., 2017). The difference in peak temperatures observed during polymerisation for *in-vitro* and *in-vivo*, may be attributed to a local cooling effect of circulating blood (Monzón et al., 2019; Ranjan et al., 2017).

1.4.2 The use of bone cement in surgery

The international standard ISO 5833:2002 (Implants for surgery — Acrylic resin cements) defines all of the requirements for bone cements, including mechanical testing, visual appearance, packaging and documentation, stability, doughing and setting times, and how to formally construct a report (ISO 5833, 2002). There are four stages of cement preparation which take a total of around 5 -10 minutes in total to complete (Monzón et al., 2019; Whitehouse & Evans, 2010): mixing phase, waiting phase, working phase and hardening phase (Vaishya et al., 2013; Whitehouse & Evans, 2010). The mixing phase takes around 1 minute (Vaishya et al., 2013). After mixing, the waiting phase takes around 1-3 minutes, this is where the cement becomes less sticky and more dough-like; the ISO 5833 standard calls this phase the doughing time which is a period of time when the cement no longer forms fibres once in contact with a gloved hand (ISO 5833, 2002). The working phase is the period where its viscosity is low enough to be extruded through a delivery system to a site of application. The cement must be able to penetrate cancellous bone, which is essentially bone that is porous and less dense than compact bone (Wear, 2020); moreover, the cement's viscosity must be high enough to resist the patient's pressure from bleeding to micro interlock with bone (Monzón et al., 2019; Hosseinzadeh et al., 2013). This period is approximately 2-4 minutes (Whitehouse & Evans, 2010). The hardening phase which is around 1-2 minutes is the final period of the whole curing process; this is also associated

with the highest amount of heat energy produced by the polymerisation process (Whitehouse, M. R. and Evans, 2010). Several mixing methods exist for bone cement (Monzón et al., 2019; Vaishya et al., 2013). There are several mixing methods: manual mixing, centrifugation mixing and vacuum mixing (Monzón et al., 2019). Manual mixing is performed by mixing the bone cement components in a bowl with a spatula. However, manual mixing is associated air entrapment and therefore an increase in the number of pores; it has been observed that bone cement prepared in this way is mechanically weaker than bone cement prepared by other methods that do not cause for an increase in porosity (Dunne et al., 2001). A modified mixing bowl allows mixing to be performed at a lower pressure of -30 kPa is also used, which causes for a reduction in air entrapment and consequently contains less pores within the bone cement (Dunne et al., 2001; Monzón et al., 2019). Centrifugation mixing therefore shows an improvement over the manual mixing method, as the centrifugation process removes air from the mixing process (Ranjan et al., 2017). A higher quality bone cement with reduced pore formation was produced using centrifugation mixing, and also demonstrating improved mechanical properties (Wixson, 1992). It was also shown that even though centrifugation and vacuum mixing produce less pores than manual mixing, that the lowest porosity was achieved when using vacuum mixing (Wixson, 1992). Vacuum mixing is the most commonly used mixing method by operating surgeons (Monzón et al., 2019). Once mixed, application of bone cements to the site can be performed manually using a syringe or cement gun (Ranjan et al., 2017). Depending on the cement viscosity whilst in the dough phase, the operating surgeon will use their judgement to assess whether the cement can be extruded from a cement gun, syringe or manual application (Vaishya et al., 2013). However, successful application from a cement gun or syringe depends on the viscosity of the cement; the surgeon decides which is the best method of extrusion to use, as per the viscosity, once the cement is in the dough phase. A low viscosity cement can be injected through a syringe and higher viscosity can be injected with a cement gun or it can even be manually compacted into the bone cavity (Vaishya et al., 2013). Use of a syringe results in a deeper penetration than manual application (Lutz et al., 2009). The cement gun allows surgeons to effectively force more cement into bone cavities than any other method, due to its higher application, compared to the other application methods (Vaishya et al., 2013).

1.5 Revision Surgery

Currently, TJRs are considered to be the standard for treatment of end-stage arthritis and other severe indications (Chang & Haddad, 2020); however, despite these successful

procedures which are life enhancing, with high levels of patient satisfaction (Chang & Haddad, 2020; Tande & Patel, 2014), failures occur, requiring further surgery (Chang & Haddad, 2020; King & Phillips, 2016; Tande & Patel, 2014). TJRs have been shown to last up to around 15 years (Cook et al., 2019; Evans et al., 2019). For THRs, 58% lasted for 25 years, 70% lasted for 20 years and 89% lasted for 15 years (Evans et al., 2019); whereas for TKRs, 70% lasted for 25 years, 72% lasted for 20 years and 77% lasted for 15 years (Cook et al., 2019). Revisions account for approximately 12% of all THR (Evans et al., 2019; Patel et al., 2015) and 6% of all TKR procedures (Cook et al., 2019; Patel et al., 2015) performed annually in the UK. The most common indications for TJR revision surgeries include unexplained pain (10%), where pain is still experienced over several years due to possible loosening, prosthetic fracture or instability, and infection (King & Phillips, 2016; Tande & Patel, 2014). Aseptic loosening is the most common indication requiring revision surgery (30%). Studies show that in the short term, infection is the most common indication for TJR revision, whereas, in the long term, aseptic loosening is the most common indication of TJR revision in patients (Jafari et al., 2010). Aseptic loosening of joint implants can affect patients 10 to 20 years after TJR surgery (Abu-Amer et al., 2007); more than 25% of all TJRs will eventually demonstrate some degree of loosening (Cobo & Del Pozo, 2011). Prosthetic joint infections (PJI) are a major indication for revisions (15%), defined as an infection of the joint prosthesis and tissue (Tande & Patel, 2014), which require a biopsy in order to identify the causative organism (King & Phillips, 2016). PJI is reported to occur in around 1-2% of all patients undergoing TJRs. PJIs in TKRs are slightly higher than for THRs as there is less soft tissue coverage around the knee (King & Phillips, 2016). It has been observed in several studies that around 60% to 70% of infections in patients occurred within the first 2 years, and that around 30% of infections occurred between 2 to 10 years (Khan et al., 2016; Kurtz et al., 2010; Tande & Patel, 2014). Revisions are generally more complex than primary TJRs, due to defects in bone and soft tissue (BOZIC et al., 2005; Vanhegan et al., 2012; Weber et al., 2018). Revision surgery takes longer to perform than primary surgery, and patients' hospital stay is usually longer, which incurs more costs (Vanhegan et al., 2012). Furthermore, revisions are associated with a higher risk of failure (Vanhegan et al., 2012). There is also the added cost of revision surgery (Weber et al., 2018); on average, the cost for revision surgery is around twice the cost of primary TJR (Vanhegan et al., 2012). Moreover, revisions due to infection are more expensive to perform than revisions due to aseptic loosening (Patel et al., 2015). It is also worth noting that infections is the leading cause of failure following revisions to TJRs (Parvizi et al., 2016).

1.6 Prosthetic joint infections (PJI)

As previously discussed, prosthetic joint infections are a major cause for revisions for TJRs, moreover, it is the leading cause for revisions within the first two years after surgery (Khan et al., 2016; Oliveira et al., 2017; Parvizi et al., 2016), as well as being the leading cause following all types of revision (Parvizi et al., 2016). PJI is considered to be the biggest problem following TJR procedures as PJIs (Cobo & Del Pozo, 2011; Davidson et al., 2019). Problems associated with PJIs are that they are difficult to diagnose, in particular as onset times are variable (Cobo & Del Pozo, 2011; W. Zimmerli, 2014); and the resistance of causative microorganisms to existing antibiotics and therapy (Tsang et al., 2018).

1.6.1 Microorganisms in PJI

The most common isolated microorganisms in PJIs are Gram-positive *staphylococcal* species such as *S. aureus*, and coagulase negative *staphylococci* such as *S. epidermidis* (Linke et al., 2022). Infections are classified according to their time of onset, following surgery as either early, delayed and late onset (Arciola et al., 2018; Davidson et al., 2019). Early onset is where the time of onset is less than 3 months, delayed onset is where the time of onset is between 3 and 24 months, and late onset is where the time of onset is 24 months onwards (Arciola et al., 2018). It is thought that for early and delayed onsets of infection, the reason is due to contamination during the surgery itself (Arciola et al., 2018; Cobo & Del Pozo, 2011; Davidson et al., 2019; Tande & Patel, 2014). Early onset of infection is caused by virulent bacteria e.g. *S. aureus*, whereas delayed onset infection is caused by microorganisms of low virulence such as coagulase-negative *staphylococci* and *P. acnes* (Arciola et al., 2018; Fsadni & Peter, 2013; Tande & Patel, 2014). Late onset infection, starting at 24 months, is caused by haematogenous seeding from infections in other parts of the body (Arciola et al., 2018; Davidson et al., 2019; Fsadni & Peter, 2013). Once bacteria have entered a surgical site, they can exist in three forms: planktonic, intracellular or biofilm (McConoughey et al., 2014). Planktonic bacteria are the single cell form and are easily cleared by the host's natural defences and by antibiotic therapy. However, planktonic bacteria can develop into biofilms if allowed to colonise surfaces within patients; moreover, they are able to grow in joint fluid during acute infection (McConoughey et al., 2014). Intracellular bacteria are able to enter and survive within host cells such as osteoblast and endothelial cells, to avoid antibiotic molecules and immune cells (McConoughey et al., 2014). Biofilms are an assembly of microorganisms which are able to adhere themselves on

to surfaces and form three-dimensional colonies (McConoughey et al., 2014; Reffuveille et al., 2017). A biofilm forms on an implant surface in several stages: first, free floating bacteria adhere to the surface implant which is coated with biotic protein from the host's blood; this process is also influenced by the surface wettability of the implant. Cell aggregation and biofilm maturation occur, followed by cellular detachment (Davidson et al., 2019). The microorganisms within the biofilm become enclosed in a polymeric matrix, which is produced by the microorganisms themselves, and this effectively shields them from the host's immune cells and from antibiotic molecules. Formation of a biofilm causes the implant to become colonised, thus infection is further propagated (Davidson et al., 2019). Compared with planktonic bacteria, bacteria biofilms greatly increase their ability to resist antimicrobial agents by around 500 - 5000 times (Cobo & Del Pozo, 2011). Furthermore, biofilm formation reduces the minimal inoculum of *S. aureus* required to cause infection by a factor of over 100,000 (Zimmerli et al., 2004). The majority of prosthetic joint infections are caused by microorganisms growing in biofilms (Cobo & Del Pozo, 2011; Davidson et al., 2019; Fsadni & Peter, 2013; McConoughey et al., 2014). *S. aureus*, *S. epidermis*, and *P. aeruginosa* make up around 75% of all biofilms found in medical devices (McConoughey et al., 2014).

1.7 Prophylaxis in joint replacement surgery

Antibiotics are currently used to treat bacterial infections, of which there are several antibiotics used for this purpose (Oliveira et al., 2017). Moreover, the type of antibiotic prescribed will depend on several factors including the infection severity and the particular bacterial strain present (Tai & Hsieh, 2013). The introduction of biomaterials into the body during orthopaedic surgery causes for an increased risk of developing deep infections (Bistolfi et al., 2011; Davidson et al., 2019; Hinarejos et al., 2015). Antibiotic loaded bone cements are a way to proactively prevent infection (Dunne et al., 2009). Antibiotic loaded cements contain one or more incorporated antibiotics. Gentamicin, vancomycin and tobramycin are the most commonly used antibiotics in antibiotic loaded bone cements (ALBC) (Hinarejos et al., 2015). Over 90% of surgeons use ALBCs in surgery in the UK (Al Thaher et al., 2016).

1.7.1 Antibiotic resistance

One of the main drawbacks of antibiotic use is the phenomenon of antibiotic-resistance. Since the mainstream use of antibiotics in the 1940s, the incidence of disease and deaths worldwide have been reduced, however, an overuse has resulted in bacteria becoming more resistant to antibiotics (Ghorbani et al., 2016). This phenomenon is considered to be a significant public health risk (Lee et al., 2018). The WHO describes antibiotic resistance as being “one of the biggest threats to global health, food security, and development today” (World Health Organisation, 2017). Methicillin resistant *Staphylococcus aureus* (MRSA) emerged in the UK in 1960s (Bhattacharya et al., 2016; Lee et al., 2018). *S. aureus* can become resistant to β -lactam antibiotics by the expression of a foreign penicillin-binding protein (PBP), PBP2a that is resistant to action by methicillin (Guo et al., 2020; Stapleton & Taylor, 2002). Methicillin-resistant *S. aureus* isolates are also resistant to a large number of different classes of antibiotics (Guo et al., 2020; Kaur & Chate, 2015). It is described as a multidrug resistant bacteria (Guo et al., 2020; Slane et al., 2015), which is resistant to aminoglycosides, cephalosporins, chloramphenicol, lincomycin, macrolides, quinophthalones, rifampicin, sulfonamides and tetracyclines (Guo et al., 2020). MRSA is the cause of around 30% of all serious infections (Bhattacharya et al., 2016; Lora-Tamayo et al., 2013). In the context of bone cement, concerns regarding antibiotic resistance appear credible, as a study by Hope *et al.* (1989) showed that resistant Staphylococcal organisms were identified in 90% of infected TJRs where ABLC was used, in comparison to just 16% of cases where cement not containing antibiotic was used (Hope et al., 1989).

1.8 Gentamicin sulfate

Gentamicin is a well-established antibiotic belonging to the aminoglycoside family (Ali et al., 2011; Hayward et al., 2018). Amongst other antibiotics, ALBCs include other aminoglycosides such as neomycin, tobramycin and streptomycin; vancomycin, a glycopeptide antibiotic, is also used (Chen, A.F. and Parvizi, 2014). Gentamicin sulfate is a broad-spectrum aminoglycoside antibiotic that is effective against Gram-negative bacteria and limited Gram-positive bacteria (Hayward et al., 2018; Tai & Hsieh, 2013); in particular, it is useful for treating bacteria that are resistant to other antimicrobials (Hayward et al., 2018). Gentamicin works by inhibiting bacterial protein synthesis by binding to the 30S ribosomes (Vestergaard et al., 2019). Gentamicin is currently on the WHO list of essential Medicines (World Health Organization, 2019) and on the list of critically important antimicrobials for

human medicine (World Health Organization, 2018). Gentamicin is produced via fermentation of *Micromonospora purpurea* (Isoherranen et al., 2000; Joseph & Rustum, 2010). Commercially available gentamicin is described as a gentamicin complex, composed of a complex of five gentamicin components (Friesen et al., 2018; Isoherranen et al., 2000). The gentamicin components differ in the degree of substitution indicated by R2 and R3 on the 6-position carbon of the purpurosamine unit, and R1 on the nitrogen atom connected to the 6-position carbon (Figure 5). The components of gentamicin API (active pharmaceutical ingredient) are listed in the British Pharmacopoeia (BP) monograph for gentamicin sulfate (Figure 5). The BP lists 5 components: C1, C1a, C2, C2a and C2b (British Pharmacopoeia, 2021). C1, C1a, C2 and C2a are the major components, comprising around 92-99% of the complex (Friesen et al., 2018; Mullins et al., 2016). It is worth noting that there are actually several known minor components found in commercial gentamicin sulfate; however, C2b is considered to be the most relevant minor component, as it is found to constitute around 1.3-2.1% of the total gentamicin components, and is therefore listed as a constituent component of gentamicin sulfate (British Pharmacopoeia, 2021; Friesen et al., 2018).

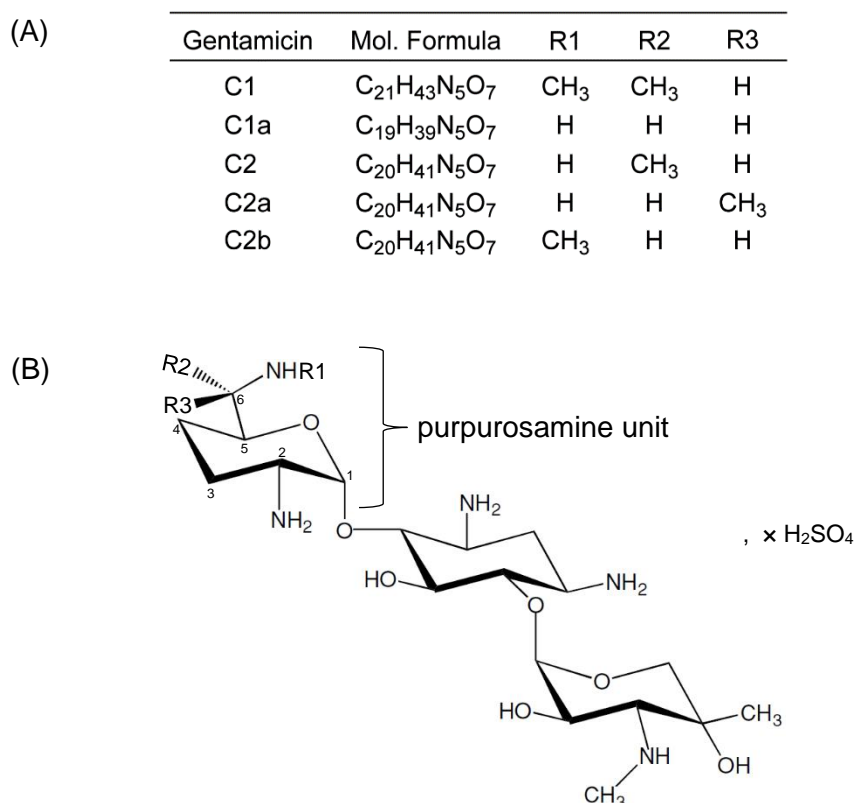


Figure 5: List of the five individual components, C1, C1a, C2, C2a and C2b, found in gentamicin sulfate complex (A). The gentamicin components differ in the degree of substitution indicated by R2 and R3 on the 6-position carbon of the purpurosamine unit, and R1 on the nitrogen atom connected to the 6-position carbon (B) (British Pharmacopoeia, 2021).

Gentamicin is the most commonly incorporated antibiotic in commercial bone cements (Chen & Parvizi, 2014; Hinarejos et al., 2015), therefore gentamicin has been the focus of this work.

1.8.1 Antibiotic loaded bone cement (ALBC)

Bone cement loaded with gentamicin for total joint replacement surgery was initially investigated with great success by Buchholz & Engelbrecht (1970); it was described as the antibiotic of choice for the following reasons: broad spectrum activity against Gram-negative and Gram-positive bacteria, good water solubility, thermal stability and low allergy profile (Buchholz & Engelbrecht, 1970; Dunne et al., 2008). ALBC containing gentamicin sulfate has been shown to be effective against several prosthetic related infections including *S.epidermidis*, *S. aureus* and *P. aeruginosa*. Furthermore, gentamicin has been shown to have the longest duration of antibacterial activity against MRSA (Tai & Hsieh, 2013). The aforementioned physical characteristics (thermal stability and water solubility) are favourable for antibiotic release from PMMA bone cement. Solubility in water is required, as there is a relationship between the ability of PMMA bone cement to elute a given drug and the level of water absorption of the bone cement (Whitehouse & Evans, 2010). Thermal stability is required, as the polymerisation temperature (curing) of PMMA could potentially be as high as 100 °C (Monzón et al., 2019; Webb & Spencer, 2007; Whitehouse & Evans, 2010). Therefore, thermal stability of gentamicin is required, so that its potency will not degrade as a result of such augmented temperatures. It has been demonstrated that gentamicin sulfate is thermally stable up to a temperature of 100 °C (Wang, 2005).

1.8.2 Characterisation of gentamicin

Due to its inherent physico-chemical properties, gentamicin sulfate and its related compounds cannot be analysed directly using conventional laboratory techniques such as HPLC-UV-vis (High-pressure liquid chromatography with a UV-Vis detector) or by UV-Vis (Ultraviolet–visible spectroscopy). UV–Vis spectroscopy, in general, is one of the most commonly used analytical techniques for the analysis of compounds, due to the fact that many molecules absorb radiation within the UV-Vis region (190-800 nm) (Palacios-Morillo et al., 2013). UV-Vis spectroscopy allows for good sample recovery and separation between compounds, without the need of derivatising compounds of interest (NicDaéid, 2019). Furthermore, in chromatography, UV-Vis detection is by far the most commonly used

technique (Swartz, 2010). Gentamicin (and all aminoglycosides) does not possess a strong UV (Ultraviolet) absorbing chromophore, therefore direct analysis by UV absorption is not possible (Farouk et al., 2015). This means that analysis cannot be performed by taking aliquots of eluent and injecting them directly onto an HPLC system attached to a UV-Vis detector or by performing scans of them on a UV-Vis spectrophotometer. Furthermore, its strongly polar nature means that it cannot be used directly with gas chromatography techniques such as GC-FID (gas chromatography with a flame ionization detector) which is the most commonly used gas chromatography method (Zheng et al., 2018); requiring derivatisation to increase its volatility (Anyakudo et al., 2020). The fact that gentamicin sulfate characterisation cannot be performed directly using conventional detectors, requiring derivatisation, has proven to be challenging (Zhou et al., 2020). A number of methods have been used to assay gentamicin such as derivatisation methods and microbiological assays (Clarot et al., 2004; Lecároz et al., 2006; Zheng et al., 2018). Microbiological assays are inexpensive, however, they are time consuming and lack adequate sensitivity and specificity (Zheng et al., 2018). Techniques not requiring chromophores can be successfully applied for the detection of gentamicin and aminoglycosides such as capillary electrophoresis (CE); and HPLC applied to other detectors such as mass spectrometry (MS), pulsed amperometric detector (PAD), as evaporative light-scattering detection (ELSD) and refractive index (RI) (British Pharmacopoeia, 2021; Lecároz et al., 2006; Zheng et al., 2018). However, these detectors are not common in most laboratories (Zheng et al., 2018). By using derivatisation methods, conventional UV-Vis detectors can be used. The amino group on the aminoglycoside molecules can be reacted with several derivatisation agents e.g., *o*-phthalaldehyde to form a stable derivative which can be analysed using a UV-Vis detector (Lecároz et al., 2006; Zheng et al., 2018). However, derivatisation techniques can cause loss of analytes by incomplete derivatisation, and for possible interfering compounds to be introduced in the analysis such as derivatisation reagents and by-products (Zheng et al., 2018). As with microbiological methods, they either lack specificity or sensitivity compared to more direct and more advanced methods such as high-performance liquid chromatography-mass spectrometry (LC-MS) (Clarot et al., 2004; Lecároz et al., 2006; Zheng et al., 2018). Moreover, as it has been shown experimentally by Lecároz *et al.* (2006) that microbiological and derivatisation assays are less sensitive than LC-MS (Clarot et al., 2004; Lecároz et al., 2006), therefore LC-MS is preferred for the characterisation of gentamicin for this thesis.

1.9 Effect of antibiotic on mechanical properties

The mechanical properties of PMMA bone cements are vital for successful total joint replacements (Whitehouse & Evans, 2010). It has been documented in several publications that the addition of antibiotics to PMMA bone cement causes a reduction in mechanical properties (Al Thaher et al., 2016; Dunne et al., 2008); however, it is generally accepted that incorporation of up to 1 g of antibiotic in 40 g of PMMA bone cement will not significantly decrease its mechanical properties, whereas higher amounts can be significantly detrimental to mechanical properties (Al Thaher et al., 2016; Ayre et al., 2015; Lewis & Janna, 2006). Several factors have been attributed as causes of mechanical weakness (Ayre et al., 2015; Hinarejos et al., 2015), such as poor dispersion and formation of agglomerations of the powdered antibiotic in the bone cement (Ayre et al., 2015; Dunne et al., 2008); the antibiotic powder itself is thought to cause weakness via the channelling effect, causing porosity upon contact with aqueous fluid, and therefore causing mechanical weakness in the bone cement (Diez-Pena et al., 2002; Hinarejos et al., 2015).

1.10 Drug release of antibiotics in bone cement

There have been a number of studies aimed at improving antibiotic release from PMMA bone cements (Al Thaher et al., 2016; Chen et al., 2021; Miola et al., 2013), which include the use of surfactants (Ayre et al., 2015; Oh et al., 2016) and various nanotechnology-based delivery systems (Al Thaher et al., 2016). However, there have been few studies into the actual mechanism of drug release from PMMA bone cement, which is still not fully understood (Martínez-Moreno et al., 2015; Miola et al., 2013). It has been shown that water must be absorbed in the cement for drug release to occur (Diez-Pena et al., 2002; Gálvez-López et al., 2014). It has been suggested that drug elutes through spaces in the PMMA matrix such as pores, cracks and voids (Gálvez-López et al., 2014). Moreover, antibiotic release is aided by the channelling effect of the antibiotic itself, effectively being dissolved by the uptake of water, creating further channels within the cement (Diez-Pena et al., 2002). From studies carried out so far, it has been postulated that drug release is affected by the following factors: surface and bulk characteristics (Baker & Greenham, 1988; van Belt et al., 2000); mixing methods (Martínez-Moreno et al., 2015); antibiotic type (Anagnostakos & Kelm, 2009); cement type (Lewis, 2015); quantity of antibiotic used (Anagnostakos & Kelm, 2009; Diez-Pena et al., 2002). It is known that most incorporated antibiotic remains inside the bone cement and is not released. *In vitro* studies show that up to 90% of the initial

incorporated antibiotic may be retained within the bone cement matrix (Dunne et al., 2009; Diez-Pena et al., 2002). Ideally, antibiotic loaded bone cement should release high concentrations of antibiotic and have a sustained drug release profile; moreover, drug release should proceed for long enough periods of time, releasing clinically significant concentrations of antibiotic to prevent infections, not releasing sub-inhibitory levels which can increase the potential for antimicrobial resistance (Anagnostakos & Kelm, 2009). However, in reality, commercially loaded antibiotic bone cement is characterised by a short burst within the first hours, mainly from surface agglomerations, subsequently releasing sub-inhibitory levels thereafter (Ayre et al., 2015; Dunne et al., 2008).

1.11 Nanotechnology and nanoparticles

The delivery of drugs by conventional administrative methods is hindered by a number of challenging factors such as poor absorption, poor bioavailability, poor selectivity, poor penetration of target-tissues, low effectiveness and cytotoxicity issues (Moss & Siccardi, 2014; Wilczewska et al., 2012). Nanoparticles have been explored to overcome the issues previously highlighted with existing drug delivery methods (Abed & Couvreur, 2014; Moss & Siccardi, 2014). Nanoparticles are defined as being particles of any shape, having dimensions of 1 nm to 100 nm (Vert et al, 2012), although in practice, the term nanoparticle is also often used for particles which are up to several hundred nanometres (Wilczewska et al., 2012). In general, nanoparticles have many physiochemical properties that can be exploited for drug loading efficiency, toxicity and drug delivery: such as chemical composition, stability, size, shape, surface area and surface charge amongst others (Gatoo et al., 2014). Drugs can be loaded inside nanoparticles by way of encapsulation, adsorption to the outer surface and also by chemical conjugation (Bharti et al., 2015; Moss & Siccardi, 2014). Nano formulations can be used to overcome the drawbacks of antibiotics, which include cytotoxicity and antibiotic resistance (Kalhapure et al., 2015), as well as improving the release kinetics of antibiotics (Ayre et al., 2015).

1.12 Nano-formulations in antibiotic loaded cements

The localised release of antibiotic is to ensure that a high concentration of the antibiotic reaches the joint, particularly due to limited circulation in the area adjacent to the implant (Ranjan et al., 2017); furthermore, through oral administration via the systemic circulatory

system there is an increase in serious adverse side effects observed such as neurotoxicity and nephrotoxicity (Omri, 2008). Nano-delivery systems containing antibiotic incorporated in bone cement have gained increasing popularity as an area of interest over recent years (Al Thaher et al., 2016). The following are examples of nanoparticles used to deliver antimicrobial agents from PMMA bone cements:

1.12.1 Carbon nanotubes (CNT)

Carbon nanotubes (CNT) are carbon allotropes, which are molecules of cylindrical sp² hybridised carbons arranged hexagonally. These cylinders are tubular having several favourable properties including a very high aspect ratio and easy functional group surface modification (Aboofazeli, 2010; Bianco et al., 2005). Single or multiple graphene sheets are rolled through cylinders to form the tubes which are one single atom thick. Single walled tubes (SWNT) or Multiple walled tubes (MWNT) are used with wide therapeutic agents both by external linkage or internal loading (Bianco et al., 2005) (Figure 6).

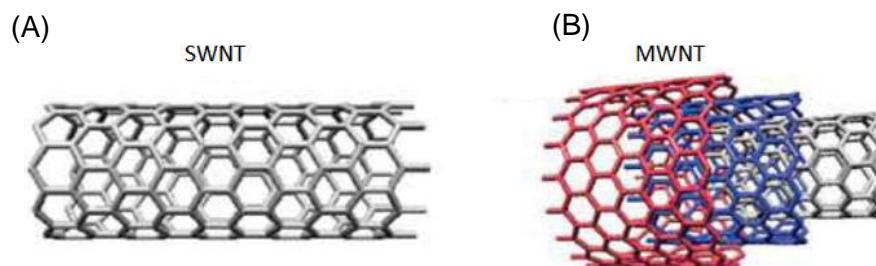


Figure 6: Structures of (A) single walled nanotubes (SWNT) and (B) multiple walled nanotubes (MWNT) (Aboofazeli 2010).

In an in-vitro study by Shen *et al.* (2016) to document the drug release kinetics from bone cement using gentamicin (Shen et al., 2016), it was reported that the incorporation of 5% w/w of gentamicin loaded carbon nanotubes in the cement formulation could cause 75% of the incorporated gentamicin to be released over 80 days; however, the mechanical strength was significantly reduced. This formulation could only achieve around 10% of the mechanical strength for compression and bending modulus, compared to the commercial cement, therefore failing the requirements of ISO 5833. Furthermore, CNT showed high toxicity (Shen et al., 2016). Moreover, there was no data on the release profile after 80 days, or whether sub-inhibitory concentrations were released after this initial time-period.

1.12.2 Mesoporous silica nanoparticles (MSN)

Mesoporous silica nanoparticles have a regular morphology with porous structure and are characterised by a large surface area; MSNs contain a high density of silanol groups at the surface which can easily be chemically modified depending on the hydrophobicity of a given drug, and they are biocompatible (Bharti et al., 2015; Wilczewska et al., 2012). Their pore size ranges from 2-10 nm. There are several types of MSN, of which the patented MCM-41 (Figure 7) is the most well-known and commonly used (Mehmood et al., 2017; Wilczewska et al., 2012). MCM-41 is characterised by a regular hexagonal arrangement of cylindrical mesopores, forming a one dimensional pore system (Bharti et al., 2015; Mehmood et al., 2017; Wilczewska et al., 2012).

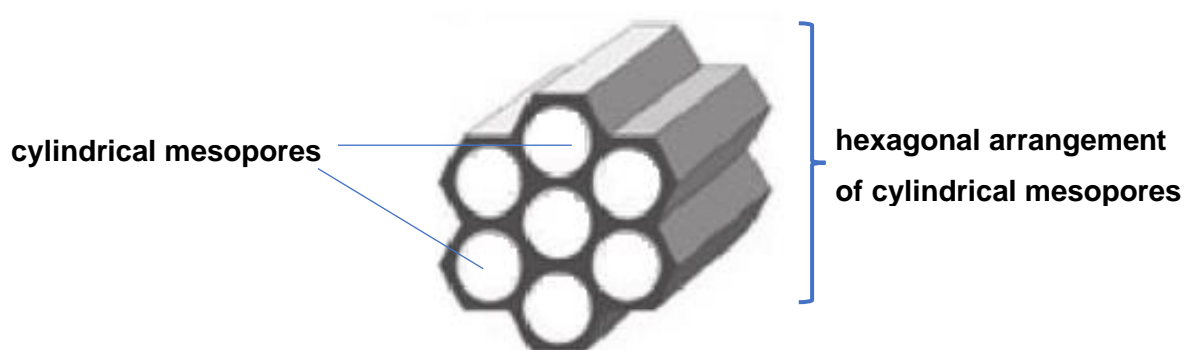


Figure 7: Diagram showing the structure of MCM-41; the regular hexagonal arrangement and cylindrical mesopores are shown.

In an in-vitro study it was reported that the incorporation of 10% w/w of gentamicin loaded MSN in the bone cement formulation caused release of 60% of incorporated gentamicin over 80 days; furthermore, compressive strength was not significantly reduced, and it was comparable to commercial bone cement. Bending modulus was decreased by around 10% compared to the commercial bone cement, but it was still above the ISO 5833 requirement. MSN toxicity was found to be low and comparable to commercial bone cement (Shen et al., 2016). Moreover, there was no data on the release profile after 80 days, or as to whether sub-inhibitory concentrations were released after this initial time period.

1.12.3 Hydroxyapatite (HAP): $\text{Ca}_{10}(\text{PO}_4)_6(\text{OH})_2$

Hydroxyapatite is a naturally occurring mineral, and is itself the main constituent found in bones, it is therefore no surprise that it has many desirable properties such as bioactivity, biocompatibility and biodegradability (Syamchand & Sony, 2015). HAP nanoparticles are suitable as nanocarriers in controlled drug delivery by way of either encapsulation or chemical linkage (S. Jafari, 2015; Syamchand & Sony, 2015). Several studies on drug delivery with antibiotics or silver ions have been conducted (Shen et al., 2016; Syamchand & Sony, 2015). In an in-vitro study it was reported that the incorporation of 32% w/w of gentamicin loaded HAP in the bone cement formulation caused 75% of the incorporated gentamicin to be released over 80 days; however, the compressive strength and bending modulus were significantly reduced and were not comparable to commercial bone cement, failing the ISO 5833 requirements. HAP toxicity was found to be low and comparable to commercial bone cement (Shen et al., 2016). Moreover, there was no data on the release profile after 80 days, or as to whether sub-inhibitory concentrations were released after this initial time-period.

1.12.4 Halloysite nanotubes (HNT)

Halloysite Nanotubes (Figure 8) is the naturally abundant form of halloysite, which is an aluminosilicate clay of the kaolin group (Yuan et al., 2015). HNT shows good biocompatibility and dimensions are diameter of around 50 nm, 15 nm lumen and length 500–1000 nm (Kamble et al., 2012; Wei et al., 2012). HNT can exist as single walled and multi walled forms (Kamble et al., 2012).

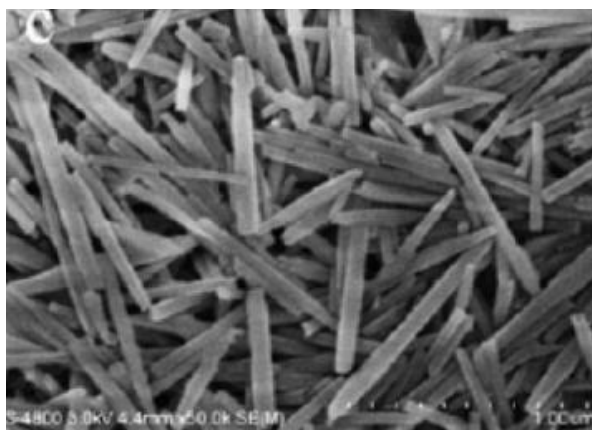


Figure 8: Electron micrograph of halloysite nanotubes SEM image of HNT (Wei et al. 2012).

In an in-vitro study by Wei *et al.* (2012) gentamicin release was investigated using gentamicin loaded HNT (Wei et al., 2012). It was shown that incorporation of 5% w/w - 8% w/w of HNT caused a sustained release of gentamicin for up to 10 days, and release for up to 16 days. It is also claimed that the addition of HNT improved mechanical strength of the cement; however, mechanical testing was not performed as per ISO 5833 requirements, so it is not possible to draw on any conclusions as testing was performed differently. Moreover, there was no data on the release profile after 16 days, or as to whether sub-inhibitory concentrations were released after this initial time period.

1.12.5 Chitosan nanoparticles (CS)

Chitosan (poly(1,4),-b-D-glucopyranosamine) is a natural, linear long-chain polymer (Shi et al., 2006), produced by reacting chitin crustacean shell with alkali, and then processed into various forms such as beads, films, fibre and other forms (Ghadi et al., 2014; Shi et al., 2006). Chitosan is the name of a group of chitin compounds which are partially or fully deacetylated. Chitosan nanoparticles are colloidal solid particles of 1-1000 nm diameter (Sailaja et al., 2010). Chitosan has a broad spectrum of antimicrobial activity and low toxicity for mammalian cells (Shi et al., 2006). In a study by Shi *et al.* (2006) chitosan and quaternary ammonium chitosan-derivatives (QCS) were incorporated into PMMA bone cement. QCS were used as they are more soluble and have more antibacterial potential (Shi et al., 2006). It has been shown that an increase in the chain length of the alkyl substituent causes for an increase in antibacterial activity (Shi et al., 2006). It was found that QCS incorporated in bone cement at around 15% w/w caused a decrease of only 3% of Young's

and bending moduli; it was also demonstrated that against *S. aureus* and *S. epidermidis*, they provided effective antibacterial action. Furthermore, it was also shown that they could be used in gentamicin containing cement to effectively add to the antibacterial action of the gentamicin powder (Shi et al., 2006). It should be noted that compression was not tested; moreover, that an in-vitro drug-release profile was not established, making this impossible to compare with, it is therefore unknown as to what quantities have been released over time, and if they are therapeutic quantities or sub inhibitory.

1.12.6 Silver nanoparticles (AgNP)

AgNP vary in morphology and range between 1-100 nm in size. AgNP systems possess several interesting properties: activity against a broad range of microbes, effective at low doses in the magnitude of $\mu\text{g/ml}$ for full growth-inhibition of bacteria; moreover, at low doses, there is little concern about systemic toxicity (Kalhapure et al., 2015). Size, dosage and morphology are key factors for effective antibacterial efficacy of AgNP (Le et al., 2010). Silver nanoparticles are capped meaning that they are functionalised with organic ligands to alter the nanoparticle morphology i.e. size and shape (Battocchio et al., 2012; Prokopovich et al., 2015). Capping is achieved by reacting with chelating agents such as oleic acid, citrates and glutamic acid amongst others (Prokopovich et al., 2015). Several studies have been conducted with PMMA bone cement containing AgNP. Due to the phenomenon of antibiotic resistance, silver nanoparticles have become an area of interest to researchers. In particular, silver nanoparticles have shown excellent antimicrobial efficacy against a broad range of bacteria (Amaro et al., 2021; Prokopovich et al., 2015), as well as good antimicrobial efficacy. It was thought initially that bacteria would not develop resistance to such nanomaterials (K. K. Y. Wong & Liu, 2010), however, recent studies have shown that bacteria are able to tolerate increasing concentrations of silver nanoparticles (Panáček et al., 2018; Valentin et al., 2020). Few studies investigating AgNP technology have documented mechanical testing to ISO 5833 (Slane et al., 2015). However, in studies where mechanical testing was performed, it was shown that an incorporated amount of up to 1% w/w does not affect mechanical properties, as per ISO 5833 (Prokopovich et al., 2015; Slane et al., 2015). Low amounts of AgNP, as low as 0.025% w/w were effective against bacteria such as MRSA, *S. aureus* and *S. epidermis* (Prokopovich et al., 2015). AgNP were also found to be effective against biofilms (Slane et al., 2015).

1.12.7 Liposomes

Liposomes are small phospholipid vesicles, composed of either natural or synthetic phospholipids (Castañeda-Reyes et al., 2020; New, 2003). They consist of one or more closed lipid bilayers, which contain discrete, enclosed, aqueous and lipophilic spaces (Castañeda-Reyes et al., 2020; New, 2003; Sercombe et al., 2015). Due to the ability of liposomes to entrap hydrophilic and lipophilic molecules, a diverse range of compounds can be encapsulated by these vesicles (New, 2003; Sercombe et al., 2015).

1.12.7.1 Phospholipids used for liposome preparation

Phospholipids are well established excipients used in the pharmaceutical industry (USP, 2020; van Hoogevest & Wendel, 2014). In particular, they are used as excipients in formulations such as emulsifiers and wetting agents; and as components of liposomes, micelles (mixed and inverted) fat-emulsions, mixed micelles. (van Hoogevest & Wendel, 2014). The basic structural components of biological and liposomal membranes are phospholipids (Drescher & van Hoogevest, 2020; New, 2003). The structure of a general phospholipid is shown in Figure 9. Phospholipids are based around a glycerol backbone where the carbons 1 and 2 positions (Figure 9) of the glycerol backbone are esterified with two fatty acids of varying degree of saturation and carbon chain length; phosphoric acid is esterified to the carbon 3 position, where itself becomes esterified with an alcohol. Depending on the structure of the alcohol at this reaction step, R3 will be different (Figure 9) i.e. different phospholipids will be synthesised e.g. phosphatidylcholine (PC), phosphatidylserine (PS), phosphatidylglycerol (PG), phosphatidylinositol (PI) and phosphatidylethanolamine (PE) (Drescher & van Hoogevest, 2020). The head group is polar whereas the fatty acid chains are non-polar (Figure 9). Naturally occurring phospholipids usually contain palmitic and oleic acids; however, synthetic phospholipids can be synthesised with other fatty acids. Common molecules (R3) attached to the phosphate moiety are listed in Table 2. The most common molecule attached to the phosphate moiety is choline which forms the overall headgroup phosphorylcholine, therefore making phosphatidylcholine molecules the most common phospholipids (Burri et al., 2012; Drescher & van Hoogevest, 2020; New, 2003). PC and PE both are zwitterionic and have an overall neutral charge at pH 7, whereas PG, PI and PS all have an overall negative charge at pH 7 (Drescher & van Hoogevest, 2020; New, 2003).

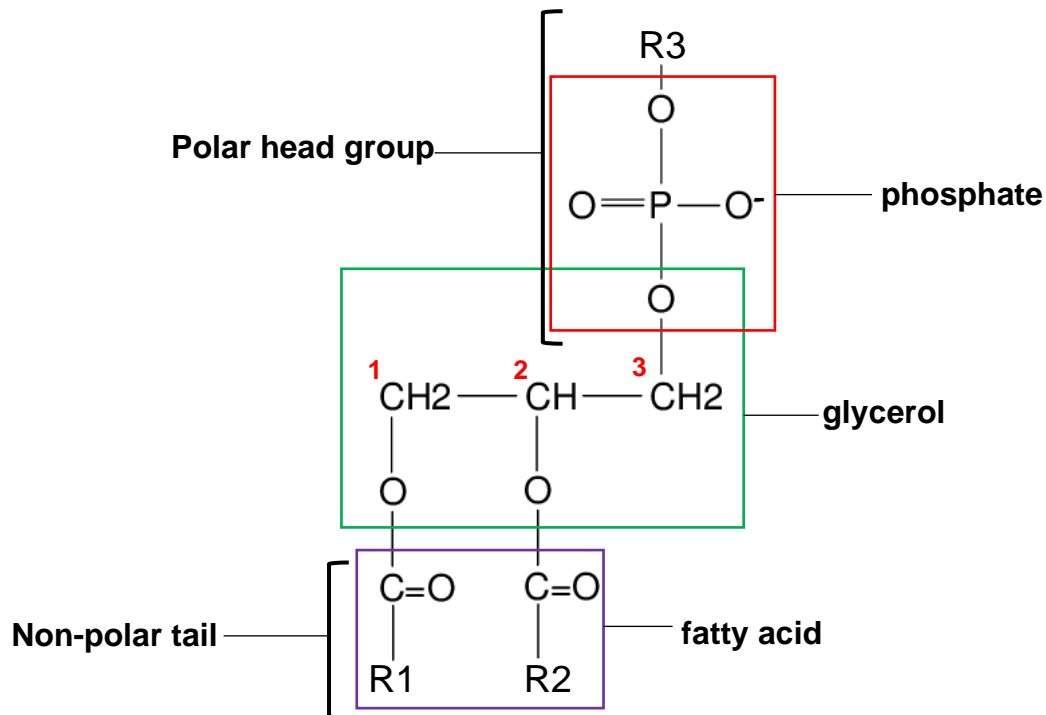
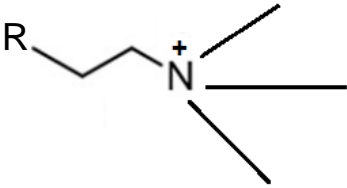
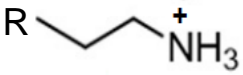
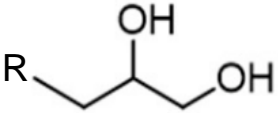
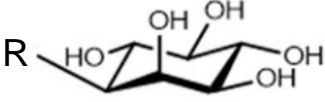
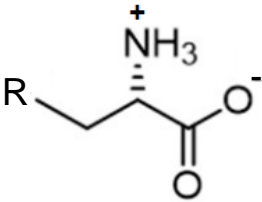


Figure 9: General chemical structure of a phospholipid molecule, with the three adjacent carbon positions on the glycerol backbone labelled 1,2 and 3 in red. The different moieties that make up phospholipid molecules are labelled phosphate, glycerol and fatty acid. R1 and R2 represent hydrocarbon chains. R3 represents different molecules such as choline, serine, glycerol, inositol or ethanolamine, that are part of the polar head group.

Table 2: Common naturally occurring phospholipids are listed. Phospholipids are denoted by the general chemical structure R, attached to atoms/molecules that make up the polar head groups. Note that atoms/molecules completing the polar head groups shown in this table represent R3 that is attached to the generic phospholipid molecule shown in Figure 9.

| Phospholipid general chemical structure | Head group (R3) | Name of phospholipid | Lipid |
|---|-----------------|-------------------------------|--------------|
| $R - H$ | Hydrogen | Phosphatidic acid (PA) | Hydrogen |
|  | Choline | Phosphatidylcholine (PC) | Choline |
|  | Ethanolamine | Phosphatidylethanolamine (PE) | Ethanolamine |
|  | Glycerol | Phosphatidylglycerol (PG) | Glycerol |
|  | Inositol | Phosphatidylinositol (PI) | Inositol |
|  | Serine | Phosphatidylserine (PS) | Serine |

Due to its low cost, relative abundance, neutral charge and relative stability (Sanarova et al., 2019), PC is the phospholipid that is most used in liposome preparation (Drescher & van Hoogevest, 2020; Du et al., 2019; New, 2003; Sanarova et al., 2019). PC is a major component of biological membranes and is obtained by mechanical extraction using hexane from a variety of natural sources such as egg yolk, soy beans and mammalian sources such as bovine heart (Drescher & van Hoogevest, 2020; Sanarova et al., 2019). PC is often termed as lecithin; however, it should be noted that whilst PC is a part of the lecithin group of animal and plant and tissue, lecithin itself is described as a mixture of phosphatidylcholine and other compounds (Drescher & van Hoogevest, 2020; USP, 2020). The United States Pharmacopeia (USP), in its monograph, describes lecithin as a complex mixture of phospholipids, consisting mainly of PC, PE, PI, and PA, with other compounds such as carbohydrates, fatty acids and triglycerides (USP, 2020). The USP also recommends checking the certificate of analysis for confirmation of the constituent compound ratios. Drescher *et al.* (2020) recommend only using lecithin where the product contains >80% w/w of PC. PC is not soluble in water, in practical terms; when it is in aqueous media, in order to minimise thermodynamically unfavourable interactions between its hydrocarbon chains and aqueous media, they orient themselves into stable planar bilayer sheets. The planar sheets then curve into spherical structures, containing no edges. The formation of this structure completely eliminates any unfavourable interactions between the phospholipid and aqueous media (New, 2003). Due to the orientation of the phospholipids in the bilayer, the hydrophobic tails are oriented towards each other, with the polar head outside, forming an aqueous core and hydrophilic bilayer (New, 2003; Sanarova et al., 2019). Figure 10 is a schematic representation of the formation of a unimellar liposome in aqueous solution. It is worth noting that the centre of the liposome is an aqueous core, capable of solubilising hydrophilic compounds (polar), whereas the bilayer is capable of solubilising hydrophobic compounds (non-polar) (New, 2003); the orientation of the phospholipids within the bilayer are shown.

aqueous media

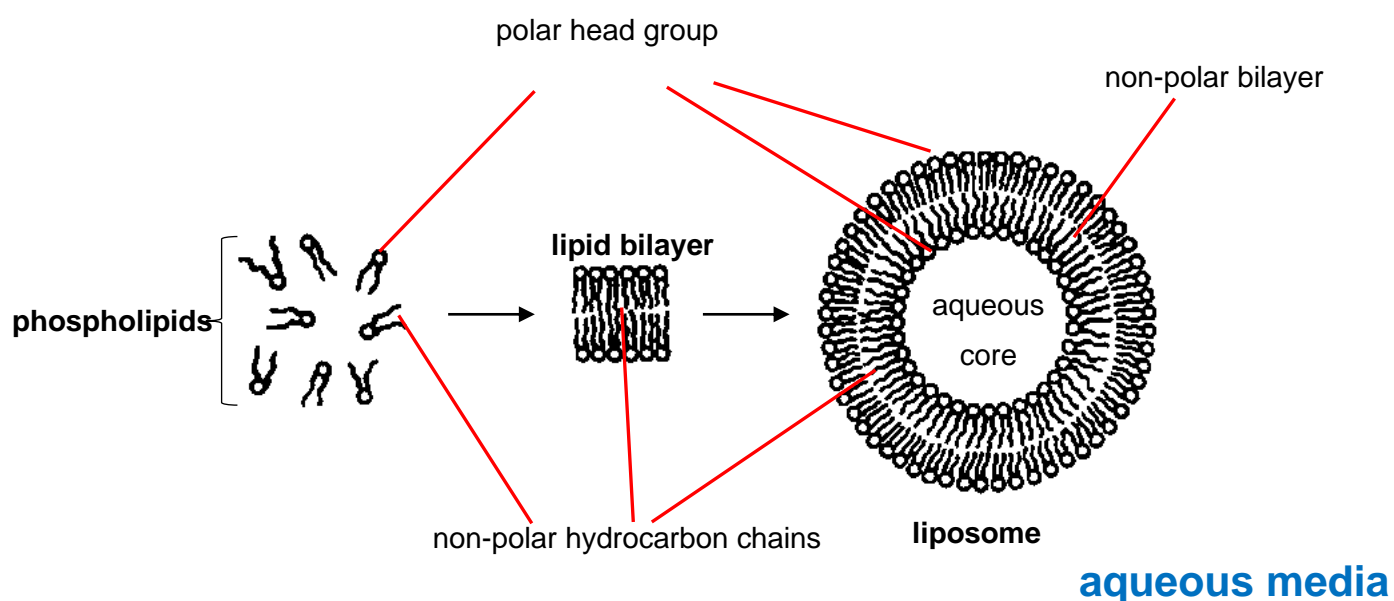


Figure 10: Schematic diagram of representation of phospholipids, lipid bilayer and liposome, all in aqueous media. The polar head and non-polar hydrocarbon chains are shown on the phospholipids at the different stages of liposome formation. Note that for the purpose of this illustration, the liposome diagram shows just one bilayer (unilamellar liposome); and the liposome is shown in 2D, when in fact liposomes are 3D objects.

All lipids have a phase transition temperature (T_c), where they change phase from gel to liquid, meaning that at the T_c , the fluidity of their bilayer changes (Chen et al., 2018; New, 2003; Sanarova et al., 2019). T_c is directly proportional to the length and saturation of the phospholipid hydrocarbon tail, whereby an increase in length or saturation causes an increase in T_c (Chen et al., 2018; New, 2003). T_c is an important parameter affecting many liposome properties required for their manufacture and applications; T_c determines properties such as fusion, permeability, stability and aggregation, as well as affecting way their behaviour in biological systems (New, 2003). More rigid membranes are able to retain encapsulated compounds, preventing leakage (New, 2003; Sanarova et al., 2019).

To increase T_c , sterols are often added (New, 2003). Sterols are found in most natural membranes; incorporation of sterols into the lipid bilayer can change the liposome properties (New, 2003). Sterols can be obtained from mammals, fungi and plants. The most abundant sterol in mammals is cholesterol, and commonly found plant sterols include sitosterol, and stigmasterol, whereas ergosterol is found in fungi (New, 2003). Cholesterol (Figure 11)

is the most commonly encountered sterol in liposome manufacture (Sanarova et al., 2019). Cholesterol by itself does form bilayers (New, 2003), however, as it is an amphipathic compound, it inserts itself into the bilayer with its hydroxyl group oriented towards the polar, aqueous surface and its aliphatic chain aligned parallel to the phospholipid hydrocarbon tails in the centre of the phospholipid bilayer. The addition of cholesterol stabilises the liposomes by increasing Tc of the membrane, therefore increasing rigidity, and causing a decrease in the permeability of the bilayer (New, 2003).

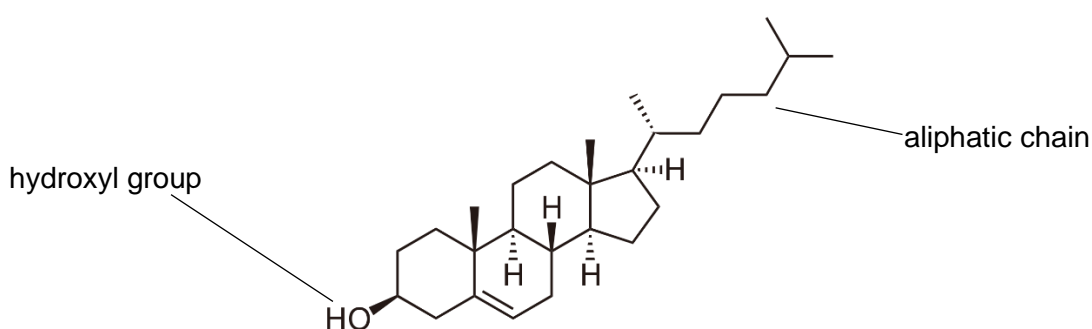


Figure 11: Molecular structure of cholesterol with particular emphasis on its hydroxyl group and aliphatic carbon chain.

1.12.7.2 Liposome manufacture and uses

Liposomes were the first nanoparticles investigated as drug carriers (Wilczewska et al., 2012), and are used in drug delivery for a number of cosmetic and pharmaceutical applications (Akbarzadeh et al., 2013; Bozzuto, 2015). In particular, there are currently several approved liposomal formulations (Ateeq et al., 2018; Sanarova et al., 2019): Liposomes are able to encapsulate a wide range of therapeutic compounds (hydrophobic and hydrophilic) and generally have excellent biocompatibility, biodegradability, and low toxicity (Akbarzadeh et al., 2013).

There are several methods in literature for the preparation of liposomes which include classical, conventional methods as well as novel methods (Akbarzadeh et al., 2013; Nkanga et al., 2019; New, 2003; Sanarova et al., 2019). Conventional methods are the most commonly used methods in liposome preparation (Nkanga et al., 2019); they involve four basic stages: drying of the lipids from organic solvents; dispersion of the lipids in aqueous media; purification of the liposomes, and characterisation of the final product (Akbarzadeh et

al., 2013; Ateeq et al., 2018; Nkanga et al., 2019; New, 2003; Sanarova et al., 2019). However, any method used for the preparation of liposomes requires that the lipids be combined with an aqueous phase, by some means (Maherani et al., 2011; New, 2003). The following methods are some of the most commonly applied methods for preparing liposomes: film hydration method, reverse phase evaporation method, solvent injection method, detergent method, solubilisation method and heating method (Nkanga et al., 2019; Maherani et al., 2011; New, 2003).

The film hydration method, also known as the Bangham method is considered to be the earliest documented method for liposome preparation (Bangham et al., 1965; Laouini et al., 2012; Maherani et al., 2011; Trucillo et al., 2020). The process involves dissolving lipids in an organic solvent, and consequently removing the organic solvent to form a lipid film. The final stage of this method is the film hydration, or simply put, it is the dispersion of the lipid film in aqueous media using agitation (Maherani et al., 2011; New, 2003). This method produces large multilamellar liposomes of size around 500 – 5000 nm (Table 3). Following film hydration, the liposomes can be re-sized, using either sonication or extrusion, to form smaller liposomes (Akbarzadeh et al., 2013; Isalomboto Nkanga et al., 2019; New, 2003). Sonication produces small unilamellar vesicles (Table 3), however, this process is often associated with degradation of liposomes and pharmaceutical ingredients, as a result of the mechanical heat produced (Nkanga et al., 2019). Resizing of liposomes can also be performed by extruding liposomes through polycarbonate membrane filters of defined size (Akbarzadeh et al., 2013; New, 2003).

Reverse phase evaporation is an alternative method to the hydration method, and was first documented by Szoka & Papahadjopoulos (1978) (Szoka & Papahadjopoulos, 1978). This process involves forming a water-in-oil emulsion of the aqueous phase and the organic phase which contains lipids (New, 2003). The emulsion is sonicated and the organic solvent is removed by rotary evaporation, producing a liposome suspension. The liposomes can be isolated using separation methods such as dialysis, centrifugation, or size exclusion (Nkanga et al., 2019; Maherani et al., 2011; New, 2003). A disadvantage of this method is that due to the fact that all compounds involved in the liposome production are in contact with the organic solvent during the entire process, encapsulated compounds should be resistant to the solvent being used (Maherani et al., 2011). Therefore the process is not suitable for fragile compounds such as peptides (Meure et al., 2008).

The solvent injection method involves a rapid injection of a solution containing lipid in solvent, either ethanol or diethyl ether, into an aqueous phase, forming liposomes (New,

2003). In the ethanol injection method, phospholipids dissolved in ethanol, are rapidly injected into water, to produce liposomes (Nkanga et al., 2019; Kanda et al., 2021). Liposomes of particle sizes between 30 – 100 nm are produced using this method (Kanda et al., 2021). A drawback to this method is that ethanol mixes azeotropically with water (Franzè et al., 2020; Kanda et al., 2021). This makes it very difficult to completely remove the residual ethanol from the liposome dispersion making it difficult to completely remove ethanol from the liposome dispersion (Kanda et al., 2021). Furthermore, removal of ethanol from a liposome solution requires distillation of the azeotropic ethanol/water mixture by heating, which can cause for degradation of liposomes and any encapsulated contents (Kanda et al., 2021). In the ether injection method, phospholipids dissolved in diethyl ether, are injected into water that is heated to around 60 °C (Nkanga et al., 2019; Kanda et al., 2021); during this process, the diethyl ether evaporates, and the liposomes are formed (Kanda et al., 2021). The diameter of the liposomes prepared by this method is around 70–190 nm (Kanda et al., 2021). However, there is concern that the relatively high temperatures used to evaporate diethyl ether, could cause the degradation of encapsulated compounds, therefore, heat stable compounds should be used (Kanda et al., 2021). Moreover, there is concern over residual diethyl ether remaining inside the liposomes (Kanda et al., 2021). High encapsulation efficiencies have been achieved using injection methods. Jaafar-Maalej et al., used the injection method with diethyl ether and observed encapsulation efficiencies of around 100% for a hydrophobic drug and around 16% for a hydrophilic drug (Jaafar-Maalej et al., 2010).

The detergent solubilisation method is a mild process for the production of liposomes (Maherani et al., 2011). Phospholipids are dissolved in aqueous solution, containing detergents at their critical micelle concentrations (CMC) (Nkanga et al., 2019; New, 2003). Phospholipids are brought into contact with the aqueous phase by the detergents, which form lipid-detergent micelles with the phospholipids (Maherani et al., 2011; New, 2003). As the detergent is removed, phospholipid molecules self-assemble into bilayered structures forming liposomes (Nkanga et al., 2019). The main disadvantages of this method are that the final concentration of liposomes in dispersion is low and the encapsulation efficiency of hydrophobic compounds is also low (Maherani et al., 2011).

The heating method is an organic solvent-free method (Nkanga et al., 2019; Maherani et al., 2011). This method involves hydration of phospholipids above the transition temperature (T_c) of the phospholipids in an aqueous solution containing 3% v/v of glycerol, a hydrating agent (Nkanga et al., 2019; Maherani et al., 2011). Heating occurs between 60 °C and 120 °C (Maherani et al., 2011), depending on whether cholesterol is part of the formulation,

due to its high melting point (Nkanga et al., 2019; Maherani et al., 2011). Glycerol, a water soluble, physiologically acceptable material (Castañeda-Reyes et al., 2020; Nkanga et al., 2019; Maherani et al., 2011), acts as an isotonic additive (Maherani et al., 2011), and increases the stability of liposomes by preventing coagulation and sedimentation. (Castañeda-Reyes et al., 2020; Nkanga et al., 2019; Maherani et al., 2011). This method has several advantages including that no organic solvents are required therefore removing toxic chemicals and waste (Nkanga et al., 2019); the hydrating agent, glycerol, does not need to be removed, as it is considered physiologically acceptable and is well-established as a pharmaceutical excipient (Nkanga et al., 2019; Simonzadeh & Ronsen, 2012); sterilisation is not required for this product when sufficiently high temperatures are used in the process i.e. 120 °C (Maherani et al., 2011).

The main difference between the different methods is the way that the liposome components are dispersed in the aqueous media prior to forming the lipid bilayer (New, 2003). Methods of drug loading are either passive or active loading (Akbarzadeh et al., 2013; Ateeq et al., 2018; New, 2003). Passive loading is where the encapsulated compounds are introduced into the liposomes during the manufacturing process, whereby the liposomes are effectively formed around the encapsulated compounds; and active loading is where the encapsulated compounds are introduced into the liposomes after the liposomes have been formed (Akbarzadeh et al., 2013; New, 2003). In passive loading, hydrophobic drugs e.g., amphotericin B can be directly encapsulated with liposomes. The encapsulation efficiency is dependent on the drug/lipid interactions and the solubility of the drug in the liposome membrane (Akbarzadeh et al., 2013).

Liposomes are mainly characterised by their size and number of bilayers (New, 2003; Sanarova et al., 2019). Size is classed as small, intermediate or large; the number of bilayers is classed as unilamellar or multilamellar vesicles (New, 2003). Table 3 shows a list of the different liposome classifications based on size and number of bilayers.

Table 3: Different classes of liposome based on size and number of bilayers (Castañeda-Reyes et al., 2020; New, 2003)

| Liposome classification | Abbreviation | Size range | Number of bilayers |
|-----------------------------------|---------------------|-------------------|---------------------------|
| Small unilamellar vesicles | SUV | 25 - 100 nm | 1 |
| Intermediate unilamellar vesicles | IUV | 100 - 1000 nm | 1 |
| Large unilamellar vesicles | LUV | >1000 nm | 1 |
| Multilamellar vesicles | MLV | 500 nm – 5000 nm | Usually 5 or more |

Liposomes were the first nanoparticles investigated as drug carriers (Wilczewska et al., 2012), and are used in drug delivery for a number of cosmetic and pharmaceutical applications (Akbarzadeh et al., 2013; Bozzuto, 2015). In particular, there are currently several approved liposomal formulations (Ateeq et al., 2018; Sanarova et al., 2019): Liposomes are able to encapsulate a wide range of therapeutic compounds (hydrophobic and hydrophilic) and generally have excellent biocompatibility, biodegradability, and low toxicity (Akbarzadeh et al., 2013).

1.13 Liposomal cement

Ayre *et al.* (2015) incorporated gentamicin loaded 100 nm liposomes into bone cement, comparing mechanical and elution properties (Ayre et al., 2015). Despite the miscibility issues posed by dissolving liposomes into a non-polar matrix, due to the liposome polar surface, it was shown that by using a poloxamer (Pluronic), a uniform dispersion was achieved. Uniform dispersion is not achieved within the current gentamicin loaded commercial cements and is characterised by observable agglomerations. Poloxamers are non-ionic block copolymers composed of polyethylene oxide (PEO) and polypropylene oxide (PPO) (Patel et al., 2009). It is proposed that the polar Pluronic PEO chains attach themselves to the liposome polar head groups on the surface, and the non-polar Pluronic PPO chains interact with the non-polar environment (Figure 12) (Ayre et al., 2015).

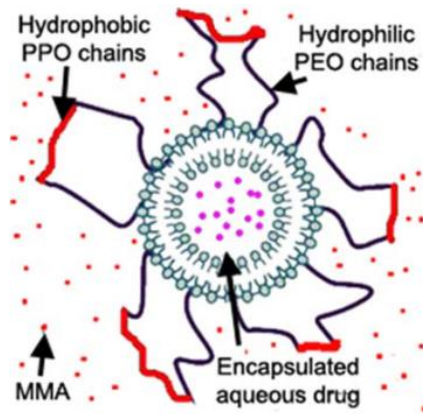


Figure 12: Proposed liposome-Pluronic structure, showing the interactions of Pluronic with respect to MMA molecules and the liposome surface; allowing the liposomes to be suspended in MMA (Ayre et al. 2015).

After a small initial burst from surface liposomes, the liposomal cement demonstrated a more linear and gradual prolonged release of antibiotic compared to the commercial gentamicin cement. Over a period of 60 days the liposomal cement had released more of the incorporated gentamicin (22%) compared to the commercial cement (9%). There was a significant reduction in the compressive strength compared to the commercial gentamicin cement, however, the compressive strength was above the ISO 5833 standard requirement. Other mechanical properties such as bending strength, fracture toughness, glass transition temperature and Vickers hardness were improved relative to the commercial gentamicin bone cement, as well as the plain cement (Ayre et al., 2015). This formulation has been patented by Ayre *et al.* (2016) (Ayre et al. 2016. Liposomal drug delivery system for bone cements. US9895466.)

1.13.1 Pluronic

Pluronic is a brand name for poloxamers, which are triblock copolymers (A-B-A) containing units consisting of a central propylene oxide unit (PO), with two ethylene oxide units either side (EO). EO is hydrophilic and PO is hydrophobic. The general structure is $EO_x-PO_y-EO_x$, where x and y are the number of sub-units. HLB number (hydrophilic lipophilic balance) is used to classify them, which is the ratio of hydrophilic/hydrophobic groups. For non-ionic surfactants a number above 10 indicates hydrophilic character, and below 10 is hydrophobic character. Furthermore, the Pluronic name indicates information about its structure (Belisle et al. 2015. Colloidal Coomassie stain. US9034652B2., 2015; Costanzo et al., 2021): the first letter tells us its state, the first number multiplied by 30 gives us an approximate molecular

weight (Mw) and the second number multiplied by 10 tells us the percentage of polyoxyethylene content (Belisle et al. 2015. Colloidal Coomassie stain. US9034652B2.). For example, L61: the preceding letter, L, indicates a liquid; the first number, 6 (6 here is 60) multiplied by 30, $60 \times 30 = 1800$ Mw; and the second digit, 1 is multiplied by 10, $1 \times 10 = 10$ percent of polyoxyethylene content.

1.14 Current status of liposomal bone cements

A search of the main patent databases such as the World Intellectual Property Organization (WIPO) and the European Patent Office (EPO) shows that other than the patent by Ayre *et al.* (2016), there is one significant patent application for a liposomal bone cement system. There is also one study of interest regarding liposomal cement.

1.14.1 Disinfectant bone and dental filler materials comprising liposomes

This patent application in 2017 (European patent) and 2020 (world patent) is for dental or bone filler materials, having antimicrobial properties against bacteria that are commonly responsible for bone and dental infections such as *E. coli*, *E. faecalis*, *P. acnes*, *P. aeruginosa* and *S. aureus*. The invention comprises of a cement matrix material with liposomes containing an antimicrobial active ingredient such as chlorhexidine or just the cationic liposomes by themselves (Raddi, 2017). Although the patent author has only shown experimental data for calcium hydroxide and calcium silicate cements, fifteen other matrix materials are mentioned within the patent which include hydroxyapatite, silicone, alginate, collagen, hydroxyapatite, and calcium phosphate. The aim of this invention is to release an antimicrobial compound for at least 15 days, effectively killing bacteria. It was observed that with incorporation of chlorhexidine API into commercial bone filling materials, a lower release of chlorhexidine was observed than for cement with liposomes containing chlorhexidine. Chlorhexidine by itself in cement was released at much lower concentrations than clinically effective concentrations. This was also observed with relatively higher incorporated concentrations of chlorhexidine (5% w/w); whereas 1% w/w in cement of liposomes containing chlorhexidine released more than 6 times the mass amount of chlorhexidine, which was also found to be above the relevant MICs. The optimal liposomal cement was found to be calcium trisilicate material containing neutral liposomes, loaded with

chlorhexidine solution. Neutral liposomal cement: 1% w/w neutral liposomes composed of dipalmitoylphosphatidylcholine (DPPC) and cholesterol (C) containing chlorhexidine solution. It is worth noting that although the author makes the claim that un-loaded cationic liposomes composed of dipalmitoylphosphatidylcholine (DPPC), cholesterol (C) and Stearylamine (SA) are effective in cement for the aims given in the patent, no test data was provided. Drug release was not performed for more than the 15 days reported, so it is not known what quantities of chlorhexidine are released thereafter. Moreover, several studies suggest that bacterial resistance to chlorhexidine can be achieved through exposure to sub-inhibitory concentrations of chlorhexidine (Kampf, 2016). The type of material in the invention is primarily used for root canal sealing, which requires testing as per the ISO 6876:2012 standard (Dentistry — Root canal sealing materials), of which no test data has been provided within this patent. Tests in the standard include flow properties, setting time, film thickness, solubility and radiopacity (Ashraf et al., 2017). Furthermore, compressive strength of such materials should be assessed, as this demonstrates the cement's resistance to forces under load in its clinical applications such as repair procedures and pulp capping (Forough et al., 2021). There is also no data for encapsulation efficiency, which would tell us how much chlorhexidine is actually incorporated into the cement. It is claimed that the liposomes exit the cement intact, and this is stated as a benefit due to the interaction between liposomes and cells/biofilms; however, there has been no characterisation or measurement of liposomes exiting the cement.

1.14.2 Liposomal bone cement containing amphotericin

Cunningham *et al.* (2012) prepared an antifungal loaded liposomal bone cement (Cunningham et al., 2012). Ambisome, an already existing lyophilised liposomal amphotericin B formulation was used in bone cement to decrease systemic toxicity and to improve its poor drug-release due its hydrophobic character (Cunningham et al., 2012; Goss et al., 2007). Previously, a mixture of amphotericin B and deoxycholate was used to improve drug release. Bone cement containing 800 mg of liposomal formulation was shown to inhibit planktonic fungi (*C. albicans*) compared to the same mass amount of amphotericin B/deoxycholate. The liposomal cement released over 20 times more drug mass amount than the cement containing B/deoxycholate. It was also shown that increasing the amount of incorporated liposomal content, increased the amount of drug released. However, the mechanical properties were severely compromised: the compressive strength for cement containing this mass amount was below the ISO 5833 standard. Drug release from the bone cement was assessed for toxicity; it was shown that *in vitro* cytotoxicity occurred, however,

no adverse tissue reaction was observed *in vivo* using mouse tissue. This study did not investigate whether liposomes exited the tissue intact (Roberts et al., 2015)

1.15 Scope of thesis

Total joint replacement (TJR) is commonly used for the treatment of end stage arthritis, particularly for hip and knee replacements. The use of antibiotic loaded bone cement (ALBC) is a well-established standard in the prevention of post-surgical infections. Currently, ALBCs have several limitations including: < 10% antibiotic release and compromised mechanical properties. The study aims to optimise a liposome delivery system, to effectively incorporate and disperse gentamicin sulfate within bone cement achieving sustained drug release, whilst maintaining suitable mechanical properties. The objectives of this study are:

- To validate and characterise the current liposomal delivery system.
- To optimise and enhance the liposomal delivery system.
- To incorporate hydrophilic and hydrophobic additives into antibiotic loaded bone cement to obtain a better understanding of drug release mechanisms.

Chapter 2

2 General Methods

This chapter outlines some of the common methods used throughout the thesis. Methods that are specific to a particular chapter will be described in detail in the relevant chapter.

2.1 Cement and liposome preparation

2.1.1 PMMA bone cement preparation

PMMA bone cement was prepared as per the manufacturer's instructions and in accordance with the ISO 5833 standard. A ratio of PMMA powder component to MMA liquid component (2:1) was prepared by weighing the components and mixing them together, using a PTFE rod and bowl. Freshly mixed cement was placed in PTFE moulds, pre-treated with silicone mould release spray, and clamped on both sides using steel plates to make the required sample shape.

2.1.2 Liposome preparation

Liposome preparation was performed as per the methodology found in the patent and academic research paper on this subject by Ayre *et al.* (Ayre et al. 2016. Liposomal drug delivery system for bone cements. US9895466.; Ayre et al., 2015) Phosphatidylcholine (175 mg) and cholesterol (25 mg) were weighed and mixed together in a 7:1 ratio, dissolved in minimal chloroform (5 ml) in a round bottom flask. The chloroform was evaporated under vacuum at 60 °C using a Rotavapor R-300 rotary evaporator (Buchi Ltd, UK). The residue (lipid-bilayer) was resuspended in 40 ml of a solution of 5 mg/mL of gentamicin sulfate by vortexing. This suspension was held for 30 minutes at 60 °C prior to extruding vertically under nitrogen pressure (≤ 8 bars), using a Lipex extruder (Evonik Canada Inc., British

Columbia, Canada). Five separate extrusions were performed sequentially using different pore size polycarbonate membranes of 400 nm, 200 nm and 100 nm (Whatman, UK).

2.1.3 Liposome pellet preparation

Liposome pellet preparation was performed as per the method described in the patent and academic research paper by Ayre *et al.* (Ayre et al. 2016. Liposomal drug delivery system for bone cements. US9895466.; Ayre et al., 2015). 2% w/w Pluronic L43, with respect to the lipid mass quantity, was added to the liposomes and centrifuged using a Beckman Optima LE-80K ultra-centrifuge (Beckman Coulter Ltd, UK) at 107,000 g for 1 hour and 30 minutes at 4 °C. The pellet was resuspended in 20 ml of the Palacos liquid component MMA by trituration, ready to be mixed with the bone cement powder component.

2.1.4 Release of antibiotic and lipids from cement discs

Cement discs were placed in 5 mL of phosphate buffered saline (PBS) pH 7.4, at 37 °C for specified amounts of time. At each time point, the liquid was removed, stored at -20 °C, and replaced by fresh PBS until the next time point. Frozen solutions were thawed for 4 hours, and then appropriate aliquots were removed for spectroscopic analysis. At each stage, the samples were protected from light. Samples were analysed in triplicate, using three separate cement discs (n=3). Antibiotic release from bone cement is expressed as the mass amount released at each time point (μg), and as the cumulative mass amount of drug release (μg), calculated by addition of the drug mass amount released at each given time point, and the sum of the mass amounts of drug released at the time points previous to it.

For comparative purposes, the percentage of cumulative drug mass amount released (%) is also used, where necessary. The percentage of cumulative drug mass amount at each time point, from the initial mass amount of drug incorporated into the bone cement disc, is expressed as the cumulative percentage release:

$$\%Cg = \frac{CMg}{I_0} \times 100$$

Where:

%Cg is the cumulative percentage of gentamicin base released at a given time point.

CMg is the cumulative mass of gentamicin base released at a given time point (μg).

I_0 is the theoretical mass amount of gentamicin base incorporated into a given bone cement disc (μg).

2.2 Particle size and zeta potential of liposomes

The mean particle diameter and surface zeta potential (surface charge) of liposomes were characterised using a Malvern Zetasizer NanoZS (Malvern Instruments Ltd, Worcestershire, UK). Particle size measurements were carried out by placing the liposome suspension into a polystyrene cuvette. Zeta potential measurements were carried out by filling a capillary zeta cell with liposome suspension. Both the cuvette and the capillary zeta cell were placed into the sample holder and checked for bubbles. Samples were analysed in triplicate ($n=3$). Measurements were performed at 22 °C using Malvern Zeta Software (Malvern Instruments Ltd, Worcestershire, UK).

2.3 Contact angle measurement

Contact angles of freshly prepared cement discs were measured. Individual cement discs were mounted on to the OneAttension Theta Lite Optical Tensiometer (Biolin Scientific, Finland) and a single drop containing 5 μl of deionised water was dispensed onto the disc surface using the OneAttension software (Biolin Scientific, Finland). Measurements were taken over 10 seconds, and the mean value of the left and right values was taken. Samples were analysed in triplicate, using three separate cement discs ($n=3$). Measurement of the contact angle was performed using OneAttension software.

2.4 Mechanical testing

Mechanical testing was performed as per the requirements of ISO 5833: compressive strength, bending modulus and bending strength (ISO 5833, 2002). As required by the standard, testing was performed using five separate cement sample preparations (n=5).

2.4.1 Compressive strength

Compression testing was performed, as per the requirements of ISO 5833, using a Lloyd LR10K Plus materials testing machine (Ametek, Pennsylvania, USA.). Cylindrical compression samples (6 mm diameter, 12 mm length) were tested at a cross-head speed of 20 mm/min. Five cement preparations were used for testing (n=5). The compressive strength (F) was calculated as per the formula specified in ISO 5833 and expressed in mega Pascals (MPa):

$$F = P/A$$

Where:

P is the force applied to cause fracture (N).

A is the cross-sectional area of the cylinder (mm²).

2.4.2 Bending modulus

Bending modulus testing was performed, as per the requirements of 5833:2002, using a Lloyd LF Plus materials testing machine (Ametek, Pennsylvania, USA.). Rectangular bending samples (75 mm length, 10 mm width, 3.3 mm thickness) were tested at a cross-head speed of 5 mm/min in four-point bending. Five cement preparations were used for testing (n=5). The bending modulus (E) was calculated as per the formula specified in ISO 5833 and expressed in mega Pascals (MPa):

$$E = \frac{\Delta F a}{4 f b h^2} \cdot (3l^2 - 4a^2)$$

Where:

- f is the difference between the deflections under the loads of 15 N and 50 N in millimetres (mm).
- b is the average measured width of the specimen, in millimetres (mm).
- h is the average measured thickness of the specimen, in millimetres (mm).
- l is the distance between the outer loading points (60 mm).
- ΔF is the load range (50 N – 15 N = 35 N).
- a is the distance between the inner and outer loading points (20 mm).

2.4.3 Bending strength

Bending strength testing was performed, as per the requirements of 5833:2002, using a Lloyd LF Plus materials testing machine (Ametek, Pennsylvania, USA.). Rectangular bending samples (75 mm length, 10 mm width, 3.3 mm thickness) were tested at a cross-head speed of 5 mm/min in four-point bending. Five cement preparations were used for testing (n=5). The bending modulus (B) was calculated as per the formula specified in ISO 5833 and expressed in megapascals (MPa):

$$B = \frac{3Fa}{bh^2}$$

Where:

- F is the force at break, in newtons (N).
- b is the average measured width of the specimen, in millimetres (mm).
- h is the average measured thickness of the specimen, in millimetres (mm).
- a is the distance between the inner and outer loading points (20 mm).

2.5 Stewart assay (determination of phospholipid content)

The Stewart assay was used to characterise liposome phospholipid content released from cement discs, stored for 5 days in PBS solution (pH 7.4) at 37 °C. This assay is used for measurement of phospholipids based on the reaction between phospholipids and

ammonium ferrothiocyanate forming a complex molecule, which can be measured directly using a UV-vis spectrophotometer. This method has several advantages over other established assays such as the Bartlett assay, that inorganic phosphates do not interfere with the reagent, meaning that phosphate buffer can be used in experiments (Charles & Stewart, 1980). Ammonium ferrothiocyanate reagent was prepared by dissolving 27.03 g of ferric chloride hexahydrate and 30.4 g of ammonium thiocyanate in 1 litre of deionised water. The phosphatidylcholine standard was prepared by accurately weighing 25 mg of phosphatidylcholine in a 25 ml volumetric flask and adding chloroform up to the mark, to obtain a 1 mg/ml stock solution of phosphatidylcholine in chloroform. One part of the stock solution and nine parts of fresh solvent (chloroform) were mixed together (1:10) to give 0.1 mg/ml of the phosphatidylcholine standard solution. For construction of the standard curve, the reagents and standard solution were pipetted into glass test tubes using the scheme for addition of reagents (Table 4):

Table 4: Scheme for the addition of reagent volumes to each tube: the tube for the blank sample contains only addition of chloroform and ammonium ferrothiocyanate with no addition of the standard solution. The test sample tubes labelled 1-6 contain different volumes of the standard solution with the addition of chloroform and ammonium ferrothiocyanate.

| Sample tube | Phosphatidylcholine standard (ml) | Chloroform (ml) | Ammonium ferrothiocyanate (ml) |
|-------------|-----------------------------------|-----------------|--------------------------------|
| Blank | 0 | 2.0 | 2.0 |
| 1 | 0.1 | 1.9 | 2.0 |
| 2 | 0.2 | 1.8 | 2.0 |
| 3 | 0.4 | 1.6 | 2.0 |
| 4 | 0.6 | 1.4 | 2.0 |
| 5 | 0.8 | 1.2 | 2.0 |
| 6 | 1.0 | 1.0 | 2.0 |

The test tubes were individually vortexed for 20 seconds and centrifuged at 1000 rpm for 10 minutes. After centrifugation, the tubes were removed from the centrifuge, and the top aqueous layer of the tubes were removed and discarded using a glass Pasteur pipette. Samples were placed into quartz cuvettes and absorbance was measured at 485 nm using

an Agilent Cary 60 UV-Vis spectrophotometer (Agilent, USA); concentrations were obtained by calculations based on the standard curve.

2.6 Extraction of lipids in solution using the Bligh and Dyer method

The Bligh and Dyer extraction method is a method used for the extraction of triacylglycerols, fatty acids and phospholipids (Bligh, E.G. and Dyer, 1959; Jensen, 2008). The method was carried out using glass test tubes which were pre-cleaned with chloroform. The following additions were made sequentially to each test tube containing 1 ml of sample, and each test tube was individually vortexed for 20 seconds after each addition. First, 3.75 ml of a mixture containing 1:2 (v/v) chloroform:methanol was added to 1 ml of sample and vortexed. 1.25 ml of chloroform was added to the mixture and vortexed. A volume of 1.25 ml of deionised water was further added to the mixture and vortexed. The test tube was centrifuged at 1000 RPM for 5 minutes at room temperature resulting in two phases giving an aqueous top layer and an organic bottom layer. Recovery of the organic layer (bottom layer) was performed using a Pasteur pipette by carefully withdrawing the bottom layer through the pipette.

2.7 Liquid chromatography–mass spectrometry (LC–MS) analysis of gentamicin

Two separate instruments and methods were used for the analysis of gentamicin:

2.7.1 Method 1 (Thermo Spectra System P4000)

The instrument used for the chromatographic separation was a High-performance liquid chromatography (HPLC) Thermo Spectra System P4000 (Thermo, USA), using a Licrospher C8 60, 250 mm x 4 mm reverse phase column obtained from Merck (Merck Millipore, USA), maintained at 50 °C with an injection volume of 25 µl. The mobile phase used was a mixture of 20 mM Pentafluoropropionic anhydride (PFPA) and methanol (60:40). Elution was isocratic at a flow rate of 1 ml/min. The HPLC was coupled with an atmospheric pressure electrospray ionization (ESI) mass spectrometer Thermo Finnigan LCQ (Thermo, USA).

Ionisation was performed using Selected Ion Monitoring mode; the ion m/z value was 478.30 for gentamicin. Capillary and fragmentor voltages were 4000 V and 140 V respectively. Nebuliser (60 psi) and drying gas (12 l/min) were both nitrogen; temperature was 350 °C. Xcalibur software was used for the data acquisition and analysis.

2.7.2 Method 2 (Bruker Amazon SL)

Analysis was performed using a method for analysis of all aminoglycoside antibiotics which is currently used in the School of Chemistry. The method was validated using ICH guidelines. A Bruker Amazon SL ion trap mass spectrometer (Bruker Corp, USA) coupled to a thermo ultimate 3000 HPLC system (Thermo Fisher Scientific, USA), using a Restek raptor C18 column (50 mm x 2.1 mm) (Restek corporation, USA.) maintained at 40 °C was used with an injection volume of 25 µl. The mobile phase was composed of 50% v/v acetonitrile in water, containing 0.1% v/v formic acid. Elution was isocratic at a flow rate of 0.1 ml/min. Mass spectrometry was performed in positive ion mode using selected ion monitoring for ion 478.3 m/z. Synapt analyser software (Waters corporation USA) was used for the data acquisition and analysis.

2.8 Analysis of lipids using fluorescence spectrophotometry

Two different methods using different diluents were developed and validated for analysis of fluorescent lipid 18:1-06:0 NBD PC:

2.8.1 Development and validation of method for analysis of fluorescent lipids in methanol

Analysis was performed using a fluorescence spectrophotometry method, developed and validated, to analyse samples using fluorescent labelled lipids. Emission and excitation wavelengths were found by the iterative wavelength determination process. This process is performed by keeping either the excitation or emission wavelength at a known value and scanning the sample for the other unknown wavelength; by performing further scans in a stepwise manner, until the excitation and emission wavelengths do not change with further scans, accurate emission and excitation wavelengths can be obtained. Limit of detection

(LOD) and limit of quantification (LOQ) were calculated using the calibration curve method, based on the standard error of the calibration curve and the calibration curve gradient, using the following equations (Kelner et al., 2009):

$$LOD = \frac{3.3 \times \sigma}{S} \qquad LOQ = \frac{10 \times \sigma}{S}$$

Where:

σ is the standard error of the calibration curve.

S is the gradient of the calibration curve.

The method was validated for use with methanol as the diluent, due to environmental and safety concerns over chloroform. Methanol is a less toxic and environmentally friendly solvent than chloroform (Capello et al., 2007). Emission and excitation wavelengths were determined to be 467 nm and 535 nm respectively using a Cary Eclipse Fluorescence Spectrometer (Agilent Technologies, USA). Cary WinFLR software (Agilent Technologies, USA) was used for the data acquisition and analysis.

Liposomes and pellets were prepared as specified in Sections 2.1.2 and 2.1.3 respectively; however, 1% w/w of topfluor fluorescent lipid, 18:1-06:0 NBD PC (Avanti Polar Lipids Inc, USA) was incorporated into the liposome preparation. Liposome pellets were incorporated into cement discs by resuspending in MMA liquid and mixing with PMMA powder as per the methods in Sections 2.1.1 and 2.1.3. Samples were protected from light at all stages. Cement samples were stored for 1, 2 and 5 days at 37 °C in PBS. The PBS solution was removed, and the lipid was extracted using the Bligh and Dyer method as in Section 2.5. Samples were then dried under nitrogen and reconstituted in 1 ml of methanol for analysis.

2.8.2 Analysis of fluorescent lipids in chloroform

Analysis was performed using a developed and validated fluorescence spectrophotometry method, where the emission and excitation wavelengths were provided by Avanti for the fluorescent labelled phosphatidylcholine lipid (18:1-06:0 NBD PC) dissolved in chloroform (Avanti Polar Lipids. 18:1-06:0 NBD PC. [online] Available at: <https://avantilipids.com/product/810132> [Accessed 10 Dec. 2020]). The emission and excitation wavelengths were confirmed as 464 nm and 531 nm respectively using a Cary

Eclipse Fluorescence Spectrometer (Agilent Technologies, USA). Cary WinFLR software (Agilent Technologies, USA) was used for the data acquisition and analysis. Limit of detection (LOD) and limit of quantification (LOQ) were calculated using the calibration curve method, based on the standard error of the calibration curve and the calibration curve gradient, using following equations in Section 2.8.1.

Liposomes and pellets were prepared as specified in Sections 2.1.2 and 2.1.3 respectively; however, 1% w/w of topfluor fluorescent lipid, 18:1-06:0 NBD PC (Avanti Polar Lipids Inc, USA) was incorporated into the liposome preparation. Liposome pellets were incorporated into cement discs by resuspending in MMA liquid and mixing with PMMA powder as per the methods in Sections 2.1.1 and 2.1.3. Samples were protected from light at all stages. Cement samples were stored for 1, 2 and 5 days at 37 °C in PBS. The PBS solution was removed, and the lipid was extracted using the Bligh and Dyer method as in Section 2.5. Samples were then dried under nitrogen and reconstituted in 1 ml chloroform for analysis.

2.9 Antimicrobial testing methods

All Antimicrobial testing was carried out using the procedures specified in this section. This includes sterilisation of glassware, media sterilisation, sample sterilisation, quantitative suspension tests, and analysis of biofilm formation.

2.9.1 Sterilisation of glassware and media

Sterilisation of all media and glassware was carried out in accordance with the British Pharmacopoeia requirements as set out in appendix XVIII, Methods of Sterilisation. Steam sterilisation was carried out using an autoclave (Fisher Scientific, UK) for 15 minutes at 121 °C (*Br. Pharmacopoeia*, 2017). All plastic labware used was pre-sterilised by the manufacturer.

2.9.1.1 Sterilisation of samples prior to testing

PMMA bone cement discs were lightly sprayed with ethanol 70% (v/v) in a fume cupboard and allowed to evaporate fully for 15 minutes prior to testing.

2.9.2 Quantitative suspension test

Analysis was performed using a method adapted from the standard EN 13727:2012+A2:2015, Chemical disinfectants and antiseptics — Quantitative suspension test for the evaluation of bactericidal activity in the medical area (British Standards Institution, 2015).

For all experiments, *S. aureus* strain NCTC 10788 was used; moreover, NCTC 10788 is a biofilm producing strain (Gwynne et al., 2021).

Day 1: preparation of *S. aureus* bacteria culture was carried out by transferring an aliquot of frozen *S. aureus* on to an agar plate and streaked across the plate using a loop. The plate was inverted and placed in an incubator overnight at 37 °C for 18 hours. Tryptone sodium chloride medium (TSC) was prepared by dissolving 1.0 g of tryptone 1.0 g and 8.5 g of sodium chloride in 1 litre of deionised water. Tryptone soya broth (TSB) was prepared by dissolving 30 g of the product in 1 litre of deionised water.

Day 2: the bacteria culture plate was removed from the 37 °C incubator, and a loop was used to transfer bacteria from the agar plate to a 10 ml falcon tube containing 10 ml of TSB. The tube was mixed using a vortexer. The tube was then placed on a shaking incubator (150 rpm) at 37 °C for 24 hours.

Day 3: the 10 ml falcon tube was removed from the shaking incubator and placed on the centrifuge at 5000 rpm for 10 minutes; after spinning, the supernatant was discarded, and the pellet was resuspended in 10 ml of TSC. This process was repeated three times in total to produce a stock bacteria suspension. Since the starting bacteria concentration was approximately 10^9 cells per ml. Using a pipette, serial dilutions of 1 ml of stock into 10 ml of TSC, then a further 1 ml was diluted into 100 ml of TSC to give a starting inoculum of approximately 10^6 cells per ml. 10 ml of inoculum was added to individual 50 ml falcon tubes containing individual cement disc samples. The tubes were placed in an incubator at 37 °C for 4 hours. After 4 hours, the tubes were removed and allowed to cool for 10 minutes. For each sample tube, an aliquot of 100 µl was added to 900 µl of TSC in 1 ml Eppendorf tubes (100 µl into 1000 µl); 4 further serial dilutions were carried out by dilution, 100 µl into 1000 µl. 10 µl of each dilution was spotted on a marked agar plate. Agar plates were placed in an incubator at 37 °C for 18 hours, at which point any resulting colonies were counted. The

result was expressed in terms of colony forming units per millilitre (CFU/ml); calculated using the following formula:

$$CFU/ml = \frac{C \times d}{V}$$

C is the number of colonies observed.

d is the dilution factor.

V is the volume plated.

2.9.3 Analysis of biofilm formation

Each disc was placed in a reagent bottle containing 1 g of pre-weighed glass beads, 1 ml of TSC was added to each bottle, and each bottle was shaken on a vortexer for 2 minutes. 10 µl aliquots were placed on agar plates for each sample. Agar plates were placed in an incubator at 37 °C for 18 hours, at which point any resulting colonies were counted. The result was expressed in colony forming units per millilitre (CFU/ml). The calculation was the same as in Section 2.9.2.

2.10 Scanning electron microscopy

Samples were attached to pin stubs with either adhesive double-sided carbon tabs (Agar Scientific Ltd) or Leit-C carbon cement (Agar Scientific Ltd) and coated in a very fine layer of gold in a DRS1 Sputter coater (Vac Techniche Ltd, UK) The samples were imaged (5 kV) using a TESCAN VEGA3 SEM (Tescan, Brno, Czech Republic).

2.11 Statistical analysis

Data is represented as the mean ± standard deviation (SD), from a minimum of three independent repeats (n=3). Statistical significance was determined by using the Student's t-test to compare the means between two groups; ANOVA was used to compare the means between three or more groups. All statistical analyses were performed using GraphPad Prism software (GraphPad Software Inc., California).

Chapter 3

3 Validation and characterisation of the liposomal delivery system

3.1 Introduction

A liposomal formulation, LCP, was previously incorporated into a commercial bone cement (Palacos R) to enhance antibiotic release and material properties (Ayre et al. 2016. Liposomal drug delivery system for bone cements. US9895466.; Ayre et al., 2015). The formulation was composed of pelleted, 100 nm phosphatidylcholine liposomes, containing gentamicin sulfate, functionalised with various Pluronic block copolymers (L31, L43, L64) to achieve stability and dispersion within the PMMA cement (Ayre et al., 2015). The study demonstrated that the liposomes in this formulation were fully dispersed within the PMMA bone cement. Testing for mechanical properties (compressive strength, bending strength and bending modulus) were carried out according to ISO 5833. The liposomal bone cement was found to exceed the ISO 5833 requirements for all the mechanical tests.

Due to the ability of the liposomes to successfully disperse within the PMMA bone cement, drug dispersion was therefore assumed to be improved, compared to the current powdered commercial cement formulations (e.g., Palacos R+G). The novel formulation also showed an improved and more sustained drug-release profile.

Antimicrobial efficacy was previously performed using agar diffusion assays against *S. aureus*. Palacos R+G produced larger zones of inhibition showing that it had a higher level of efficacy than LCP-CEMENT in inhibiting *S. aureus* growth; however, despite results being inconsistent between sample repeats for Palacos R+G, LCP-CEMENT was shown to inhibit *S. aureus* in a much more consistent manner, potentially due to the more sustained antibiotic release. The previous study by Ayre *et al.* (2015) measured drug release using the o-phthalaldehyde (PHT) method by Sampath & Robinson (1990) (Ayre et al., 2015). This

method is an established, validated colorimetric method using an ultraviolet–visible (UV-Vis) spectrophotometer for analysis of analysis of a derivatised compound (Sampath & Robinson, 1990); however, liquid chromatography-mass spectrometry (LC-MS) is a superior analytical method due to its high selectivity and sensitivity, compared to UV-Vis, and its relatively short preparation time, in comparison to the o-phthaldialdehyde method (Zheng et al., 2018). Moreover, due to the far superior sensitivity of this method, it can detect much lower limits of quantification, allowing trace amounts of drug to be measured (Lecároz et al., 2006).

The study reported in this chapter aims to validate LCP-CEMENT and to assess its reproducibility in terms of mechanical properties, antimicrobial activity, and drug-release. Antimicrobial activity and drug release will be assessed using more effective methods compared to previous studies. In doing so, this chapter will also aim to establish an LC-MS method for the analysis of gentamicin sulfate from bone cement. Finally, this chapter will also explore the role of the individual excipients (i.e., Pluronics) on drug release properties and will investigate whether the liposomes themselves are being released from LCP-CEMENT.

3.2 Methods

3.2.1 Materials

Phosphatidylcholine (PC) from egg yolk ($\geq 99\%$), cholesterol (99%), pentafluoropropionic acid ($\geq 97\%$), gentamicin sulfate ($\geq 590 \mu\text{g}$ Gentamicin base per mg), phosphate buffered saline (10 \times concentrate), iron (III) chloride hexahydrate ($\geq 99.9\%$), ammonium thiocyanate ($\geq 97.5\%$), Sephadex G-50 and Pluronic L31 and L61 were obtained from Sigma Aldrich (Sigma Aldrich Ltd, Gillingham, UK). Chloroform (HPLC grade $\geq 99.8\%$), methanol (HPLC grade $\geq 99.9\%$), sodium chloride, tryptone and tryptone soy broth were purchased from Fisher Scientific (Fisher Scientific UK, Loughborough, UK). Pluronic L43 was obtained from BASF Corp (BASF Corporation, USA). Palacos cements R and R+G were provided by Heraeus (Heraeus Medical, Newbury, UK). Fluorescent labelled phosphatidylcholine (18:1-06:0 NBD PC) was obtained from Avanti Polar Lipids (Avanti Polar Lipids, Alabama USA). *Staphylococcus aureus* (*S. aureus*, NCTC 10788) was used.

3.2.2 Liposome preparation

Liposomes and pellets were prepared as specified in Sections 2.1.2 and 2.1.3 respectively.

3.2.3 Cement preparation

Cements were prepared as per the method specified in Section 2.1.1.

3.2.4 Zeta potential and particle size

Particle size and zeta potential were performed using a Malvern Zetasizer NanoZS (Malvern Instruments Ltd, Worcestershire, UK), as specified in Section 2.2.

3.2.5 Contact angle measurement

Water contact angles were measured using the Attension contact angle analyser as specified in Sections 2.3.

3.2.6 Mechanical testing

All mechanical testing was performed using the methods specified in Section 2.4. The compressive strength, bending modulus and bending strength were tested as specified in Sections 2.4.1 and 2.4.2 and 2.4.3 respectively.

3.2.7 Release of antibiotic and lipids from cement discs

The methods for gentamicin and phospholipid release from the cement discs, as well as storage of the release samples is described in Section 2.1.4. Calculations for cumulative gentamicin released are also described in Section 2.1.4.

3.2.8 Stewart assay

The Stewart assay for determination of phosphatidylcholine content was carried out using the method specified in Section 2.5.

3.2.9 LC-MS

Gentamicin was assayed using LC-MS. Two LC-MS methods, using separate instruments (Thermo Spectra System P4000 and Bruker Amazon SL), as specified in Section 2.7.1 and 2.7.2 respectively, were used for the analysis of gentamicin. The method in Section 2.7.1 was developed as part of this study and the method in Section 2.7.2 is an in-house method for aminoglycoside antibiotics, currently used by the School of Chemistry at Cardiff University. Limits of quantification and limits of detection were established using signal-to-noise (S/N) ratios. S/N of at least 10 was accepted for the limit of quantification (British Pharmacopoeia, 2021), and a S/N of between at least 3 was considered acceptable for the limit of detection (ICH, 2005; Wang et al., 2019). The S/N ratio was calculated by injecting low concentrations of gentamicin to obtain chromatographic peaks, and using the following equation to calculate their signal-to-noise ratios (British Pharmacopoeia, 2021):

$$S/N = 2H/h$$

Where:

h is the height of the highest point from the maximum to the apex of the noise peaks, over a time equivalent to at least 5 times the width of the principal peak at half its height.

H is the height of the principal peak measured from its maximum to the extrapolated baseline of the noise peaks over a time equivalent to at least 5 times the width of the principal peak at half its height.

3.2.10 High performance liquid chromatography (HPLC) analysis of lipids

HPLC analysis was performed using a validated method used for the quantitative analysis of dipalmitoylphosphatidylcholine (DPPC) and related substances such as phosphatidylcholine (PC). Samples were injected on to the HPLC: Thermo Scientific UltiMate 3000 (Thermo Fisher Scientific, USA), using a Kinetex® 5µm C18 100 Å, LC Column 250 x 4.6 mm with SecurityGuard ULTRA Holder, maintained at 25 °C. Injection volume was 50 µl. The mobile phase was composed of premixed methanol/water (70/30). Elution was isocratic at a flow rate of 1 ml/min. A wavelength of 211 nm was used to detect phosphatidylcholine. Chromelion analyser software (Thermo Fisher Scientific, USA) was used for the data acquisition and analysis.

3.2.11 Determination of encapsulation efficiency

The determination of encapsulation efficiency was performed by separation of liposomes, using the Sephadex minicolumn centrifugation method (Fry et al., 1978). 10 g of Sephadex G50 (Sigma G50150) was left overnight at room temperature to swell in 120 ml of 0.9% w/v NaCl solution, then stored in a fridge. The plungers were removed from 5 ml syringes, and the base of the barrel was plugged with a piece of cotton wool which was surrounded on the top and bottom with 2 layers of Whatman GF/B filter paper which have been cut to size. The syringe was rested in a 15 ml falcon tube and filled to the top with Sephadex, and then centrifuged at 1800 rpm for 3 minutes. After centrifugation, the eluate was discarded. 1 ml of liposome solution was slowly injected onto the dehydrated Sephadex column using a pipette. The column was centrifuged at 1800 rpm for 3 minutes and the eluate containing liposomes with no unentrapped solution was stored at -20 °C for analysis by LC-MS.

3.2.12 Analysis of lipids using fluorescence spectrophotometry

Analysis of fluorescent lipid (18:1-06:0 NBD PC) was performed using a fluorescence spectrophotometer; Two separate methods were used for analysis of the fluorescent lipid. The first method in Section 2.8.1 was developed and validated for use of methanol as a diluent, and the second method in Section 2.8.2 was developed for use of chloroform as the diluent. Fluorescent labelled liposomes were prepared using 18:1-06:0 NBD PC. The

liposomes were prepared in the same way as in Section 2.1.2; however, 2% w/w of 18:1-06:0 NBD PC was incorporated into the formulation, with respect to the amount of total lipid.

3.2.13 Antimicrobial testing

Overnight cultures of *S. aureus* (NCTC 10788) were prepared as described in Section 2.9. All antimicrobial testing was carried out using the methods specified in Section 2.9. This includes sterilisation of glassware, media sterilisation, sample sterilisation; quantitative suspension tests, and analysis of biofilm formation.

3.2.14 Scanning electron microscopy

Scanning electron microscopy (SEM) was carried out using the method specified in Section 2.10.

3.2.13 Statistical analysis

Statistical analysis was performed as described in Section 2.11.

3.3 Results

3.3.1 Zeta potential and particle size of liposomes

Table 5 shows the average particle diameter and zeta potential of liposome samples. Average particle diameter is reported as the intensity average, since a unimodal distribution was observed for all samples. The mean diameter of the non-loaded liposomes was 113.2 ± 2.5 nm and 114.3 ± 0.98 nm for the gentamicin-loaded liposomes after extrusion through polycarbonate membranes. The mean surface zeta potentials for the non-loaded and gentamicin loaded liposomes were -2.3 ± 0.4 mV and 3.5 ± 1.0 mV respectively. The mean diameter of the NBD labelled liposomes was 107.9 ± 2.2 nm and the mean surface zeta potential of the fluorescent labelled liposomes was -14.1 ± 1.5 mV. Polydispersity index for all liposome preparations was between 0.05 and 0.12.

Table 5: Particle size (nm), Polydispersity index (PDI) and zeta potential measurements (mV) for gentamicin loaded liposomes, non-loaded liposomes and non-loaded NBD labelled liposomes. (n=3). Average particle diameter is reported as the intensity average, since a unimodal distribution was observed for all samples.

| Sample | Particle size (nm) | Polydispersity index (PDI) | Zeta Potential (mV) |
|-------------------------------------|--------------------|----------------------------|---------------------|
| Non-loaded liposomes | 113.2 ± 2.5 | 0.09 ± 0.02 | -2.3 ± 0.4 |
| Gentamicin loaded liposomes | 114.3 ± 0.98 | 0.05 ± 0.03 | 3.5 ± 1.0 |
| NBD labelled liposomes (non-loaded) | 107.9 ± 2.2 | 0.12 ± 0.02 | -14.1 ± 1.5 |

3.3.2 Contact angle measurement

Figure 13 shows the different contact angles obtained for Palacos R, Palacos R+G, LCP-CEMENT and Palacos R + G discs containing different amounts of pluronics (L31, L43 and L61). Palacos R, which is PMMA cement with no gentamicin added, had the highest contact angle ($116 \pm 0.8^\circ$), followed by LCP-CEMENT ($115 \pm 3.9^\circ$). Palacos R+G had a much lower contact angle ($98 \pm 0.8^\circ$). The Palacos R+G cements containing various Pluronic of differing percentages (1% w/w, 5% w/w and 10% w/w) showed consistent contact angles across the Pluronic range tested. The much higher percentage of 10% w/w for all Pluronic (L31, L43 and L61) resulted in lower contact angles than Palacos R. 1% w/w and 5% w/w for all Pluronic (L31, L43 and L61) did not appear to significantly affect the contact angle with respect to Palacos R, as was the case with all Pluronic at these two concentrations ($p > 0.05$). The lowest contact angle for the Pluronic samples was for 10% Pluronic L61. With respect to Palacos R, only Palacos R+G and all of the 10% w/w Pluronic samples (L31, L43 and L61) showed a significant reduction in contact angle ($p = 0.0177$, $p = 0.0003$, 0.0088 and $p < 0.0001$ respectively). Only LCP-CEMENT, Palacos R and L61 5% cement discs showed a significant difference with respect to Palacos R+G, ($p = 0.0177$, $p = 0.0250$ and $p = 0.0413$ respectively).

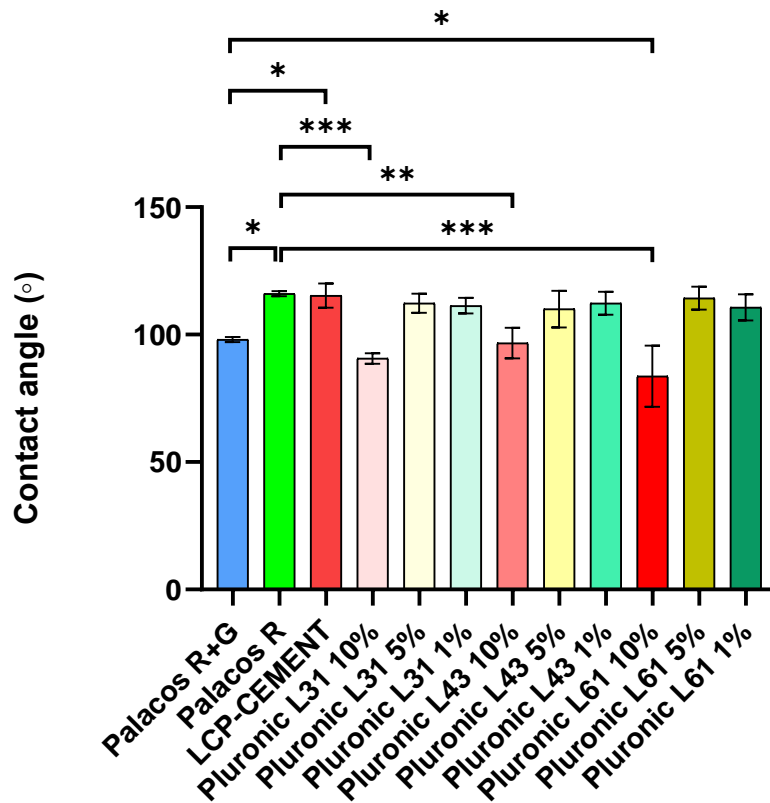


Figure 13: Contact angle measurements for commercial cements Palacos R and Palacos R+G, LCP-CEMENT, commercial R+G cement containing different Pluronic concentrations ranging from 1 – 10% w/w. (n=3). Asterisks indicate the level of significance (* p<0.05, ** p<0.01, * p<0.001).**

3.3.3 Mechanical properties

Mechanical testing was performed as per the requirements of ISO 5833: compressive strength, bending modulus and bending strength (ISO 5833, 2002). As required by the standard, testing was performed using five separate cement sample preparations (n=5).

3.3.3.1 Compressive strength

The compressive strengths of Palacos R, Palacos R+G and LCP-CEMENT prepared and left for 24 hours in air are shown in Figure 14. Palacos R showed the highest compressive strength of 81 ± 4 MPa, followed by Palacos R+G which had a compressive strength of 73 ± 2 MPa. Both Palacos R and R+G were above the ISO 5833 limit for of 70 MPa. LCP-CEMENT had a compressive strength of 67 ± 5 MPa which was just under the ISO 5833

limit. With respect to Palacos R, Palacos R+G was not significantly lower ($p=0.1221$) whereas LCP-CEMENT showed a significant reduction in compressive strength ($p= 0.0129$).

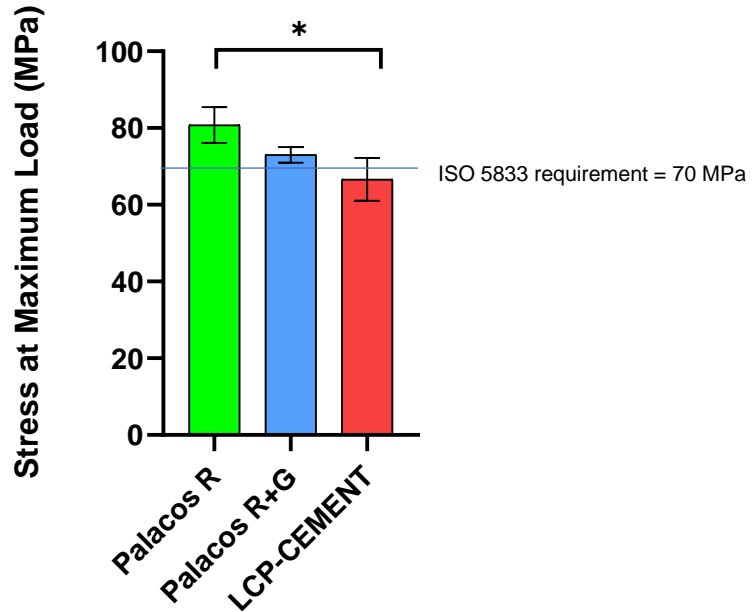


Figure 14: Compressive strength results for Palacos R and Palacos R+G and LCP-CEMENT. Data is presented as mean \pm standard deviation ($n=5$). Asterisks indicate the level of significance (* $p<0.05$, ** $p<0.01$, * $p<0.001$).**

3.3.3.2 Bending Modulus

The bending modulus of Palacos R, Palacos R+G and LCP-CEMENT prepared and left for 24 hours in air are shown in Figure 15. Palacos R showed the highest bending modulus of 3163 ± 51 MPa, followed by Palacos R+G which had a bending modulus of 3101 ± 54 MPa and then LCP-CEMENT which had a bending modulus of 2991 ± 69 MPa. All samples were above the ISO 5833 limit of 1800 MPa. With respect to Palacos R, Palacos R+G was not significantly different ($p=0.2541$), whereas LCP-CEMENT showed a significant reduction in bending modulus ($p=0.0024$).

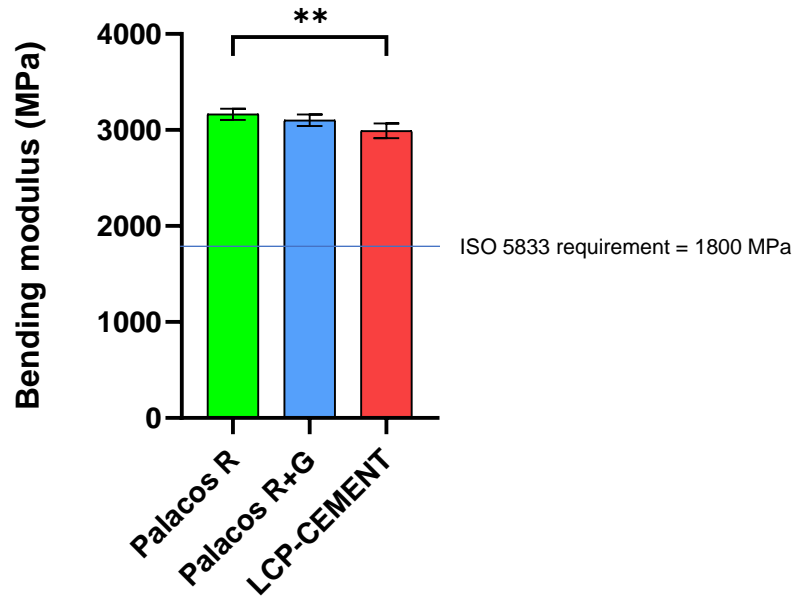


Figure 15: Bending modulus results for Palacos R and Palacos R+G and LCP-CEMENT. Data is presented as mean \pm standard deviation ($n=5$). Asterisks indicate the level of significance (* $p<0.05$, ** $p<0.01$, * $p<0.001$).**

3.3.3.3 Bending Strength

The bending strength of Palacos R, Palacos R+G and LCP-CEMENTS prepared and left for 24 hours in air are shown in Figure 16. Palacos R had the highest bending strength of 82 ± 7 MPa, followed by LCP-CEMENT which had a bending strength of 74 ± 7 MPa and then Palacos R+G which had a bending strength of 63 ± 5 MPa. All samples were above the ISO 5833 limit of 50 MPa for bending strength. With respect to Palacos R, bending strength for LCP-CEMENT was not significantly lower ($p=0.2335$) whereas Palacos R+G showed a significant reduction ($p=0.0035$).

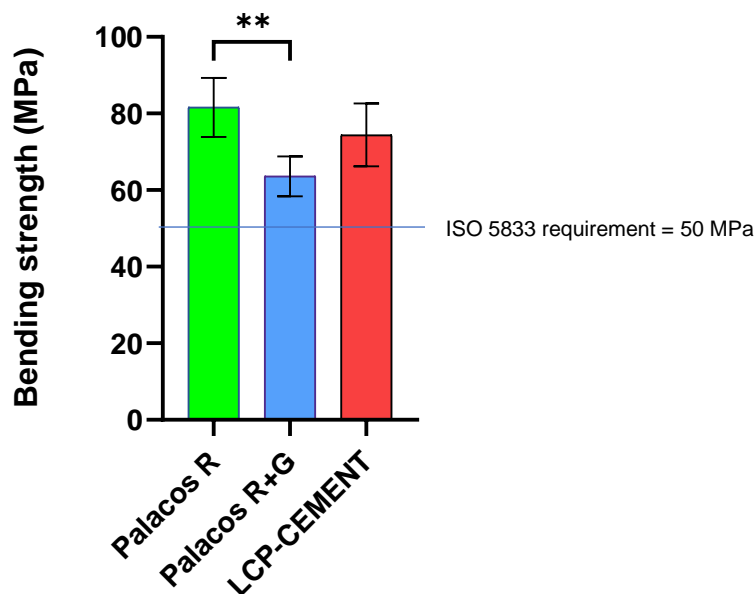


Figure 16: Bending strength results for Palacos R and Palacos R+G and LCP-CEMENT. Data is presented as mean \pm standard deviation ($n=5$). Asterisks indicate the level of significance (* $p<0.05$, ** $p<0.01$, * $p<0.001$).**

3.3.4 LC-MS method optimisation (Thermo Spectra System P4000)

Figure 17 shows clear identifiable peaks observed for gentamicin base at high concentrations of gentamicin (60 $\mu\text{g/ml}$) and at the lower concentration (3 $\mu\text{g/ml}$). The retention time was approximately 5-7 minutes, and no interfering peaks were observed.

Figure 18 shows linearity of the different injections of gentamicin at different concentrations. An R^2 value of 0.995 shows that a strong linear correlation was observed between the gentamicin and the mass-spectrometer detector at single ion monitoring mode for m/z 478.30, using concentrations between 3 $\mu\text{g/ml}$ to 60 $\mu\text{g/ml}$ of gentamicin base (Figure 17). Six replicate injections of 5 $\mu\text{g/ml}$ were injected (Table 6) showing injection repeatability by calculating the percentage relative standard deviation (% RSD) of peak areas. This was found to be 4.7%, which is below the limit of 5% as recommended by ICH (Pinto et al., 2017). Figure 19 shows the signal to noise ratios calculated for the limits of quantification and detection (LOQ and LOD). LOD and LOQ were determined as 1 $\mu\text{g/ml}$ and 3 $\mu\text{g/ml}$ respectively (Table 7).

It is worth noting that for effective release of antibiotic from an implant, a concentration above its minimum inhibitory concentration (MIC) is required to provide protection against

infection (S. Dukhin & Labib, 2012). The MIC of an antimicrobial agent, expressed in mg/L ($\mu\text{g/ml}$), is defined as the lowest concentration that will inhibit visible growth of an organism, after overnight incubation (Andrews, 2001; Kowalska-Krochmal & Dudek-Wicher, 2021). The MIC of gentamicin sulfate required to inhibit bacteria growth of *S. aureus* is 0.0125 mg/ml (12.5 $\mu\text{g/ml}$) (Figuroa et al., 2008). The LOQ for gentamicin should be a lower concentration than the MIC value, so that lower quantities (equivalent to the MIC value or lower) of gentamicin sulfate released from bone cement can be quantified and compared to the MIC value. Concentrations that are lower than the MIC value are termed sub-inhibitory concentrations. The LOD, which is the lowest concentration of released gentamicin that can be detected, is used for confirmation of low, sub-inhibitory levels of drug release, rather than for quantification purposes.

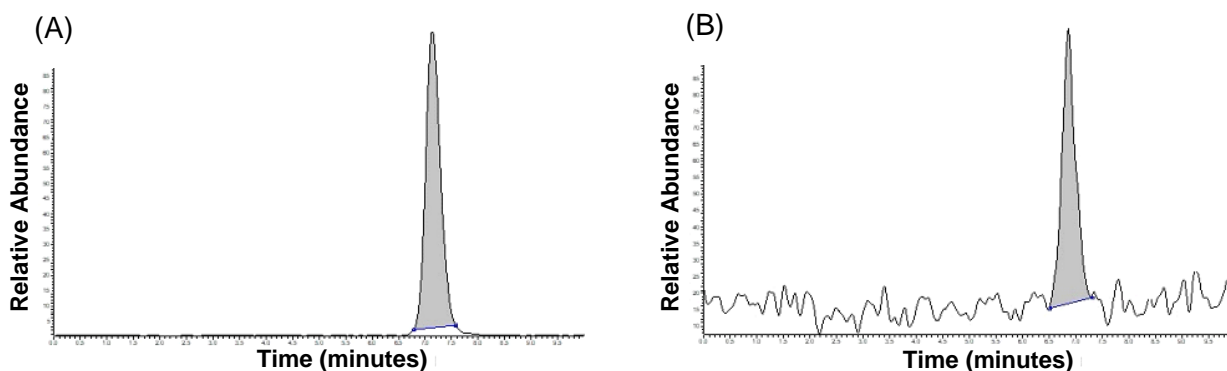


Figure 17: Examples of gentamicin peaks for concentrations of (A) 3 $\mu\text{g/ml}$ (LOQ) and (B) 60 $\mu\text{g/ml}$ (upper quantification limit), showing clear identifiable peaks at retention time of around 7 minutes.

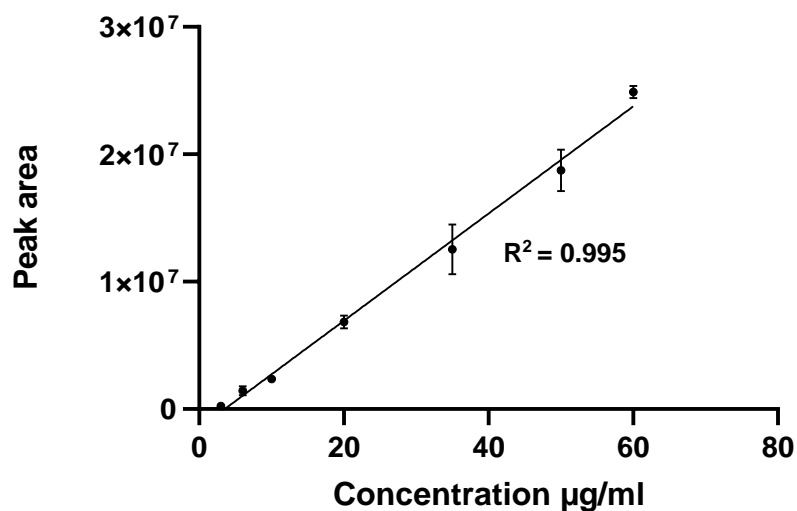


Figure 18: Calibration curve of gentamicin base by the LC-MS method (Thermo Spectra System P4000) for concentrations ranging from 3 µg/ml (LOQ) to 60 µg/ml (upper quantification limit) (n=3). R² (>0.99) is deemed acceptable (Pinto et al., 2017).

Table 6: %RSD of the gentamicin peak areas for repeat injections of 5 µg/ml gentamicin (n=6). %RSD of <5% is deemed acceptable (Pinto et al., 2017).

| Injection | Peak area |
|-------------|-----------|
| Injection 1 | 518554 |
| Injection 2 | 493978 |
| Injection 3 | 490772 |
| Injection 4 | 540044 |
| Injection 5 | 559397 |
| Injection 6 | 511474 |
| mean | 519036 |
| SD | 22534 |
| % RSD | 4.7 |

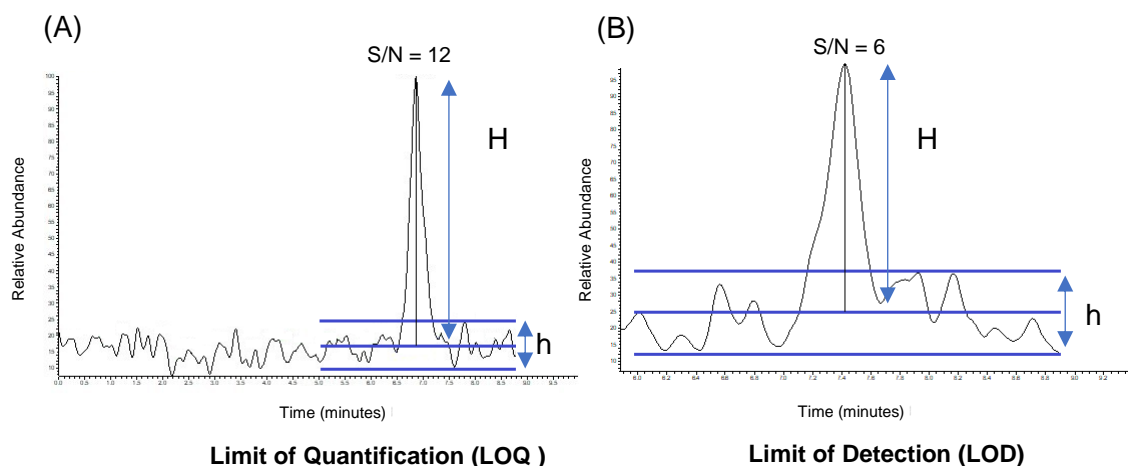


Figure 19: Chromatograms showing (A) LOQ and (B) LOD, using concentrations of 3 µg/ml (LOQ) and 1 µg/ml (LOD). Signal-to-noise ratios of at least 3 and 10 were deemed acceptable for the limits of detection and quantification respectively (Wang et al., 2019).

Table 7: Signal-to-noise ratios for validation of method (Thermo Spectra System P4000). LOQ (3 µg/ml) and LOD (1 µg/ml) (n=3).

| Gentamicin concentration (µg/ml) | 3 Replicates | | | Mean S/N |
|----------------------------------|--------------|-----|-----|----------|
| | S/N | S/N | S/N | |
| 3 | 12 | 10 | 10 | 11 |
| 1 | 6 | 5 | 4 | 5 |

3.3.4.1 Encapsulation efficiency of gentamicin in liposomes

Following separation and lysis of the liposomes (n=3), encapsulated gentamicin was assayed by LC-MS. The encapsulation efficiency of gentamicin was determined as 14.7 ± 2.6 % using the following equation:

$$\text{Encapsulation Efficiency (\%)} = \frac{\text{Amount of gentamicin in liposomes}}{\text{Initial amount of gentamicin loaded}} \times 100$$

3.3.4.2 Antibiotic release from liposomal and commercial bone cements

The initial mass quantity of gentamicin release for LCP-CEMENT was $267.1 \pm 14.7 \mu\text{g}$ in the first 48 hours, rising to $496.6 \pm 13.6 \mu\text{g}$ at 3200 hours (4.5 months). The Palacos R+G cement released $470.5 \pm 7.7 \mu\text{g}$ at 48 hours and $822.4 \pm 9.6 \mu\text{g}$ at 3200 hours (4.5 months) (Figure 20 and Figure 21). An unpaired t-test was performed to compare the means of the cumulative mass quantities of gentamicin released at different time points: at 6 hours, there was a significantly higher mass quantity of gentamicin released from Palacos R+G than LCP-CEMENT ($p < 0.0001$); at 720 hours (1 month), Palacos R+G released a significantly higher mass quantity of gentamicin than LCP-CEMENT ($p < 0.0001$); and at 3200 hours (4.5 months), Palacos R+G released a significantly higher mass quantity of gentamicin than LCP-CEMENT ($p < 0.0001$).

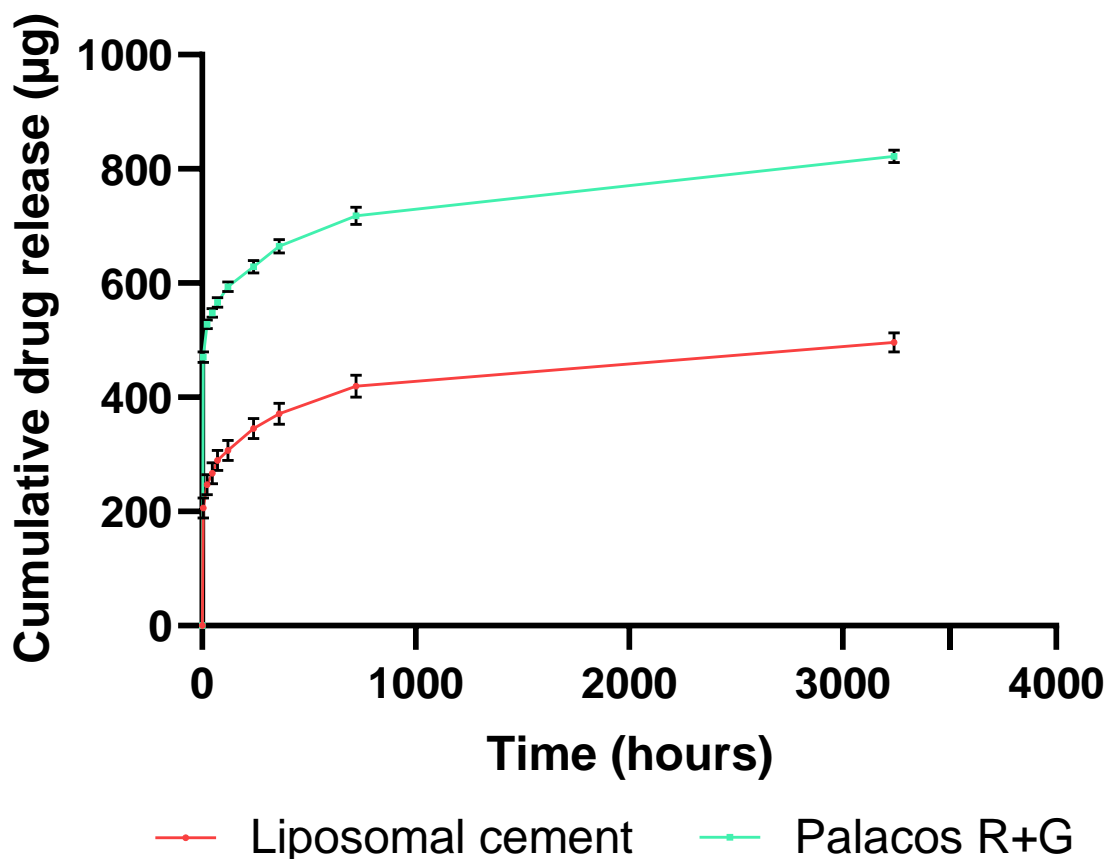


Figure 20: Cumulative drug release of GS (μg) from PMMA bone cement stored in PBS solution (pH 7.4, 37°C) at different time points (0 to 3240 hours). Error bars indicate standard deviation from the mean of experimental data performed in triplicate ($n=3$).

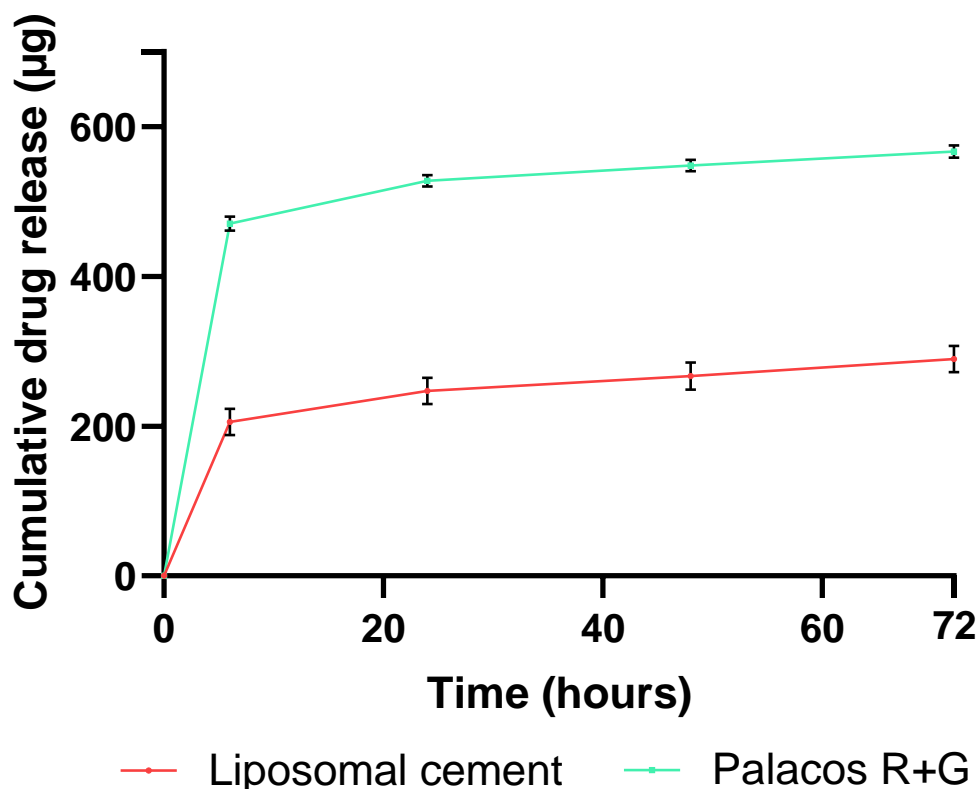


Figure 21: Cumulative drug release of GS (μg) from PMMA bone cement stored in PBS solution (pH 7.4, 37 °C) from time points 0 to 72 hours. Error bars indicate standard deviation from the mean of experimental data performed in triplicate ($n=3$).

3.3.4.3 Antibiotic release from Palacos R+G containing different incorporated percentages of Pluronic L31, L43 and L61

The LC-MS method using the Bruker Amazon SL ion trap mass spectrometer described in 2.7.2 was used to analyse the samples containing different amounts of Pluronics. Validation parameters were investigated according to the ICH Q2 guidelines (ICH, 2005), such as, specificity, linearity, range, accuracy, and LOD and LOQ, to confirm its suitability as an analytical method for PMMA bone cement samples. Linearity was demonstrated by an R^2 value of 0.997, showing that a strong linear correlation was observed between gentamicin and the mass-spectrometer detector at single ion monitoring mode for m/z 478.30, using concentrations within the range of 1 $\mu\text{g}/\text{ml}$ to 120 $\mu\text{g}/\text{ml}$ of gentamicin base (Figure 22). Specificity was assessed by injecting the diluent (PBS), a solution of PBS of which Palacos R disc had been stored in for one week at 37 °C, and solutions containing 1% w/v of

Pluronic L31, L43 and L61 in PBS at pH 7.4; none of which caused any interfering peaks to be observed. Limits of detection and quantification were determined as 0.5 µg/ml and 1 µg/ml respectively.

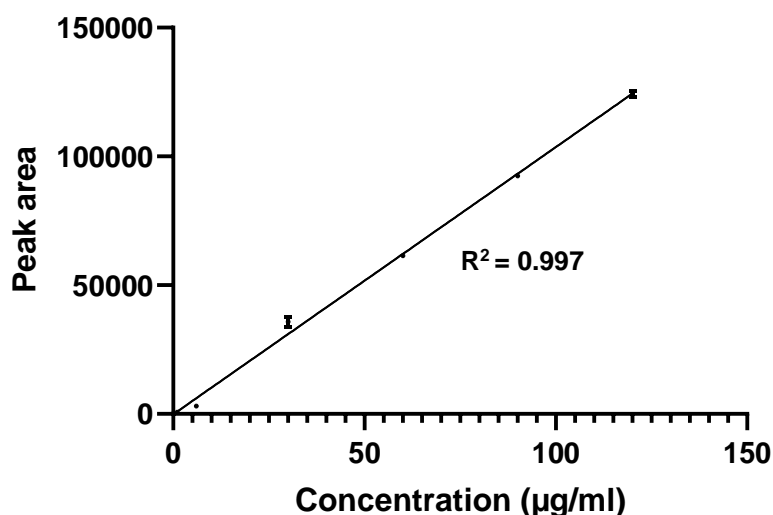


Figure 22: Calibration curve for gentamicin base determination, by LC-MS method (Bruker Amazon SL) for concentrations ranging from 1 µg/ml (LOQ) to 120 µg/ml (upper quantification limit) (n=3). R^2 (>0.99) is deemed acceptable (Pinto et al., 2017).

The Pluronic samples released different mass quantities of gentamicin at the start of elution, as measured at the first time point, but also as measured at the final time point, 2160 hours (3 months) (Figure 23 and Figure 24). Overall, the highest releasing cement discs were L43 10% (1273 ± 212.3 µg), L43 5% (1091 ± 204.5 µg) and L31 5% (1010 ± 168.8 µg). The lowest releasing cement discs overall were L61 10% (476.3 ± 119.9 µg), L31 10% (476.7 ± 147.2 µg), L61 5% (535.8 ± 72.4 µg) and L31 1% (544.8 ± 222.4 µg). In this experiment Palacos R+G released a cumulative gentamicin mass quantity of 747.8 ± 203.9 µg at the final time point 2160 hours (3 months). At 12 hours, Palacos R+G released 632.4 ± 237.9 µg gentamicin, meaning that Palacos R+G had the smallest difference in gentamicin release between those time points (115.4 µg), compared to all the Pluronic cement discs (Table 8). It is worth noting that with the exception of L43 1%, L61 1% and L61 5%, standard deviations range between 119.9 and 222.4 at time point 2160 hours. Standard deviations for L43 1%, L61 1% and L61 5% are 58.7 µg, 28.0 µg and 72.4 µg respectively, indicating more consistent mass release amongst cements from those groups. At the 2160 hours (3 months) time point, all cement discs containing Pluronic were not significantly different to Palacos R+G ($p > 0.05$).

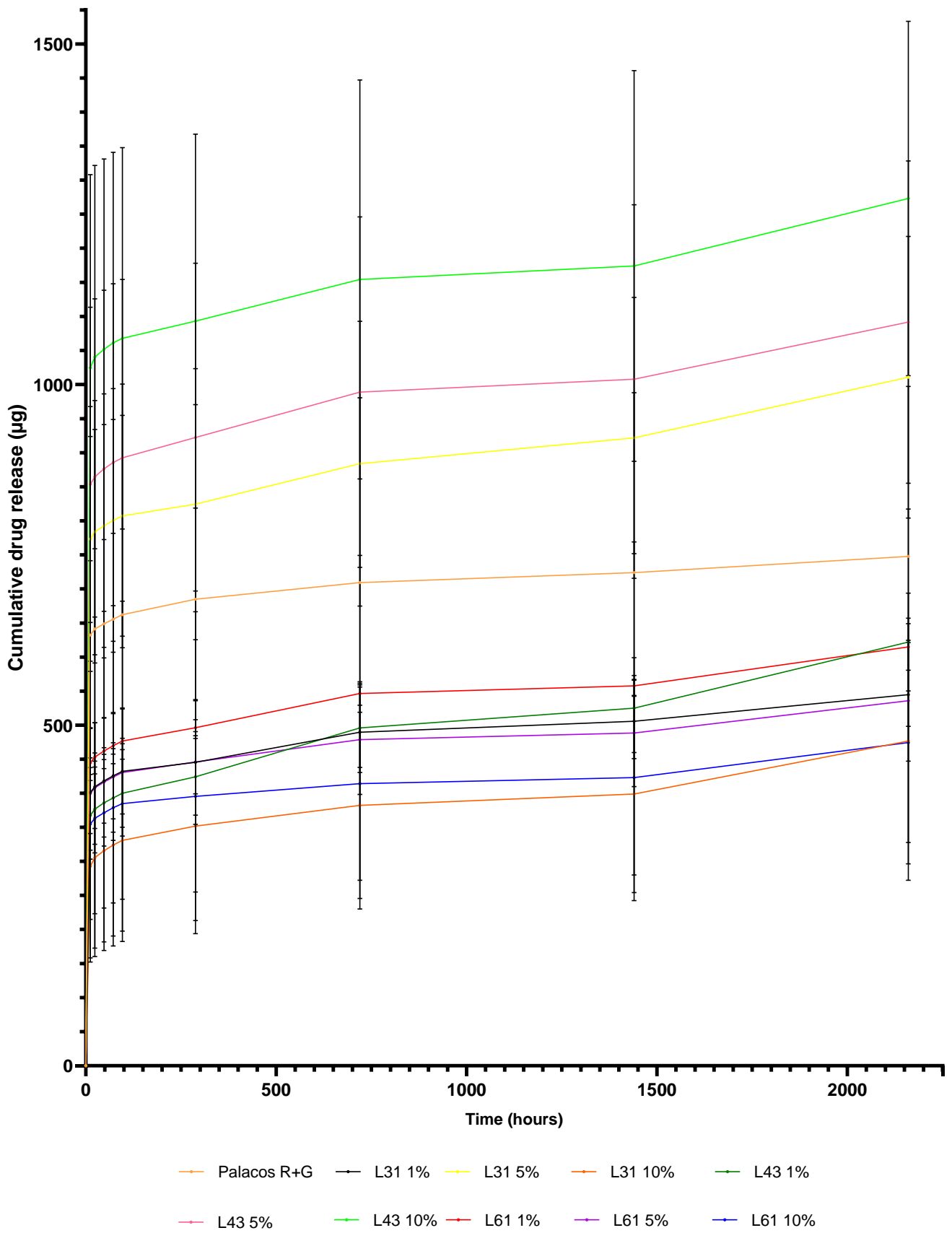


Figure 23: Cumulative drug release of GS (μg) from PMMA bone cement samples containing different incorporated percentages of Pluronic L31, L43 and L61 all stored in PBS solution (pH 7.4, 37 °C) from time points 0 to 2160 hours. (n=3).

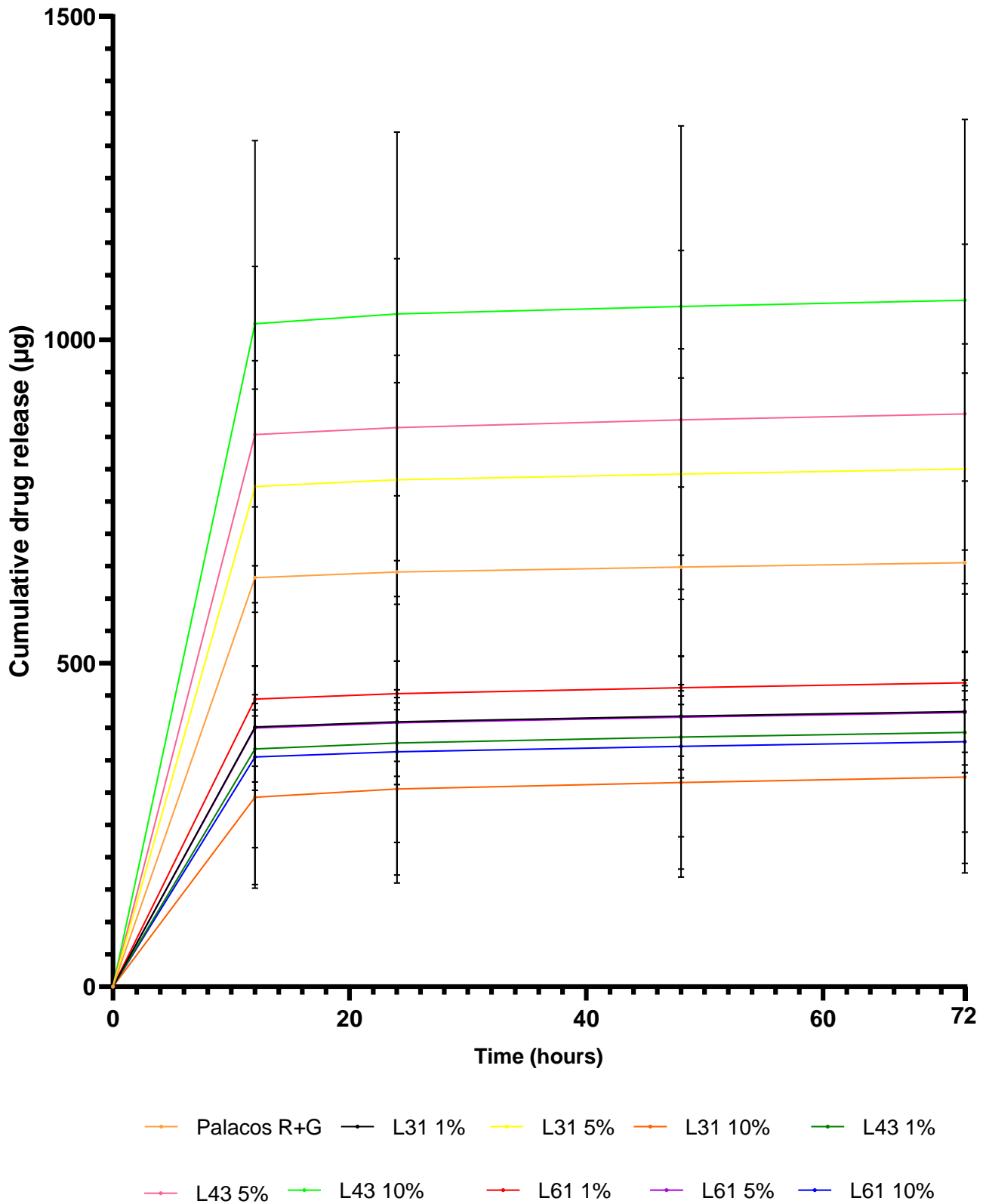


Figure 24: Cumulative drug release of GS (μg) from PMMA bone cement samples containing different incorporated percentages of Pluronic L31, L43 and L61 all stored in PBS (pH 7.4, 37 °C) from time point 0 to 72 hours. (n=3). Note that lines for two sets of data (L31 1% and L61 5%) are indistinguishable from one another at these times points.

Table 8: Difference in mass quantity of gentamicin released (μg), between 12 hours and 2160 hours (3 months), for each sample (Palacos R+G, all cements containing Pluronic L31, L43 and L61).

| Sample | Drug release at 12 hours (μg) | Drug release at 2160 hours (μg) | Difference in drug release mass quantity (12 to 2160 hours) (μg) |
|---------|--|--|---|
| R+G | 632.4 \pm 237.9 | 747.8 \pm 203.9 | 115.4 |
| L31 1% | 401.6 \pm 203.6 | 544.8 \pm 222.4 | 143.2 |
| L43 1% | 367.6 \pm 41.8 | 622.0 \pm 58.7 | 254.4 |
| L61 1% | 444.9 \pm 5.8 | 614.7 \pm 28.0 | 169.9 |
| L31 5% | 773.2 \pm 158.8 | 1010.7 \pm 168.8 | 237.5 |
| L43 5% | 853.7 \pm 212.2 | 1091.6 \pm 204.5 | 237.9 |
| L61 5% | 399.9 \pm 78.7 | 535.8 \pm 72.4 | 136.0 |
| L31 10% | 292.8 \pm 110.1 | 476.7 \pm 147.2 | 183.8 |
| L43 10% | 1024.8 \pm 231.3 | 1273.1 \pm 212.3 | 248.3 |
| L61 10% | 355.1 \pm 114.6 | 474.3 \pm 119.9 | 119.2 |

3.3.5 Antimicrobial testing

Antimicrobial efficacy was assessed by using a quantitative suspension test. Cement discs were incubated for 4 hours, at 37 °C in a suspension of *S. aureus*. After 48 hours, cement discs were vortexed with glass beads to dislodge any microbial biofilm attachment which may have formed on the discs.

3.3.5.1 Quantitative suspension test

Results from the antimicrobial quantitative suspension test are shown in Figure 25. All samples tested showed some level of efficacy in reducing *S. aureus* bacteria count. The starting bacteria count in solution was 1×10^6 colony forming units per mL (CFU/ml). Components of the cement formulations were also tested individually. A quantity of 0.01 g of gentamicin sulfate was found to kill all *S. aureus* bacteria (0 CFU/ml); two quantities of methyl methacrylate (MMA) were tested (0.01 g and 0.1 g), both quantities caused a reduction in bacteria count: 0.01 g MMA (2.7×10^5 CFU/ml) and 0.1 g MMA (9×10^4 CFU/ml)

(Figure 26). Palacos R was the least effective cement sample, resulting in 2.8×10^5 CFU/ml. Palacos R+G was the most effective sample resulting in 1.1×10^5 CFU/ml. The Pluronic samples all resulted in around 2×10^5 CFU/ml with the exception of Pluronic L61 1% sample which resulted in 2.4×10^5 CFU/ml. Compared to Palacos R+G, all samples were significantly different ($p < 0.05$), except for Pluronic L31 5% w/w which showed no significant difference ($p > 0.1167$).

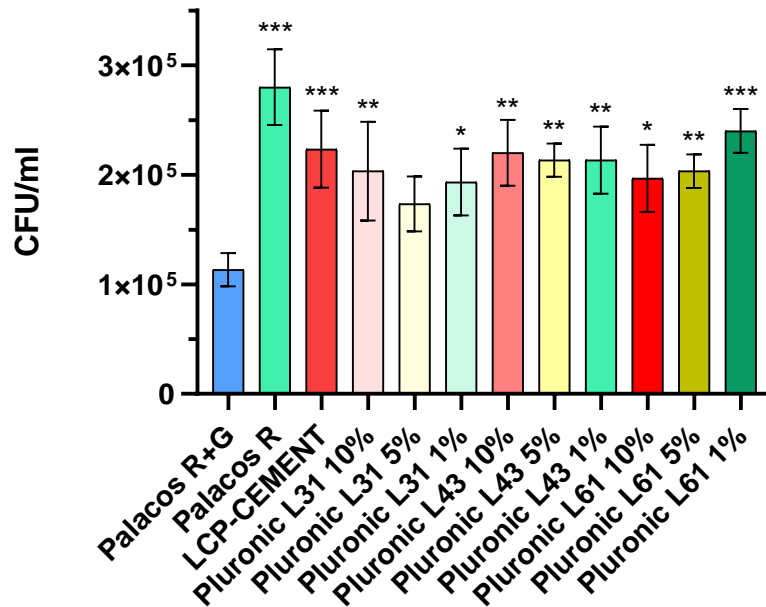


Figure 25: Colony forming units (CFU) for samples after 4 hours contact with *S. aureus* cultures in TSB at 37 °C (n=3). Asterisks indicate the level of significance with respect to Palacos R+G (* $p < 0.05$, ** $p < 0.01$, * $p < 0.001$).**

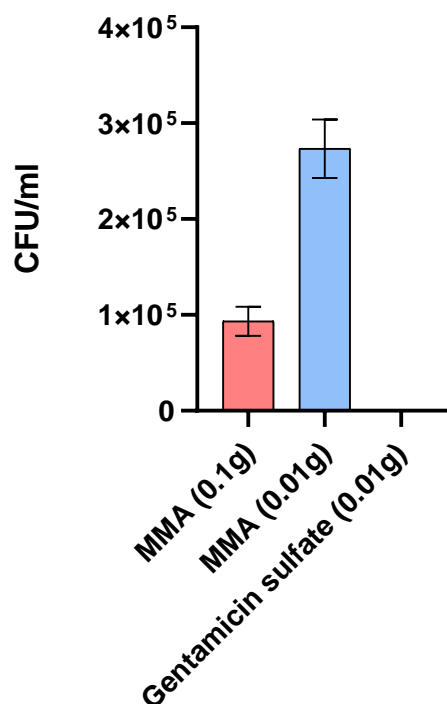


Figure 26: Colony forming units (CFU) for 0.01 g GS, 0.01 g and 0.1 g of MMA after 4 hours contact with *S. aureus* cultures in TSB at 37 °C (n=3).

3.3.5.2 Analysis of biofilm formation

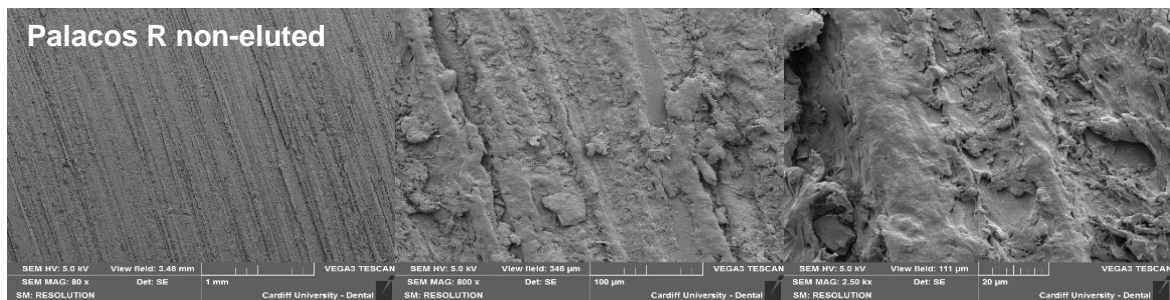
The cement discs stored in inoculum were removed after 48 hours, vortexed with glass beads and sonicated to dislodge any biofilm formed around the cement discs. Any dislodged *S. aureus* biofilm was allowed to regrow on plates. For all cement discs tested, no colony forming units were observed after incubation of the agar plate for 18 hours (0 CFU/ml for all samples), meaning that *S. aureus* was not detected.

3.3.6 Scanning electron microscopy (SEM) of cement disc surface

SEM was used to characterise all of the cement disc formulations' surface morphology after manufacture; moreover, the discs were also analysed to see the difference in surface morphology before and after incubation in PBS for one week. Figures 27 to 38 show SEM images, at magnifications of 80, 800 and 2.5k, for Palacos R, Palacos R+G, LCP-CEMENT, Palacos L31 (1%, 5% and 10%), Palacos L43 (1%, 5% and 10%) and Palacos L61 (1%, 5% and 10%). All cement discs were imaged as freshly prepared cement discs (non-eluted) and

imaged after an incubation period in PBS at 37 °C for one week (eluted). When prepared freshly, all cement discs, with the exception of Palacos R, showed large air-pockets/pores present on the surfaces. It can also be seen with all of the samples with the exception of Palacos R, that there are fused round PMMA particles on the solid sample surfaces, which are approximately 20 µm in diameter. Examples of fused PMMA particles and pores are shown with orange and blue arrows on the images. For all eluted cement discs, it was not possible to observe any significant pore formation compared to the eluted cement discs. This indicates that water does not significantly penetrate bone cement.

(A)



(B)

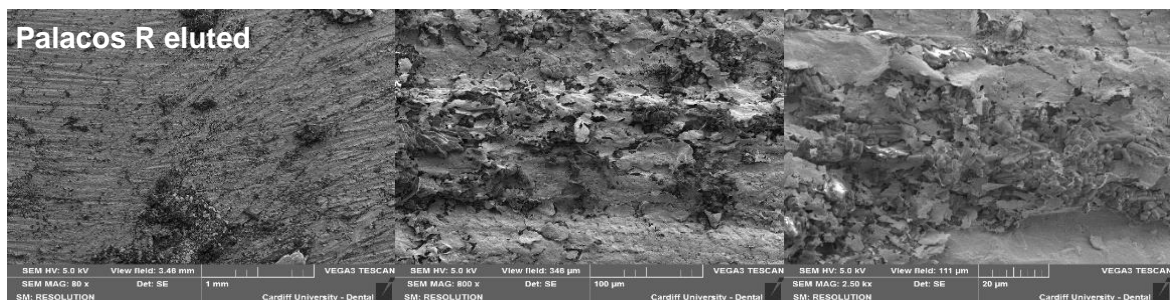
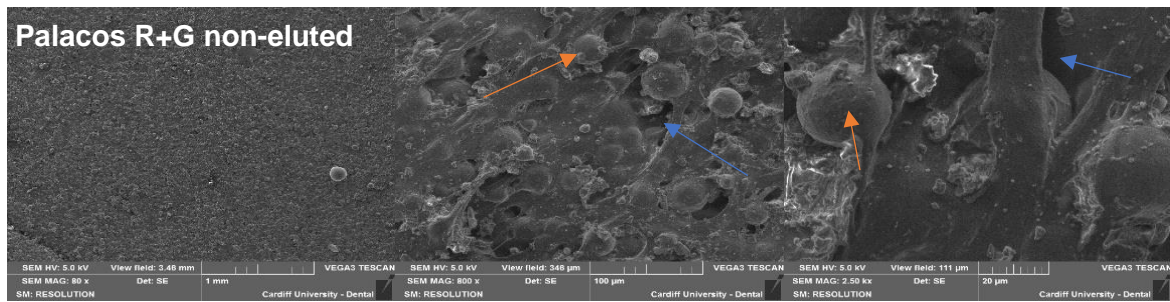


Figure 27: SEM surface images of Palacos R samples (A) before and (B) after incubation in PBS for one week at 37 °C; sample magnifications are x80, x800 and x2.5k respectively.

(A)



(B)

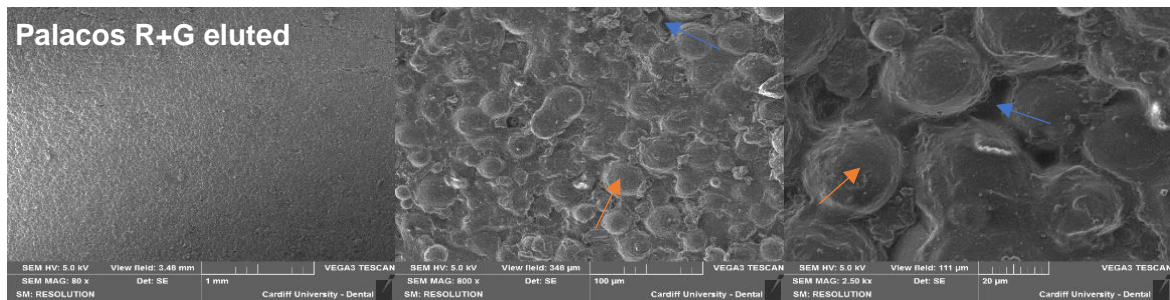
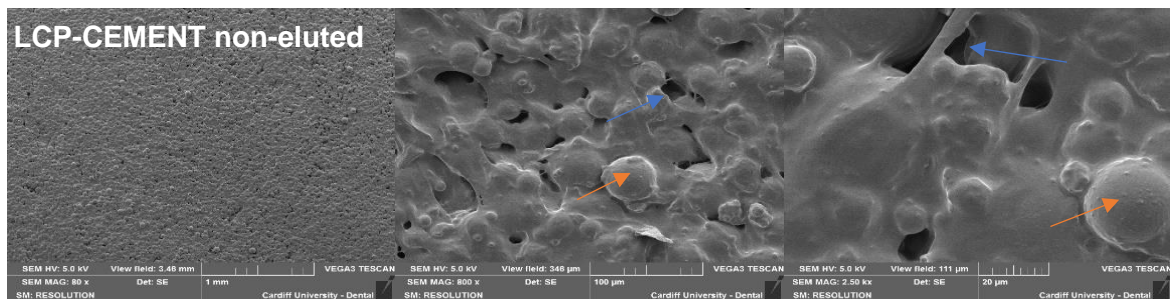


Figure 28: SEM surface images of Palacos R+G samples (A) before and (B) after incubation in PBS for one week at 37 °C; sample magnifications are x80, x800 and x2.5k respectively. Arrows indicate PMMA particles (orange) and pores (blue).

(A)



(B)

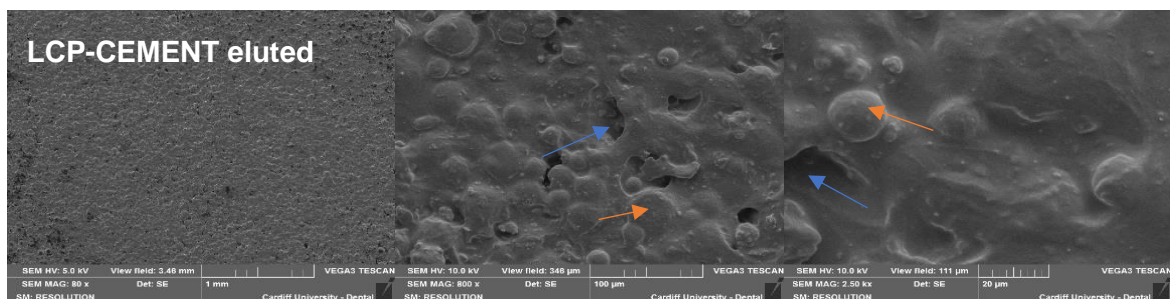
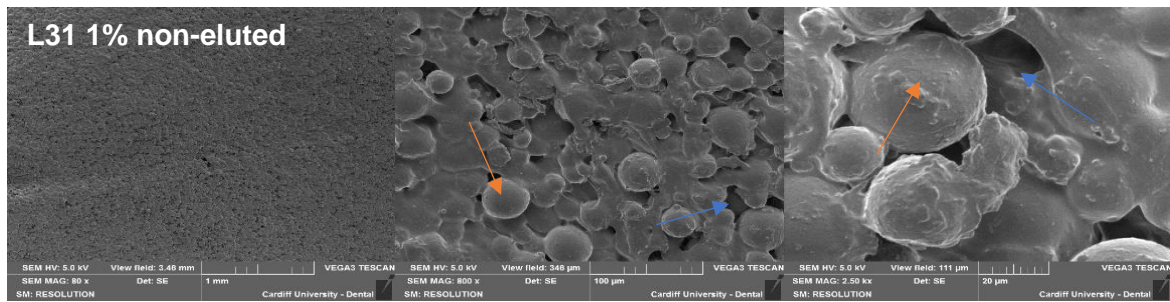


Figure 29: SEM surface images of LCP-CEMENT samples (A) before and (B) after incubation in PBS for one week at 37 °C; sample magnifications are x80, x800 and x2.5k respectively. Arrows indicate PMMA particles (orange) and pores (blue).

(A)



(B)

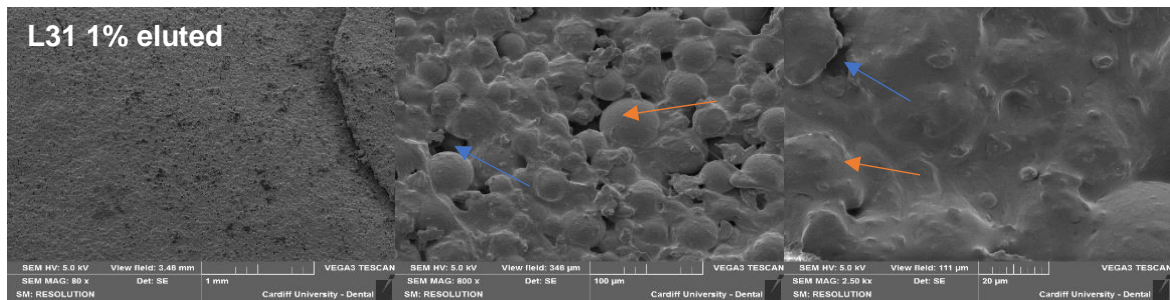
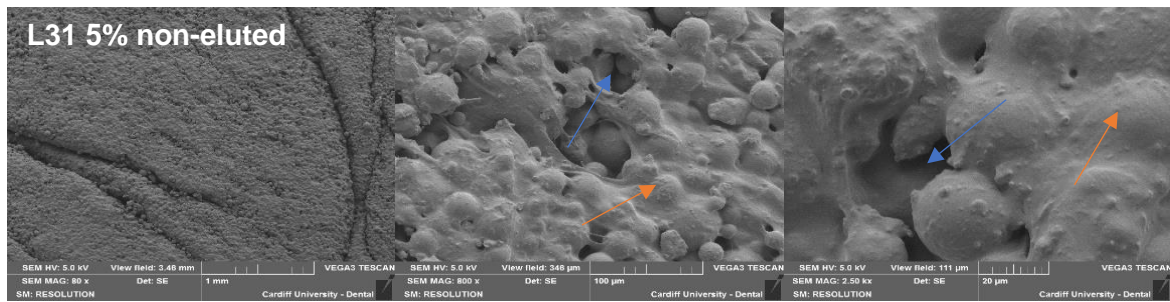


Figure 30: SEM surface images of Palacos R+G cement samples containing 1% w/w of Pluronic L31 (A) before and (B) after incubation in PBS for one week at 37 °C; sample magnifications are x80, x800 and x2.5k respectively. Arrows indicate PMMA particles (orange) and pores (blue).

(A)



(B)

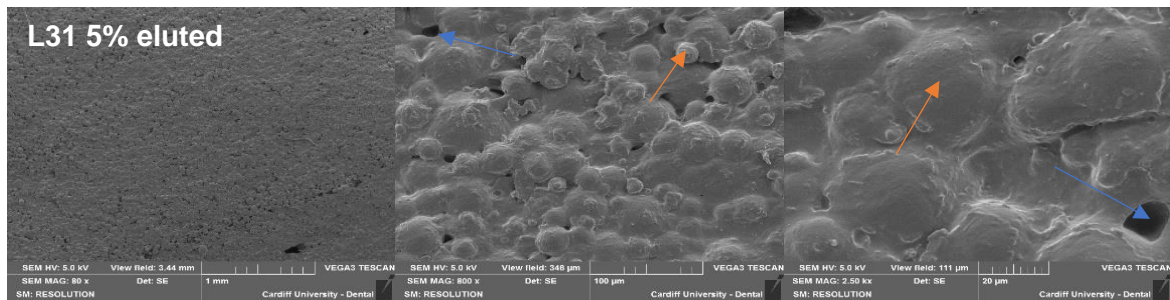
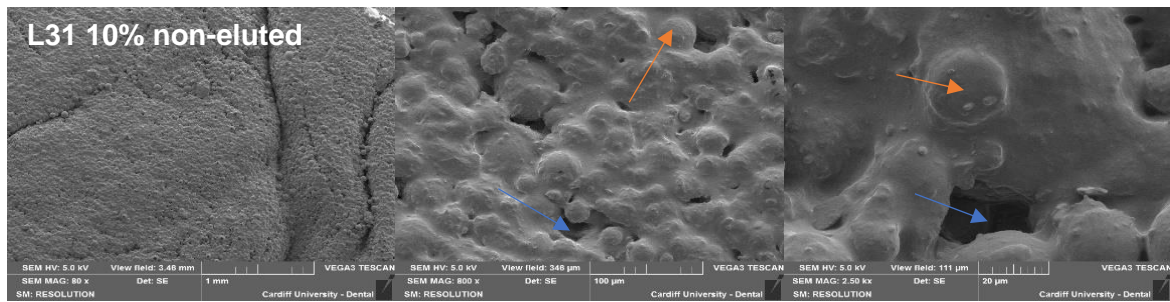


Figure 31: SEM surface images of Palacos R+G cement samples containing 5% w/w of Pluronic L31 (A) before and (B) after incubation in PBS for one week at 37 °C; sample magnifications are x80, x800 and x2.5k respectively. Arrows indicate PMMA particles (orange) and pores (blue).

(A)



(B)

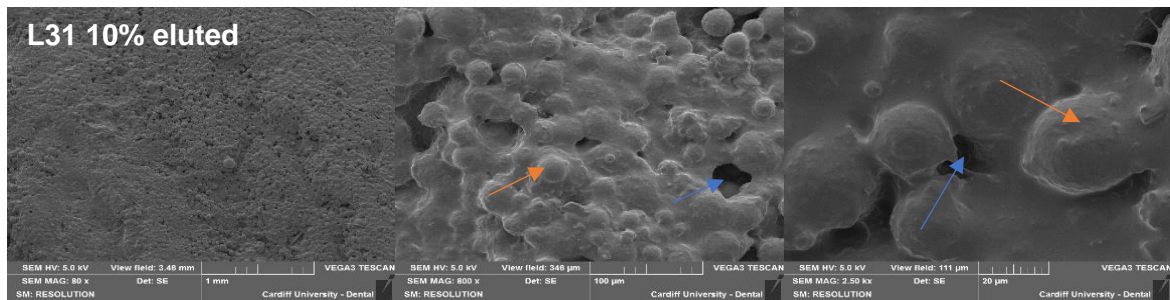
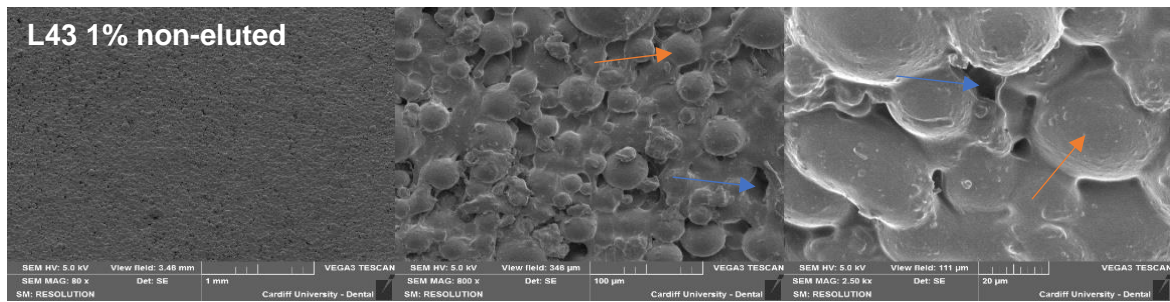


Figure 32: SEM surface images of Palacos R+G cement samples containing 10% w/w of Pluronic L31 (A) before and (B) after incubation in PBS for one week at 37 °C; sample magnifications are x80, x800 and x2.5k respectively. Arrows indicate PMMA particles (orange) and pores (blue).

(A)



(B)

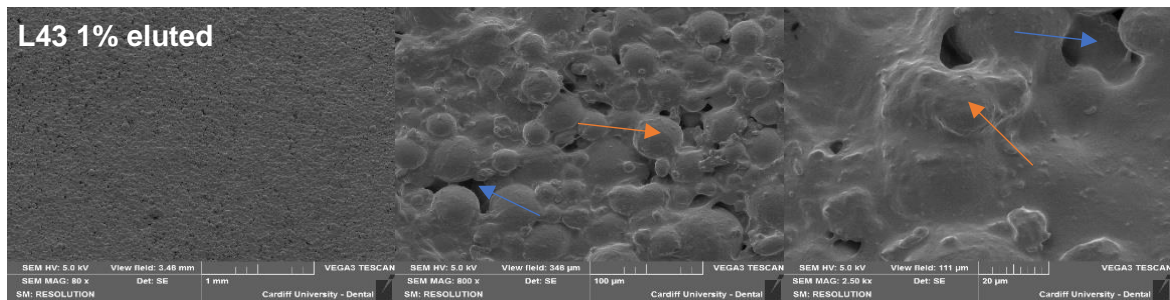
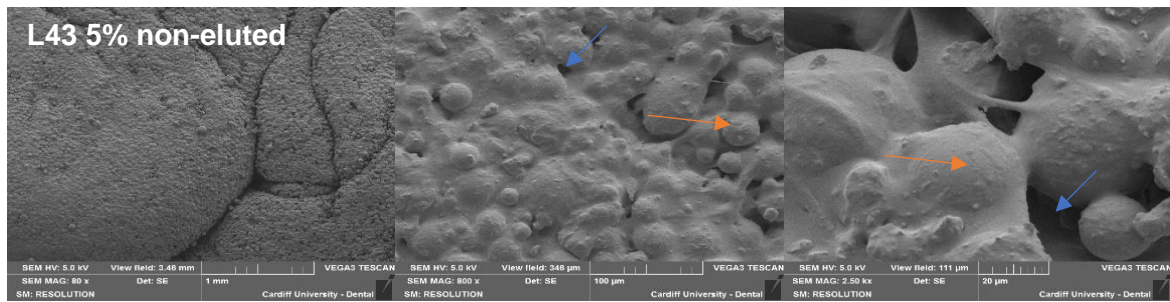


Figure 33: SEM surface images of Palacos R+G cement samples containing 1% w/w of Pluronic L43 (A) before and (B) after incubation in PBS for one week at 37 °C; sample magnifications are x80, x800 and x2.5k respectively. Arrows indicate PMMA particles (orange) and pores (blue).

(A)



(B)

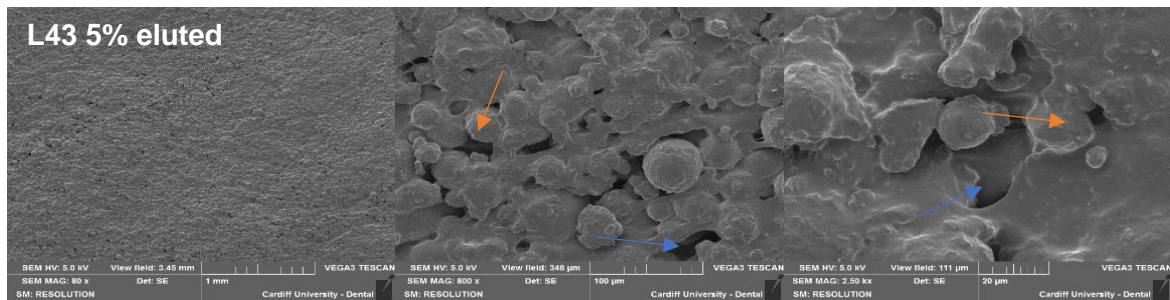
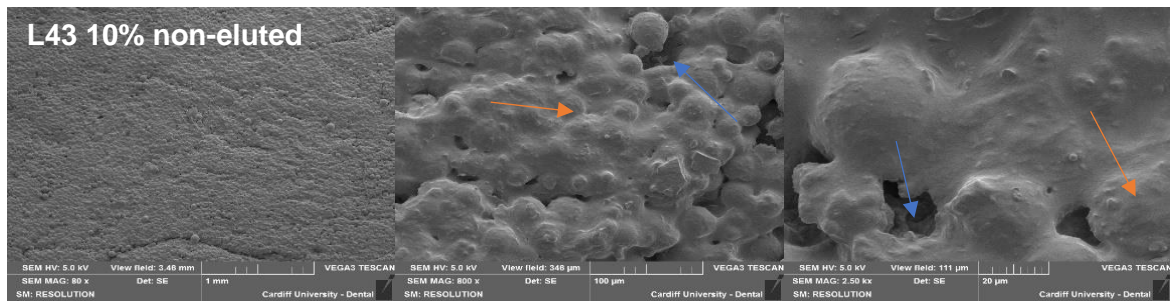


Figure 34: SEM surface images of Palacos R+G cement samples containing 5% w/w of Pluronic L43 (A) before and (B) after incubation in PBS for one week at 37 °C; sample magnifications are x80, x800 and x2.5k respectively. Arrows indicate PMMA particles (orange) and pores (blue).

(A)



(B)

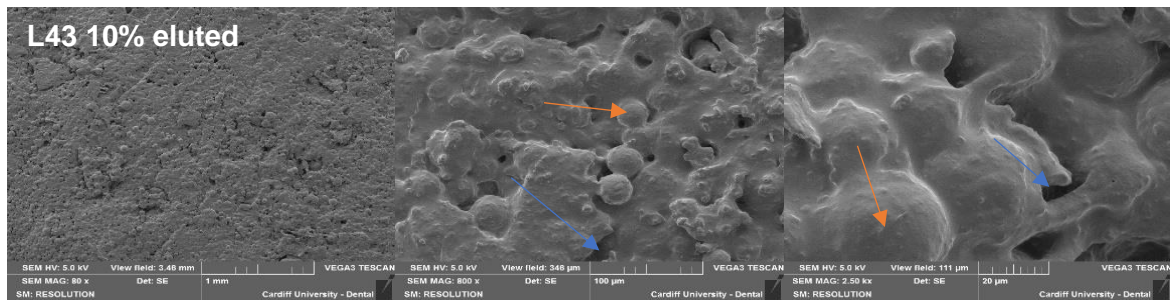
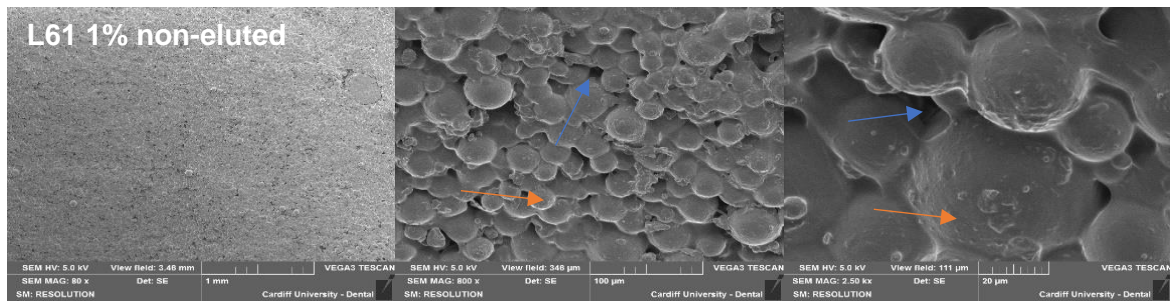


Figure 35: SEM surface images of Palacos R+G cement samples containing 10% w/w of Pluronic L43 (A) before and (B) after incubation in PBS for one week at 37 °C; sample magnifications are x80, x800 and x2.5k respectively. Arrows indicate PMMA particles (orange) and pores (blue).

(A)



(B)

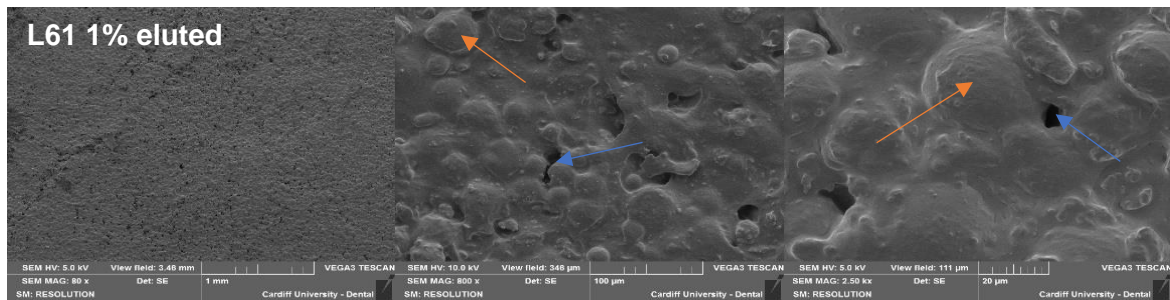
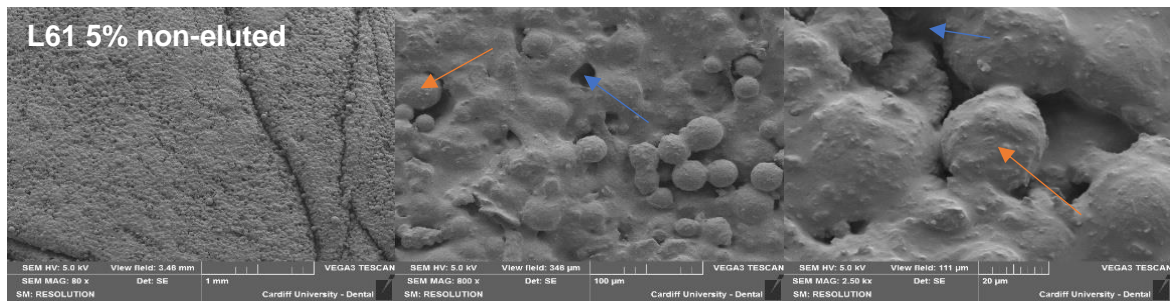


Figure 36: SEM surface images of Palacos R+G cement samples containing 1% w/w of Pluronic L61 (A) before and (B) after incubation in PBS for one week at 37 °C; sample magnifications are x80, x800 and x2.5k respectively. Arrows indicate PMMA particles (orange) and pores (blue).

(A)



(B)

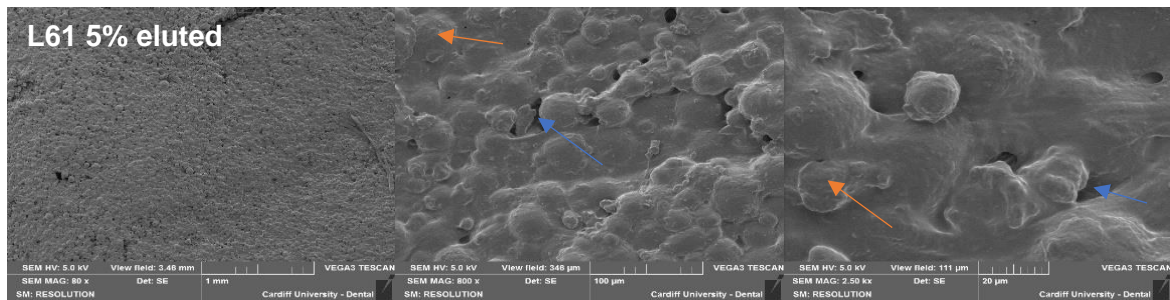
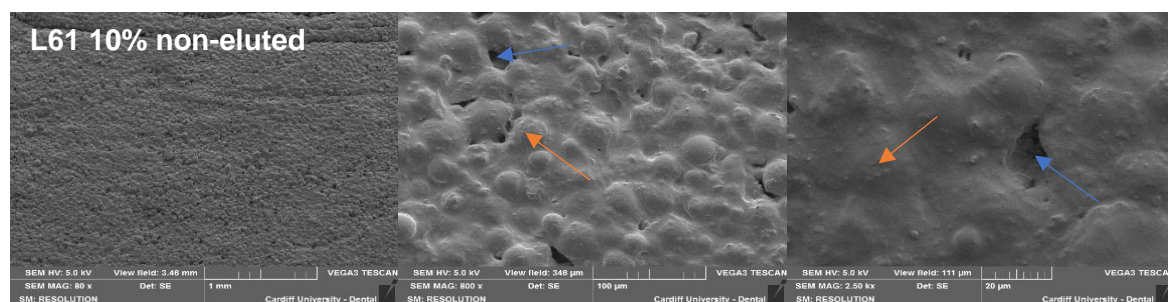


Figure 37: SEM surface images of Palacos R+G cement samples containing 5% w/w of Pluronic L61 (A) before and (B) after incubation in PBS for one week at 37 °C; sample magnifications are x80, x800 and x2.5k respectively. Arrows indicate PMMA particles (orange) and pores (blue).

(A)



(B)

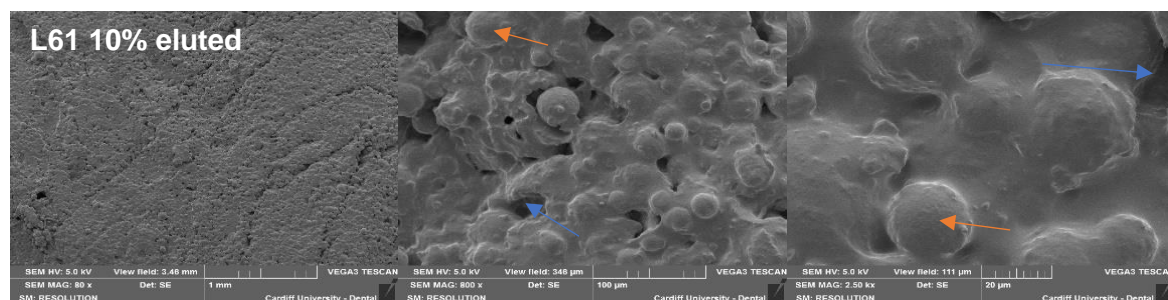


Figure 38: SEM surface images of Palacos R+G cement samples containing 10% w/w of Pluronic L61 (A) before and (B) after incubation in PBS for one week at 37 °C; sample magnifications are x80, x800 and x2.5k respectively. Arrows indicate PMMA particles (orange) and pores (blue).

3.3.7 Determination of lipid release from cement

Several methods including analysis using UV-Vis, HPLC-UV-Vis and fluorescence spectrophotometry, for analysis of fluorescent labelled liposomes, were used to assess the release of the phospholipid contents of liposomal cement, after incubation in PBS at 37 °C, over specific time periods.

3.3.7.1 Detection of phospholipids by Stewart assay

A strong linear correlation was observed between the phosphatidylcholine lipid concentration and absorbance at 485 nm using the Stewart method for concentrations of phosphatidylcholine between 0.01 and 0.1 mg/ml (R^2 value of 0.994) (Figure 39). Results for the analysis of phosphatidylcholine in PBS (incubated cement discs), using the Stewart assay are shown in Table 9. Control samples of eluents from Palacos R, Palacos R+G stored in PBS at 37 °C for 5 days were analysed using this assay; absorbance values

obtained from these samples were below the limit of detection (LOD), meaning that bone cement components and gentamicin sulfate do not interfere with this analysis. Samples of LCP-CEMENT discs stored in PBS at 37 °C for 1, 2 and 5 days were analysed (Table 9) . The absorbance values obtained for all samples were below the LOD, meaning that lipid concentration could not be determined.

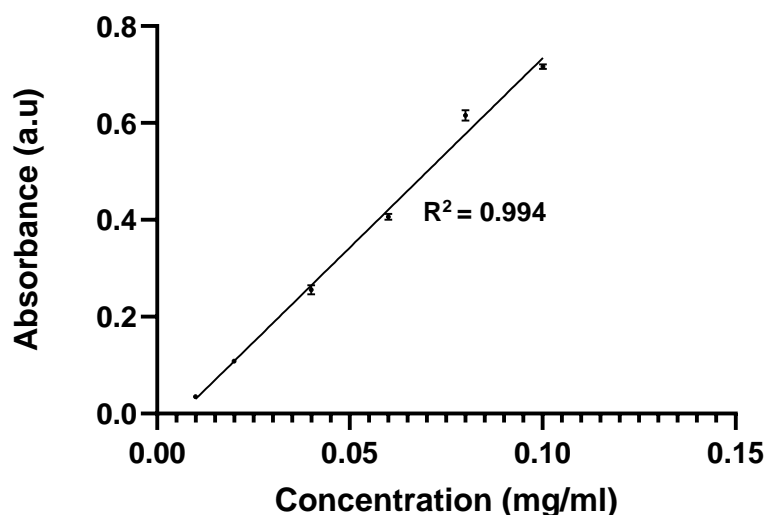


Figure 39: Calibration curve for phosphatidylcholine determination, using the Stewart assay (n=3). R2 (>0.99) is deemed acceptable (Pinto et al., 2017).

Table 9: Absorbances obtained for LCP-CEMENT eluents at 1, 2 and 5 days, by UV-Vis (n=3).

| Sample | Mean corrected absorbance |
|---------------------|---------------------------|
| LCP-CEMENT (1 day) | <LOD |
| LCP-CEMENT (2 days) | <LOD |
| LCP-CEMENT (5 days) | <LOD |

3.3.7.2 Detection of phospholipids using HPLC

Chromatograms obtained from the HPLC analysis of 0.5 mg/ml of PC, and eluent from Palacos R stored in PBS at 37 °C for 5 days are shown in Figure 40. PC gave rise to a single, clear sharp peak at a retention time (Rt) of 4.2 minutes. However, eluent from Palacos R cement gave rise to a broad interfering peak (Rt = 3.8 minutes), containing a shouldering peak (Rt = 4.5 minutes), covering a time period of 3 to 5 mins, meaning that analysis of phospholipids from a cement disc formulation was not possible using this method.

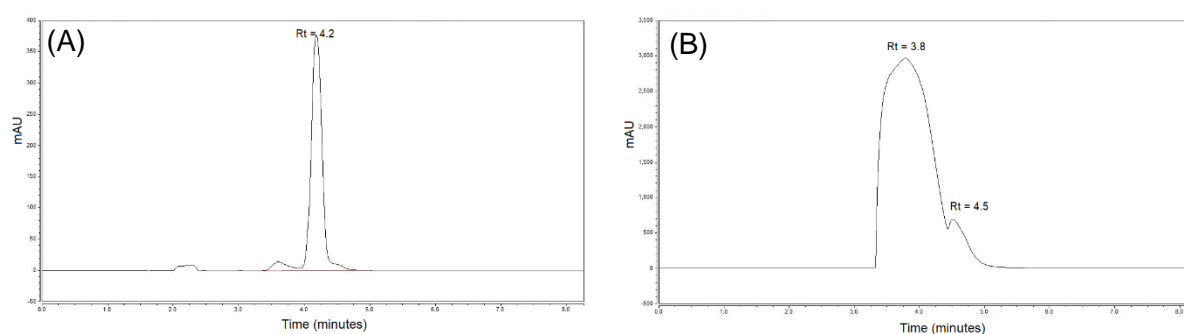


Figure 40: Chromatograms obtained from HPLC analysis of phosphatidylcholine in bone cement: (A) 0.5 mg/ml phosphatidylcholine after extraction and, (B) Palacos R cement eluent.

3.3.7.3 Assays using fluorescent labelled phospholipids

Fluorescent labelled liposomes were prepared using 2% w/w of 18:1-06:0 NBD PC with respect to the phosphatidylcholine mass amount used. The liposomes were incorporated into PMMA bone cement discs, Palacos R. The discs were incubated in PBS at 37 °C for different amounts of time (1,2 and 5 days), to allow release of phospholipid content into the PBS medium. Assays were developed and validated to characterise the release of phosphatidylcholine into PBS.

3.3.7.3.1 Using water as the diluent

Initially, water was used as a diluent, and it was attempted to determine excitation and emission wavelengths iteratively. Excitation and emission wavelengths were initially obtained at 274 nm and 548 nm respectively, however, these wavelengths were not stable over time, meaning that data obtained by this method was not repeatable.

3.3.7.3.2 Development of assay using methanol as the diluent

A method for determination of the fluorescent lipid used to label liposomes, 18:1-06:0 NBD PC, was developed and validated using methanol as the diluent. Methanol was chosen as a diluent due to safety and environmental concerns over chloroform. Excitation and emission wavelengths were determined using the iterative method (Section 2.8.1), establishing reproducible emission and excitation wavelengths for 18:1-06:0 NBD PC in methanol. These were found to be 467 nm and 535 nm respectively (Figure 41). A calibration curve was established using concentrations of 0.2 µg/ml to 20 µg/ml (Figure 42). An R^2 value of 0.998 shows that a strong linear correlation was observed between the fluorescent lipid, 18:1-06:0 NBD PC and the detector. LOD and LOQ were calculated using the calibration curve method (Section 2.8.1). LOD and LOQ were found to be 0.1 µg/ml and 0.2 µg/ml respectively. Components of the formulation that could cause possible interferences such as eluent from Palacos R, gentamicin sulfate, Pluronic L31, L43 and L61 were investigated and were all found to be consistent with baseline noise (<LOD). Control samples containing 10 µg/ml of 18:1-06:0 NBD PC were analysed in triplicate and found to have recoveries of $78.9 \pm 5.2 \%$.

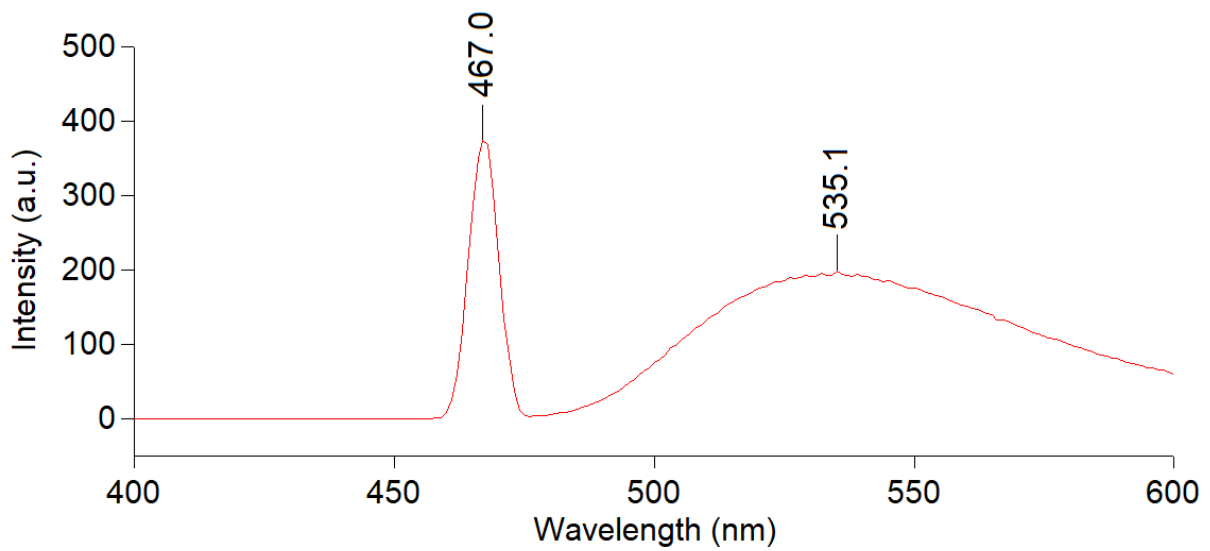


Figure 41: Emission and excitation wavelengths for 1 $\mu\text{g/ml}$ of 18:1-06:0 NBD PC fluorescent lipid in methanol. The wavelengths were determined as 467 nm (excitation) and 535 nm (emission).

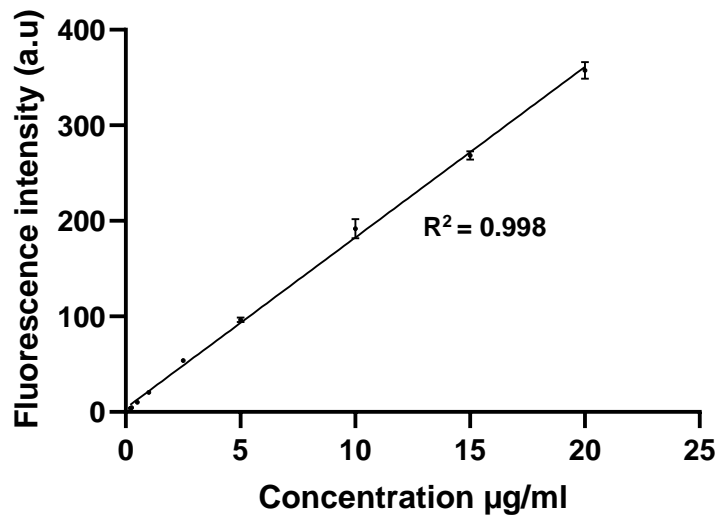


Figure 42: Calibration curve of 18:1-06:0 NBD PC phospholipid in methanol using concentrations from 0.2 $\mu\text{g/ml}$ (LOQ) to 20 $\mu\text{g/ml}$ (upper quantification limit) ($n=3$). R^2 (>0.99) is deemed acceptable (Pinto et al., 2017).

3.3.7.3.2.1 Assay of fluorescent labelled phospholipids from bone cement eluent, using the method for methanol as the diluent

Eluent from cement samples containing fluorescent labelled liposomes, stored in PBS at 37 °C for different lengths of time (1 day, 2 days, and 5 days) were assayed in triplicate and were found to be below the limit of detection, meaning that lipid concentration could not be determined.

3.3.7.3.3 Development of assay using chloroform as the diluent

The excitation and emission wavelengths for 18:1-06:0 NBD-PC dissolved in chloroform were confirmed as being 464 nm and 531 nm respectively (Figure 43). A calibration curve was established using concentrations of 0.0005 µg/ml to 3 µg/ml (Figure 44). An R² value of 0.999 shows that a strong linear correlation was observed between the fluorescent lipid, 18:1-06:0 NBD PC and the detector. LOD and LOQ were calculated using the calibration curve method (Section 2.8.1). LOD and LOQ were found to be 0.00002 µg/ml and 0.0005 µg/ml respectively. Components of the formulation that could cause possible interferences such as eluent from Palacos R, gentamicin sulfate, Pluronic L31, L43 and L61 were investigated and were all found to be consistent with baseline noise (<LOD). Control samples containing 10 µg/ml of 18:1-06:0 NBD PC were analysed in triplicate and found to have recoveries of 83.3 ± 3.3 %.

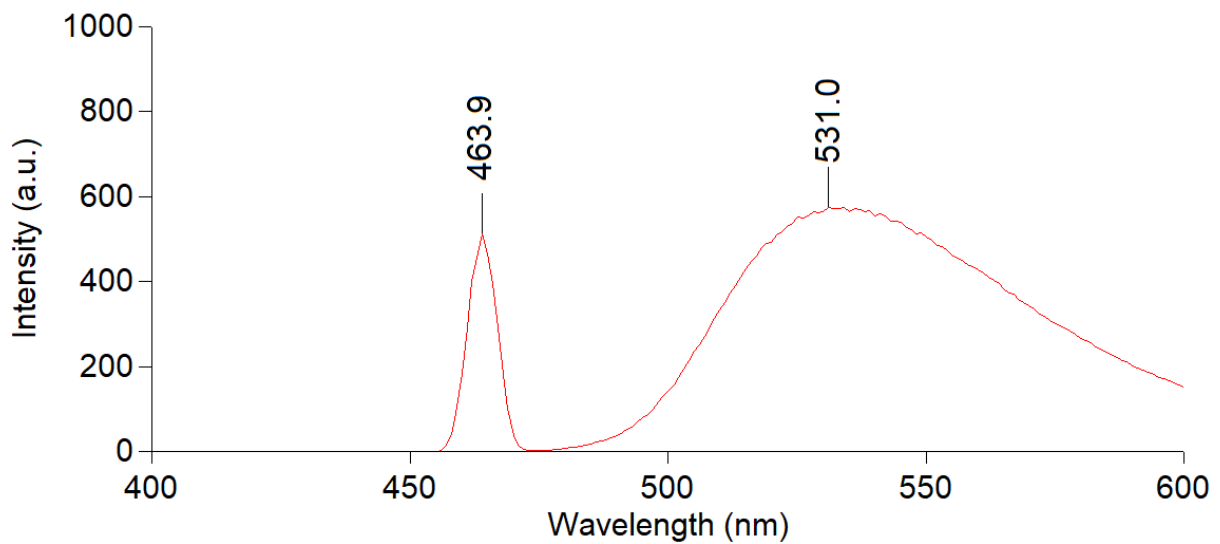


Figure 43: Emission and excitation wavelengths for 5 µg/ml of 18:1-06:0 NBD PC fluorescent lipid in chloroform. The wavelengths were determined as 464 nm (excitation) and 531 nm (emission).

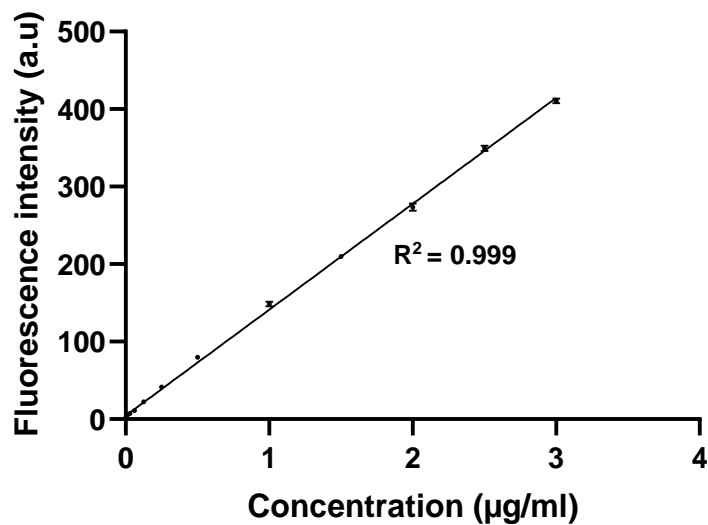


Figure 44: Calibration curve of 18:1-06:0 NBD PC phospholipid in chloroform using concentrations of 0.0005 µg/ml LOQ) to 3 µg/ml (upper quantification limit) (n=3). R2 (>0.99) is deemed acceptable (Pinto et al., 2017).

3.3.7.3.3.1 Assay of fluorescent labelled phospholipids from bone cement eluent, using the method for chloroform as the diluent

Eluent from cement samples containing fluorescent labelled liposomes, stored in PBS at 37 °C for different lengths of time (1 day, 2 days and 5 days) were assayed in triplicate and were found to be below the limit of detection, meaning that lipid concentration could not be determined.

3.4 Discussion

An LC-MS method for assaying gentamicin sulfate was successfully optimised and validated. The method was based on an existing method used to assay various aminoglycosides including gentamicin sulfate (Clarot et al., 2004); however, given the large number of samples required for injection, the method was further optimised and the retention was reduced from 10 minutes to around 5 minutes. A shorter retention time was important, not only to allow for a more rapid turnaround, but to also to reduce any potential degradation of gentamicin sulfate during the auto-sampling process. Doubling the flowrate from 0.5 ml/sec to 1 ml/sec resulted in consistent and satisfactory chromatograms in terms of peak shape. Validation using ICH guidelines was performed (ICH, 2005): repeatability was demonstrated by showing that repeat injections consistently produced the same peak areas i.e. percentage relative standard deviation (%RSD) was shown to be satisfactory according to ICH guidelines (<5% difference) (Pinto et al., 2017); linearity was demonstrated by an R^2 value of 0.995 (>0.99) (Pinto et al., 2017); selectivity was demonstrated by running samples of compounds that may be present in the injected solutions, none of which showed any interfering peaks (Eluent from Palacos R, low concentrations of Pluronics and PC, PBS at pH 7.4). Limits of detection and quantification were determined using the signal-to-noise method and found to be 1 µg/ml and 3 µg/ml respectively. Following validation, using ICH guidelines, this assay was found to be sufficiently accurate and reproducible for assaying gentamicin from PMMA bone cements between concentrations of 60 µg/ml (upper limit) and at 3 µg/ml (lower limit). Mass spectrometry methods, in particular tandem mass spectrometry LC-MS/MS, offer better sensitivity and specificity for analytes in comparison to conventional methods which include HPLC attached to conventional detectors, in particular UV-Vis (Grebe & Singh, 2011; Wong et al., 2018; Zheng et al., 2018); moreover, it is particularly useful for the analysis of compounds that are without chromophores (Wong et al., 2018). Since gentamicin does not possess a natural chromophore, several methods for the identification and quantification of gentamicin have been documented (Fernández-Ramos et al., 2006). These include both chemical and microbiological assays: gas chromatography (GC), HPLC, capillary electrophoresis (CE), enzyme immunoassay, polarization fluoro-

immunoassay, UV-Vis, fluorescence spectroscopy, electrochemical detection, and mass-spectrophotometry. Microbiological assays and immunoassays have shown poor reproducibility and can be subject to interference from other compounds (Fernández-Ramos et al., 2006). The most commonly used method is the *o*-phthaldialdehyde (PHT) derivatisation method developed by Sampath and Robinson (1990), whereby amino groups are derivatised forming chromophores, which can be detected by UV-vis or fluoro spectroscopy (Sampath & Robinson, 1990). The optimised LC-MS method (Thermo Spectra System P4000) was able to characterise gentamicin accurately with good repeatability, having demonstrated a limit of quantification of 3 µg/ml. The sensitivity achieved however was not as low as in the original method by Lecároz *et al.* (2006). In their study, the LC-MS method was compared against a derivatisation method, and the limits of quantification were determined as 0.04 µg/ml using LC-MS compared to 25 µg/ml using the derivatisation method. The LOD and LOQ of the LC-MS method used in the School of Chemistry (Bruker Amazon SL) (LOQ of 1 µg/ml and LOD of 0.5 µg/ml) were also lower than for the optimised method; however, the LOQ of 3 µg/ml and LOD of 1 µg/ml were found to be adequate for the purposes of this study. In LC-MS, the sensitivity is directly proportional to the ionisation efficiency, which relates to the production of gaseous ions. There are several parts to the method which could be investigated and adjusted to further optimise the ionisation efficiency, such as sample preparation, mobile phase and instrumental parameters. One of the factors that could certainly contribute to lower sensitivity is an increase in flow-rate (Keqi Tang, 2011). Decreasing flow rate allows the detector to capture more sample, thereby increasing sensitivity, however, in this project it was necessary to increase the flow-rate due to the high number of samples. Although it would be useful to increase the sensitivity particularly for samples that release very low (sub-inhibitory) concentrations of gentamicin, the developed method was deemed suitable, particularly given the improvements in sensitivity over the previously used PHT method.

Both gentamicin sulfate loaded and non-loaded liposomes were produced at around 100 nm, which was consistent with the previous study performed (Ayre et al., 2015). The zeta potential values in mV were as expected for neutrally charged PC liposomes (approximately -5 mV to +5 mV), indicating that the gentamicin sulfate did not affect the liposome surface charge. Particle size did not differ significantly from one another as the polydispersity index values were small and less than 0.7, which is indicative of a homogenous population (Refai et al., 2017). However, although liposomes produced by using 2% w/w 18:1-06:0 NBD PC of the total lipid content, were found to be similar in size, zeta potential values for liposomes produced using them were higher than with the neutrally charged PC lipids. This shows that

the addition of the NBD conjugated phospholipid to the liposome formulation has an effect on the overall surface charge of the liposome.

The contact angle for PMMA samples was 116 ° indicating that it is a hydrophobic polymer. Contact angles for samples of PMMA bone cement have been documented at values ranging from 70 ° and 130 ° (Letchmanan et al., 2017; Van de Belt et al., 2001; Virto et al., 2003). There are a number of reasons as to why contact angle may differ, including purity of solvent used, contamination of surfaces and surface roughness (Kubiak et al., 2011). Palacos R+G was shown to have a contact angle of 98 ° which was consistent with the addition of a hydrophilic additive such as gentamicin sulfate to the PMMA bone cement. LCP-CEMENT did not show a significant decrease in contact angle when compared to the Palacos R cement; this could be due to a much lower amount gentamicin being incorporated (200 mg per 40 g of PMMA, compared to 1 g per 40 g of PMMA for Palacos R+G). Furthermore, of the incorporated 200 mg, only a fraction was retained since the encapsulation efficiency of the liposomal formulation was found to be 15%. Incorporating 10% w/w of Pluronic caused a significant decrease in contact angle, similar to that of gentamicin in Palacos R+G, thereby further increasing surface wettability. Smaller amounts of the different Pluronics did not cause any significant effect on the contact angle, which was consistent with the contact angle for LCP-CEMENT which only contains a small amount of Pluronic (2% w/w).

The three poloxamers used to make samples, L31, L43 and L61 all have different hydrophilic–lipophilic balance values (HLB): 3, 12 and 3 respectively (Krupka & Exner, 2011; Sek et al., 2010). As a rule, HLB values greater than 10 are considered hydrophilic and an HLB value lower than 10 is considered lipophilic (Hakemi-Vala et al., 2017). The contact angle for all samples containing 1% or 5% Pluronic, showed no significant changes when compared to Palacos R, however, all of the 10% Pluronic samples had significantly lower contact angles than Palacos R. Both samples containing 10% L31 and 10% L61, which are lipophilic according to their HLB values, had slightly lower contact angles than 10% L43, which is hydrophilic, although this was not statistically significant. The reason for this may be due to the sensitivity of the technique not being able to discern very minor changes in hydrophobicity or perhaps due to other previously discussed influencing factors such as slight variations in roughness (Adhikari et al., 2016; Krupka & Exner, 2011).

Characterising the surface wettability of bone cement is important, however, as it gives an indication of its hydrophobic or hydrophilic character. The significance of this experiment relates to its behaviour upon contact with water, whereby water will have a stronger affinity

to a more hydrophilic cement and conversely less affinity to a cement showing more hydrophobic character. This means that a more hydrophilic cement will likely release more drug since increased water contact allows more chance of water infiltration into the cement, likely resulting in more drug release to kill bacteria in a clinical context. It was shown in the antimicrobial suspension test that in the first 4 hours, Palacos R+G reduced the number of bacteria (CFU/ml) more than the other samples tested. Similarly, in a study by Oh *et al.* (2016) despite the contact angle not being measured, it was demonstrated in principle that by hydrophilising bone cement using Pluronic F64, antimicrobial activity was indeed enhanced (Oh *et al.*, 2016).

The compression, bending modulus and bending strength results for all samples were above the ISO 5833 requirements, with the exception of compressive strength for the LCP-CEMENT which was slightly below the value of 70 MPa required by the ISO standard (67 MPa). The results were consistent with the study performed by Ayre *et al.* (2015) which showed Palacos R to have the highest compressive strength, followed by Palacos R+G and LCP-CEMENT. However, in the study by Ayre *et al.* (2015) all samples were above or close to the tolerance set in the standard ISO 5833 (78 and 81 MPa). The fact that it was not possible to achieve the same compression result for LCP-CEMENT in this study could be due to variations in the manufacturing method during the LCP-CEMENT preparation. Nevertheless, these mechanical testing results show that the cements all demonstrate some of the properties required to be used as orthopaedic load-bearing cements, which will be subjected to various physical challenges. Further to mechanical testing, before this formulation can be used clinically, other parameters will also need to be investigated such as setting time, temperature and cytotoxicity (Brochu *et al.*, 2014).

Palacos R+G released more total mass quantity of gentamicin than LCP-CEMENT, due to the greater amounts of incorporated powdered gentamicin (1 g per 40 g of cement). At 48 hours LCP-CEMENT released a mass quantity of 267 µg compared to Palacos R+G (471 µg). After 3200 hours (4.5 months), LCP-CEMENT released 497 µg compared to Palacos R+G (822 µg). However, in terms of the percentage of incorporated gentamicin released, LCP-CEMENT released a higher cumulative total percentage than the Palacos R+G cement (31% and 18% respectively), meaning that more gentamicin was released from the mass amount of gentamicin that was initially incorporated into LCP-CEMENT. Overall, the mass amounts of gentamicin released were similar to that shown by Ayre *et al.* (2015). Furthermore, the drug release profile for LCP-CEMENT was similar to that of Palacos R+G, albeit having released lower mass quantities at each time point. The mass amounts of released gentamicin were higher in this study than those obtained by Ayre *et al.* (2015). The

higher results could be due to the LC-MS analytical technique being a superior technique to the colorimetric PHT method. As observed during the early incubation periods, Palacos R+G had a greater initial release of gentamicin sulfate when compared to LCP-CEMENT. Both Palacos R+G and LCP-CEMENT had a burst release profile, which was not avoided by using a liposomal system. The results for drug release from LCP-CEMENT show that the liposomal formulation in the study by Ayre et al. (2016) is reproducible. The higher percentage release from LCP-CEMENT compared to Palacos R+G is possibly due to the uniform dispersion of gentamicin in the LCP-CEMENT formulation as described by Ayre *et al.* (2016) (Ayre et al. 2016. Liposomal drug delivery system for bone cements. US9895466.), where the amphiphilic Pluronic is used to effectively disperse liposomes within the cement, creating a homogenous distribution of gentamicin throughout the bulk of the cement. Ayre *et al.* (2015) described the initial incompatibility between the hydrophilic outer surface of the liposomes and the hydrophobic methyl methacrylate, which required the use of Pluronics (Ayre et al., 2015). It was proposed that the hydrophilic portion of the Pluronic attaches itself to the hydrophilic functional groups on the liposome surface, thereby allowing the hydrophobic portion of the Pluronic to attach itself to the hydrophobic MMA molecules and consequently enhance dispersion within the PMMA cement. The dispersion of LCP within the cement matrix is in stark contrast to that of the commercial cement, Palacos R+G, where the powdered antibiotic is not homogeneously dispersed within the cement matrix, causing agglomerates to be formed (Dunne et al., 2009) and only a relatively small percentage of the entire total incorporated drug to be released in an uncontrolled burst release from the surface, with the rest effectively trapped within the cement matrix (Dunne et al., 2009). Moreover, after a few weeks, the commercial antibiotic cements become incapable of releasing therapeutic levels of antibiotic, resulting in sub-inhibitory levels for prolonged periods, potentially encouraging the development of antibiotic-resistant bacteria (Dunne et al., 2007; Stravinskas et al., 2018).

Palacos R+G containing Pluronics L31 5%, L43 5% and L43 10% released the most gentamicin (1000 µg to 1300 µg). They released more gentamicin than Palacos R+G (800 µg) and also double the mass quantities (500 µg) for the lowest releasing cement discs containing Pluronic (L31 1%, L31 10%, L61 5% and L61 10%). Contact angle measurements showed addition of 10% Pluronic increased the hydrophilicity of the cements. At the final time point, 2160 hours (3 months), Palacos R+G appears to have stopped releasing gentamicin, as the curve has plateaued by this point, whereas the Pluronic samples appears to still be releasing gentamicin. The Pluronics may have hydrophilised the PMMA cement, and furthermore it is was shown in a study by Oh *et al.* (2016) using Pluronic F68, that Pluronics can homogeneously disperse gentamicin sulfate within the cement (Oh et al.,

2016). In the study by Oh *et al.* (2016), it was also thought that the Pluronic caused the hydrophilisation of PMMA bone cement, as well the creation of pores via the formation of reverse micelles. At the higher concentrations of Pluronic L43 and at 5% L31 this may be evident, however there is no data for CMC in MMA, which would need to be determined for the various Pluronics. Another mechanism of action may be through the enhanced dispersion of gentamicin powder throughout the bone cement, similar to that observed with LCP. As the Pluronic is able to bind to the hydrophilic liposome surface, it is also likely to bind to the hydrophilic gentamicin in a similar manner, improving the compatibility of the hydrophilic aminoglycoside with the hydrophobic MMA (Ayre *et al.*, 2015; Oh *et al.*, 2016). The type of static experiments performed in these studies however are limited with regards to the fact that it does not replicate *in vivo* conditions. The drug release was performed in 5 ml of PBS which has different rheological properties to that of blood. Moreover, the drug is released in a defined volume as opposed to a continuous circulation which could affect the dissolution of the antibiotic and also cause potential degradation of the cement over time (Ayre *et al.*, 2015). Although a direct comparison to clinical conditions cannot be made, this study was able to directly compare the drug release of gentamicin from different formulations of bone cements to that of the commercial gentamicin loaded cement.

The quantitative antimicrobial suspension test showed that all samples were effective at inhibiting *S. aureus*, thereby reducing the bacteria count from 10^6 CFU/ml to bacteria counts ranging from approximately 2.8×10^5 to 1.1×10^5 CFU/ml. Palacos R+G showed the highest efficacy, which is consistent with a large initial burst release since the test was carried out over a 4 hour incubation period. It was also observed that Palacos R bone cement alone also has an effect on the bacteria, reducing the count to 2.8×10^5 CFU/ml. This was confirmed by subjecting the bacteria to MMA alone, which resulted in a reduced count to 9×10^4 CFU/ml. There was no observable trend for the Palacos R+G samples containing different amounts of Pluronics. The Pluronic samples did not show the same level of efficacy as the Palacos R+G, despite containing the same amount of gentamicin. In a study performed by Oh *et al.* (2016) (Oh *et al.*, 2016), Pluronic was incorporated into commercial PMMA bone cement containing vancomycin to hydrophilise the cement matrix. The Pluronic cement was shown to have a more controlled drug release profile, which could explain why less gentamicin could have been released from the Pluronic containing samples initially (Oh *et al.*, 2016). Samples were tested over a period of 48 hours for the possible formation of biofilms, as it has been shown that 24 to 48 hours is the optimal time for biofilm formation on medical devices (Oliveira *et al.*, 2017). No biofilm formation was detected on any of the cements after 48 hours, indicating the possibility of biofilm prevention by the various cement formulations. However, although the *S. aureus* strain used in this experiment (NCTC 10788)

is known to produce biofilms (Gwynne et al., 2021), the experiment should be conducted by using a control disc made from a material where biofilm growth is known to occur e.g. glass (Marques et al., 2007; Shukla et al., 2017). The overall antimicrobial results were consistent with the study performed by Ayre *et al.* (2015). In the previous study, agar diffusion assay was used to test samples (Ayre et al., 2015). Whilst that study demonstrated that LCP-CEMENT and Palacos R+G were effective at killing *S. aureus* as demonstrated by zones of inhibition, no effect from Palacos R was observed. It was also observed that Palacos R+G did not give consistent results; however, this phenomenon was not observed in the current study. Although drug release was measured at 6 hours and not 4 hours, LCP-CEMENT was found to have released 0.041 mg/ml and Palacos R+G released 0.094 mg/ml by that time point. This is above the minimum inhibitory concentration (MIC) required to inhibit *S. aureus*. In a study by Figueroa *et al.* (2008), it was shown that the MIC of gentamicin sulfate required to inhibit bacteria growth of *S. aureus* was 0.0125 mg/ml (Figueroa et al., 2008). This experiment showed that the cement formulations were all capable of releasing sufficient antibiotic in order to inhibit bacteria growth of *S. aureus* at 4 hours; and that consequent biofilm formation at 48 hours may have been prevented, although this would need to be confirmed by further testing. It is also worth noting however that this method does not characterise gentamicin release over a prolonged period. Rather, it is measuring the effects at the first four hours i.e., at a single time point, which is similar to the first time point for drug release as measured by LC-MS. Although a defined period for antibiotic release from bone cement is not yet agreed upon, it is thought that the first two to four weeks are important in managing potential infections following joint replacement surgery (Bernard et al., 2010). Using the amount of time that a potential bacterial infection is known to occur, it would be beneficial to test the samples at different time points based on this information. This would be performed by removing samples, which are being stored in solution such as PBS, at regular intervals and incubating them in a bacteria suspension to investigate whether the release at different stages is sufficient to inhibit *S. aureus*.

All the samples produced, showed some air pockets/pores, possibly due to the mixing process. It is known for the mixing process to produce pores (Ayre et al., 2014; Dunne et al., 2001). Although not observed in the Palacos R, all of the samples appeared to be formed from fused round PMMA particles that have not fully polymerised with the MMA liquid. This may be due to additives sterically inhibiting the PMMA and MMA from fully interacting. Incomplete polymerisation is a known phenomenon that can result in a weaker cement due to the unreacted MMA acting as a plasticiser (Vallo, 2000). Incomplete polymerisation can also be a risk to a patient as MMA can leak into the surrounding area causing necrosis or embolisms (Vallo, 2000). This plasticising effect of non-reacted MMA could be a reason why

the LCP-CEMENT was slightly weaker than the Palacos R and Palacos R+G in compression. No clear changes were observed with regards to the cement surfaces between the control samples and the various drug-release samples. Not all samples appeared to have formed significant amounts of channels or pores upon storage in PBS. It was not possible to see if incubation of the discs in PBS causes for pore or channel formation.

A spectrofluorometry method for the 18:1-06:0 NBD PC fluorescent lipid in methanol (Section 3.2.12) was successfully developed and validated. Following validation, using ICH guidelines, this assay was found to be sufficiently accurate and reproducible for assaying the 18:1-06:0 NBD PC fluorescent lipid from PMMA bone cements between concentrations of 0.2 µg/ml and 20 µg/ml, the limit of detection was 0.1 µg/ml. A second spectrofluorometry method for the 18:1-06:0 NBD PC fluorescent lipid in chloroform was also successfully developed and validated. Although there was data for excitation and emission spectra for this compound in chloroform from the manufacture, there was no method for assaying the 18:1-06:0 NBD PC fluorescent lipids. Confirmation of both wavelengths were performed and were both shown to be concordant with the manufacturer's data for excitation and emission wavelengths of 467 nm and 535 nm respectively. Following validation, using ICH guidelines, this assay was found to be sufficiently accurate and reproducible for assaying the 18:1-06:0 NBD PC fluorescent lipid from PMMA bone cements between concentrations of 0.0005 µg/ml and 3 µg/ml, the limit of detection was 0.0002 µg/ml. This method was found to be more sensitive than the method using methanol as the diluent. A method was also attempted using water as the diluent, since this would be more favourable in terms of accuracy of data, particularly there would be less time required for sample preparation, as samples could be analysed immediately. Using water was not possible as it was not possible to obtain stable wavelengths for emission and excitation, and the readings were not stable. As a result, it was not possible to use this method for the detecting lipid release from the bone cement. This solvent effect is possibly due to the fact fluorescence spectroscopy is solvent dependant, and a change in polarity of solvent can cause for a molecular rearrangement of a given fluorophore (Lakowicz & Lakowicz, 1983).

The fluorescence spectroscopy assays were unable to quantify the release of fluorescent labelled lipid, 18:1-06:0 NBD PC. The results were below the LOD for both methods, and therefore it was deemed unlikely that any lipid was being released. Fluorescence spectroscopy is a highly sensitive and selective analytical tool used in drug release for low level detection (Sierra Villar et al., 2013). In this experiment, samples were analysed after storage in PBS over 1, 2 and 5 days. The reason for this was to account for the possibility of the fluorescent NBD probe degrading, although a longer time period may yield more

released lipids, it was not possible at any time point to determine lipid release. The stability of the 18:1-06:0 NBD PC could be investigated further to assess the extent of any possible degradation under the conditions that the samples were subjected to.

An HPLC method for quantification of phospholipids was used to detect and quantify PC. The method was able to detect phosphatidylcholine by itself; however, components from the Palacos cement were found to interfere with the phosphatidylcholine peak, producing a co-eluting peak. This meant that this method was not suitable for lipid release from PMMA bone cement. This co-eluting peak could have been due to MMA released from the cement, as it is well documented that MMA elutes from PMMA bone cement (Buchholz HW, 1970). Buchholz *et al.* (1970) observed that MMA eluted from PMMA for extended periods after its manufacture (Naveed, Shah, et al., 2014). No further work was performed on this method however, an investigation into the method could be carried out by investigating all the parameters including but not limited to flow rate, temperature, column choice, as well as the mobile phase composition. The Stewart assay had been shown to be suitable for this application as none of the components interfered with the analysis. Results of lipid detection by the Stewart assay were below the limits of detection and quantification, so it was not possible to confirm if lipid had been released, since it is not possible to extrapolate beyond the standard curve. It is also possible that the phosphatidylcholine lipid may have been oxidised (Al-Orf, 2011). This could be investigated using LC-MS, which can be used to identify any oxidation products of phosphatidylcholine, to see the extent of any oxidation induced by PMMA bone cement (O'Donnell, 2011).

3.5 Conclusions

An LC-MS method was successfully developed, as per ICH guidelines, for the analysis of gentamicin. Drug release from LCP-CEMENT was compared to Palacos R+G using this method. LCP-CEMENT released lower mass quantities of gentamicin than Palacos R+G. Most of the released drug mass for Palacos R+G and liposomal cement was the result of an initial burst release; however, LCP-CEMENT released a higher percentage of drug incorporated compared to Palacos R+G.

Different Pluronics which were used in the liposomal formulation were incorporated into Palacos R+G cement to investigate the effect of this excipient on antibiotic release. Over 3 months, Palacos R+G containing higher levels of Pluronic released more gentamicin than

Palacos R+G. All Pluronics showed further gentamicin mass release at the 3-month time point, whereas Palacos R+G stopped releasing significant levels of gentamicin at this point. All liposomes were reproduced and were found to be of consistent with those produced in the previous study. LCP-CEMENT mechanical properties were broadly consistent with the previous study, although the compressive strength was slightly lower than the ISO 5833 limit, which shows perhaps, some difficulties in reproducibility of LCP-CEMENT. The quantitative antimicrobial suspension test showed that all samples were effective in reducing *S. aureus* bacteria count. MMA itself was found to be effective in reducing bacteria count. Biofilm formation was not observed for either Palacos R+G, Palacos R+G containing pluronics, or for liposomal cement samples, indicating that the bone cements may have prevented biofilm formation, although this still requires confirmation by further testing, using a positive control. It was shown that the different Pluronics used did not affect the water/cement contact angle, although at higher concentrations of Pluronic, the contact angle was reduced.

An HPLC method was used to analyse phosphatidylcholine, however, the method was not suitable due to an interfering peak from the PMMA bone cement. The well-established Stewart phospholipid assay was unable to determine the presence of released lipids from bone cement. Two sensitive spectrofluorometry assays were successfully developed using different solvents to assay 18:1-06:0 NBD PC fluorescent lipids. Both methods, despite having very low limits of detection, were unable to determine fluorescent lipids released from bone cement. SEM images were taken of all PMMA samples; with exception to Palacos R, all the samples appeared to be formed of round particles, which may indicate an incomplete polymerisation; it was not possible to see clear changes between control samples and drug-release samples.

Chapter 4

4 Developing and evaluating a freeze-dried liposome-gentamicin formulation for use in bone cement

4.1 Introduction

Liposomal formulations have been successfully incorporated into commercial PMMA bone cements, to tailor and improve drug-release (Al Thaher et al., 2016). In the previous chapter, a liposomal formulation, LCP, was produced by membrane extrusion and incorporated into bone cement, LCP-CEMENT. LCP was validated and characterised with regards to its manufacture; furthermore, LCP-CEMENT was validated and characterised with regards to its drug release, mechanical properties, and antimicrobial efficacy. The manufacture of LCP was reproducible with regards its particle size and zeta potential. Moreover, although LCP-CEMENT released less drug quantities than the commercial gentamicin loaded bone cement, LCP-CEMENT released a greater percentage of its incorporated drug than the commercial gentamicin loaded bone cement, as well maintaining similar mechanical properties as observed in the previous study, in Chapter 3. The results in Chapter 3 show that the encapsulation efficiency was 15%, meaning that not all the gentamicin mass quantity was incorporated into LCP and hence LCP-CEMENT. Manufacture of LCP therefore needs to be optimised to enhance loading of gentamicin-containing-liposomes into the bone cement. Manufacture of the liposome formulation involved two main parts: first, the high-pressure extrusion of a lipid suspension through a 100 nm polycarbonate membrane and second, the ultracentrifugation of the liposome suspension in water at 107,000 g. An alternative method of manufacture for the liposome formulation is freeze-drying, which has been reported to show improved liposome stability, increased encapsulation efficiency of aminoglycoside antibiotics and improved antimicrobial efficacy (El-Nesr et al., 2010; Halwani et al., 2007). Freeze-drying is often used in the pharmaceutical industry to improve the shelf-

life of pharmaceutical products, as well (Hansen et al., 2015; Shukla, 2011). In the freeze-drying process, water is effectively frozen and then removed from the sample by sublimation (primary drying) and desorption (secondary drying). This drying process allows for the removal of water from compounds that are potentially unstable in water but are stable in a dry state (Nireesha et al., 2013). Furthermore, it is known that sugars such as disaccharides are able to protect membrane structures such as liposomes against leakage and fusion, and are able to preserve their structural integrity (Roy et al., 2016). A freeze-dried liposome formulation could therefore potentially improve drug loading and thereby subsequently increase the mass quantity of drug released from the bone cement. Moreover, a successfully freeze-dried formulation, with suitable stability would be commercially favourable, as this would mean that it could be stored appropriately, and then added to bone cement when required by an operating surgeon.

Aims of this chapter:

To improve the total mass of drug loaded into the bone cement by using a more efficient manufacturing method to produce LCP, which will contain more gentamicin-encapsulated-liposomes.

To use freeze drying, to enhance the mass of drug loaded into the cement and to compare the efficiencies of this optimised formulation to the existing liposome formulation, LCP.

Objectives of this chapter:

- To confirm the mass of gentamicin and lipids that are present in the existing gentamicin loaded liposome formulation, LCP, and to evaluate its incorporation in bone cement.
- To establish a freeze-dried liposomal gentamicin formulation, FDL, that can be stored and loaded into a bone cement when required.
- To characterise the drug release, mechanical properties and antimicrobial efficacy of the freeze-dried liposomal gentamicin formulation and compare them to the LCP formulation evaluated in Chapter 3.

4.2. Methods

4.2.1 Materials

Phosphatidylcholine (PC) from egg yolk ($\geq 99\%$), cholesterol (99%), dioleoyl-3-trimethylammonium propane (DOTAP), pentafluoropropionic acid ($\geq 97\%$), gentamicin sulfate ($\geq 590 \mu\text{g}$ Gentamicin base per mg), phosphate buffered saline (10 \times concentrate), iron (III) chloride hexahydrate ($\geq 99.9\%$), ammonium thiocyanate ($\geq 97.5\%$), Sucrose ($\geq 99.5\%$), Pluronic L31 and L61 were obtained from Sigma Aldrich (Sigma-Aldrich Ltd, Gillingham, UK). Pluronic L43 was obtained from BASF Corp (BASF Corporation, USA). Chloroform (HPLC grade $\geq 99.8\%$), methanol (HPLC grade $\geq 99.9\%$), sodium chloride, tryptone and tryptone soy broth were purchased from Fisher Scientific (Fisher Scientific UK, Loughborough, UK). Palacos cements R and R+G were provided by Heraeus (Heraeus Medical, Newbury, UK). *Staphylococcus aureus* (*S. aureus*, NCTC 10788) was used.

4.2.2 Sample preparation

4.2.2.1 Cement samples

Cement samples were prepared as per the method specified in Section 2.1.1.

4.2.2.1.1 LCP-CEMENT

The liposomal formulation LCP was added to MMA liquid during the cement manufacturing process described in Section 2.1.1.

4.2.2.1.2 Liposomal formulation (LCP)

The liposomal formulation was prepared and pelleted as per the methods specified in Section 2.1.2 and 2.1.3.

4.2.2.2.1 FDL-CEMENT

The freeze-dried formulation FDL was added to MMA liquid containing 2% Pluronic L31 with respect to the lipid mass in FDL, during the cement manufacturing process described in Section 2.1.1. Cement samples containing the equivalent of 0.15% w/w, 0.30% w/w and 0.60% w/w gentamicin base were prepared and labelled as FDL-CEMENT015, FDL-CEMENT030 and FDL-CEMENT060 respectively.

4.2.2.1.2.1 Freeze-dried liposomal formulation (FDL)

Liposomes containing phosphatidylcholine, cholesterol and DOTAP (7:1:1) were prepared as per the method in Section 2.1.2. Sucrose was added to the liposome suspension and stirred, to produce a ratio containing 5/5/1 of sucrose, gentamicin sulfate and lipid content.

4.2.2.1.2.2 Freeze drying process

Freeze-drying was carried out using the SP VirTis Genesis Lyophilizer (SP Scientific, USA), equipped with Wizard 2.0 software (SP Scientific, USA). The liposome suspension containing sucrose was freeze-dried in a cycle for approximately 51.5 hours. The product was initially frozen to -40 °C for 180 minutes before a vacuum was applied; primary drying was carried out at a shelf temperature of -40 °C with a pressure of 100 µBar; the shelf temperature was increased to -30 °C after 180 minutes and the pressure was increased to 150 µBar; temperature was maintained at -30 °C for a total of 2030 minutes with a pressure of 150 µBar; the secondary drying process increased the temperature to +20 °C for 480 minutes at a pressure maintained at 150 µBar.

4.2.3 LC-MS

Gentamicin was assayed using LC-MS. The instrument and method were used as specified in Section 2.7.2.

4.2.4 Mechanical testing

All mechanical testing was performed using the methods specified in section 2.4. The compressive strength, bending modulus and bending strength were tested as specified in sections 2.4.1 and 2.4.2 and 2.4.3 respectively.

4.2.5 Zeta potential and particle size

Particle size and zeta potential were performed using a Malvern Zetasizer NanoZS (Malvern Instruments Ltd, Worcestershire, UK), as specified in Section 2.2.

4.2.6 Contact angle measurement

The contact angle was measured using the Atenssion contact angle analyser as specified in Sections 2.3.

4.2.7 Antimicrobial testing

Overnight cultures of *S. aureus* (NCTC 10788) were prepared as described in Section 2.9. All antimicrobial testing was carried out using the methods specified in Section 2.9. This includes sterilisation of glassware, media sterilisation, sample sterilisation; quantitative suspension tests, and analysis of biofilm formation.

4.2.8 Scanning electron microscopy

Scanning electron microscopy (SEM) was carried out using the method specified in Section 2.10.

4.2.9 Statistical analysis

Statistical analysis was performed as described in Section 2.11.

4.3 Results

4.3.1 Gentamicin release from FDL-CEMENT

The concentration of gentamicin released from the FDL-CEMENTS was very low compared to the established Palacos R+G formulation. Table 10 shows drug release in µg/ml at each time point, for all FDL-CEMENT samples. At the 12-hour time point, Palacos R+G release resulted in a concentration of 126.5 µg/ml gentamicin in the 5 ml incubation medium compared to 1.3 µg/ml and 3.3 µg/ml gentamicin for FDL-CEMENT015, FDL-CEMENT030 and FDL-CEMENT060. FDL-CEMENT015 released an amount that was below the LOQ. Table 11 shows the total mass (µg) of gentamicin released at 3-months. At the 3-month time point, Palacos R+G released a total mass of 747.9 µg gentamicin, whereas FDL-CEMENT015, FDL-CEMENT030 and FDL-CEMENT060 released of 6.3 µg, 13 µg and 51 µg gentamicin respectively.

Table 10: Gentamicin release (µg) at different time-periods (non-cumulative), over a period of 2160 hours (90 days) from a Palacos R+G formulation and FDL-CEMENT samples: FDL-CEMENT015, FDL-CEMENT030 and FDL-CEMENT060 (n=3).

| Time (hours) | Mass quantity of gentamicin detected in release media (µg) | | | |
|----------------|--|---------------|---------------|---------------|
| | Palacos R+G | FDL-CEMENT015 | FDL-CEMENT030 | FDL-CEMENT060 |
| 0 | 0 | 0 | 0 | 0 |
| 12 | 632.44 ± 237.9 | <LOQ | 6.7 ± 0.5 | 16.7 ± 6.4 |
| 24 | 8.94 ± 1.4 | <LOD | <LOD | 6.3 ± 0.2 |
| 48 | 7.54 ± 0.4 | <LOD | <LOD | 7.4 ± 0.9 |
| 72 | 6.84 ± 0.6 | <LOD | <LOD | <LOQ |
| 96 | 6.84 ± 0.6 | <LOD | <LOD | <LOD |
| 288 (12 days) | 22.74 ± 8.2 | <LOD | <LOD | 6.7 ± 0.7 |
| 720 (30 days) | 24.34 ± 16.6 | <LOD | <LOD | <LOQ |
| 1440 (60 days) | 14.84 ± 10.2 | <LOD | <LOD | <LOQ |
| 2160 (90 days) | 23.94 ± 20.3 | 6.3 ± 1.0 | 6.3 ± 0.6 | 6.3 ± 0.1 |

Table 11: Total, cumulative, mass quantity (μg) of gentamicin released at 2160 hours (90 days) from Palacos R+G formulation and FDL-CEMENT samples: FDL-CEMENT015, FDL-CEMENT030 and FDL-CEMENT060 (n=3).

| Time (hours) | Total mass quantity of gentamicin detected in release media (μg) | | | |
|--------------|---|---------------|----------------|----------------|
| | Palacos R+G | FDL-CEMENT015 | FDL-CEMENT030 | FDL-CEMENT060 |
| 2160 | 747.85 \pm 203.9 | 6.3 \pm 1.0 | 13.0 \pm 0.6 | 43.6 \pm 5.5 |

4.3.2 Mechanical testing

Mechanical testing was performed as per the requirements of ISO 5833: compressive strength, bending modulus and bending strength (ISO 5833, 2002). As required by the standard, testing was performed using five separate cement sample preparations (n=5).

4.3.2.1 Compressive strength

The compressive strengths for Palacos R and Palacos R+G LCP-CEMENT and FDL-CEMENT015 and FDL-CEMENT030 (prepared and left for 24 hours in air) are shown in Figure 45. FDL-CEMENT060 failed immediately upon testing and so no data was recorded. FDL-CEMENT030 showed the highest compressive strength of 90 ± 0.52 MPa, followed by Palacos R which had a compressive strength of 81 ± 3.80 MPa and FDL-CEMENT015 had a compressive strength of 79 ± 1.23 MPa. Palacos R+G had a compressive strength of 71 ± 1.64 MPa. LCP-CEMENT had a compressive strength of 67 MPa. FDL-CEMENT015 and FDL-CEMENT030 had higher compressive strengths than both Palacos R+G and the LCP-CEMENT, and they were above the ISO 5833 minimum requirement of 70 MPa. FDL-CEMENT015 and FDL-CEMENT030 in both cases were not significantly different to Palacos R ($p=0.9978$ and $p=0.0503$ respectively). FDL-CEMENT015 and FDL-CEMENT030 in both cases showed a significant increase in compressive strength in comparison to LCP-CEMENT ($p=0.0057$ and $p<0.0001$ respectively). FDL-CEMENT030 showed a significant increase in compressive strength compared to FDL-CEMENT015 ($p=0.0313$). With respect to Palacos R, Palacos R+G, FDL-CEMENT015 and FDL-CEMENT030 were not significantly lower ($p=0.1443$, $p=0.9978$ and $p=0.0503$ respectively) whereas LCP-CEMENT showed a significant reduction in compressive strength ($p= 0.0037$).

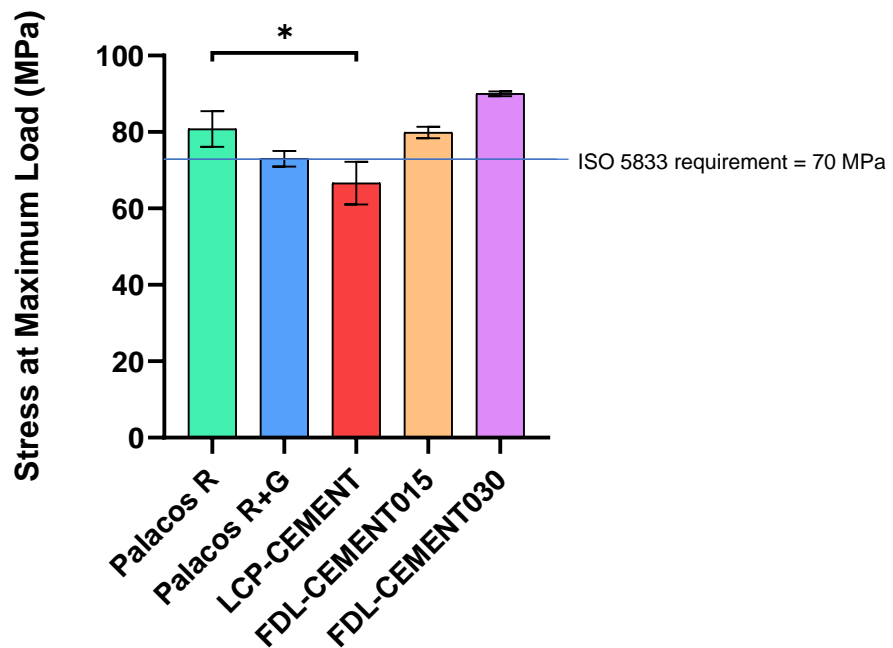


Figure 45: Compressive strength results for Palacos R and Palacos R+G, LCP-CEMENT, FDL-CEMENT015 and FDL-CEMENT030. Data is presented as mean \pm standard deviation (n=5). Asterisks indicate the level of significance (* $p<0.05$, ** $p<0.01$, * $p<0.001$).**

4.3.2.2 Bending modulus

The bending modulus for Palacos R and Palacos R+G, LCP-CEMENT, FDL-CEMENT015 and FDL-CEMENT030 (prepared and left for 24 hours in ambient conditions) are shown in Figure 46. Palacos R showed the highest bending modulus of 3163 ± 51 MPa, followed by Palacos R+G which had a bending modulus of 3101 ± 54 MPa, and then LCP-CEMENT which had a bending modulus of 2991 ± 69 MPa. FDL-CEMENT060 failed immediately upon testing. FDL-CEMENT015 had a bending modulus of 2153 ± 48 MPa, and FDL-CEMENT030 had a bending modulus of 2054 ± 75 MPa. All formulations, except for FDL-CEMENT060, were above the ISO 5833 minimum requirement of 1800 MPa. FDL-CEMENT015 and FDL-CEMENT030 in both cases showed a significant reduction in bending modulus in comparison to Palacos R ($p<0.0001$ for both FDL-CEMENT015 and FDL-CEMENT030). FDL-CEMENT015 and FDL-CEMENT030 in both cases showed a significant reduction in bending modulus in comparison to LCP-CEMENT ($p<0.0001$ for both FDL-CEMENT015 and FDL-CEMENT030). There was no significant difference between FDL-CEMENT015 and FDL-CEMENT030 ($p=0.4193$).

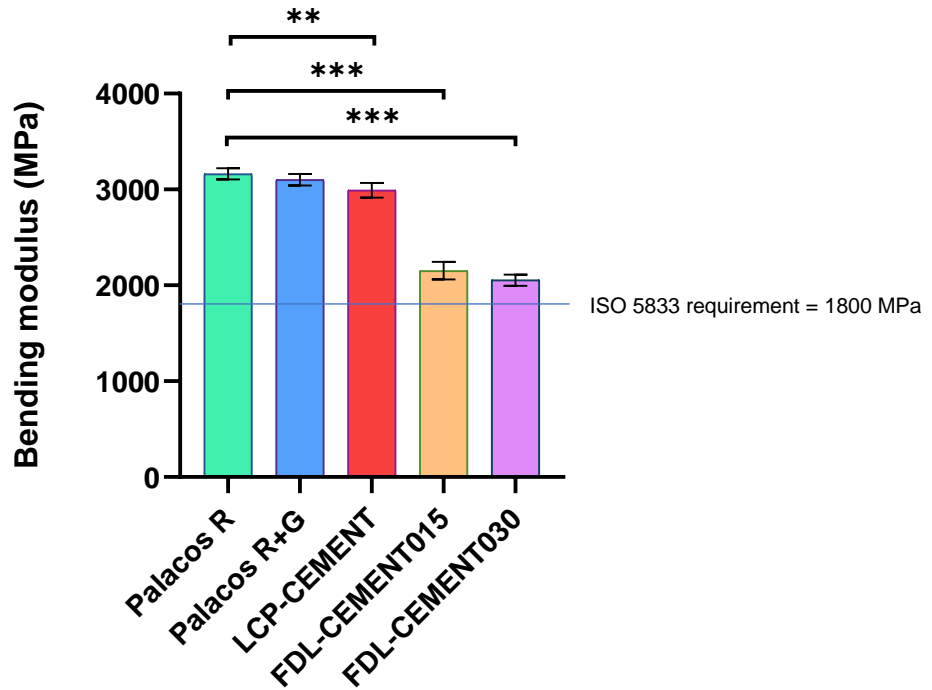


Figure 46: Bending modulus results for Palacos R and Palacos R+G, LCP-CEMENT, FDL-CEMENT015 and FDL-CEMENT030 (n=5). Data is presented as mean \pm standard deviation (n=5). Asterisks indicate the level of significance (* $p < 0.05$, ** $p < 0.01$, * $p < 0.001$).**

4.3.2.3 Bending strength

The bending strength for Palacos R, Palacos R+G, LCP-CEMENT and FDL-CEMENT015 and FDL-CEMENT030 (prepared and left for 24 hours in air) are shown in Figure 47. Palacos R showed the highest bending strength of 82 ± 7 MPa, followed by liposomal cement which had a bending strength of 74 ± 7 MPa and then Palacos R+G which had a bending strength of 63 ± 5 MPa. FDL-CEMENT060 was unable to be tested due to the sample failing immediately upon testing. FDL-CEMENT015 had a bending strength of 55 ± 8 MPa, and FDL-CEMENT030 had a bending modulus of 45 ± 7 MPa. All samples except for FDL-CEMENT030 and FDL-CEMENT060 freeze-dried cements, were above the ISO 5833 limit of 50 MPa. FDL-CEMENT015 and FDL-CEMENT030 in both cases showed a significant reduction in bending strength in comparison to Palacos R ($p=0.0014$ and $p < 0.0001$ respectively). FDL-CEMENT015 and FDL-CEMENT030 in both cases showed a significant reduction in bending strength in comparison to LCP-CEMENT ($p=0.0186$ and $p=0.0007$ respectively). There was no significant difference between FDL-CEMENT015 and FDL-CEMENT030 ($p=0.5759$).

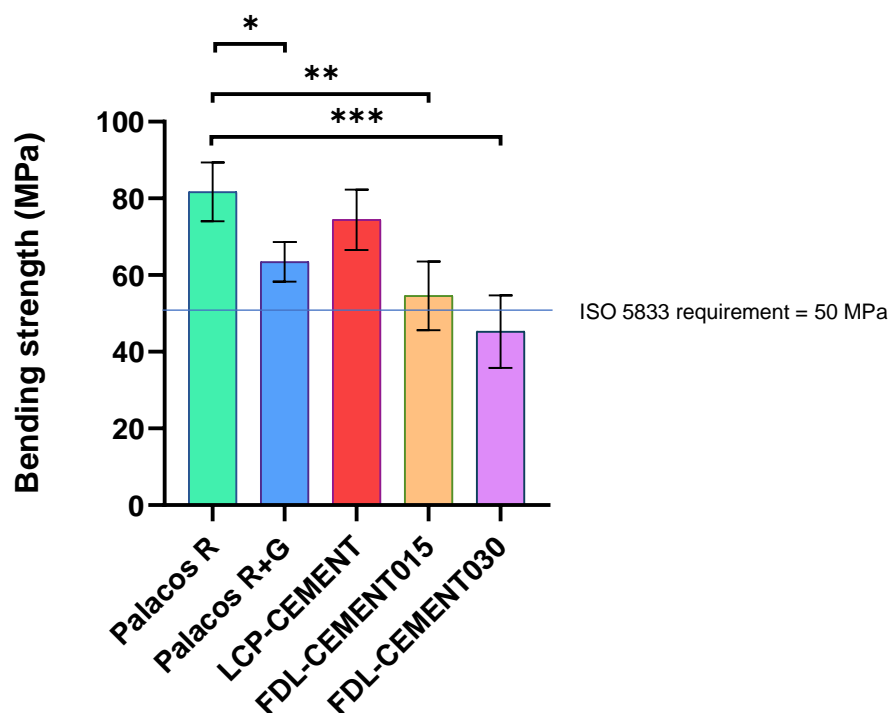


Figure 47: Bending strength results for Palacos R and Palacos R+G, LCP-CEMENT, FDL-CEMENT015 and FDL-CEMENT030 (n=5). Data is presented as mean \pm standard deviation (n=5). Asterisks indicate the level of significance (* $p < 0.05$, ** $p < 0.01$, * $p < 0.001$).**

4.3.3 Characterising the components of the freeze-dried liposome-gentamicin formulation to be used in cements (FDL)

The contents of the freeze-dried liposomal formulation were analysed. The mass amounts of gentamicin base and phosphatidylcholine were assayed. The mean particle diameter and zeta-potential of the liposomes were measured.

4.3.3.1 Analysis of Freeze-dried formulation vial contents

Gentamicin and lipid content in the freeze-dried vials were assayed after freeze-drying to see how much of each constituent is present, to give an indication of loss from the process or by storage. The mean net weight of freeze-dried product in each vial was 9.7 ± 0.2 mg. The mean mass of PC lipid in the freeze-dried vials, measured by Stewart assay, was 0.39 ± 0.02 mg. The mean mass content of total gentamicin sulfate found in the freeze-dried measured by LC-MS, was found to be 2.46 ± 0.21 mg. This means that at the time of

assaying the vials, the mass amounts of both gentamicin and PC were around half the initial mass amounts used to make up each vial.

4.3.3.2 Particle size and zeta potential of freeze-dried liposome-gentamicin formulations

Table 12 shows the average particle diameter and zeta potential for the samples tested. The average particle diameter, measured by dynamic light scattering (DLS), for the freeze-dried liposomes (3 days) is reported as the intensity average, since a unimodal distribution was observed. The average particle diameter for the freeze-dried liposomes (12 months) is reported as the volume average, since a bimodal distribution was observed for these samples. The freeze-dried formulation was characterised at 3 days after its production, and at 12 months after production. Particle size was measured to see if the liposome membrane structure was maintained after freeze-drying. The mean diameter of freeze-dried liposomes, 3 days after manufacture, was found to be 280.6 ± 16.1 nm, the mean polydispersity index was 0.2 ± 0.1 . After 12 months storage, the freeze-dried liposomes increased in size and were found to be 1483.3 ± 386.5 nm, the mean polydispersity index was 0.9 ± 0.1 . Polydispersity index gives an indication of the particle size distribution for each measurement, values closer to zero indicate more homogenous particle size. The mean surface zeta potential for freeze-dried liposomes 3 days after manufacture was found to be 40.0 ± 1.4 mv, and 12 months the zeta potential was found to be 1.7 ± 0.5 mv.

Table 12: Average particle size (nm), zeta potential measurements (mV) and polydispersity index for gentamicin-loaded freeze-dried liposomes measured at 3 days and 12 months after freeze-drying and (n=3). Note that the formulation measured at 3 days is reported as the intensity average particle size and the formulation measured at 12 months is reported as the volume average particle size.

| Sample | Particle size (nm) | Polydispersity index (PDI) | Zeta Potential (mV) |
|--------------------------------------|--------------------|----------------------------|---------------------|
| Freeze-dried formulation (3 days) | 280.6 ± 16.1 | 0.2 ± 0.1 | 40.0 ± 1.4 |
| Freeze-dried formulation (12 months) | 1483.3 ± 386.5 | 0.9 ± 0.1 | 1.7 ± 0.5 |

4.3.4 Contact angles for cement discs

Figure 48 shows the different contact angles obtained for discs prepared from Palacos R, Palacos R+G, LCP-CEMENT as prepared in the previous Chapter, FDL-CEMENT015, FDL-CEMENT030 and FDL-CEMENT060. Palacos R had the highest contact angle ($116 \pm 0.8^\circ$), followed by LCP-CEMENT ($115 \pm 3.9^\circ$). Palacos R+G had a much lower contact angle ($98 \pm 0.8^\circ$). The Palacos R cements containing various amounts of the freeze-dried formulation had lower contact angles than Palacos R and LCP-CEMENT cement: FDL-CEMENT015 and FDL-CEMENT060 both had contact angles of $106 \pm 2.9^\circ$, whereas FDL-CEMENT030 had a contact angle of $111 \pm 4.0^\circ$. FDL-CEMENT015 and FDL-CEMENT060 cements showed a significant reduction in contact angle compared to Palacos R ($p=0.0477$ for both FDL-CEMENT015 and FDL-CEMENT060) whereas FDL-CEMENT030 did not show a significant difference compared to Palacos R ($p=0.5934$). Compared to Palacos R+G, FDL-CEMENT030 showed a significant reduction in contact angle ($p=0.0055$), whereas FDL-CEMENT015 and FDL-CEMENT060 did not show a significant difference ($p=0.1032$ for both FDL-CEMENT015 and FDL-CEMENT060). FDL-CEMENT015, FDL-CEMENT030 and FDL-CEMENT060 did not show a significant difference in contact angle compared to LCP-CEMENT ($p=0.0705$, $p=0.7260$ and $p=0.0705$ respectively). FDL-CEMENT015, FDL-CEMENT030 and FDL-CEMENT060 were not significantly different from each other (FDL-CEMENT015 and FDL-CEMENT030 $p=0.5270$, FDL-CEMENT015 and FDL-CEMENT060 $p>0.9999$, and FDL-CEMENT030 and FDL-CEMENT060 $p=0.5270$).

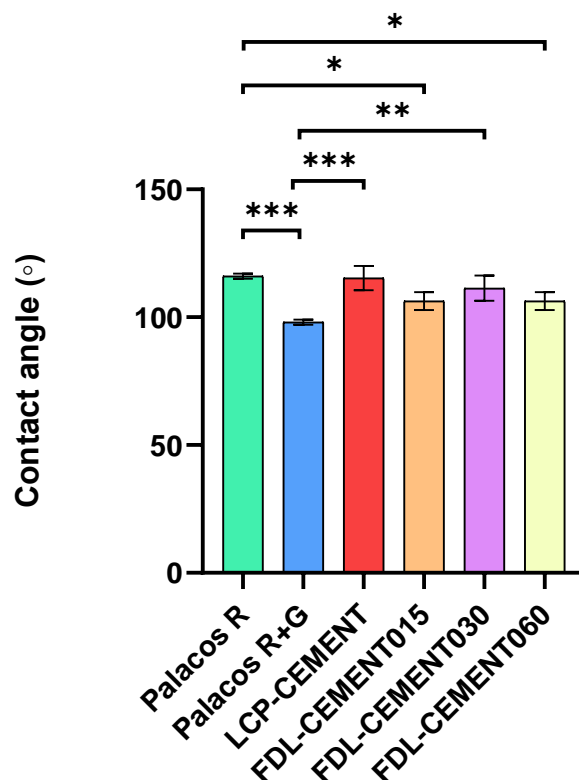


Figure 48: Contact angles for Palacos R and Palacos R+G, LCP-CEMENT, FDL-CEMENT015, FDL-CEMENT030 and FDL-CEMENT060 (n=3). Data is presented as mean ± standard deviation (n=3). Asterisks indicate the level of significance (* p<0.05, ** p<0.01, * p<0.001).**

4.3.5 Antimicrobial testing

Antimicrobial efficacy was assessed by using a quantitative suspension test. Cement discs were incubated for 4 hours, at 37 °C in a suspension of *S. aureus*. After 48 hours, cement discs were vortexed with glass beads to dislodge any microbial biofilm attachment which may have formed on the discs.

4.3.5.1 Quantitative suspension test

Results from the antimicrobial quantitative suspension test are shown in Figure 69. All formulations tested showed some level of efficacy in reducing the growth of *S. aureus*. The starting bacteria count in solution was 1×10^6 colony forming units per mL (CFU/ml). The freeze-dried cement samples were the most effective in reducing *S. aureus* bacteria count. FDL-CEMENT015, FDL-CEMENT030 and FDL-CEMENT060 showed results of 1.3×10^4 CFU/ml, 1.7×10^4 CFU/ml, 1.3×10^4 CFU/ml respectively, whereas Palacos R, Palacos R+G

and LCP-CEMENT were less effective, showing results of 2.8×10^5 CFU/ml, 1.1×10^5 CFU/ml and 2.2×10^5 CFU/ml respectively. FDL-CEMENT015, FDL-CEMENT030 and FDL-CEMENT060 in each case showed a significant reduction in colony forming units in comparison to Palacos R ($p < 0.0001$ for FDL-CEMENT015, FDL-CEMENT030 and FDL-CEMENT060); Palacos R+G ($p = 0.0199$, $p = 0.0043$ and 0.0011 respectively); and LCP-CEMENT ($p < 0.0001$ for FDL-CEMENT015, FDL-CEMENT030 and FDL-CEMENT060). FDL-CEMENT015, FDL-CEMENT030 and FDL-CEMENT060 were not significantly different from each other (FDL-CEMENT015 and FDL-CEMENT030 $p = 0.9354$, FDL-CEMENT015 and FDL-CEMENT060 $p = 0.4948$, and FDL-CEMENT030 and FDL-CEMENT060 $p = 0.9405$).

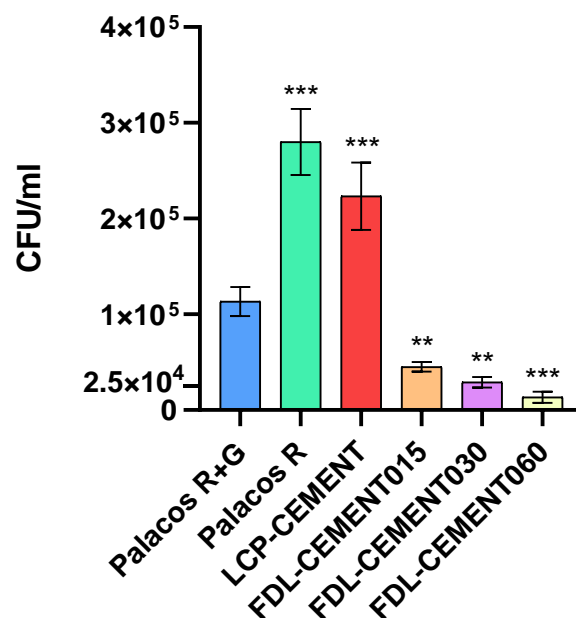


Figure 49: Colony forming units (CFU) for Palacos R and Palacos R+G, LCP-CEMENT, FDL-CEMENT015, FDL-CEMENT030 and FDL-CEMENT060 (n=3). Data is presented as mean ± standard deviation (n=3). Asterisks indicate the level of significance with respect to Palacos R+G (* $p < 0.05$, ** $p < 0.01$, * $p < 0.001$).**

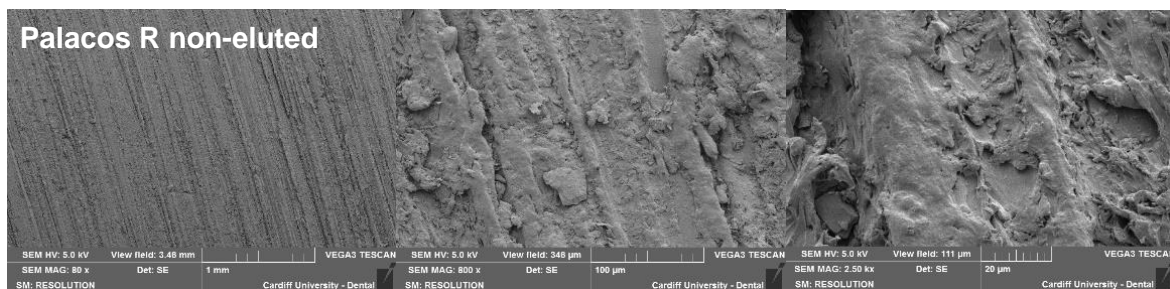
4.3.5.2 Analysis of biofilm formation

The cement discs stored in inoculum were removed after 48 hours, vortexed with glass beads and sonicated to dislodge any biofilm formed around the cement discs. Any dislodged *S. aureus* biofilm was allowed to regrow on plates. For all cement discs tested, no colony forming units were observed after incubation of the agar plate for 18 hours (0 CFU/ml for all samples), meaning that *S. aureus* was not detected.

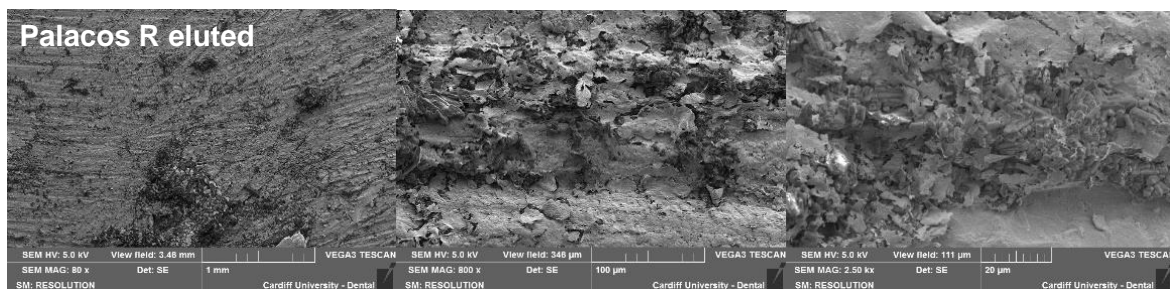
4.3.6 SEM images of cement disc surface

SEM was used to characterise all of the cement disc formulations' surface morphology after manufacture; moreover, the discs were also analysed to see the difference in surface morphology before and after incubation in PBS for one week. Figure 50 shows SEM images, at magnifications of 80, 800 and 2.5K, of Palacos R, Palacos R+G, LCP-CEMENT, FDL-CEMENT015, FDL-CEMENT030 and FDL-CEMENT060, freshly prepared (non-eluted) and after an incubation period in PBS at 37 °C for one week (eluted). All of the cement discs, both eluted and non-eluted discs, with the exception of Palacos R, contained fused round PMMA particles and pores/air-pockets. Examples of round particles and pores are shown by orange and blue arrows respectively. It was not possible to confirm by looking at the SEM images, whether incubation had an effect on pore/channel formation.

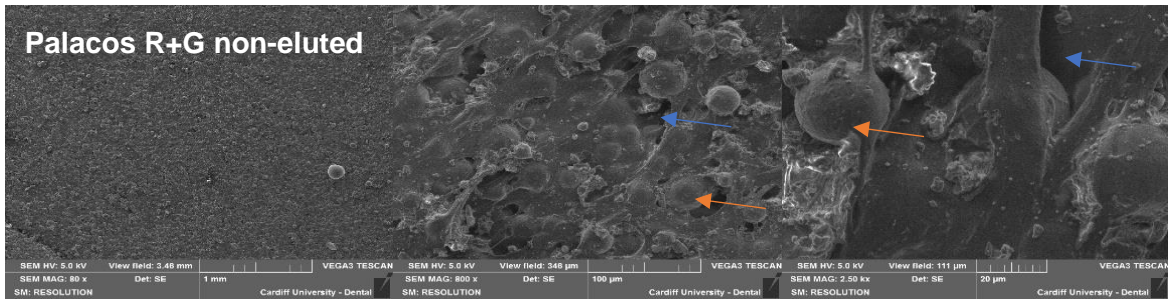
(A)



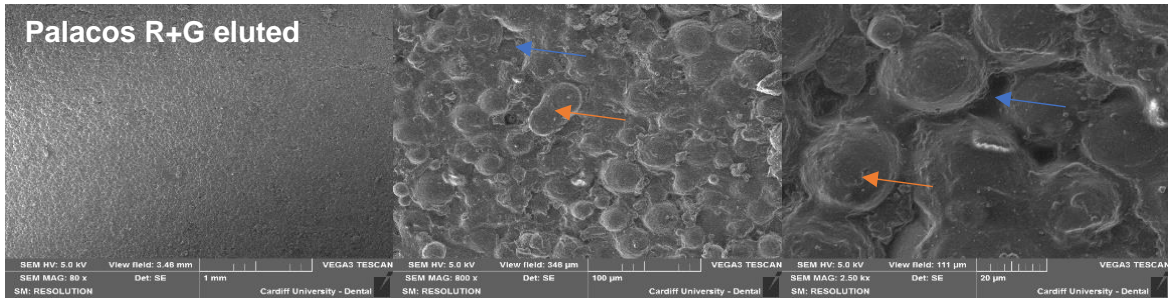
(B)



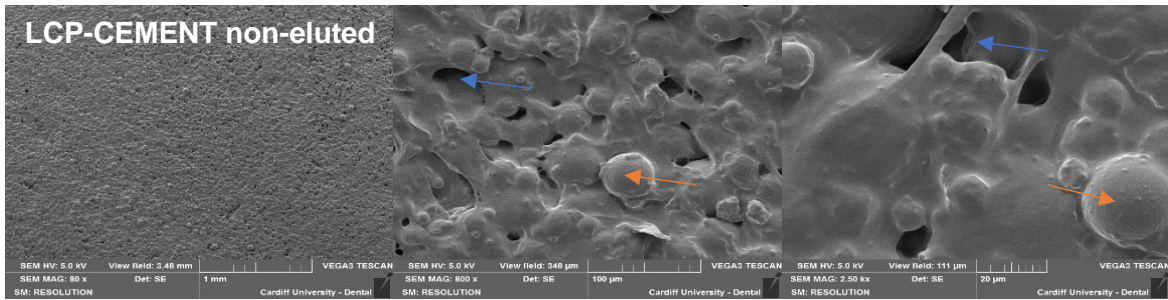
(A)



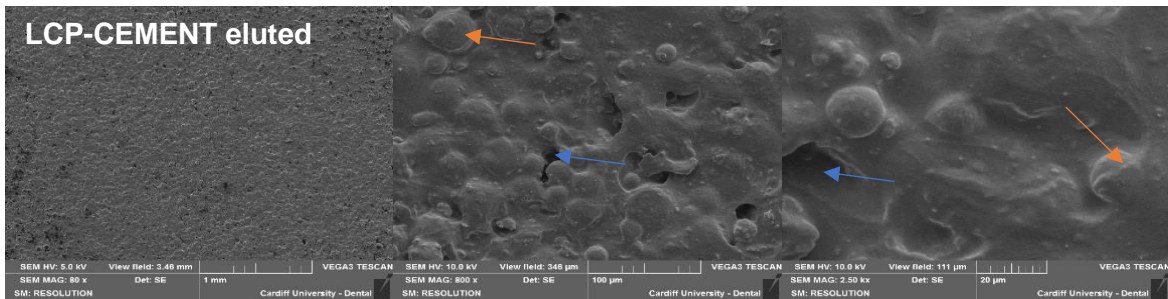
(B)



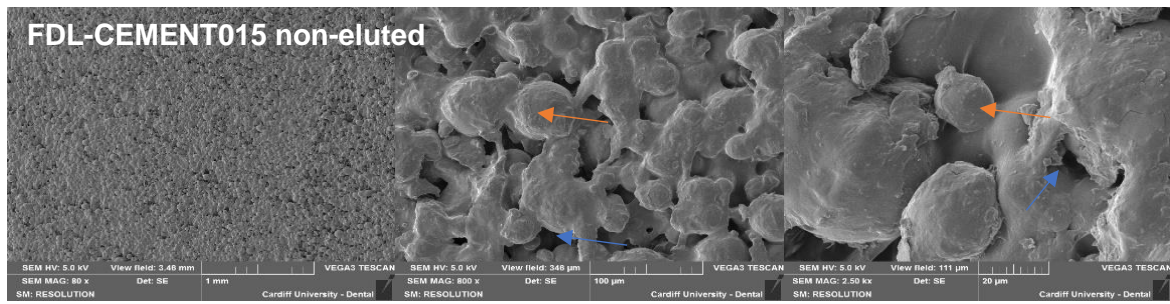
(A)



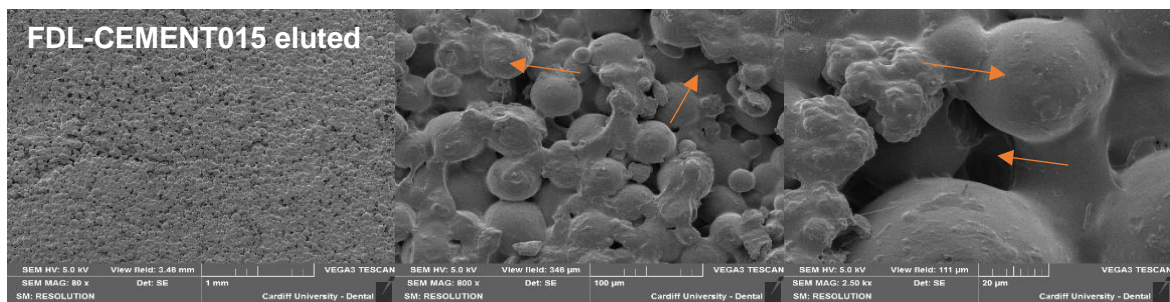
(B)



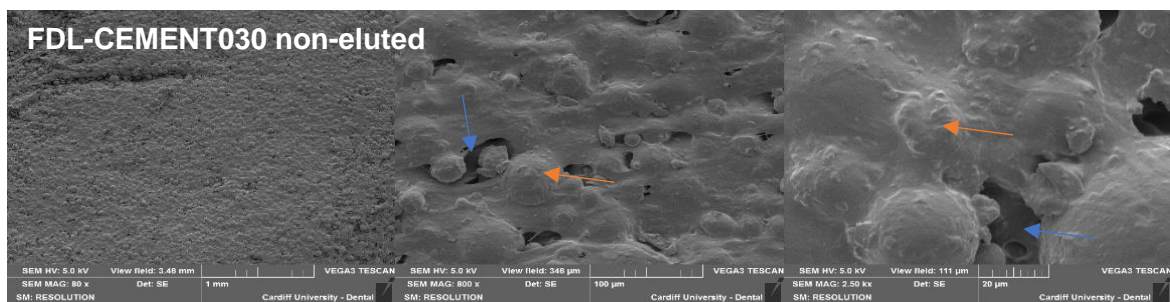
(A)



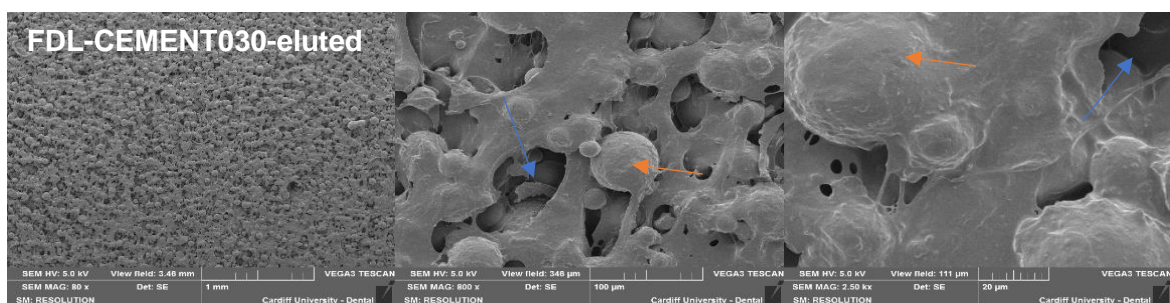
(B)



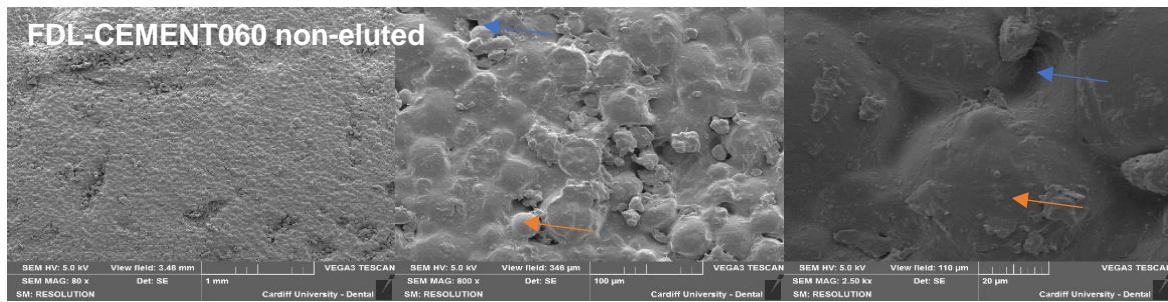
(A)



(B)



(A)



(B)

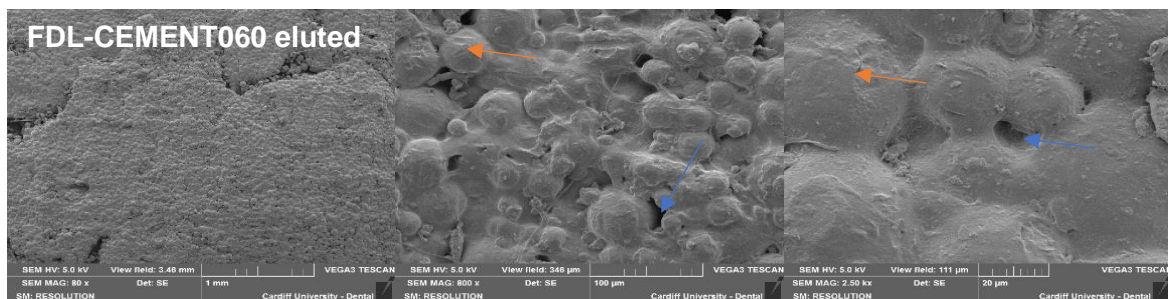


Figure 50: SEM surface images for Palacos R and Palacos R+G, LCP-CEMENT, FDL-CEMENT015, FDL-CEMENT030 and FDL-CEMENT060; (A) before and (B) after incubation in PBS for one week at 37 °C; sample magnifications are x80, x800 and x2.5k respectively. Arrows indicate PMMA particles (orange) and pores (blue).

4.3.7 Measurement of phosphatidylcholine loss during liposome manufacturing processes

Loss of phosphatidylcholine at different stages of liposome manufacture was assessed. Phosphatidylcholine mass content was measured using the colorimetric Stewart assay, after extrusion through polycarbonate membranes and after ultracentrifugation. SEM images were taken of the polycarbonate membranes to observe any residue from phosphatidylcholine.

4.3.7.1 Assay of phosphatidylcholine during liposome membrane extrusion process

The initial mass of phosphatidylcholine lipid used at the start of the process to make the liposomes was assayed using the Stewart assay, and then after the process of making and extruding liposomes through polycarbonate membranes, the final mass of phosphatidylcholine was assayed using the same method. Assaying the starting mass

quantity of phosphatidylcholine and the mass amount after extrusion shows how much phosphatidylcholine had been lost during this process. The mean initial mass used was 23.8 ± 0.6 mg and the mean final extruded amount was 19.8 ± 0.5 mg. The lipid lost during this process was around one sixth of the starting material (16.8 ± 3.3 %).

4.3.7.2 SEM images of 100 nm, 200 nm and 400 nm polycarbonate Whatman track-etched Membranes (controls and after extrusion):

SEM images of the polycarbonate filters used during liposome extrusion were taken to visualise any retained lipid on the membranes during the extrusion process. This helps to show that lipids are effectively lost during this process.

Figure 51 shows SEM images at various magnifications of 1K to 15K of surfaces of the polycarbonate Whatman Track-Etched Membranes used during the liposome extrusion process. Images of control membranes (unextruded) and membranes used for liposome extrusion are shown (pore sizes: 100 nm, 200 nm and 400 nm). It can be seen that on the membranes used for extrusion, there is residual material that is not present on the control membranes. The 400 nm pore membrane, which was the first membrane used in the process, contains the most residual lipid, followed by the 200 nm and 100 nm filter papers. The 400 nm filter paper is more uniformly coated with residual lipid, whereas the 100 nm and 200 nm filter papers are coated with smaller quantities.

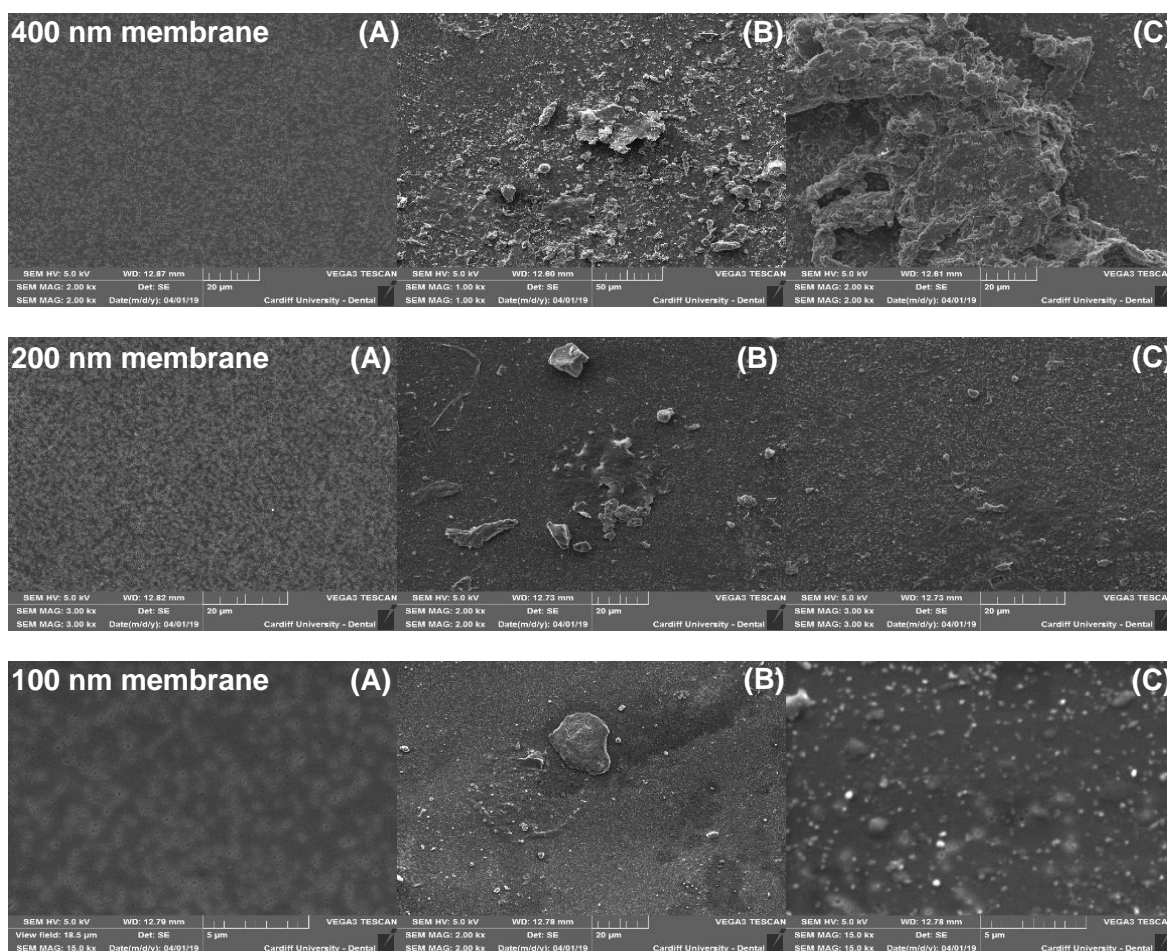


Figure 51: SEM images of Whatman Track-Etched Membranes, of pore sizes 100 nm, 200 nm and 400 nm. Images taken show control samples that have not been extruded (A) and membranes after liposome extrusion (B) and (C). All images taken at various magnifications (1k to 15k).

4.3.7.3 Measure of phosphatidylcholine mass loss during ultracentrifugation process using 107, 000 g

The phosphatidylcholine mass content of the liposome suspension produced after the extrusion process was measured using the Stewart assay (Section 4.3.7.1), prior to the ultracentrifugation process to form a liposome pellet. The mass quantity of phosphatidylcholine measured prior to ultracentrifugation was compared to the final phosphatidylcholine mass content in the resulting liposome pellet and in its respective supernatant liquid, after ultracentrifugation for different lengths of time (1.5 hours, 3 hours and 4.5 hours). The sum of the mass content of phosphatidylcholine determined individually in each pellet and supernatant liquid, for the different centrifugation times, corresponded to the total starting mass content, showing that no phosphatidylcholine was lost during the

centrifugation process. Increasing the centrifugation time caused the amount of phosphatidylcholine contained in the pellet to increase, and consequently a decrease in the amount contained within the supernatant liquid was observed. All of the pellets formed showed a significant increase in phosphatidylcholine mass content by increasing the time of centrifugation from 1.5 hours to 3 hours and 4.5 hours (1.5 hours and 3 hours $p=0.0014$, 1.5 hours and 4.5 hours $p<0.0001$, and 3 hours and 4.5 hours $p=0.0019$). The supernatant liquids at 3 hours and 4.5 hours showed a significant decrease in phosphatidylcholine mass content compared to the supernatant liquid at 1.5 hours ($p<0.0001$ for both supernatant liquids at 3 hours and 4.5 hours). The supernatant liquids at 4.5 hours did not show a significant decrease in lipid mass content compared to the supernatant liquid at 3 hours ($p=0.9813$). It was shown that increasing the centrifugation time from 1.5 hours to 4.5 hours caused for an increase in the pellet phosphatidylcholine mass content from 25% to 50% (Figure 52). It was also shown that larger diameter liposomes were present in the pellet and smaller diameter liposomes were present in the supernatant liquid, after centrifugation. At 1.5 hours the average particle diameters of the pellet and supernatant liposomes were found to be 130 nm and 110 nm respectively; at 4.5 hours, the average particle diameters of the pellet and supernatant liposomes were found to be 125 nm and 107 nm respectively. The average particle diameter for non-centrifuged liposomes was 114 nm (Figure 53).

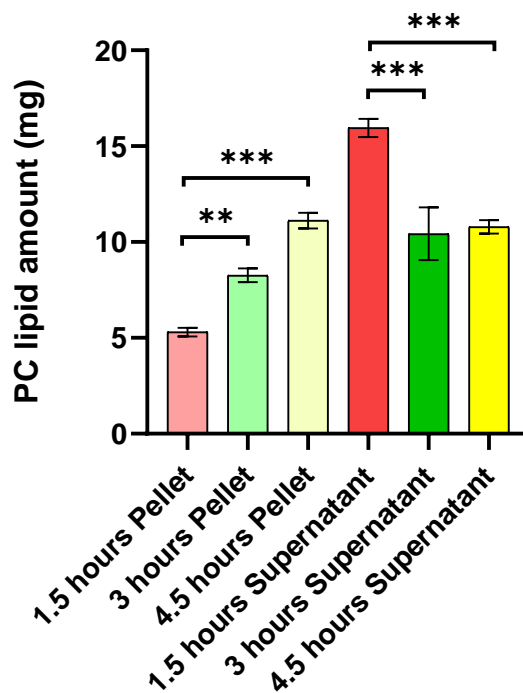


Figure 52: Amount of lipid measured in mg for both the pellet and supernatant after centrifugation at an average force of 107,000 g at time points of 1.5, 3.0 and 4.5 hours (n=3). Asterisks indicate the level of significance (* $P<0.05$, ** $P<0.01$, * $P<0.001$).**

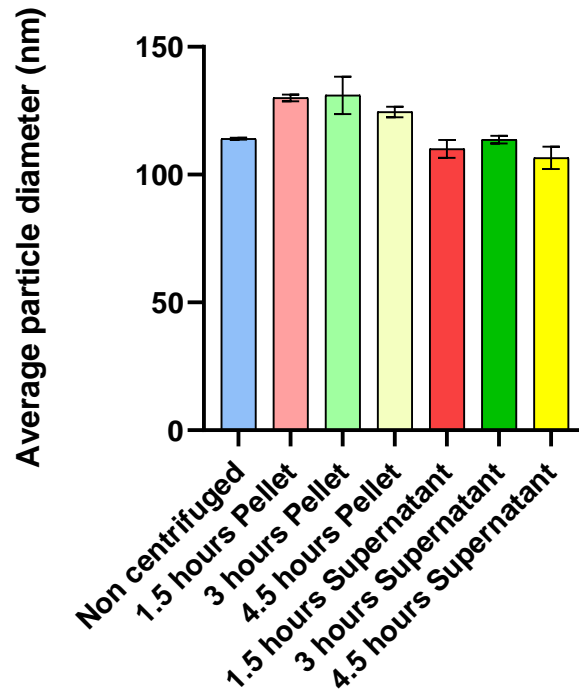


Figure 53 Average particle diameter measure for liposomes in both the pellet and supernatant after centrifugation at an average force of 107,000 g at time points of 1.5, 3.0 and 4.5 hours (n=3).

4.3.7.4 Measure of phosphatidylcholine mass loss during ultracentrifugation process using 207, 000 g

Because particles of different size and density sediment at different rates, larger and denser particles will sediment faster. This means that smaller and lighter liposomes are likely to remain in the supernatant liquid; sedimentation for these can be increased by using increasing the rotation speed and therefore the centrifugal force. The phosphatidylcholine mass content of the liposome suspension, produced by liposome extrusion, was measured using the Stewart assay prior to ultracentrifugation. The mass quantity of phosphatidylcholine measured prior to ultracentrifugation, using a faster rotor of average force of 207,000 g, was compared to the final phosphatidylcholine mass content in the resulting liposome pellet and in its respective supernatant liquid, after ultracentrifugation for different lengths of time (1.5 hours and 3 hours). The sum of the mass content of phosphatidylcholine determined individually in each pellet and supernatant liquid, for the different centrifugation times, corresponded to the total starting mass content, showing that no phosphatidylcholine was lost during the centrifugation process. Increasing the centrifugation time caused for an increase in the amount of lipid contained in the pellet, and

consequently a decrease in the amount contained within the supernatant liquid. It was shown that increasing the centrifugation time from 1.5 hours to 3 hours caused for an increase in the pellet lipid mass content from 83% to 95% (Figure 54). The pellet formed at 3 hours showed a significant increase in lipid mass content compared to the pellet formed at 1.5 hours ($p=0.0007$). The supernatant liquid at 3 hours showed a significant decrease in lipid mass content compared to the supernatant liquid at 1.5 hours ($p<0.0035$). It was shown that after centrifugation for 1.5 hours, larger diameter particles were present in both the pellet and the supernatant liquid, after centrifugation. The average particle diameters of the pellet and supernatant liposomes were found to be 154.4 ± 5.9 nm and 124.7 ± 11.7 nm respectively. The average particle diameter for non-centrifuged liposomes was 114.0 ± 0.3 nm (Figure 55).

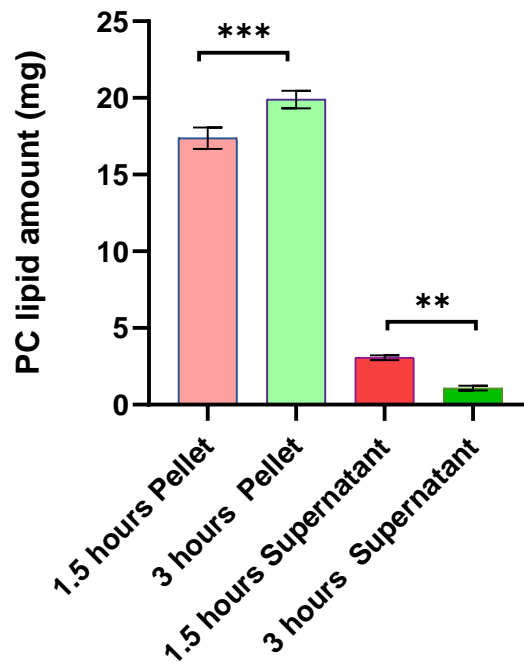


Figure 54: Amount of lipid measured in mg for both the pellet and supernatant after centrifugation at an average force of 207,000 g at time points of 1.5 and 3.0 hours ($n=3$). Asterisks indicate the level of significance (* $p<0.05$, ** $p<0.01$, * $p<0.001$).**

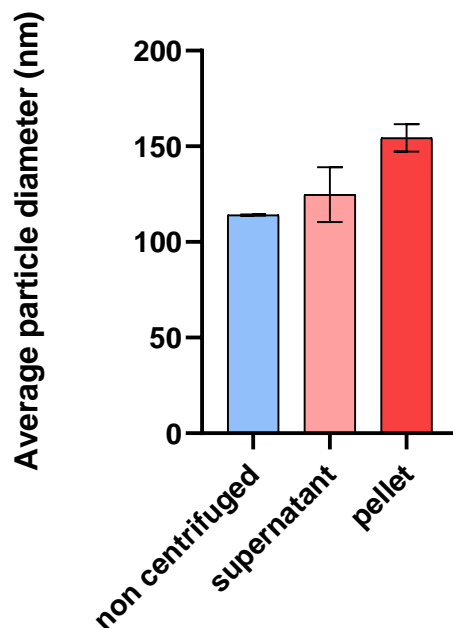


Figure 55: Average particle diameter of measure for liposomes in both the pellet and supernatant after centrifugation at an average force of 207,000 g at 1.5 hours (n=3).

4.4 Discussion

This chapter aimed to establish a freeze-dried liposomal formulation based on the liposomal formulation developed and patented by Ayre *et al.* (2016) (Ayre *et al.* 2016. Liposomal drug delivery system for bone cements. US9895466.; Ayre *et al.*, 2015). Liposomes were freeze-dried and various quantities of the freeze-dried liposomes, containing different mass amounts of gentamicin base were incorporated into bone cement. FDL-CEMENT015, FDL-CEMENT030 and FDL-CEMENT060 released very low mass quantities of gentamicin. The mass quantities of gentamicin released by the FDL-CEMENTS over 90 days were compared to the gentamicin release from the commercial product Palacos R+G, and LCP-CEMENT. Results for the FDL-CEMENTS were compared to the commercial product, Palacos R+G, as commercial antibiotic loaded bone cement is the most commonly used material in orthopaedic surgery and is currently considered to be the gold standard for drug delivery (Karaglani *et al.*, 2020; Singh *et al.*, 2019). FDL-CEMENTS were also compared to the LCP-CEMENT, to see if incorporation of freeze-dried liposomes into bone cement affects antibiotic release. Palacos R+G cement released 632 µg of gentamicin base on the first day of drug-release, and in total, a cumulative mean mass quantity of 748 µg of gentamicin at 90 days. However, at 90 days, FDL-CEMENT015, FDL-CEMENT030 and FDL-CEMENT060 released total cumulative mean mass quantities of 6 µg, 13 µg, and 51 µg respectively. The

mass quantities of gentamicin released by all of the FDL-CEMENTS were not comparable with the mass quantities of gentamicin released from LCP-CEMENT tested in Chapter 3, as they were significantly lower. LCP-CEMENT released 206 µg of gentamicin on the first day, and further mass quantities of between 18 µg and 77 µg at each consecutive time point after that up until 135 days. An initial burst of gentamicin was observed for both Palacos R+G and LCP-CEMENT, however, despite the initial burst of gentamicin from the surface of the Palacos R+G and LCP-CEMENT, further drug release was observed. Currently, all antibiotic loaded cements show a burst release profile, as they release antibiotic in a biphasic manner, effectively releasing most antibiotic in the first hours (Cyphert et al., 2018; Mori et al., 2011). Since drug release from PMMA bone cement is primarily a surface phenomenon (Letchmanan et al., 2017; van Belt et al., 2000), most antibiotic is released at the outset upon contact between dissolution medium and the PMMA surface. The characteristic burst release was not observed for FDL-CEMENTS suggesting that there were no significant mass amounts of gentamicin sulfate on the PMMA disc surface. It is also worth noting that for the FDL-CEMENTS, only a very small percentage of the incorporated gentamicin mass content was released. FDL-CEMENT015 and FDL-CEMENT030 released approximately 1% of the incorporated amount of gentamicin, and FDL-CEMENT060 released approximately 3%. This is in stark contrast to Palacos R+G and LCP-CEMENT which released 18% and 31% of their total incorporated gentamicin contents respectively. Of the FDL-CEMENT discs tested, the highest gentamicin mass content release was from FDL-CEMENT060, which contained the largest mass content of gentamicin base and of the cryopreservant, sucrose. The increased release of gentamicin from FDL-CEMENT060 could be due to the channelling effect, as it contains the highest amount of channelling agents (Sudha et al., 2010; Zakaria et al., 2019). Channelling agents such as sucrose (Igbinaduwa et al., 2019) and gentamicin sulfate itself (Virto et al., 2003), which are soluble in the dissolution medium, are incorporated into the formulation, forming pores and capillaries by which the drug can diffuse through them and be released into the dissolution medium. Moreover, the incorporation of more hydrophilic material in FDL-CEMENT060 could cause for hydrophilisation of the bulk cement and therefore increase the wettability (El-Fallal et al., 2009; Oh et al., 2016; van Belt et al., 2000), as was observed by contact angle measurements; meaning that increased penetration of water into pores via the PMMA cement surface would therefore cause for an increase in drug release (van Belt et al., 2000). In a study where porogens were incorporated into bone cements, producing pores within the bone cement matrix, gentamicin release was increased with further addition of porogens, i.e., increased pores in the bone cement matrix (Wu, 2016); this is similar to the increase in concentration of the freeze-dried formulation within Palacos R bone cement, as an increase in the amount of incorporated freeze-dried material in bone cement, effectively means more incorporated gentamicin

sulfate and sucrose, both of which are channelling agents, capable of creating pores in the bone cement after storage in water.

Contact angles indicate the wettability of a given surface. These were measured to ascertain whether the bone cement formulations had increased or decreased wettability in comparison to the commercial bone cement, Palacos R+G. It is likely that a surface with increased wettability will release higher mass quantities of antibiotic, as the increased wettability means that a higher degree of water contact between the disc surface and water has been achieved. FDL-CEMENTS showed similar contact angles to Palacos R and the LCP-CEMENT. However, FDL-CEMENTS showed an increase in contact angle compared to Palacos R+G, which could be due to there being more gentamicin sulfate (hydrophilic compound) present in the Palacos R+G cement discs, and therefore more gentamicin sulfate on the disc surface. Moreover, gentamicin sulfate is found in agglomerates in commercial cement (Dunne et al., 2009), meaning that larger mass amounts of gentamicin sulfate could be on the surface and in contact with the test droplet, making the overall contact angle lower due to a much more hydrophilic surface. Low contact angles denote good contact between water and a surface, whereas high contact angles denote the ability of a surface to repel water (Huhtamäki et al., 2018). Too low of a contact angle could therefore cause for insufficient contact between water and bone cement, which could affect the levels of drug release from the cement by causing less water absorption into the cement, and therefore less drug release (Shinsako et al., 2008). However, given that the contact angles for FDL-CEMENTS are similar to LCP-CEMENT which released mass amounts comparable to the antibiotic release by Palacos R+G (Chapter 3), it can be assumed that the contact angles for FDL-CEMENTS are sufficient for water absorption. This indicates that the low levels of mass quantities of gentamicin released by the FDL-CEMENTS were not necessarily due to insufficient contact between their surfaces and water.

The mean mass of gentamicin sulfate in the freeze-dried vials was found to be 2.5 mg, which is approximately half the mass of gentamicin sulfate mass amount that was in each vial prior to freeze-drying. This could mean that either there has been loss of sample during the freeze-drying process or that the stability of the gentamicin sulfate has not been maintained. Each vial contained 1 ml of the freeze-dried formulation, which was composed of 1 mg/mL of lipid content, 5 mg/mL of gentamicin sulfate and 5 mg/mL of sucrose. This means that each vial should contain 11 mg in total, approximately 10% of the mass quantity has been lost during the process. It can be assumed that a fraction of the lipids was lost during the extrusion process, as it was shown in Section 4.3.7.1 that around one sixth of the phospholipid content was lost during this stage of the liposome manufacture, which may

account for some of the loss of the freeze-dried material. In terms of product transfer, it is unlikely that the constituents were retained on the hydrophobic surfaces of the polypropylene plastic tubes where the liposome suspension and pre-freeze-dried formulation were stored (Barbosa et al., 2019; Watson et al., 2009) as liposome surfaces, gentamicin sulfate and sucrose are hydrophilic (Kubica et al., 2014; New, 2003; Prior et al., 2000); this also applies to the pipette tips used for dispensing the liposome suspension. Although gentamicin sulfate is known to be thermally stable up to higher temperatures of even up to 100 °C (Wang et al., 2004), there are not many studies investigating the stability of gentamicin sulfate at sub-zero temperatures or after freeze-drying. There are several studies which involve the freeze-drying of gentamicin sulfate in various formulations (Blanco-Príeto et al., 2002; Dorati et al., 2018; Kunz et al., 2019), however, none of them have investigated the stability of gentamicin sulfate after the freeze-drying process itself, so it cannot be established as to whether the freeze-drying process has affected the gentamicin potency. Moreover, stability has been characterised by microbiological assays in these studies, meaning that accurate degradation data cannot be obtained. A loss of 50% of the active ingredient suggests that degradation of gentamicin sulfate may have been accelerated during the process. A degradation of 50% for gentamicin sulfate is considered high, as the general degradation of gentamicin due to exposure to UV-light, water and temperature is well documented (Waheed, et al., 2014). In a study performed to ICH and WHO guidelines, a gentamicin water-based-gel formulation was subjected to accelerated aging for 6 months, and gentamicin was found to have degraded by only 11% of its original total content (Sombié et al., 2014). This study therefore gives an indication of the long-term stability of gentamicin in water. However, it is possible that one of the other constituents from the freeze-dried formulation, in this study, may have affected gentamicin sulfate. In a study, a formulation containing 5% w/w dextrose mixed with gentamicin sulfate, it was shown that gentamicin was degraded much faster than a control sample containing just gentamicin sulfate and water alone. The degradation with dextrose occurred at room temperature, producing several known degradation products; however, these degradation compounds that were observed, were not all present in a control mixture of gentamicin sulfate in water without dextrose. The presence of further degradation products when gentamicin sulfate is mixed with dextrose indicates a chemical reaction between the two compounds (Graham et al., 1997). At room temperature, the gentamicin sulfate content degraded by 37% when mixed with dextrose, whereas gentamicin sulfate in water alone showed no significant degradation (Graham et al., 1997). Sucrose is a disaccharide formed by monomers of glucose and fructose joined together by an ether known as a glycosidic bond, via a dehydration reaction (Das, 2015; Sánchez-Lozada et al., 2010), glucose is also known as dextrose (Latorre & Baez-nieto, 2013). Due to the molecular and functional group similarities of both sucrose and dextrose molecules, it may be possible

that sucrose interacts with gentamicin sulfate in the same way, or that perhaps the glycosidic bond is broken, and that glucose reacts with gentamicin. Further investigations into the interaction of gentamicin and sucrose should be performed, by mixing sucrose with gentamicin sulfate, followed by LC-MS assay of gentamicin to characterise degradation quantitatively. Loss of gentamicin during the manufacturing process, prior to freeze-drying, should also be investigated, as a significant loss in gentamicin mass quantities was not anticipated; although no significant loss is expected as LCP-CEMENTS released significant mass quantities of gentamicin sulfate. Given the possible degradation of gentamicin with sucrose, it is not expected that FDL-CEMENTS will release significant mass quantities after 3 months. If degradation of gentamicin by sucrose is confirmed, degradation is likely to continue further, even if gentamicin is released into the release media, as sucrose will also be present in the release media.

The concentrations of gentamicin released by the discs were compared to the minimum inhibitory concentration (MIC) for gentamicin. The MIC is the lowest concentration of an antimicrobial that prevents visible growth of a microorganism after overnight incubation (Andrews, 2001). In two separate studies, using a collection of different strains of *S. aureus*, the minimum inhibitory concentration of gentamicin sulfate was determined as being 0.016 µg/ml (Gentilini et al., 2000) and as 0.06 µg/ml (Mottola et al., 2016). The gentamicin release by Palacos R+G has exceeded these concentrations at each time point up until three months. FDL-CEMENT060 has also exceeded the MIC up until the 72-hour mark, although at 96 hours it is not known if the MIC was exceeded, since the concentration obtained was below the LOQ for the LC-MS method (1 µg/ml), as well as being below the LOD (0.5 µg/ml). As the LOQ and LOD concentrations are much higher than the MIC concentrations obtained by both studies, it is possible that gentamicin sulfate was released at concentrations higher than the MIC at the time points where the concentration is lower than the LOQ. The same applies to FDL-CEMENT015 and FDL-CEMENT030 which did not release concentrations above the LOQ over several time points. FDL-CEMENT015 released concentrations of gentamicin that were below the LOQ at all time points except for the three-month time point; FDL-CEMENT030 released 1.3 µg/ml. It is worth noting that the MIC values in both studies were not actually determined by spectroscopic analysis, rather they were calculated by serially diluting known concentrations of gentamicin sulfate, which is why much lower concentrations were determined in comparison to the LC-MS method (Gentilini et al., 2000; Mottola et al., 2016). The fact that FDL-CEMENT060 has released gentamicin above the MIC value for three days consecutively shows us that it will inhibit bacteria growth for at least three days. It has been shown experimentally that following TJR, 24 hours is the critical time-period where biofilm formation occurs; at this stage, an infection becomes more

difficult to treat, and usually requires removal of the implants (Webb et al., 2013). However, due to the fact that after the 72-hour time point, the antibiotic release is below the detection limit of the LC-MS, it is not known whether gentamicin above the MIC value has been released, or if sub-inhibitory concentrations have been released at this point. Administering sub-inhibitory levels of antibiotic could cause for the formation of antibiotic resistant bacteria (Jiranek et al., 2006). Furthermore, it has been shown experimentally, that bacteria such as *S. aureus* are able to effectively colonise different biomaterials, including antibiotic-loaded PMMA bone cement which provides an optimal surface for bacteria, which could be cause for concern, if the bacteria count is not reduced (Jiranek et al., 2006; McConoughey et al., 2015). The quantitative antimicrobial suspension test showed that the freeze-dried samples were in fact the most effective in reduction of bacteria count. FDL-CEMENT015, FDL-CEMENT030 and FDL-CEMENT060 all caused for larger reductions of the bacteria count, from 10^6 CFU/ml to 10^4 CFU/ml. Whereas Palacos R, Palacos R+G and LCP-CEMENT were all less effective than the FDL-CEMENTS, causing reduction of the bacteria count, from 10^6 CFU/ml to 10^5 CFU/ml. The results for the freeze-dried cement discs are not consistent with the other cement disc results. Moreover, given the very low assay results for gentamicin by LC-MS for the freeze-dried cements, it would not be expected that these discs would exceed the other gentamicin containing discs for bacteria colony reduction, particularly as the mass amounts of gentamicin released by these samples were largely below the limit of quantification; moreover, the gentamicin mass content released was much lower than for the Palacos R+G and for the liposomal formulation. This experiment should be repeated to confirm this result. No biofilm formation was detected on any of the cements after 48 hours, indicating that biofilm may have been prevented by the various cement formulations. However, although the *S. aureus* strain used in this experiment (NCTC 10788) is known to produce biofilms (Gwynne et al., 2021), the experiment should be conducted by using a control disc made from a material where biofilm growth is known to occur e.g. glass (Marques et al., 2007; Shukla & Rao, 2017). Given the low assay result of gentamicin by LC-MS for the freeze-dried cements, these findings are unexpected, as the mass amounts of gentamicin released by these samples was much lower than for the Palacos R+G and for the liposomal formulation. The osmotic effect on bacteria caused by high sucrose concentrations is documented (Mizzi et al., 2020). It was reported that *S. aureus* is completely inhibited at a concentration of 195 g of sucrose per 100 g of water (Akiyama et al., 1998), and much less sucrose is incorporated into this formulation. Moreover, it was shown in Chapter 3 that 10 mg of MMA alone causes for a reduction in bacteria count for *S. aureus*. A possibility is that more MMA may have eluted from the bone cement due to increased pores in the cement caused by the channelling effect, due to sucrose. It is known that MMA elutes from the cement disc as demonstrated in an original study (Buchholz HW,

1970). It is also possible that the combination of sucrose and gentamicin caused for an improved effect on the bacteria. The combination of sugar and antibiotics has been investigated in a study aimed at killing persistent bacteria (Allison et al., 2011). The results showed that sugar can make gentamicin more effective in killing *S. aureus* persisters when used in combination with antibiotics; however, in that study, which used several different sugars, only fructose was shown to be effective against persisters, however, it should be noted that sucrose was not used in the study. The effect of incorporating just a channelling agent into Palacos R should be investigated, as well as the mass amount of MMA being released. If it is possible to release MMA from bone cement in larger mass quantities, it could be useful; however, it should be noted that although PMMA bone cement is considered safe, there are documented side effects including tissue complications and systemic problems, which may be attributed to MMA (Gosavi et al., 2010; Kitajima & Ogawa, 2021). Moreover, there are several in-vitro studies suggesting MMA as being cytotoxic (Ansteinsson et al., 2013; Pradeep & Sreekumar, 2012), so the use of MMA as a tool for reduction in bacteria should be treated with caution. The current benchmark in preventing infection is the commercial gentamicin loaded cement, Palacos R+G (Karaglani et al., 2020), any successful test sample will either match its result or exceed it, as even though there are currently no set limits for the release of antibiotic, the commercial product is known to be an effective treatment for infection prophylaxis in orthopaedic surgery (Al Thaher et al., 2016). As stated in the previous chapter, one of the limitations of this test is that only one time-period was tested, the first 4 hours of drug release. The reason for testing one single time point was due to time-constraints during this study. It is thought that the first two to four weeks are important in managing potential infections following joint replacement surgery (Bernard et al., 2010). It would therefore be beneficial to test a sample over several time points, over at least two weeks, to observe whether the test samples are capable of reducing the bacteria count at key time points, since the issue with the commercial product is that it demonstrates a burst release profile and does not release in a controlled, sustained, manner after the initial first hours (Neut et al., 2010). Even though, the FDL-CEMENTS caused the largest reduction in bacteria count, it is unknown whether these test samples would continue to reduce the bacteria count after this time point (4 hours); moreover, due to the very low gentamicin release observed by LC-MS, it is unclear at this stage as to their mechanism of antimicrobial activity i.e., whether the antibiotic in combination with sugar has an effect, if larger quantities of MMA are being released, or if there is another reason.

Overall, Palacos R was the strongest material in all tests, except for compressive strength, where FDL-CEMENT030 had the highest compressive strength. FDL-CEMENT060 failed all of the mechanical tests outright, therefore, no data was obtained for it. FDL-CEMENT015

and FDL-CEMENT030 passed the ISO 5833 requirements for compressive strength and bending modulus, however, FDL-CEMENT030 failed the requirement for bending strength. For compressive strength, both freeze-dried samples showed improved mechanical strength and were in fact stronger than Palacos R+G and the current liposomal formulation; FDL-CEMENT030 obtained the highest result outright, and FDL-CEMENT015 had a compressive strength marginally lower than Palacos R. Addition of the FDL formulation to Palacos R caused for a reduction in bending modulus and bending strength. These mechanical testing results show that the FDL-CEMENTS can improve compressive strength and are able to pass various requirements as established in the ISO 5833 standard. It is worth noting that large volumes of freeze-dried material were added to Palacos R, in comparison to the LCP formulation which required a smaller volume of material, as a pellet, to be added to Palacos R. As a result of the relatively large volumes of FDL formulation added, the highest quantity that could be mixed into Palacos R was a mass amount containing the equivalent of 0.60% w/w of gentamicin base (FDL-CEMENT060). The results show that addition of the FDL formulation, up until 0.30% w/w of gentamicin base, caused for an increase in compressive strength, and a decrease in bending strength and bending modulus. FDL-CEMENT060 failed all the tests and FDL-CEMENT030 failed bending strength, and therefore are not suitable for clinical use due to their inferior mechanical properties. FDL-CEMENT015 passed all of the ISO 5833 requirements and from the mechanical testing perspective, it could be considered suitable for clinical use. The mechanical properties are clinically important so that loads may be transmitted through the joint into the bone and muscle over long periods of time. The function of bone cement in a cemented hip replacement is to transmit loads through the joint over very long periods of time; moreover, forces are transmitted through the joints and bone cement is subjected to high stresses (C. Lee, 2017). Currently, the commercial cements, both those containing antibiotic and without antibiotic, demonstrate the highest mechanical testing results.

The zeta potential of freeze-dried liposomes at 3 days after manufacture was found to be 40 mV, indicating that the liposomes have good colloidal stability at this stage; whereas after storage for 12 months, the zeta potential of freeze-dried liposomes was found to be 1.7 mV, indicating that flocculation is likely to have occurred due to low colloidal stability (Kumar & Dixit, 2017; Lowry et al., 2016). The average particle diameter of the freeze-dried liposomes after 12 months was found to be 1483 nm, showing that particle size was not maintained long term, after storage at 2-8 °C for 12 months, as particle size had increased significantly from the initial measurement of 281 nm. Moreover, the polydispersity index for the liposomes measured at 3 days was found to be 0.2, indicating that the particle size at this stage is homogenous (Refai et al., 2017), whereas at 12 months the polydispersity index was found

to be 0.9, which is above 0.7, indicating that the particle size distribution is not homogeneous (Refai et al., 2017). It was thought that after removal of water during the freeze-drying process, sucrose could be used as a cryopreservant, replacing water molecules at the lipid head group, thus maintaining the lipid bilayer structure, while retaining the original size of the liposome (New, 2003). However, the increase in liposome size suggests that the liposomes have been transformed from SUV to LUV, possibly by the process of fusion (Franzé et al., 2018). Fusion can be caused by the difference in packing, causing intermembrane fusion in the SUV, at temperatures below the phase transition temperature (T_c), where lipid chains become disordered forming a glass-like structure; therefore, causing tight packing, in particular in the inner monolayer, causing a reduction in flexibility and motion in the bilayer (New, 2003). The complexity of the freeze-drying process certainly plays a role in this, and it should be noted that for freeze-drying of the liposomal formulation, the freeze-drying characteristics of the formulation were not investigated beforehand. Choosing the process parameters and the right cryopreservative additives for protection of membrane integrity, from the stresses which are due to freezing and dehydration is a complex task (Franzé et al., 2018). Due to the fact that liposomes contain water, when the water is removed, the liposomes can spontaneously reassemble causing for an irreversible, alteration of their structure (Chen et al., 2010).

All FDL-CEMENT discs contained air pockets and pores. It is known that the PMMA mixing methods influence the degree of cement porosity (Shiramizu et al., 2008). As with the cement produced from the current liposomal formulation, all of the freeze-dried samples appeared to be formed from fused round particles. The round particles appear to be PMMA particles that have not fully polymerised. This may be due to additives sterically inhibiting the PMMA and MMA from fully interacting together. It is possible to see pore formation on the surface of the freeze-dried samples of samples stored in PBS, as well as pores formed in the control samples (non-eluted). The pores present in the cements containing round pores may be due areas of the cement that have not polymerised as well as gaps between round particles. As has already been discussed, since the freeze-dried formulations contain sucrose, which is a channelling agent, formation of pores and channels would be expected in FDL-CEMENT, after incubation in PBS.

The mean amount of total phosphatidylcholine found in the vials containing freeze-dried product was found to be 0.39 mg, which means that the amount of phosphatidylcholine in each vial is lower than what was initially used to prepare the FDL formulation. Since the amount of phosphatidylcholine per vial should be 0.78 mg, it can be assumed that 50% of phosphatidylcholine has been degraded or been lost during the manufacturing process such

as during the extrusion process where one sixth of the lipid content was found to be lost and retained on the polycarbonate membrane. The liposomes may have degraded prior to the freeze-drying process due to several lengthy processes which include the lipid extrusion process. It is known that phosphatidylcholine can oxidise during storage for a number of reasons including general processing, hydrolysis and exposure to air (Al-Orf, 2011; Franzé et al., 2018). It has been shown that lipid oxidation is adversely affected by the freeze-drying process itself for various lipids (Raikos et al., 2015). There have been some developments and studies in freeze-drying processes for phosphatidylcholine liposomes, however, data regarding oxidation and freeze-drying of liposomes remains limited (Franzé et al., 2018). Products from the oxidation of phosphatidylcholine could be detected and assayed by several methods. This would confirm if the product has undergone degraded by oxidation. The simplest and most established method is to assay by UV-Vis absorbance as oxidised phospholipids are detected at a wavelength of 234 nm (Kim & LaBella, 1987; Weinstein et al., 2000). There are also other methods such as LC-MS providing high-sensitivity quantitation, if needed (O'Donnell, 2011). As it is unclear as to whether the manufacturing process prior to freeze-drying, or if freeze-drying is responsible for the loss of lipid content, phosphatidylcholine should be assayed prior to freeze-drying and immediately after freeze-drying using the Stewart assay, in order understand at which point phosphatidylcholine content has been lost.

It was found by measuring the amount of phosphatidylcholine in the starting material prior to lipid extrusion and after lipid extrusion, that 17% phosphatidylcholine was lost during the extrusion process, showing that significant loss of lipid occurred at this stage of the manufacturing process. SEM images were taken of the Whatman membranes before and after lipid extrusion. Images of the membranes of pore size 100 nm, 200 nm and 400 nm were obtained, and it was shown that 400 nm pore filter paper contained the most residual lipid, followed by the 200 nm and 100 nm filter papers. The 400 nm paper contained the most residual lipid content from a single extrusion, whereas the smaller pore size membranes contained less residual lipid content from multiple extrusions. Although these images show that there is loss of lipid at this stage, it does not give information on how much lipid has actually been lost due to this process. Recovery of the membrane filters and consequent assay by the Stewart assay would show the amount contained on the membranes at this stage. Moreover, analysis of the membrane residue by SEM-EDX elemental analysis could possibly have confirmed or indicated the presence of phosphatidylcholine by specifying the presence of phosphorous. Although no studies showing the retention of phospholipids by polycarbonate membranes were found, some studies have shown the retention of molecules containing polar groups on polycarbonate

membrane surfaces. Surfactants have been adsorbed on to the polycarbonate filter surface by way of polar end groups interacting with the polycarbonate surface molecules (Apel et al., 2006). In another study, the movement of lipid-based polymeric nanoparticles through a polycarbonate membrane has been documented (Coulman et al., 2009): a reduction of nanoparticles through the membrane was observed due to the blockage of pores and the accumulation of nanoparticles on the membrane itself. The blockage and accumulation of particles on to the membrane was attributed to the interaction between the lipid-based polymeric nanoparticles and the polycarbonate membrane. Polycarbonates are polymers with carbonate linkages and contain aromatic moieties in their structure (Antonakou & Achilias, 2013). Phosphatidylcholine is composed of a charged choline headgroup, glycerophosphoric acid and two fatty acids (saturated and unsaturated) (Drescher & van Hoogevest, 2020). There are several possible intermolecular interactions that could be responsible for the adsorption of phosphatidylcholine onto a polycarbonate membrane. A number of interactions at the surface are possible such as electrostatic interactions and non-polar interactions like Van der Waals dispersive forces between both molecules, since each contains hydrophilic and hydrophobic moieties due to polar and non-polar groups.

The mass quantity of phosphatidylcholine present in both pellet form and in the supernatant liquid, at centrifugation times of 1.5 hours, 3 hours and 4.5 hours using an average force of 107,000 g was measured using the Stewart assay. The sum of the mass quantities of phosphatidylcholine determined in either the pellet or supernatant liquid for each tube, was equal to the initial total mass quantity of lipid, indicating that the process of ultra-centrifugation did not cause for any noticeable loss or degradation of phosphatidylcholine. An increase in centrifugation time caused for an increase in the amount of lipid in the pellet. It was shown that by increasing the centrifugation time from 1.5 hours to 4.5 hours, an increase in the mass quantity of phosphatidylcholine in the pellet was observed. The increase was from 25% phosphatidylcholine to 50% phosphatidylcholine respectively. It was also shown that larger diameter liposomes were present in the pellet and that smaller diameter liposomes were present in the supernatant liquid, after centrifugation. Since the rate of particle sedimentation is proportional to particle size, and furthermore, the number of particles in a pellet are dependent on the centrifugation time (R.H. Burdon, P.H. van Knippenberg, 1988), it is therefore beneficial to investigate the production of liposomes containing a higher proportion of larger particle sizes which will result in a pellet containing a higher phosphatidylcholine mass content due to increased particle sedimentation.

The mass quantity of phosphatidylcholine present in both pellet form and in the supernatant liquid, at centrifugation times of 1.5 hours and 3 hours using an increased average force of

207,000 g was measured using the Stewart assay. The sum of the mass quantities of phosphatidylcholine determined in either the pellet or supernatant liquid for each tube, was equal to the initial total mass quantity of lipid, indicating that the process of ultra-centrifugation at an increased average force of 207, 000 g did not cause for any noticeable degradation of phosphatidylcholine. An increase in Relative Centrifugal Force (RCF or g) caused for an increase in the amount of lipid mass content. It was shown that by increasing the centrifugation time at 207, 000 g from 1.5 hours to 3 hours caused for an increase in lipid mass amount in pellet of 83% phosphatidylcholine to 95% phosphatidylcholine, which is approximately double the amount found in the pellet at 4.5 hours using the 107,000 g rotor. The increase in phosphatidylcholine mass content can be explained as the rate of particle sedimentation is proportional to particle size and gravitational force; furthermore, the number of particles in a pellet are dependent on the centrifugation time (R.H. Burdon, P.H. van Knippenberg, 1988). The average particle diameters of liposomes found in the pellet and supernatant liquid were found to be 154 nm and 125 nm respectively, compared to the mean particle diameter for non-centrifuged liposomes which was 114 nm, prior to ultra-centrifugation. As most of the lipid was found to be in the pellet at 1.5 hours, it can be inferred that the liposome size had increased. It is also worth noting that there are no documented studies that have used higher than 107, 000 g. As there are several factors governing particle sedimentation during centrifugation (R.H. Burdon, P.H. van Knippenberg, 1988), it can be seen that an increase in gravitational force has caused for the largest increase in particle sedimentation.

4.5 Conclusions

A freeze-dried gentamicin liposomal cement formulation (FDL-CEMENT) was made and compared to the liposomal formulation manufactured by incorporating a liposome pellet into bone cement (LCP-CEMENT). The freeze-dried liposomal formulations was incorporated into the bone cement up to a maximum amount equivalent to 0.60% w/w of gentamicin base, to produce cements FDL-CEMENT015, FDL-CEMENT030 and FDL-CEMENT060. Gentamicin release from FDL-CEMENTS were compared to Palacos R+G and the liposomal cement, using LC-MS. It was found that not only did the cement discs containing freeze-dried gentamicin loaded liposomes release much less gentamicin than the Palacos R+G and the liposomal formulation cement discs, but the amounts of gentamicin released by the freeze-dried formulation were of rather negligible mass quantities. FDL-CEMENT060 released antibiotic mass quantities above the MIC at time points of up to 72 hours,

thereafter, releasing quantities below the LOQ. FDL-CEMENT015 did not release mass quantities above the MIC, and FDL-CEMENT030 released mass quantities above MIC at 12 hours only. FDL-CEMENT060 failed all the mechanical testing outright whereas FDL-CEMENT015 passed all of the ISO 5833 requirements. FDL-CEMENT030 had the strongest compressive strength of all samples, including Palacos R, although it failed the bending strength. The contact angles of the FDL-CEMENTS were found to be lower than for Palacos R and higher than Palacos R+G. The quantitative antimicrobial suspension test showed that the freeze-dried samples were in fact the most effective at reducing *S. aureus* bacteria count, despite releasing less gentamicin than the other cement discs. No biofilm formation was detected on any of the cement discs, indicating that biofilm formation may have been prevented by the various cement formulations; however, further testing is required to confirm this. SEM images were taken of the freeze-dried cements which contained round particles, which is perhaps indicative of an incomplete polymerisation due to the large amount of material added to the cement. SEM images also showed that pores were formed on the FDL-CEMENTS, after storage in PBS. Analysis of the FDL formulations showed that the liposomes had increased in size from approximately 300 nm to approximately 1800 nm, possibly converting through fusion from SUVs to LUVs. Moreover, the mass quantities of phosphatidylcholine and gentamicin sulfate in each vial of freeze-dried product were both around half of the mass quantities expected per vial after freeze-drying. Further studies on the phospholipid oxidation should be performed. Moreover, the interaction between sucrose and gentamicin should be investigated, as there is the possibility of increased degradation when combined. It was shown by assay that during the liposome extrusion process, around one sixth of the phosphatidylcholine content is lost prior to centrifugation. SEM images also showed that residual lipid remained on the extrusion membrane filters. Using ultracentrifugation at approximately 107, 000 g at different time points, it was shown that liposomes are still present in the supernatant liquid and have therefore not been completely sedimented. However, by increasing the centrifugation time threefold, the mass quantity of lipid content measured in the pellet doubled, although there was still a significant amount of lipid content remaining in the supernatant liquid. Doubling the time and centrifugal force to 207, 000 g, caused for 95% of lipid to be present in the pellet. The freeze-dried formulation was shown to have a significantly lower mass amount of gentamicin sulfate than was initially incorporated, meaning that loss or degradation of gentamicin is caused by this process. This means that this freeze-dried liposomal formulation is not an option and requires further investigation. Producing liposomes by extrusion and centrifugation, as in Chapter 3, was shown to be a wasteful process, as significant mass quantities of reagents are lost during the process; and is therefore not considered a suitable alternative to using a freeze-dried product.

Chapter 5

5 Incorporation of hydrophilic and hydrophobic additives

5.1 Introduction

It was shown in chapter 4 that the method of manufacture of the liposomal formulation (Ayre *et al.*, 2015) gives rise to substantial loss of phospholipids during the manufacturing process; in particular, only a small fraction of liposomes is actually incorporated into the bone cement, approximately one quarter of the initial starting amount is used in the bone cement. Although it was possible to improve the liposome yield to well over 90% by increasing the centrifugation force and spin time, other properties such as particle size were compromised, and moreover, this process is time-consuming and therefore may not be a financially viable option, should commercialisation be sought. A freeze-dried formulation was investigated and incorporated into bone cement, in quantities comparable to the mass amount of gentamicin incorporated into bone cement in the study by Ayre *et al.* (2015). The mass amounts of gentamicin released from the freeze-dried liposome bone cement discs were found to be very low in comparison to the commercial bone cement and previous liposomal formulation. Moreover, mechanical properties were generally compromised by increased addition of the freeze-dried liposomes. It was therefore concluded that the freeze-dried formulation was not a viable option for incorporation into bone cement as a drug-delivery system. In Chapter 3, the drug release from three different Pluronic types differing in hydrophilic and hydrophobic character (Pluronics L31, L43 and L61) were incorporated into commercial gentamicin-loaded bone cement, showing different characteristics, whereby the most hydrophilic Pluronic resulted in approximately twice as much drug release than the least hydrophilic Pluronic. In a study by Diez-Pena *et al.* (2002), PMMA bone cement was loaded with amounts of 1% w/w to 24% w/w of gentamicin sulfate for drug release, it was found that the total percentage of drug release from the bone cements increased with an increase in mass amount of incorporated gentamicin sulfate. In fact, according to this study, the bone cement

containing 24% w/w of gentamicin sulfate released almost all of its incorporated drug (Diez-Pena et al., 2002). This was mainly attributed to gentamicin sulfate acting as a channelling agent due to its hydrophilic nature. Oh et al. (2016) attributes the increase in drug release, upon addition of hydrophilic additives, to the hydrophilisation of the material itself (Oh et al., 2016). To date, there have been many studies which have looked at improving drug delivery from PMMA bone cements (Miola et al., 2013), however, there have been few studies into the actual mechanism of drug release from PMMA bone cement, which is still not fully understood (Martínez-Moreno et al., 2015; Miola et al., 2013). A better understanding of the mechanisms of drug release from bone cements would allow for more effective drug delivery systems to be produced. This chapter investigates the effects of two commonly used pharmaceutical excipients, lactose and magnesium stearate, which are hydrophilic and hydrophobic respectively. Magnesium stearate (Figure 56) is a metallic salt with molecular formula $\text{Mg}(\text{C}_{18}\text{H}_{35}\text{O}_2)_2$, containing a magnesium cation and two stearic acid equivalent anions (Hiremath & Agrahari, 2019; Hobbs et al., 2017). Magnesium stearate is an established pharmaceutical excipient used in various formulations including tablets, capsules and powders (Gönen et al., 2015; Hobbs et al., 2017). Its applications exploit its properties which include insolubility in polar solvents, softness and low toxicity (Cheng et al., 2008; Hobbs et al., 2017; Okolo, 2019). It is often used as a lubricant in the manufacture of pharmaceutical tablets or as a release agent (Hobbs et al., 2017). It has also been used to improve aerosol performance of micronized drug powders by coating particles with magnesium stearate particles to decrease agglomerate strength of powders (Gönen et al., 2015). Other industrial uses include its use as a thermal stabiliser and plasticiser in polymers such as rubber and thermoplastics (Gönen et al., 2015); it is also widely used in the food industry in the manufacture of dietary supplements, chewing gums and baking ingredients due to its properties as a binder, thickener, antifoaming and anticaking agent (Hobbs et al., 2017). Magnesium stearate is the most commonly used metallic salt lubricant (Hiremath & Agrahari, 2019). Its lubricant effect is due to the polar moiety which adheres to powders, whilst the lipophilic moiety is oriented away from the powder surface, effectively forming a partial hydrophobic layer around particles (Jójárt et al., 2012). However, its ability to form a layer around particles affects water penetration, therefore affecting drug dissolution and causing drug release retardation (Hiremath & Agrahari, 2019; Rashid et al., 2010).

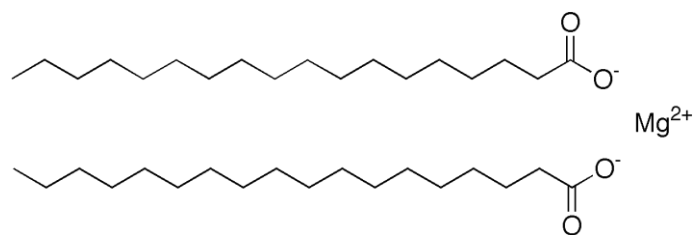


Figure 56: Chemical structure of magnesium stearate which exists as a salt containing two stearate anion equivalents and one magnesium cation.

Lactose is a disaccharide sugar composed of glucose and galactose subunits (Figure 57). The molecular formula of lactose is $C_{12}H_{22}O_{11}$ (Newburg & Neubauer, 1995). Lactose exists in several forms, both crystalline and amorphous. Crystalline forms of lactose are anhydrous α -lactose, anhydrous β -lactose and α -lactose monohydrate (Johnson & Conforti, 2003). Lactose is used as a carrier in tablets due to its low toxicity, mild sweetness, water solubility, non-hygroscopic character and its suitability for direct compression, whilst maintaining good disintegration properties (Gamble et al., 2010; Johnson & Conforti, 2003). In pharmaceutical tablet manufacture, the main form of lactose used is α -lactose monohydrate (Johnson & Conforti, 2003).

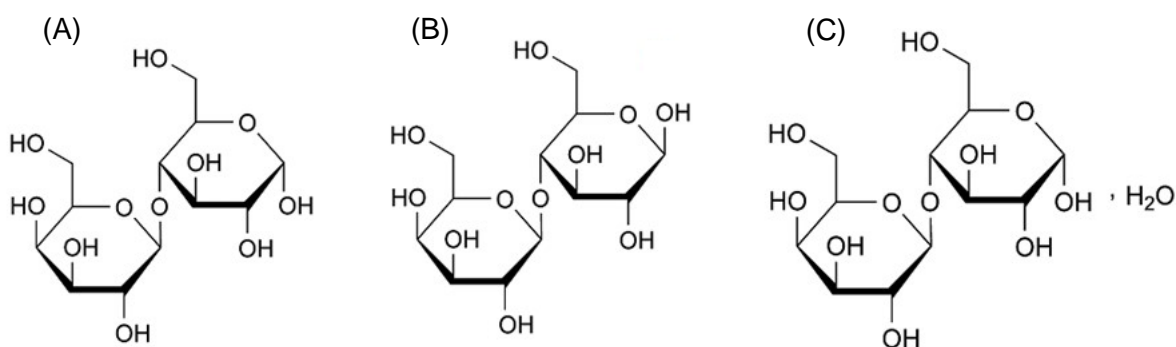


Figure 57: Chemical structures of A) anhydrous α -lactose B) anhydrous β -lactose and C) α lactose monohydrate.

Aims of this chapter:

To incorporate lactose and magnesium stearate into commercial bone cement and to investigate drug release and mechanical properties.

Objectives of this chapter:

- To incorporate lactose and magnesium stearate into bone cement.
- To characterise the drug release profiles, mechanical properties and antimicrobial efficacies of these bone cements, comparing them to those of Palacos R+G and LCP-CEMENT cements used in Chapter 3.
- To characterise channels, pore formation and structural changes to the bone cements after storage in PBS, using micro computed tomography and scanning electron microscopy.

5.2. Methods

5.2.1 Materials

Pentafluoropropionic acid ($\geq 97\%$), gentamicin sulfate ($\geq 590 \mu\text{g}$ Gentamicin base per mg), phosphate buffered saline (10 \times concentrate), magnesium stearate, lactose monohydrate, methanol (HPLC grade $\geq 99.9\%$), sodium chloride, tryptone and tryptone soy broth were purchased from Fisher Scientific (Fisher Scientific UK, Loughborough, UK). Palacos cements R and R+G were provided by Heraeus (Heraeus Medical, Newbury, UK). *Staphylococcus aureus* (*S. aureus*, NCTC 10788) was used.

5.2.2 Cement preparation

Cements were prepared as per the method specified in Section 2.1.1. Different compositions of bone cements containing different concentrations of lactose (10% w/w to 80% w/w) and magnesium stearate (10% w/w to 25% w/w) were prepared by carefully mixing each compound with PMMA powder (Palacos R+G) by geometric dilution; the final mixture was mixed with an amount of MMA equivalent to half of the total weight of PMMA mixed with

either additive to produce bone cement. The final percentage of each compound refers to the additive percentage weight in PMMA. Cement discs were labelled as either lactose or MgSt and their percentage of incorporation in PMMA e.g., lactose 10% refers to 10% w/w of lactose incorporated into PMMA (Palacos R+G) bone cement.

5.2.3 LC-MS to assay gentamicin release from cement discs

Gentamicin release from the cement discs was assayed using LC-MS. Sampling, storage and handling are described in Section 2.1.4. Cement discs prepared as described in Section 5.2.2, were placed in 5 ml bijoux vials containing PBS (pH 7.4) and incubated at 37 °C; at each time point, the PBS was removed for analysis and replaced with fresh PBS. Analysis was conducted in triplicate. The instrument and method were used, as specified in Section 2.7.1.

5.2.4 Antimicrobial testing

Overnight cultures of *S. aureus* (NCTC 10788) were prepared as described in Section 2.9. All antimicrobial testing was carried out using the methods specified in Section 2.9. This includes sterilisation of glassware, media sterilisation, sample sterilisation; quantitative suspension tests, and analysis of biofilm formation.

5.2.5 Mechanical testing

All mechanical testing was performed using the methods specified in Section 2.4. The compressive strength, bending modulus and bending strength were tested as specified in Sections 2.4.1 and 2.4.2 and 2.4.3 respectively.

5.2.6 Scanning electron microscopy

Scanning electron microscopy (SEM) was carried out using the method specified in Section 2.10.

5.2.6.1 Cutting cement disc

In this chapter, surfaces of the disc samples were visualised, using SEM, prior to and after incubation in PBS at 37 °C; furthermore, cement discs were split vertically through the middle to observe differences due to penetration of water from the top surface of the disc. Cutting through samples to observe differences due to water ingress, using SEM, was not performed in previous studies, which have generally sought to observe differences in surface morphology. Figure 58 shows a schematic representation of a cement disc where line (A) is the point where a diamond saw was used to cut through the disc approximately 2-3 mm in depth along the direction of line (B). After sawing into the disc, a flat metal screwdriver tip was inserted, and the disc was split into two equal halves by rotating the screwdriver tip.

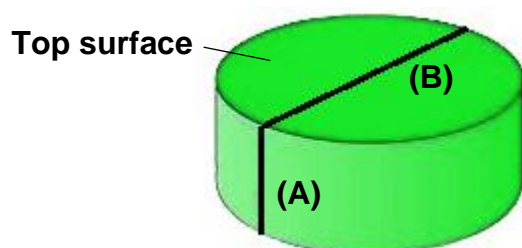


Figure 58: Schematic diagram of a cement disc used for characterising changes due to penetration of water from the top surface. Line (A) is where the saw is placed and cut in the direction of line (B).

5.2.7 Analysis of cement discs by micro computed tomography

Micro computed tomography (microCT) data was collected using a SkyScan 1272 high-resolution MicroCT system (SkyScan, Kontich, Belgium). Three separate cement discs were scanned after incubation in PBS at 37 °C for one week: Palacos R+G was used as a control sample and Palacos R+G containing 25% w/w and 80% w/w of lactose were analysed. All three sample discs were stacked within a plastic polyethylene tube and separated from one another with polystyrene discs, as these polystyrene and plastics are considered as radiolucent and therefore do not interfere with the analysis (Meftah et al., 2019; Pugmire et al., 2015). The sample tube was mounted on to the sample holder between the x-ray source and the charge-coupled device (CCD) detector. The samples were scanned using the following parameters: source voltage 100 kV, source current 100 μ A, copper filter 0.11 mm,

rotation step 0.2°, pixel size 5.0 µm, frame averaging (2), rotation 360°. After scanning, the micro-CT images were reconstructed using the NRecon software (v.1.6.3, SkyScan, Belgium). Three-dimensional images (3D) were generated using CTVOX software (v. 3.3.0, SkyScan, Belgium) and the CTan software (v.1.18.1.0, SkyScan, Belgium) was used for porosity measurements. Analysis of porosity refers to the counting of empty space and characterising their connections in relation to solid matter. Empty space and solid matter are characterised by different coloured voxels. Figure 59 is a schematic diagram of an object containing (A) two open pores, and (B) one closed pore. The green area (C) denotes solid material within the object volume.

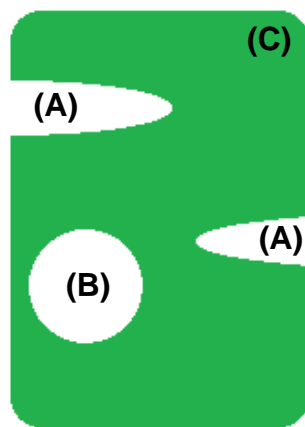


Figure 59: Schematic diagram of an object with (A) two open pores and (B) one closed pore. Solid matter (C), within the object, is coloured green.

Open porosity relates to empty space within a sample volume that is connected to the outside surface of that sample. An open pore is defined in a 3D model as any space located within a solid object that is connected to the outside surface of the solid object (Bruker-microCT, 2012). Percentage open porosity (open porosity %) is defined as the volume of open pores as a percentage of the total sample volume (Bruker-microCT, 2012).

Closed porosity relates to empty space within a sample volume, that is not connected to the outside surface of that sample. A closed pore in a 3D model is defined as a connected network of empty volume (black voxels) that is surrounded on all sides by solid material (white voxels). Percentage closed porosity (closed porosity %) is defined as the volume of closed pores as a percentage of the total sample volume (Bruker-microCT, 2012).

Total porosity is the sum of the volumes of all open and closed pores. Percentage total porosity (total porosity %) is defined as the volume of open and closed pores as a percentage of the total sample volume (Bruker-microCT, 2012).

5.2.8 Contact angle measurement

Water contact angles were measured using the Attension contact angle analyser as specified in Section 2.3.

5.2.9 Sample weight loss after storage in PBS

Sample weight loss was characterised for discs incubated in PBS for 7 days at 37 °C. Samples were dried to constant weight meaning that drying was continued until two consecutive weighings where the sample weight did not differ by more than 0.5 mg (British Pharmacopoeia, 2021). The samples were weighed before and after incubation in PBS, using an analytical balance measuring up to four decimal places. Samples were individually placed in 5 ml bijoux vials containing PBS. After 7 days, sample discs were removed from PBS and dried at 65 °C to constant weight for 6 hours. Prior to being weighed, the samples were placed in a vacuum desiccator for 30 minutes. Percentage weight loss was determined by calculating the percentage difference between the initial sample weight and the final sample weight after 7 days in PBS:

$$\text{percentage weight loss} = \frac{W_i - W_f}{W_i} \times 100$$

Where:

W_i is the initial weight of the disc as freshly prepared, prior to incubation in PBS.

W_f is the final weight of the disc after removal from BPS and dried to constant weight.

5.2.10 Statistical analysis

Statistical analysis was performed as described in Section 2.11.

5.3. Results

5.4.1 Antibiotic release from Palacos R+G containing different incorporated percentages of lactose and magnesium stearate

The cumulative mass quantities of release of antibiotic from Palacos R+G and all of the cement discs containing 10% w/w and 25% w/w of either lactose or magnesium stearate are shown in Figure 60 (1296 hours (2 months)) and Figure 61 (72 hours). The results show that after 2 months, a much greater total mass amount of gentamicin has been released from both lactose cement discs: lactose 25% released $1425.5 \pm 253.4 \mu\text{g}$ of gentamicin, and lactose 10% released $1100.0 \pm 134.8 \mu\text{g}$ of gentamicin. MgSt 25% cement disc released the next largest quantity of gentamicin ($882.4 \pm 68.5 \mu\text{g}$), followed by Palacos R+G ($819.4 \pm 187.3 \mu\text{g}$), and MgSt 10% ($741.0 \pm 137.7 \mu\text{g}$) releasing the least amount of gentamicin. Burst release was observed over the first hours for all of the cement discs, followed by lower levels of gentamicin release. However, MgSt 10% and 25% both showed a more controlled release than Palacos R+G and lactose 10% cement discs, releasing gentamicin in a more sustained manner, over the first 456 hours. Lactose 25% cement disc also showed a sustained release, which was due to it releasing the largest quantities of gentamicin over the first 456 hours, meaning that at each time point prior to 456 hours, the cement discs continued to release further quantities of gentamicin; thus, showing an extended-release profile. Palacos R+G released $398.7 \pm 54.0 \mu\text{g}$ of its gentamicin content in the first 24 hours, which is around half of the total amount that it released after 1296 hours ($819.4 \pm 187.3 \mu\text{g}$); whereas MgSt 10% and 25% both released $226.9 \pm 72.4 \mu\text{g}$ and $289.8 \pm 22.1 \mu\text{g}$ of gentamicin at 24 hours respectively, which is around one third of the total mass amount released at 1296 hours. Therefore, the magnesium stearate cements released gentamicin at a slower rate than Palacos R+G. At 1296 hours (2 months), compared to Palacos R+G, only lactose 25% showed a significant difference in mass amount of drug release ($p=0.0045$), whereas all the other cements did not release significantly different quantities to Palacos R+G ($p>0.05$); lactose 10% and 25% did not release significantly different quantities of gentamicin to each other ($p=0.1399$); and MgSt 10% and 25% did not release significantly different quantities of gentamicin to each other ($p=0.7845$). Furthermore, at this final time point (1296 hours), MgSt 10% and MgSt25% released significantly lower mass quantities of gentamicin than lactose 25% ($p=0.0019$ and $p=0.0096$ respectively), whereas MgSt 25% and MgSt 10% both released mass amounts that were not significantly different to lactose 10% ($p=0.0932$ and

p=0.4489 respectively). There was no significant difference between mass quantities released for MgSt 10% and 25% at this time point (p=0.7845).

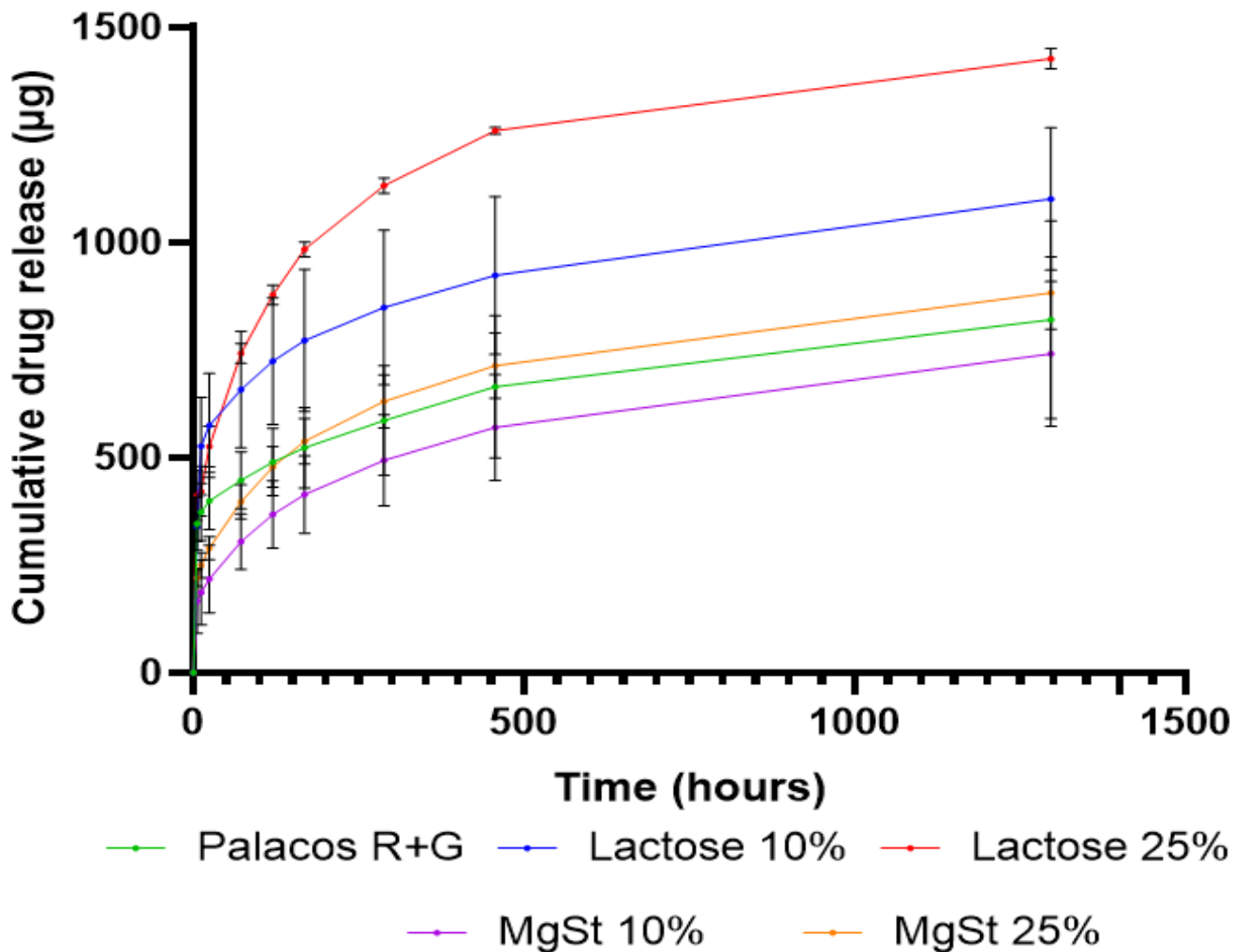


Figure 60: Cumulative drug release of GS (µg) from Palacos R+G, and Palacos R+G containing 10% w/w and 25 % w/w of magnesium stearate cement discs all stored in PBS solution (pH 7.4, 37 °C) from time point 0 to 1296 hours. (n=3).

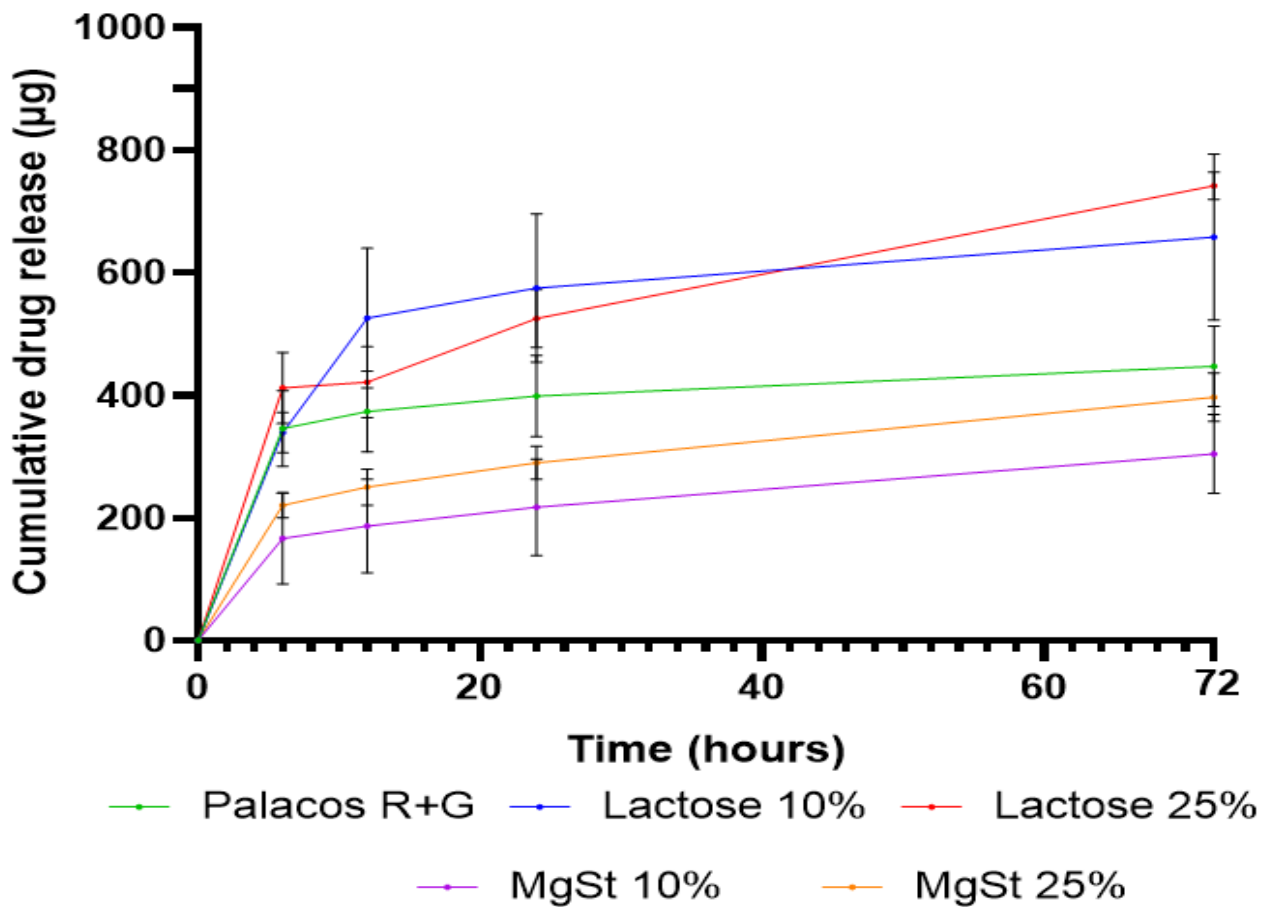


Figure 61: Cumulative drug release of GS (μg) from Palacos R+G, Palacos R+G containing 10% w/w and 25% w/w of lactose and Palacos R+G containing 10% w/w and 25% w/w of magnesium stearate cement discs all stored in PBS solution (pH 7.4, 37 °C) from time point 0 to 72 hours. (n=3).

5.4.1 Antimicrobial testing

Antimicrobial efficacy was assessed by using a quantitative suspension test. Cement discs were incubated for 4 hours, at 37 °C in a suspension of *S. aureus*. After 48 hours, cement discs were vortexed with glass beads to dislodge any microbial biofilm attachment which may have formed on the discs.

5.4.1.1 Quantitative suspension test

Results from the antimicrobial testing (quantitative suspension test) are shown in Figure 62. All samples tested showed some level of efficacy in reducing *S. aureus* bacteria count. The starting bacteria count in solution was 1×10^6 colony forming units per mL (CFU/ml). Lactose 10% and 25% and MgSt 10% and 25% reduced the CFU/ml to 8.7×10^4 CFU/ml, 6.7×10^4 CFU/ml, 10.3×10^4 CFU/ml and 8.0×10^4 CFU/ml respectively. Palacos R+G cement discs reduced the CFU/mL to 1.3×10^5 CFU/ml. Palacos R was the least effective, reducing the CFU/ml to 2.8×10^5 CFU/ml. All lactose, magnesium stearate cements and Palacos R+G showed a significant reduction in colony forming units compared to Palacos R (all results compared to Palacos R were $p < 0.0001$). All the lactose and magnesium stearate samples (lactose 10%, lactose 25% and MgSt 25%), except for MgSt 10%, showed a significant reduction in colony forming units compared to Palacos R+G ($p = 0.0257$, $p = 0.0015$ and $p = 0.0097$ respectively) except for MgSt 10%, which showed no significant difference ($p = 0.2619$). There was no significant difference between the lactose and magnesium stearate samples in terms of CFU/mL reduction ($p > 0.05$).

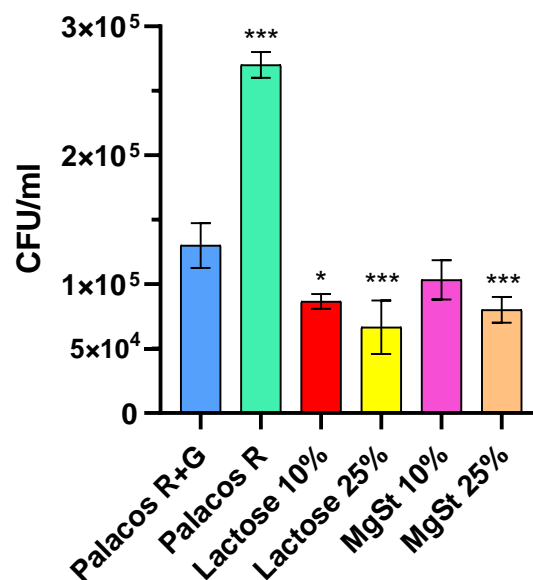


Figure 62: Colony forming units (CFU) for Palacos R, Palacos R+G, and for lactose 10% and 25%, and MgSt 10% and 25% cement discs. Data is presented as mean \pm standard deviation ($n=3$). Asterisks indicate the level of significance with respect to Palacos R+G (* $p < 0.05$, ** $p < 0.01$, * $p < 0.001$).**

5.4.1.2 Analysis of biofilm formation

The cement discs stored in inoculum were removed after 48 hours, vortexed with glass beads and sonicated to dislodge any biofilm formed around the cement discs. Any dislodged *S. aureus* biofilm was allowed to regrow on plates. For all cement discs tested, no colony forming units were observed after incubation of the agar plate for 18 hours (0 CFU/ml for all samples), meaning that *S. aureus* was not detected.

5.4.1 Mechanical testing

Mechanical testing was performed as per the requirements of ISO 5833: compressive strength, bending modulus and bending strength (ISO 5833, 2002). As required by the standard, testing was performed using five separate cement sample preparations (n=5).

5.4.1.1 Bending modulus

The bending modulus of commercial cements Palacos R, Palacos R+G, lactose 10% and 25%, and MgSt 10% and 25% cements (prepared and stored for 24 hours in air) are shown in Figure 63. All of the lactose and magnesium stearate cements, except for MgSt 25% were above the ISO 5833 limit of 1800 MPa. MgSt 25% (565 ± 266 MPa) was substantially lower than the ISO 5833 standard limit of 1800 MPa; furthermore, of the five replicate test samples for MgSt 25% cement, two of the samples ruptured before achieving the pre-load (load at which measurements commence, 10 N) and therefore achieved a bending modulus result of 0 MPa. MgSt 10% obtained a bending modulus result of 2407 ± 222 MPa. Lactose 10% and lactose 25% obtained bending modulus results of 2326 ± 311 MPa and 2555 ± 489 MPa, respectively. Palacos R+G showed no significant reduction in bending modulus ($p=0.9998$). All of the lactose and magnesium stearate samples, except for lactose 10%, showed a significant reduction in bending modulus compared to Palacos R (lactose 25%, MgSt 10% and MgSt 25%) ($p=0.0156$, $p=0.0345$ and $p<0.0001$ respectively). Lactose 10% showed no significant reduction ($p=0.1306$).

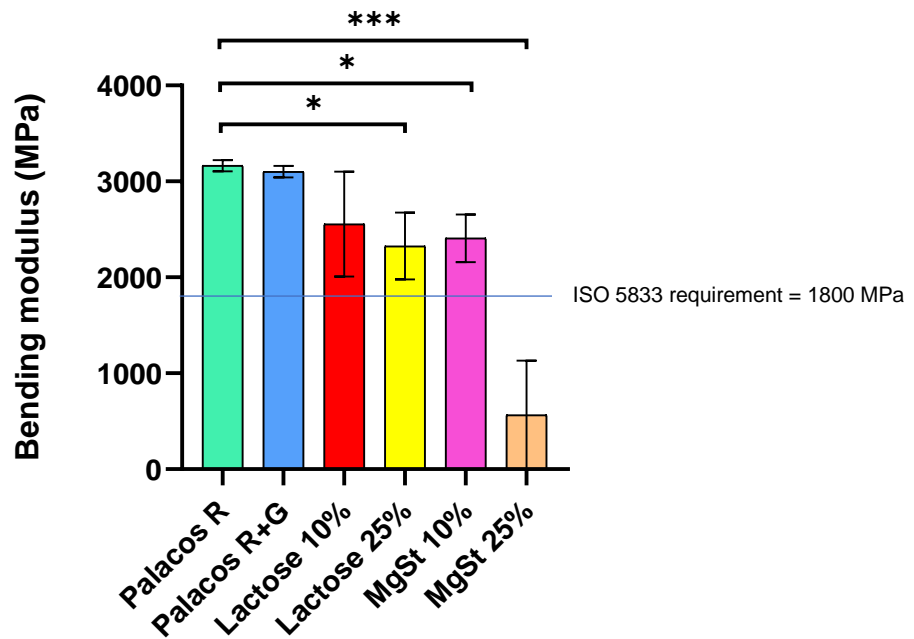


Figure 63: Bending modulus results for commercial cements, Palacos R, Palacos R+G, and cements containing 10% w/w and 25% w/w each of lactose and magnesium stearate. Data is presented as mean \pm standard deviation (n=5). Asterisks indicate the level of significance (* $p < 0.05$, ** $p < 0.01$, * $p < 0.001$).**

5.4.1.2 Bending strength

The bending strength of commercial cements, Palacos R, Palacos R+G, lactose 10% and 25%, and MgSt 10% and 25% cements (prepared and stored for 24 hours in air) are shown in Figure 64. All of the lactose and magnesium stearate samples, except for lactose 25% (40 ± 15 MPa) were above the ISO 5833 limit of 50 MPa. Lactose 10%, MgSt 10% and 25% w/w obtained bending strength results of, 77 ± 16 MPa, 80 ± 13 MPa and 94 ± 9 MPa respectively, all above the limit set in ISO 5833. Compared to Palacos R, only lactose 25% showed a significant reduction in bending modulus ($p=0.0004$); all of the other samples tested (Palacos R+G, lactose 10%, MgSt 10% and MgSt 25%) did not show a significant reduction compared to Palacos R ($p=0.2811$, $p=0.9928$, $p > 0.9999$ and $p=0.6792$ respectively).

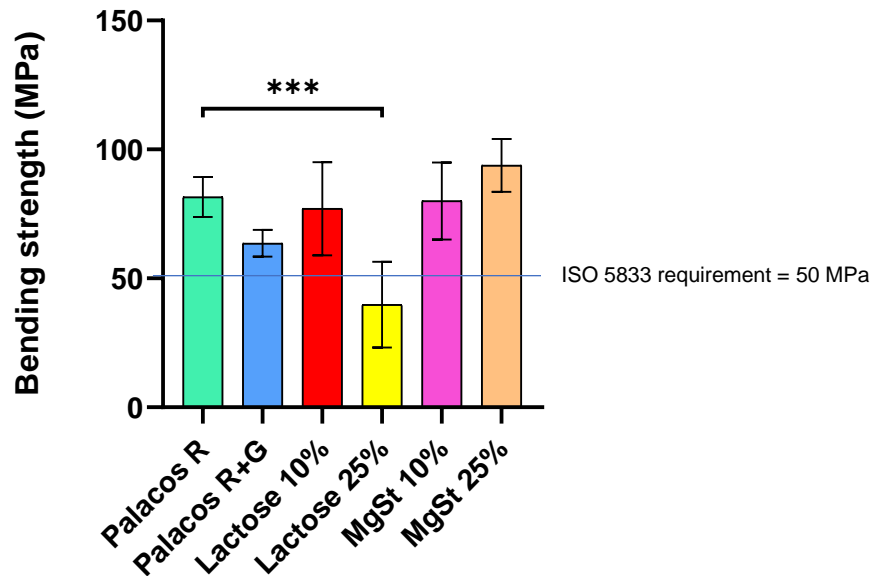


Figure 64: Bending strength results for commercial cements, Palacos R, Palacos R+G, and cements containing 10% w/w and 25% w/w lactose and magnesium stearate. Data is presented as mean \pm standard deviation ($n=5$). Asterisks indicate the level of significance (* $P<0.05$, ** $P<0.01$, * $P<0.001$).**

5.4.1.2 Compressive strength

The compressive strengths of commercial cements, Palacos R, Palacos R+G, lactose 10% and 25%, and MgSt 10% and 25% cements (prepared and stored for 24 hours in air) are shown in Figure 65. All of the lactose and magnesium cements were below the ISO 5833 limit of 70 MPa. Lactose 10% marginally failed as it had a compressive strength of 69 ± 2.5 MPa. Lactose 25%, MgSt 10% and 25% had compressive strengths of 60 ± 0.9 MPa, 52 ± 0.9 MPa and 31 ± 1.5 MPa respectively, indicating a dose-dependent reduction in compressive strength with increased lactose and magnesium stearate concentrations. Compared to Palacos R, all of the tested cement discs (Palacos R+G, lactose 10%, lactose 25%, MgSt 10% and MgSt 25%) showed a significant reduction in compressive strength ($p=0.0307$, $p=0.0012$, $p<0.0001$, $p<0.0001$ and $p<0.0001$ respectively). Compared to Palacos R+G, all of the lactose and magnesium stearate samples (lactose 25%, MgSt 10% and MgSt 25%), except for 10% w/w lactose, showed a significant reduction in compressive strength ($p=0.0006$, $p<0.0001$ and <0.0001 respectively); therefore 10% w/w lactose did not show a significant difference when compared to Palacos R+G ($p=0.4173$). All of the lactose and magnesium samples showed a significant difference in compressive strength when compared to one another ($p<0.05$).

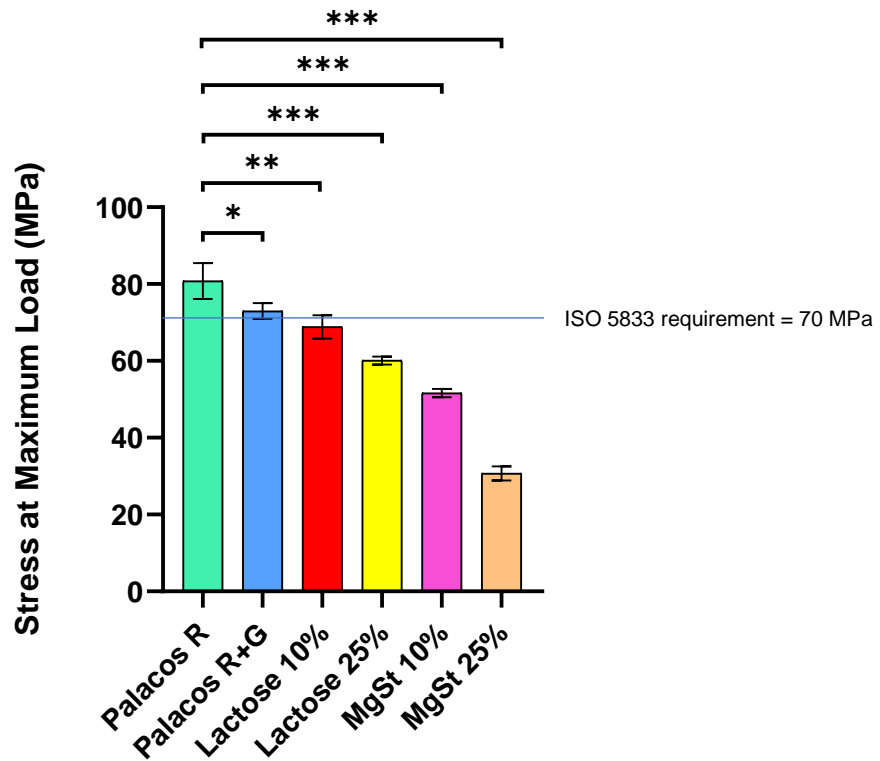


Figure 65: Compression results for commercial cements, Palacos R, Palacos R+G, and cements containing 10% w/w and 25% w/w lactose and magnesium stearate. Data is presented as mean \pm standard deviation (n=5). Asterisks indicate the level of significance (* $p < 0.05$, ** $p < 0.01$, * $p < 0.001$).**

5.4.1.1 Contact angle measurements

Figure 66 shows the different contact angles obtained for discs prepared from Palacos R, Palacos R+G, lactose 10% and 25%, and MgSt 10% and 25% cements. Palacos R had the highest contact angle ($116 \pm 0.8^\circ$), whilst Palacos R+G had the lowest contact angle ($98 \pm 0.8^\circ$). The cements containing lactose and magnesium stearate generally had higher contact angles than Palacos R; lactose 10% ($119 \pm 1.2^\circ$), lactose 25% ($117 \pm 4.5^\circ$), MgSt 10% ($121 \pm 4.5^\circ$) and MgSt 25% ($114 \pm 3.3^\circ$). Compared to Palacos R only Palacos R+G had a significant reduction in contact angle ($p=0.0007$), none of the lactose or magnesium stearate samples (lactose 10%, lactose 25%, MgSt 10% and MgSt 25%) showed a significant difference ($p=0.9435$, $p>0.9999$, $p=0.5810$ and $p=0.9671$ respectively), although all lactose and magnesium samples showed a significant increase in contact angle compared to Palacos R+G ($p=0.0002$, $p=0.0005$, $p<0.0001$ and $p=0.0024$ respectively). All

of the lactose and magnesium stearate samples did not show any significant difference when compared to each other ($p>0.05$).

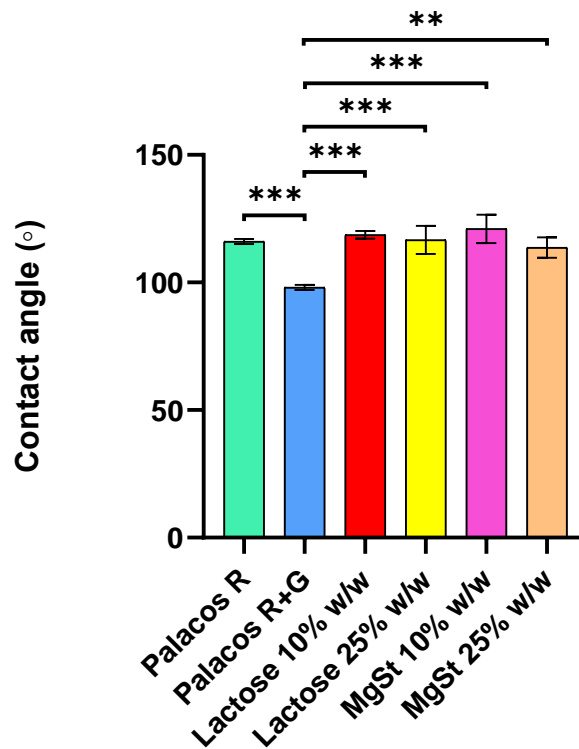


Figure 66: Contact angles for commercial cements Palacos R, Palacos R+G, and cements containing 10% w/w and 25% w/w lactose and magnesium stearate. Data is presented as mean \pm standard deviation ($n=3$). Asterisks indicate the level of significance (* $p<0.05$, ** $p<0.01$, * $p<0.001$).**

5.4.1.1 Scanning electron microscopy

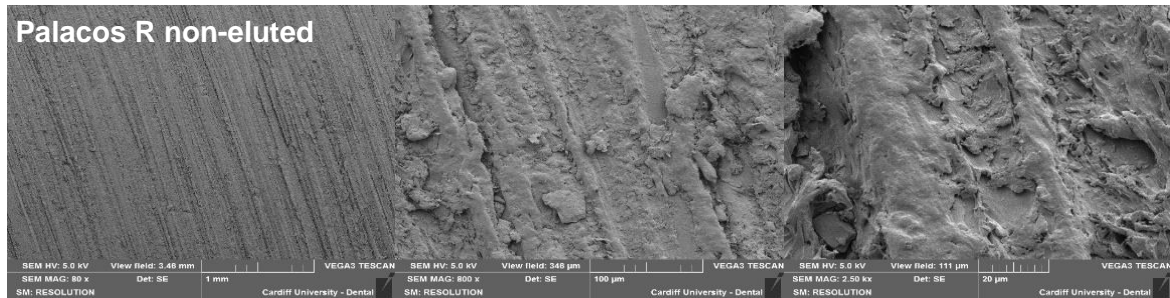
5.4.1.1.1 SEM images of cement disc surface

SEM was used to characterise all of the cement disc formulations' surface morphology after manufacture; moreover, the discs were also analysed to see the difference in surface morphology before and after incubation in PBS for one week. Figures 67 to 73 show SEM surface images at magnifications of 80, 800 and 2.5k for the surfaces of Palacos R, Palacos R+G, lactose 10% and 25%, 80%, and MgSt 10% and 25% cements discs, as prepared before and after incubation in PBS at 37 °C for one week. Cement discs containing 80% w/w lactose were prepared for the sole purpose of visualising changes due to water penetration, that may not be observable in cement discs containing smaller mass quantities of lactose, or

for magnesium stearate. It was thought that lactose 80% w/w cement discs were more likely to show changes due to water penetration, as they contained the highest mass amount of channelling agent. Lactose 80% was also used in further experiments such as microCT analysis, and weight loss of cement samples after incubation in PBS.

There were no observable changes to the surfaces of Palacos R or Palacos R+G, after incubation. Lactose 10% and 25% cements discs, contain round, fused, PMMA particles and pores prior to and after incubation. The surface of lactose 80% cement discs was covered with smaller particles around it, with what appears to be debris from the irregularly shaped lactose particles on the surface; after incubation, it was observed large pores ranging from <1 to around 100 μm are present all over the surface and the observed debris are no longer seen. The MgSt 10% and 25% cement discs both contained small pores on the surface (10 - 50 μm) which are not obvious on the discs after incubation. There are round, fused PMMA particles and round particles that are fused to a much lesser degree than those observed in Palacos R+G and lactose cements. These particles appear very prominently on the disc surface prior to incubation; however, after incubation, only well-fused particles can be observed, as the surfaces appear much flatter. The lesser-fused, round particles on the non-eluted cement surfaces, have diameters ranging from to 20 to 100 μm . Fused PMMA particles, lesser-fused particles and pores are indicated on the images using orange, yellow and blue arrows respectively. Smaller, non-pmma particles on lactose 80% w/w discs are indicated by green arrows.

(A)



(B)

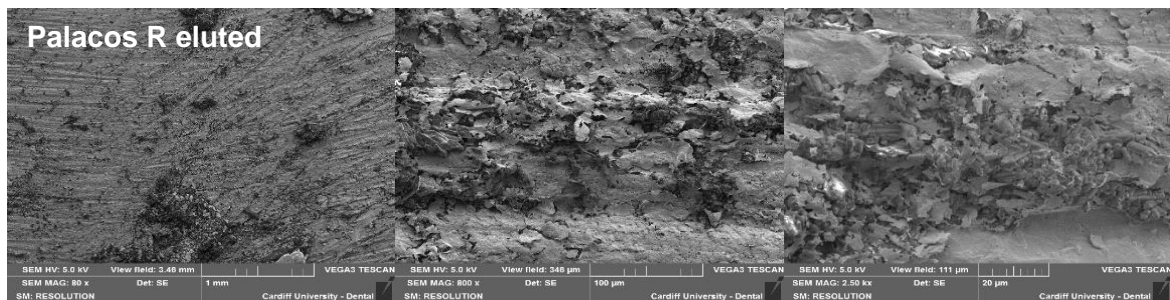
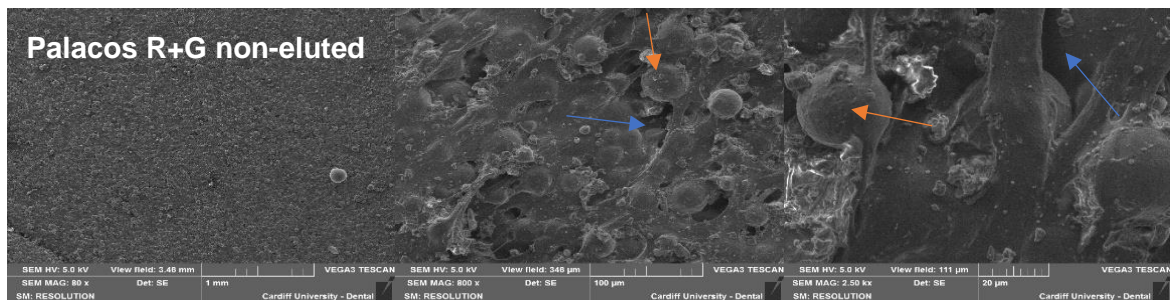


Figure 67: SEM surface images of Palacos R samples (A) before and (B) after incubation in PBS for one week at 37 °C; sample magnifications are x80, x800 and x2.5k respectively.

(A)



(B)

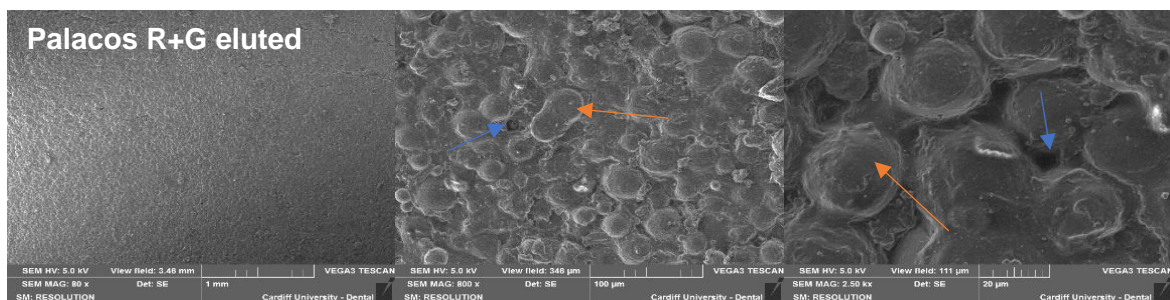


Figure 68: SEM surface images of Palacos R+G samples (A) before and (B) after incubation in PBS for one week at 37 °C; sample magnifications are x80, x800 and x2.5k respectively. Arrows indicate PMMA particles (orange) and pores (blue).

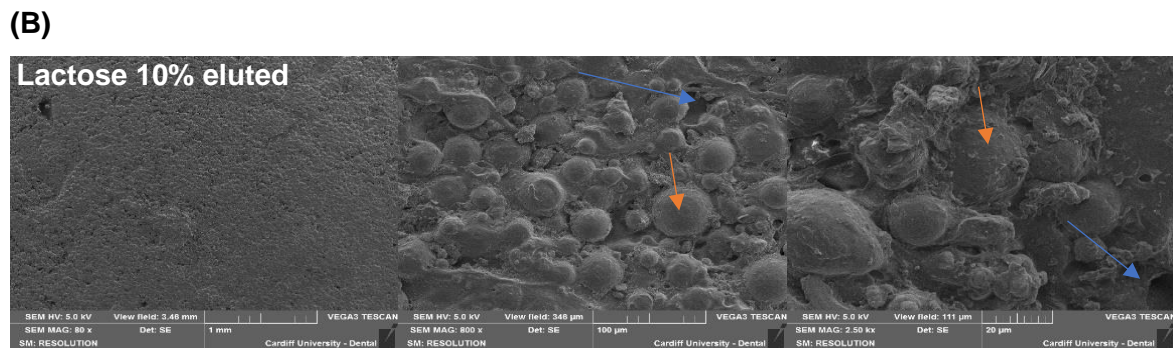
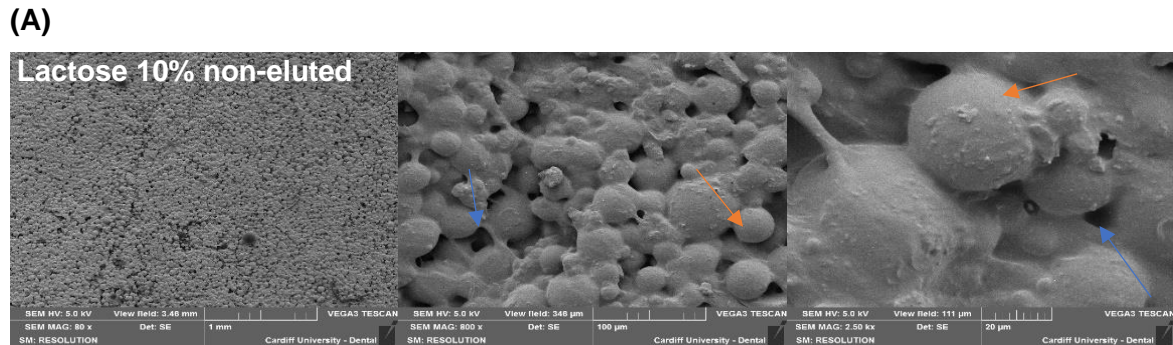


Figure 69: SEM surface images of lactose 10% (A) before and (B) after incubation in PBS for one week at 37 °C; sample magnifications are x80, x800 and x2.5k respectively. Arrows indicate PMMA particles (orange) and pores (blue).

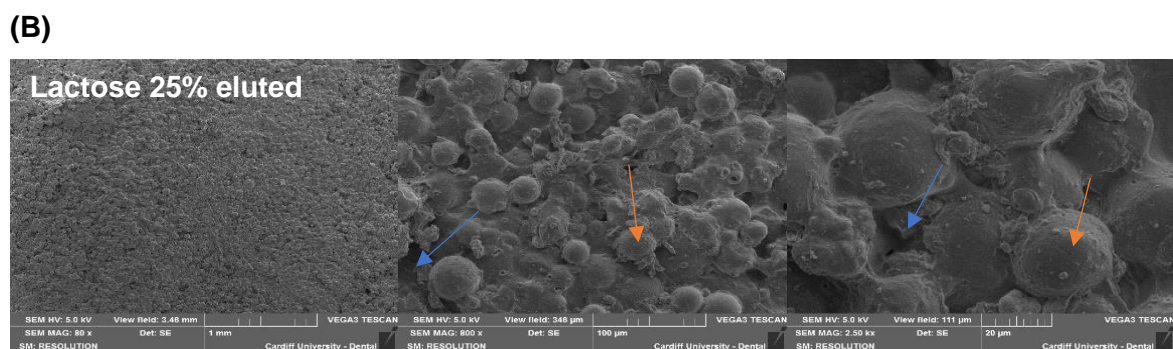
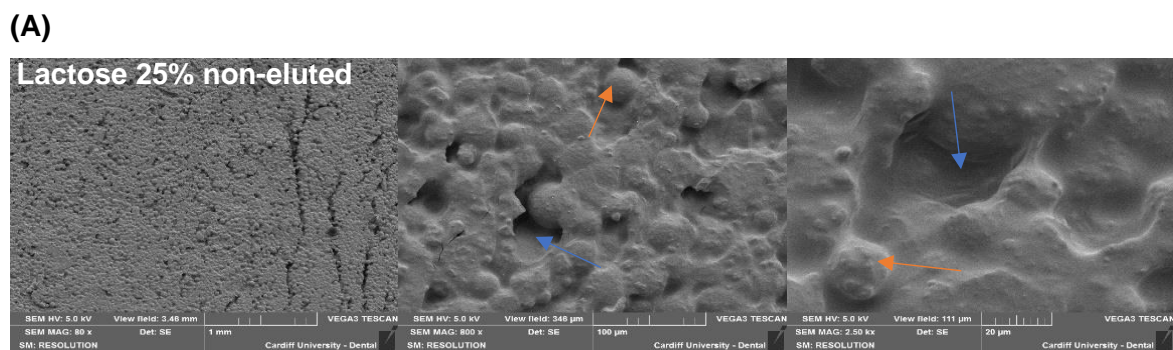
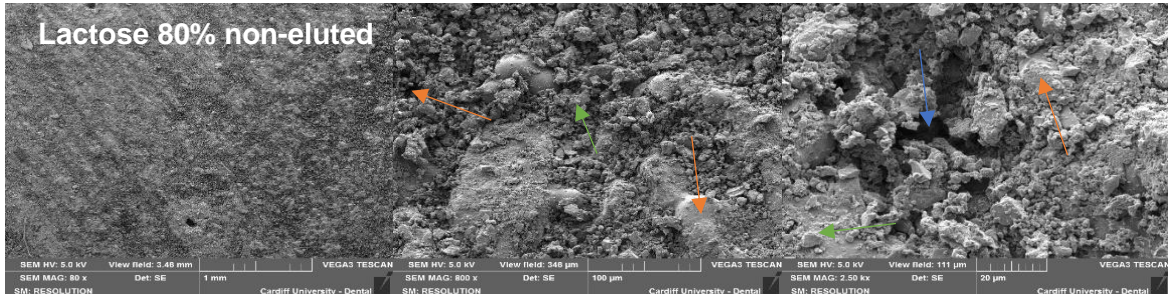


Figure 70: SEM surface images of lactose 25% (A) before and (B) after incubation in PBS for one week at 37 °C; sample magnifications are x80, x800 and x2.5k respectively. Arrows indicate PMMA particles (orange) and pores (blue).

(A)



(B)

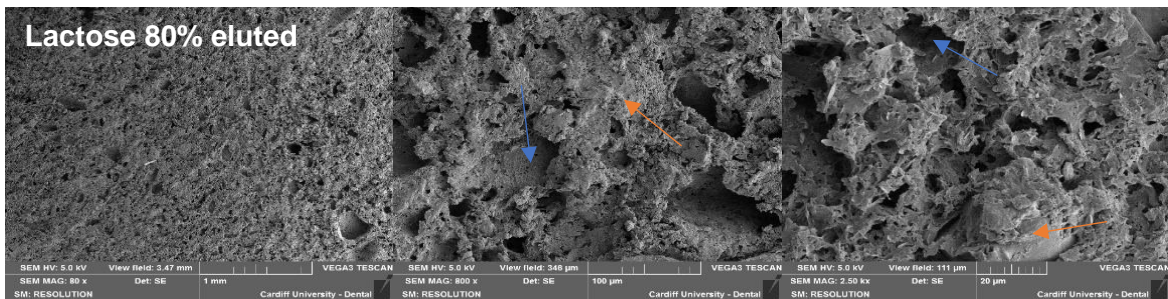
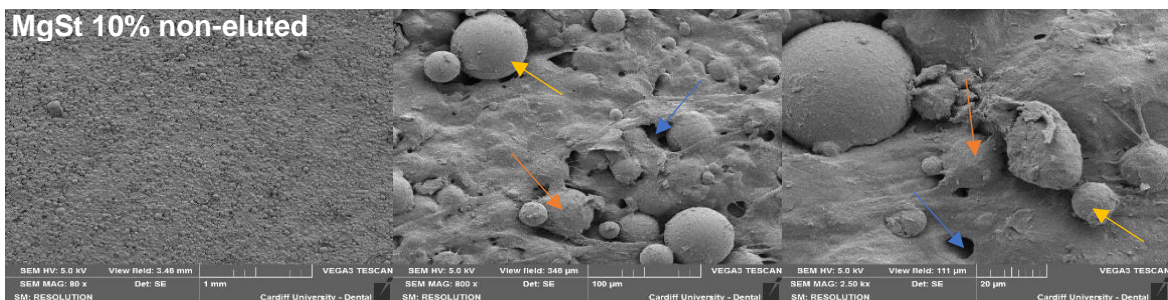


Figure 71: SEM surface images of Palacos R+G cement samples containing lactose 80% (A) before and (B) after incubation in PBS for one week at 37 °C; sample magnifications are x80, x800 and x2.5k respectively. Arrows indicate solid matrix (orange), smaller non-pmma particles (green) and pores (blue).

(A)



(B)

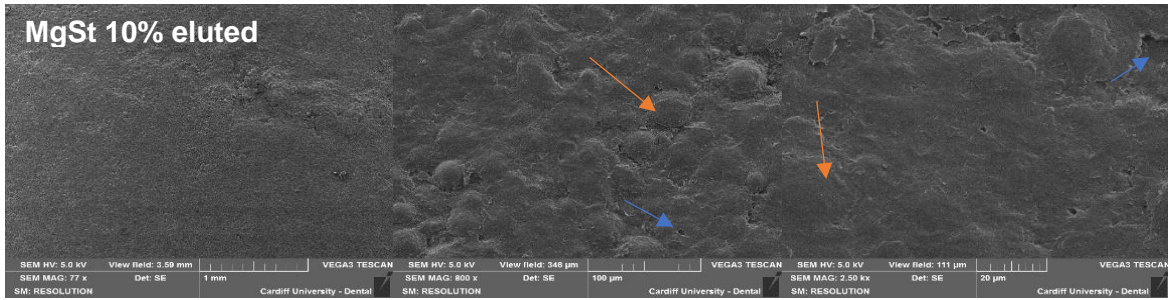
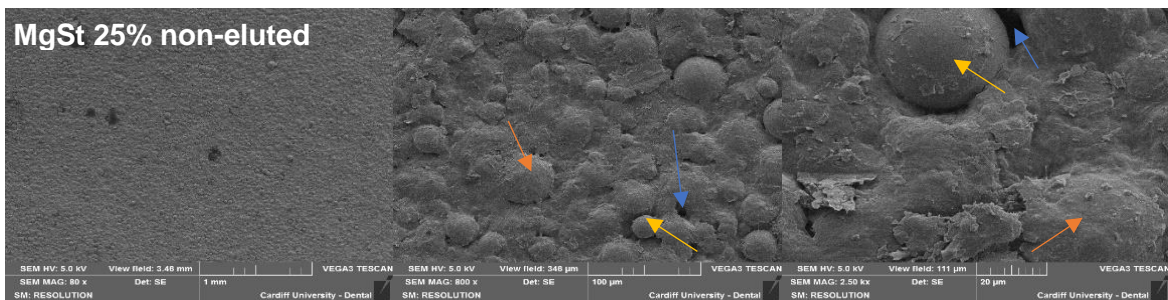


Figure 72: SEM surface images of Palacos R+G cement samples containing MgSt 10% (A) before and (B) after incubation in PBS for one week at 37 °C; sample magnifications are x80, x800 and x2.5k respectively. Arrows indicate fused PMMA particles (orange), lesser-fused PMMA particles (yellow) and pores (blue).

(A)



(B)

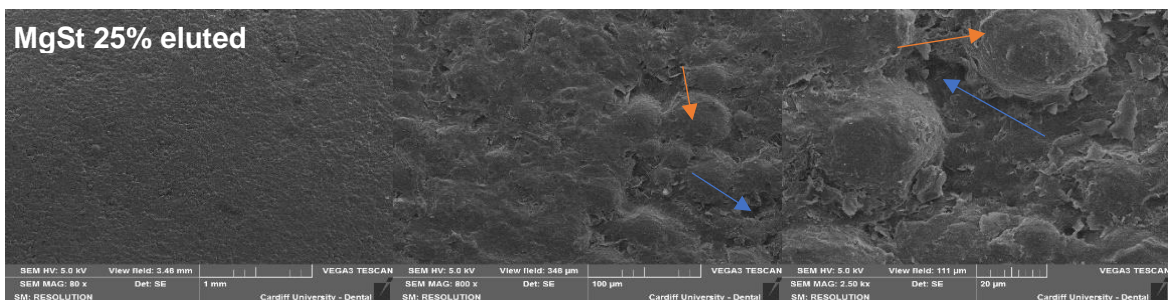


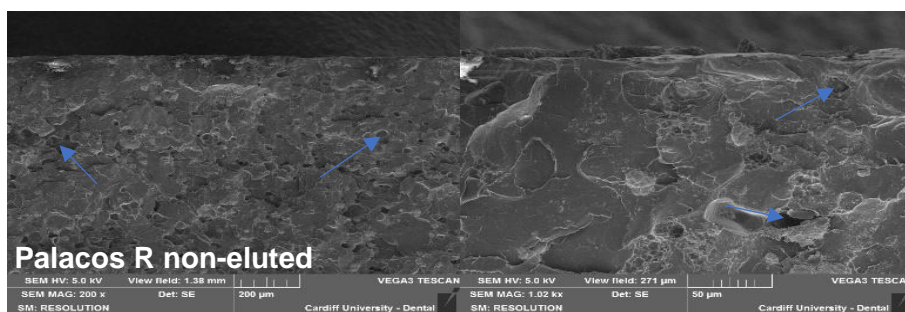
Figure 73: SEM surface images of Palacos R+G cement samples containing MgSt 25% (A) before and (B) after incubation in PBS for one week at 37 °C; sample magnifications are x80, x800 and x2.5k respectively. Arrows indicate fused PMMA particles (orange), lesser-fused PMMA particles (yellow) and pores (blue).

5.4.1.1.2 SEM images of horizontally cut cement discs

Figures 74 to 80 show SEM images at magnifications of 200 and 1k for Palacos R, Palacos R+G, lactose 10% and 25%, 80%, and MgSt 10% and 25% cements discs, as prepared and after incubation in PBS at 37 °C for one week. The images show surfaces resulting from cutting the cement discs horizontally into two parts (Section 5.2.6.1). This experiment was done to visualise the extent of water penetration through the cement disc from the surface.

No changes could be seen in the Palacos R Palacos R+G, MgSt 10% and 25%, and lactose 10% cement disc samples, after incubation. They all contained some pores on the inside surfaces prior to incubation, and it could not be determined with certainty for those samples, whether any pores observed in cements that were incubated in PBS, were the result of water penetration. The inside surface of the incubated lactose 25% cement disc appeared to have large pores that were not present prior to incubation. Although there were small round pores present prior to incubation, the shape and dimension of the pores after incubation are not the same and indicate the possibility of water penetration. Furthermore, the inside surface of the lactose 80% cement disc also shows large pores that are present after incubation, which have formed over the surface area of the entire SEM image.

(A)



(B)

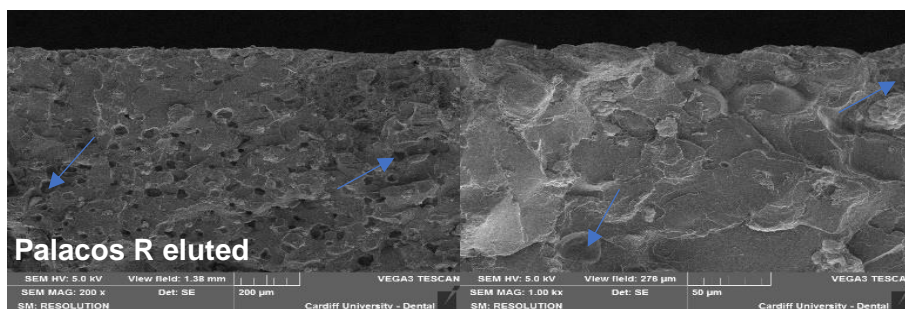
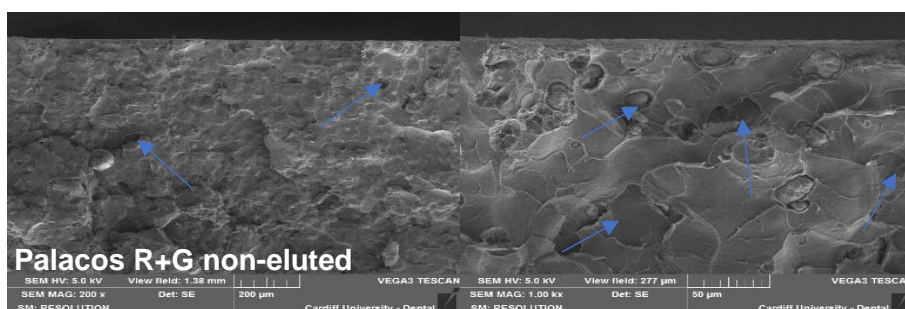


Figure 74: SEM images of inside portion of Palacos R disc cut horizontally (A) before and (B) after incubation in PBS for one week at 37 °C; sample magnifications are x200 and x1k. Arrows indicate pores.

(A)



(B)

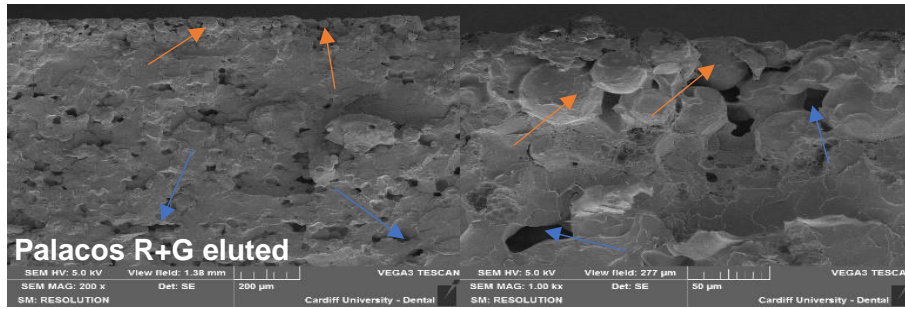


Figure 75: SEM images of inside portion of Palacos R+G disc cut horizontally (A) before and (B) after incubation in PBS for one week at 37 °C; sample magnifications are x200 and x1k. Arrows indicate PMMA particles (orange) and pores (blue).

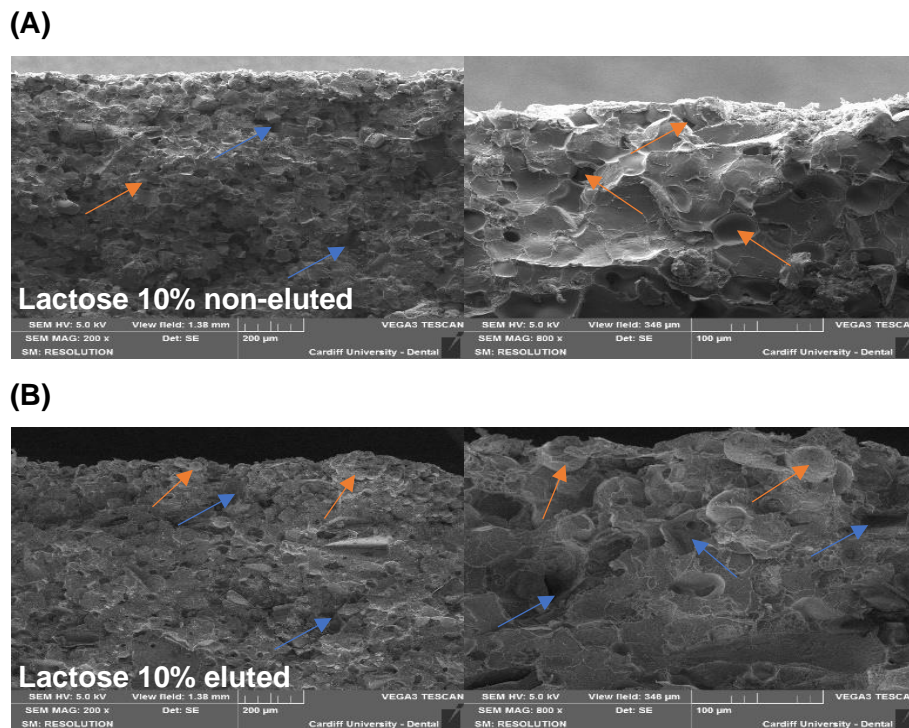
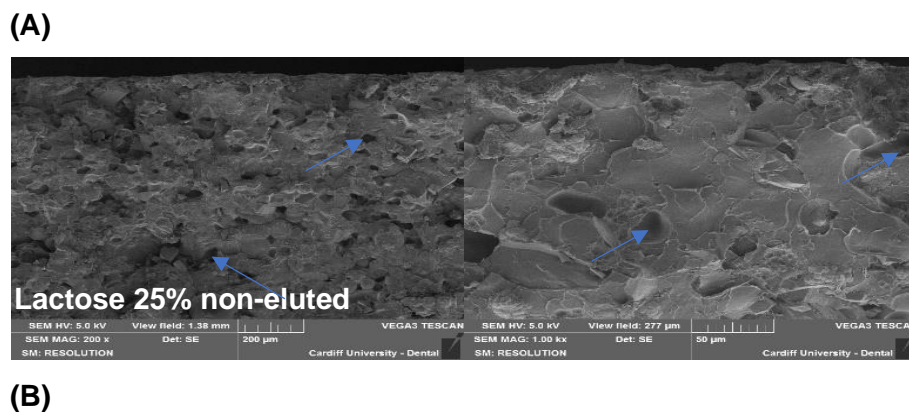


Figure 76: SEM images of inside portion of Palacos R+G disc containing lactose 10% disc cut horizontally (A) before and (B) after incubation in PBS for one week at 37 °C; sample magnifications are x200 and x1k. Arrows indicate PMMA particles (orange) and pores (blue).



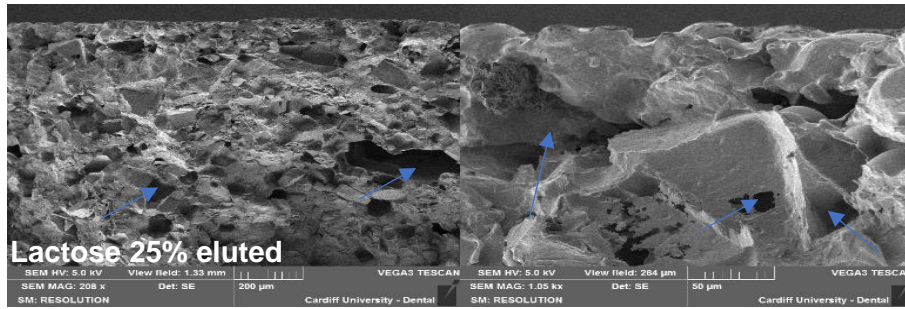
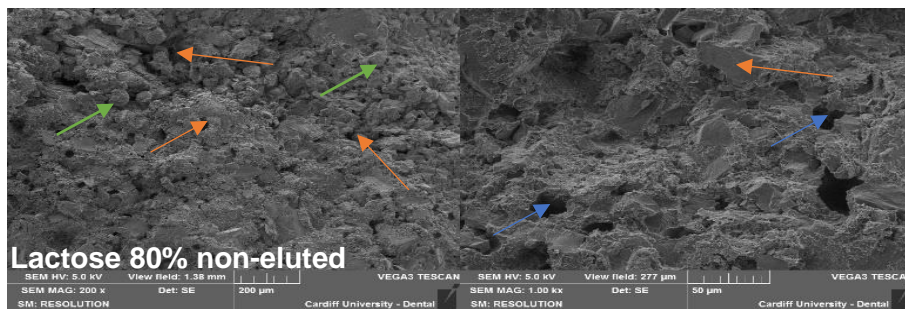


Figure 77: SEM images of inside portion of Palacos R+G disc containing lactose 25% disc cut horizontally (A) before and (B) after incubation in PBS for one week at 37 °C; sample magnifications are x200 and x1k. Arrows indicate pores.

(A)



(B)

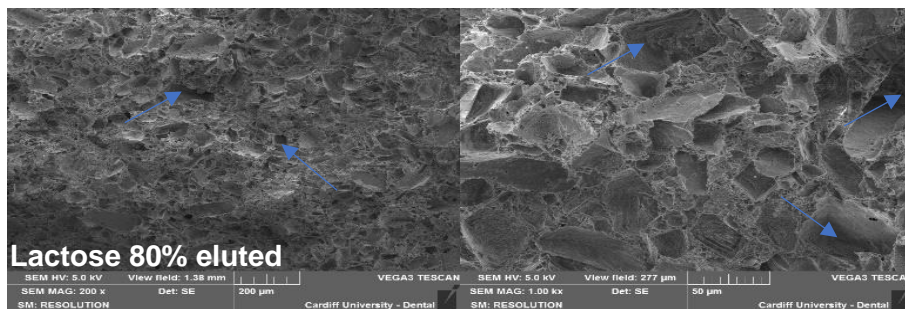
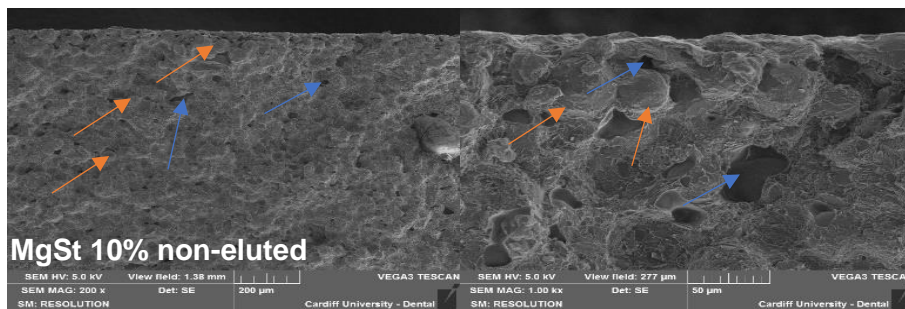


Figure 78: SEM images of inside portion of Palacos R+G disc containing lactose 80% disc cut horizontally (A) before and (B) after incubation in PBS for one week at 37 °C; sample magnifications are x200 and x1k. Arrows indicate solid matrix (orange), smaller non-pmma particles (green) and pores (blue).

(A)



(B)

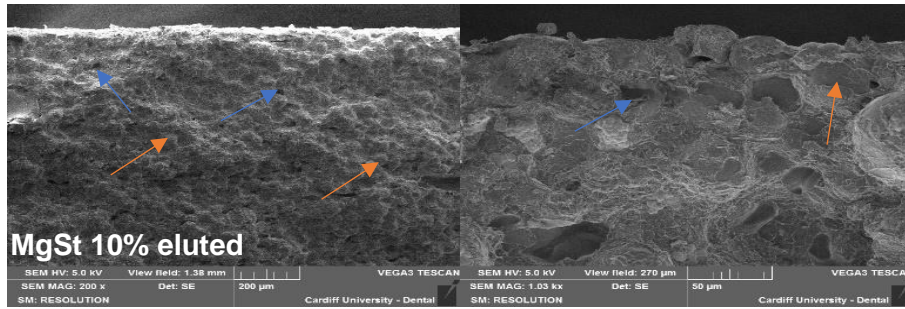
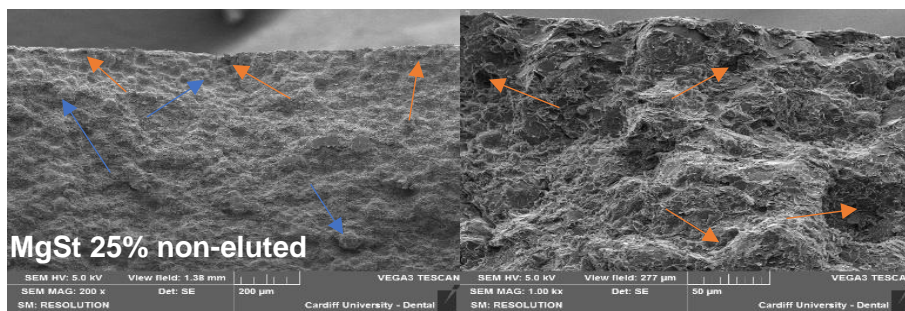


Figure 79: SEM images of inside portion of Palacos R+G disc containing MgSt 10% disc cut horizontally (A) before and (B) after incubation in PBS for one week at 37 °C; sample magnifications are x200 and x1k. Arrows indicate PMMA particles (orange) and pores (blue).

(A)



(B)

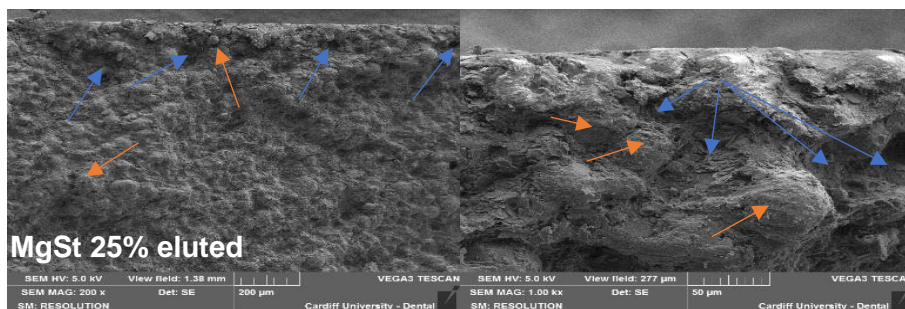


Figure 80: SEM images of inside portion of MgSt 25% disc cut horizontally (A) before and (B) after incubation in PBS for one week at 37 °C; sample magnifications are x200 and x1k. Arrows indicate PMMA particles (orange) and pores (blue).

5.4.1.1 Micro-CT analysis

Sample discs for Palacos R+G, lactose 25% and lactose 80% were analysed using microCT. Only three samples were analysed due to instrument constraints; moreover, three samples can be scanned simultaneously using the Bruker microCT instrument. Palacos R+G was chosen as a control sample. Lactose 25% was chosen as it released the largest quantity of gentamicin in the release study. Furthermore, as mentioned in Section 5.4.1.1, lactose 80%

was chosen for this experiment on the basis that it has the highest concentration of channelling agent, therefore, it has the highest water absorption of all the samples, which could give the best visualisation of water penetration, if visualisation is indeed limited. Other cement discs were not included in this experiment as they did not release the most amount of gentamicin, therefore, as use of this instrument was limited, only samples that were expected to show changes due to water penetration were scanned.

Porosity calculations from the 3D reconstructed scanned images of samples stored in PBS at 37 °C for one week were obtained and are shown in Table 13. The different types of porosity calculated are described in Section 5.2.7. Percentage of closed pores within the discs for Palacos R+G, lactose 25% and lactose 80% were calculated, as 1%, 6% and 0% respectively. Percentage of open pores within the discs for Palacos R+G, lactose 25% and lactose 80% were calculated, as 2%, 8% and 60% respectively. Percentage of total porosity within the discs for Palacos R+G, lactose 25% and lactose 80% were calculated, as 3 %, 13 % and 60 % respectively. Figures 81 to 83 show 3D reconstructions of sample discs (Palacos R+G, lactose 25% and lactose 80%); A) and B) are views of the top and side of the discs respectively, C) is a view of the inside of the reconstructed images, where the software has cut through vertically in the centre of the disc, and D) is a view of inside where the software has cut through the middle of the disc horizontally. The images C) and D) are for the purpose of seeing differences between samples due to water penetration into the discs. Images for Palacos R+G and lactose 25% both showed that the discs had several discrete holes inside the discs and on the surface (Figure 81 and Figure 82). Lactose 80% does not clearly show any discrete holes or pores on the images; however, it can be seen in Figure 83 images A), B) and C) that there are more black voxels amongst the white voxels which means that there is more empty space within the disc.

Table 13: Porosity calculations obtained for samples discs Palacos R+G and Palacos R+G discs containing 25% w/w and 80% w/w of lactose, after incubation in PBS for one week at 37 °C (n=1).

| | Palacos R+G | Lactose 25% | Lactose 80% |
|-------------------|-------------|-------------|-------------|
| Closed porosity % | 1 | 6 | 0 |

| | | | |
|------------------|---|----|----|
| Open porosity % | 2 | 8 | 60 |
| Total porosity % | 3 | 13 | 60 |

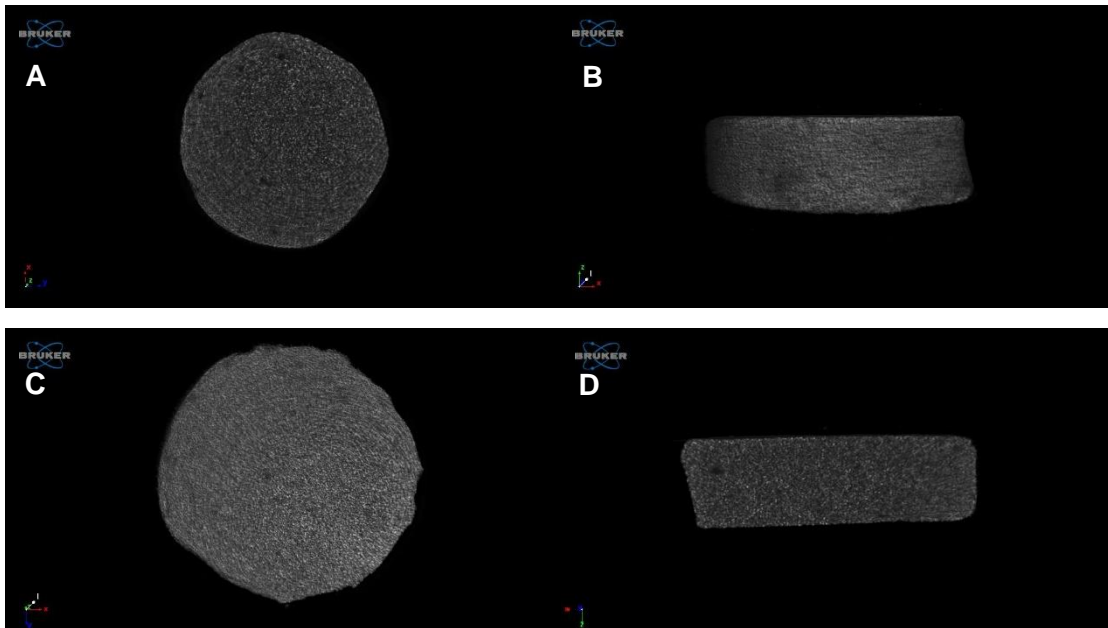
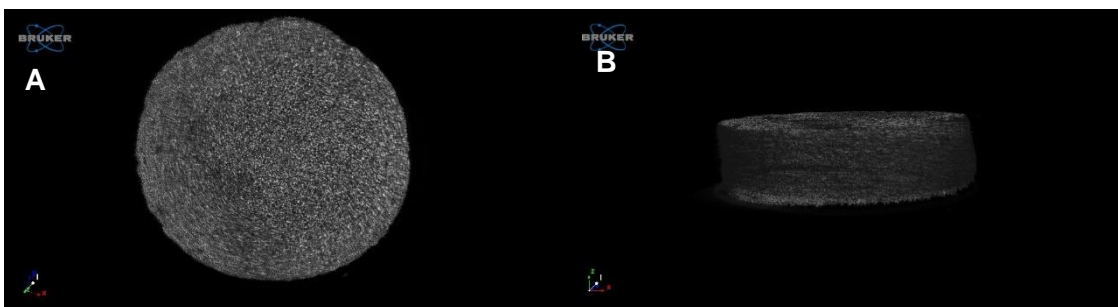


Figure 81: MicroCT 3D images obtained for control sample disc, Palacos R+G, after incubation in PBS for one week at 37 °C. A) is the top view, B) is the side view, C) is the view of the sample disc cut with the software vertically, halfway through the middle; and D) is the view of the sample disc cut with the software horizontally, halfway through the middle.



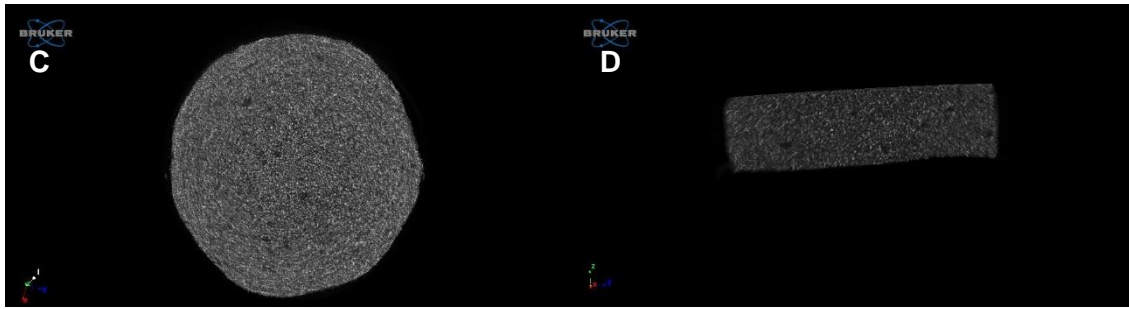


Figure 82: MicroCT 3D images obtained for sample disc, lactose 25%, after incubation in PBS for one week at 37 °C. A) is the top view, B) is the side view, C) is the view of the sample disc cut with the software vertically, halfway through the middle; and D) is the view of the sample disc cut with the software horizontally, halfway through the middle.

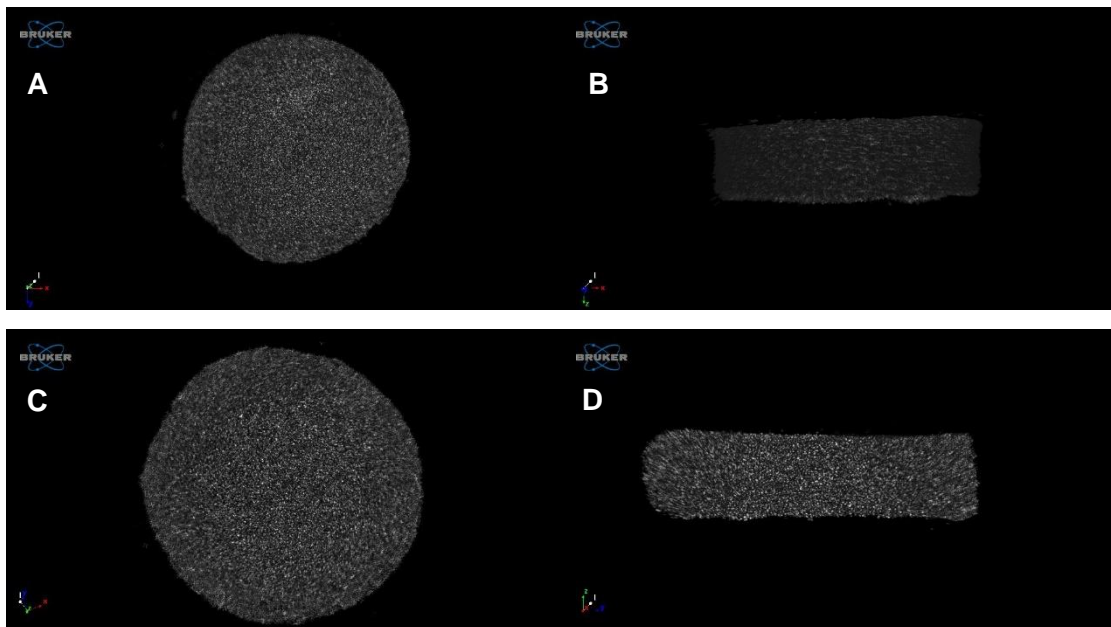


Figure 83: MicroCT 3D images obtained for sample disc, lactose 80%, after incubation in PBS for one week at 37 °C. A) is the top view, B) is the side view, C) is the view of the sample disc cut with the software vertically, halfway through the middle; and D) is the view of the sample disc cut with the software horizontally, halfway through the middle.

5.4.1.1 Sample weight loss after storage in PBS

After incubation in PBS at 37 °C, weight losses of different samples were obtained. Samples were dried at 65 °C to constant weight. It was found that by weighing the cement discs every 1.5 hours; between 4.5 and 6 hours, the weight change was less than 0.5 mg. Initially, 80% w/w lactose in Palacos R+G was prepared to visualise effects that were not as obvious in

cement discs containing lower mass amounts of lactose. 80% w/w was the largest mass amount that could be incorporated into Palacos R+G to produce a solid cement disc. In this experiment, 50% w/w lactose in Palacos R+G was prepared to see the dose dependant effect of increasing the lactose content in bone cement on cement disc weight loss, following storage in PBS and incubation at 37 °C. Figure 84 shows the percentage weight losses from Palacos R, Palacos R+G, lactose 10% and 25%, and MgSt 10% and 25% cements discs and Figure 85 shows weight losses separately for lactose 25%, 50% and 80%. Palacos R had the lowest weight loss of all the samples tested, 0.2 ± 0.0 %. Lactose 80% w/w had a weight loss of $61\% \pm 4.5$ %, which was the highest weight loss of all samples tested. Palacos R+G had a weight loss of 1.1 ± 0.1 %. Lactose 10%, 25% and 50 % had weight losses of $2.3\% \pm 0.4$ %, $8.3\% \pm 1.0$ % and $23.1\% \pm 1.2$ % respectively. MgSt 10% and 25% had weight losses of $1.2\% \pm 0.1$ % and $1.3\% \pm 0.1$ % respectively. Sample discs of Palacos R+G, MgSt 10% and 25% did not have a significant increase in weight loss compared to Palacos R ($p=0.3885$, $p=0.3885$ and $p=0.2100$ respectively); whereas lactose 10%, 25%, 50% and 80% had a significant increase in weight loss in comparison to Palacos R ($p=0.0067$ for lactose 10%, and $p<0.0001$ for lactose 25%, lactose 50% and 80%). Lactose 25%, 50% and 80% also had a significant increase in weight loss compared to Palacos R+G ($p=0.0067$ for lactose 25%, and $p<0.0001$ for both lactose 50% and 80%), whereas all other cement discs (Palacos R, lactose 10%, MgSt 10% and MgSt 25%) did not have a significant increase in weight loss compared to Palacos R+G ($p=0.9996$, $p=0.9979$, $p>0.9999$ and $p>0.9999$ respectively). MgSt 10% and 25% had weight losses that were not significantly different to one another ($p>0.9999$). Lactose 25%, 50% and 80% all had weight losses that were significantly different to one another ($p<0.05$); moreover, lactose 25%, 50% and 80% all had significantly different weight losses to MgSt 10%, 25% and lactose 10% ($p<0.05$).

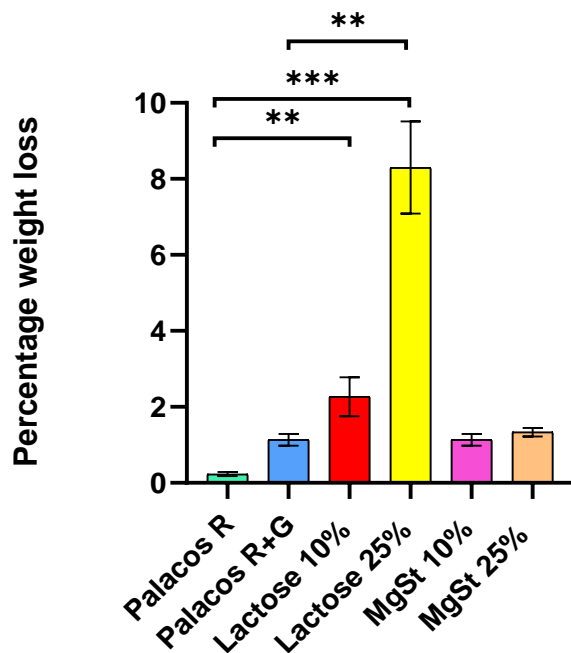


Figure 84: Percentage weight loss for Palacos R, Palacos R+G, Palacos R+G discs containing 10% w/w and 25% w/w of lactose and Palacos R+G discs containing 10% w/w and 25% w/w of magnesium stearate cement discs, after incubation in PBS at 37 °C for one week (n=3). Asterisks indicate the level of significance (* p<0.05, ** p<0.01, * p<0.001).**

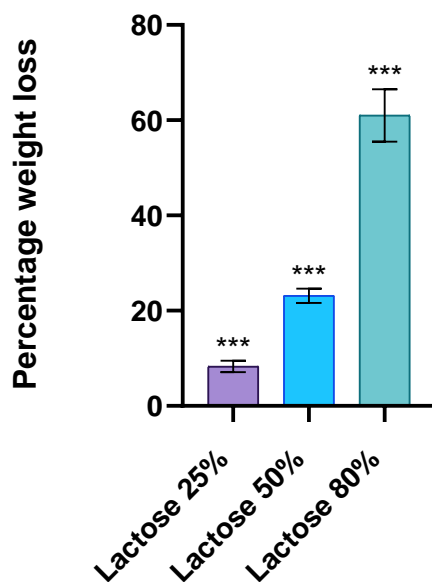


Figure 85: Percentage weight loss for discs produced from Palacos R+G containing 25% w/w, 50% w/w and 80% w/w of lactose, after incubation in PBS at 37 °C for one week (n=3). Asterisks indicate the level of significance with respect to Palacos R+G (* p<0.05, ** p<0.01, * p<0.001).**

5.5 Discussion

Following the results in Chapter 4, it was decided that liposomal cement (pelleted or freeze-dried) is not a feasible option, based on the performance of the freeze-dried cements (FDL), and the time-consuming and the wasteful nature of the pelleted liposomal system (LCP). The freeze-dried formulation, once incorporated into the bone cement, did not release therapeutic quantities of gentamicin for any length of time. It was also shown that the pelleted liposomal formulation was not commercially useful, as much of the reagents are lost during the production process, and long-term storage of the liposomal formulation is not a consideration. It was decided to investigate further additives that could enhance drug-release without compromising mechanical properties. Moreover, experimenting with different additives, of hydrophobic and hydrophilic character, would allow for a better understanding of how drug release occurs in bone cements. The aims of this chapter were therefore to investigate incorporation of lactose and magnesium stearate in bone cement to improve the drug release properties and to understand the mechanisms of drug-release from bone cement.

Different percentage amounts of lactose and magnesium stearate were incorporated into bone cement by geometric dilution. It was found that the maximum percentage of magnesium stearate that could be incorporated into bone cement, to make a solid disc, is 25% w/w. However, up to 80 w/w of lactose can be incorporated to make a solid disc. Antibiotic release was characterised, since infection prophylaxis is an important role of bone cements (Schwarz et al., 2021). Gentamicin release from the modified bone cement discs was measured over 8 weeks, using LC-MS. Results for magnesium stearate and lactose bone cements were compared to the commercial product, Palacos R+G, as commercial antibiotic loaded bone cement is the most commonly used material in orthopaedic surgery and is currently considered to be the gold standard for drug delivery (Karaglani et al., 2020; Singh et al., 2019). All the cements had a burst release at 6 hours. It has been documented in several articles that drug release from bone cement is always characterised by an initial burst release within the first hours of drug-release, regardless of formulation (Cyphert et al., 2018; Mori et al., 2011). Cements containing 10% w/w and 25% w/w of incorporated lactose, released the most gentamicin of all of the cement discs. They released more than the commercial gentamicin loaded bone cement by the final time point of 2 months; lactose 25% and lactose 10% released around 600 µg and 300 µg more than Palacos R+G, respectively. Moreover, at 24 hours, the cement discs containing lactose released more gentamicin than Palacos R+G and around twice the mass quantity of gentamicin than the cement discs

containing magnesium stearate. The magnesium stearate cement discs (MgSt 10% and 25%) released final mass quantities of gentamicin, at the final time point (1296 hours), that were comparable to the drug release by Palacos R+G; however, the magnesium stearate cements showed a more sustained release profile than Palacos R+G. The sustained drug release may be due to the dissolution retardant effect of magnesium stearate. Magnesium stearate is a known dissolution retardant due to its hydrophobic properties, it is able to repel water from entering various formulations such as tablets, therefore retarding drug release for both hydrophilic and hydrophobic drugs such as paracetamol (hydrophilic) and ibuprofen (hydrophobic), and causing a more sustained release (Uhumwangho et al., 2007). The increased gentamicin mass amount released from lactose incorporated bone cement is possibly due to channelling. The channelling effect is where a hydrophilic compound, soluble in the dissolution medium, such as lactose or gentamicin (Igbinauwa et al., 2019; Virto et al., 2003) is incorporated within a formulation, and functions by effectively being dissolved by the dissolution medium; forming channels within matrix material, therefore releasing further drug mass amounts through pores and channels (Sudha et al., 2010; Zakaria et al., 2019). Furthermore, the incorporation of hydrophilic material in bone cement can cause hydrophilisation of the bulk cement and therefore increase the wettability (El-Fallal et al., 2009; Oh et al., 2016; van Belt et al., 2000), meaning that there will be more contact between water and disc surface, therefore increased penetration of water into pores via the PMMA cement surface occurs, and therefore an increase in drug release (van Belt et al., 2000). In a study where porogens were incorporated into bone cements, gentamicin release was increased with the addition of porogens (Wu, 2016); this is similar to the increase in concentration of lactose in Palacos R+G, as an increase in lactose would create more pores after storage in PBS due to channelling. Moreover, the burst release is due to immediate dissolution of surface components attributed to antibiotic, located on the cement surface, meaning that broadly speaking, water penetration does not extend throughout the cement disc itself (Gálvez-López et al., 2014). This accounts for the immediate high-level release for most of the samples. However, the fact that lactose 25% continued to release large mass amounts of gentamicin, may be because of the large mass quantities of channelling agents contained in the cement, mainly lactose, which forms channels throughout the entire bone cement disc.

The sample weight loss experiment shows that an increase in cement weight loss is associated with an increase in incorporated channelling agent. The weight loss of Palacos R+G, Lactose 25% and Lactose 80% were 1%, 8% and 61% respectively, showing that an increase in hydrophilic content causes an increase in weight loss. Given that Palacos R which contains no gentamicin at all nor lactose, had a weight loss of 0.2%, it can be seen

that Palacos R+G has released 1% of its entire mass, of which it is assumed that most of the weight loss is due to gentamicin, as the only difference between Palacos R and Palacos R+G is just the incorporation of gentamicin sulfate. The lactose 25% percent cement released 8% of its contents, and gentamicin 80% released 61% of its contents, meaning that the degree of channel formation was extensive in the 80% w/w lactose disc, covering a large proportion of the cement disc. The porosity calculations by microCT showed that the open porosity of the cement discs, which is the porosity connected to the surface of the disc, was Palacos R+G (2%), Lactose 25% (8%) and Lactose 80% (60%) which is consistent with the weight loss values obtained for these respective discs. The closed porosity of the lactose 80% cement disc was zero, which suggests that the channelling within the disc is interconnected throughout the disc, as no discrete open pores were shown to be present. However, it was not possible to clearly visualise the extent of the channelling with the microCT images; and it was not possible to differentiate between the three separate samples visually. Although bone cements contain zirconium particles which is a radio pacifier, acting as a contrasting agent, the bone cement itself has not absorbed the x-rays well enough to show a contrast between channels and solid material. To improve on this result, the method could be altered, so that that after samples incubated in PBS are then subjected to either iodine vapour alone or iodine moieties added to an aqueous solution (Boyde et al., 2014). Iodine is known to impart a strong contrast to samples imaged by microCT, as it has a high atomic number (Boyde et al., 2014). Furthermore, it would also need to be determined how long staining should last, as this is largely an empirically determined parameter (Boyde et al., 2014). However, should a method be successfully optimised, individual pores and channels could potentially be observed in the samples, and it could be shown exactly how far into the discs, penetration by water occurs. This would be very useful in seeing how far drug release occurs in all samples and to compare the different levels of penetration based on an understanding of the properties of the excipients such lactose etc. Characterisation of the water contact angle did not shed any light on whether the lactose cement surface as a whole was hydrophilised, as the contact angles for the lactose , magnesium stearate and Palacos R cement discs were similar, and not significantly different to one another; however, all of the lactose and magnesium stearate bone cements' contact angles were significantly higher than Palacos R+G. Contact angles indicate the wettability of a given surface. These were measured to ascertain whether the bone cement formulations had increased or decreased wettability in comparison to the commercial bone cements Palacos R and Palacos R+G. It is likely that a surface with increased wettability will release higher mass quantities of antibiotic, as the increased wettability means that a higher degree of water contact between the disc surface and water has been achieved. It is expected that bone cement will become hydrophilised by the addition of a hydrophilic additive (Oh et al., 2016); therefore, an

increase in hydrophilicity would result in a decreased contact angle (Kubiak et al., 2011). The reason for the contact angle not decreasing significantly with regards to Palacos R, could be due to the water droplet dissolving surface gentamicin upon immediate contact, therefore being affected by the concentration of gentamicin within that droplet. In particular, it is documented that the water contact angle technique is sensitive to contamination of the water droplet itself, which can affect the final contact angle result (Marmur et al., 2017).

The actual concentration of gentamicin released at 6 hours for each sample, as measured by LC-MS, was above the known minimum inhibitory concentration (MIC) required to reduce *S. aureus* bacteria count; according to the study by Figueroa *et al.* (2008), it was shown that the MIC of gentamicin sulfate required to inhibit bacteria growth of *S. aureus* was 0.0125 mg/ml (Figueroa et al., 2008). The commercial cement Palacos R+G was found to have released 0.069 mg/ml, lactose 10% (0.070 mg/ml), lactose 25% (0.082 mg/ml), magnesium stearate 10% (0.033 mg/ml) and magnesium stearate 10% (0.044 mg/ml) at 6 hours. The quantitative antimicrobial suspension test showed that all of the samples were effective at reducing *S. aureus* bacteria count and caused for a reduction in colony forming units. All cement samples containing either lactose or magnesium stearate were more effective in killing *S. aureus* than the commercial Palacos R+G. No biofilm formation was detected on any of the cements after 48 hours, indicating that biofilm formation may have been prevented by the various cement formulations. However, although the *S. aureus* strain used in this experiment (NCTC 10788) is known to produce biofilms (Gwynne et al., 2021), the experiment should be conducted by using a control disc made from a material where biofilm growth is known to occur e.g. glass (Marques et al., 2007; Shukla & Rao, 2017). All samples were tested for compression, bending modulus, and bending strength as per the standard ISO 5833. Only lactose 10% passed all of the requirements. There were no observable changes to the surfaces of Palacos R or Palacos R+G, after incubation. Lactose and magnesium stearate incorporated cements all contained rounded fused particles, moreover, pores were present on the surface in between those round particles prior to incubation; however, after incubation in PBS, the degree of porosity observed prior to incubation, could not be seen, which may be the result of loosely bound PMMA particles being removed during the incubation process, particularly as it could be seen that polymerisation may have been inhibited. It was shown clearly that lactose 80%, after incubation in PBS, had formed large pores all over the surface. This is mostly likely due to the channelling effect. The cement discs were cut horizontally to visualise any possible water penetration. It was possible to see clear pores in the lactose 25% and 80% cement, showing that water penetration had occurred through the bone cement surface, at least through 600 μm , as measured on the image.

5.6 Conclusions

Lactose and magnesium stearate were incorporated into bone cement to investigate the effects of hydrophilic and hydrophobic additives on drug-release. It was possible to make bone cements containing up to 25% w/w of magnesium stearate, and up to 80% w/w lactose. It was observed that all of the bone cements including Palacos R+G and the cements containing lactose or magnesium stearate, had a burst release upon contact with water. The initial mass quantities of gentamicin released at the point of burst release (first time point) differed depending on the additives contained in the bone cement. Bone cement containing lactose showed the greatest mass quantity release of gentamicin at the first time point. Lactose 25% cement had the highest mass quantity drug release of gentamicin at the first time point; and at this time point, the release was significantly higher than the gentamicin release from both magnesium stearate cements. However, it was observed that bone cement containing magnesium stearate had a more sustained drug-release profile. Bone cement supplemented with lactose released the most amount of drug mass quantity; however, bone cement containing 25% w/w lactose also showed a sustained drug release; this was due to the large extent of channelling within the cement itself, as the cement released larger mass quantities of antibiotic at all the time points. By the final time point, bone cement supplemented with magnesium stearate released mass amounts of drug comparable with commercial gentamicin loaded bone cement. However, over the time-course, a more sustained release was observed for the cements supplemented with magnesium stearate; this was due to the dissolution retardation effect of magnesium stearate. It was possible, by SEM, to visualise clear formation of pores on the surfaces of discs for lactose 80% w/w after incubation; and surface differences could be observed on all lactose and magnesium stearate cement discs which formed as part of the disc manufacturing process. Moreover, penetration from the surface of lactose supplemented discs could be seen by horizontally cutting the lactose 25% and 80% discs in half. MicroCT was able to calculate porosity within the cement discs after incubation in PBS, although visualisation of pores was not possible using the reconstructed images. It is therefore recommended to investigate a staining method with a contrasting agent, which may allow visualisation of water penetration within the cement discs. Weight loss after incubation showed that most of the cements including Palacos R, Palacos R+G, lactose 10% and the magnesium stearate cements do not have a large weight loss, after incubation for 1 week in PBS, although lactose 80% w/w lost 60% of its initial mass, suggesting that channels are

formed throughout the cement itself. Only bone cement containing 10% w/w lactose passed the ISO 5833 requirements. All of the magnesium stearate and lactose supplemented cement discs decreased *S. aureus* bacteria counts, comparable with the commercial cement, Palacos R+G. LC-MS data showed that clinically significant levels of gentamicin were released at the 6-hour time point.

Chapter 6

6 Dry particle coating of gentamicin sulfate with magnesium stearate

6.1 Introduction

Commercial antibiotic loaded bone cement (ALBC) is characterised by antibiotic release occurring as a burst release, with most drug released in the first hours of application (Moojen et al., 2008; Neut et al., 2010). A drawback of this characteristic burst-release profile is the consequent and continual drug release at low concentrations (Cyphert et al., 2018), even releasing at sub-inhibitory concentrations after the first week (Moojen et al., 2008). Release

of aminoglycosides at sub-inhibitory amounts induce biofilm formation (Xiong et al., 2014) and can also cause antibiotic resistance (ter Boo et al., 2015). An ideal bone cement should release antibiotic at levels above the MIC for at least 1-2 months, to prevent acute orthopaedic infections, whilst maintaining its mechanical properties (Cyphert et al., 2018). In Chapter 5, lactose and magnesium stearate were added to commercial bone cement containing gentamicin sulfate, Palacos R+G, to characterise the effects of the addition of hydrophilic and hydrophobic additives, particularly on antibiotic release. Large mass amounts of lactose and magnesium stearate were added to bone cement containing gentamicin sulfate. The lactose incorporated bone cements released large mass quantities of gentamicin at each consecutive time point, releasing a total of 1400 µg of gentamicin after 2 months; this was in comparison to the commercial antibiotic loaded bone cement which released around 800 µg of gentamicin. On the face of it, a high mass amount of drug release over a period of time may appear favourable; however, a large amount of hydrophilic drug release from bone cement is also associated with increased penetration and retention of water, porosity and degradation (Karpiński et al., 2019), moreover, porosity can be the cause of the bone cement degradation (Akram et al., 2016; Karpiński et al., 2019). The bone cement containing magnesium stearate released antibiotic at a slower rate, in a more controlled manner. Magnesium stearate is a commonly used lubricant in solid dosage formulations (Wang et al., 2010), and it is known to delay tablet dissolution because of its hydrophobicity (Ariyasu et al., 2016; Uhumwangho et al., 2007). There are several studies that have successfully combined magnesium stearate with particles of interest, such as active pharmaceutical ingredients (Qu et al., 2015; Zhou et al., 2013) or pharmaceutical excipients such as dry powder inhaler carrier particles (Zhou et al., 2013). This process known as dry particle coating (Bungert et al., 2021; Sato et al., 2013) or hybrid mixing (Alyami et al., 2017; Dahmash & Mohammed, 2015), is a process that effectively coats smaller 'guest' particles on to larger 'host' particles, producing functionalised particles (Serris et al., 2013). The process of dry powder coating is indicative of strong adhesion of finer guest particles on to the surface of coarser host particles (Zhou et al., 2010). The guest particles become attached to the host particles mainly by van der Waals forces (Zheng et al., 2020). Coatings by a guest particle around a host particle are categorised by the extent of coating (Dahmash & Mohammed, 2015; Saharan et al., 2008): a partial discrete coating is a partial coating where guest particles are adhered to the host particle, in a non-regular manner; continuous coating is effectively a monolayer formed around the guest particle; embedding is where the attraction between host and guest is strong enough to cause the host particles to become embedded on to it; encapsulation is a continuous coat around the host particle when the forces between the host and guest particles are strong enough (Alyami et al., 2017; Dahmash & Mohammed, 2015). Dry particle coating methods

encompass physical processes that are effectively dry processes, which do not make use of any solvents (Zheng et al., 2019). The hydrophilic nature of gentamicin sulfate prevents it from being well dispersed within the hydrophobic PMMA cement, thus causing for poor dispersion and formation of agglomerations of the powdered antibiotic in the bone cement (Dunne et al., 2008); coating gentamicin sulfate with hydrophobic magnesium stearate could help overcome issues of poor dispersion within the cement, therefore improving the mechanical properties and causing for a more uniform drug release profile.

Methods that use a range of different mechanical forces have been employed for dry powder coating (Dahmash & Mohammed, 2015; Saharan et al., 2008). Conventional 'low shear' mixing methods include rotary mixing (Alonso et al., 1988) and mechanical tumbling (Saharan et al., 2008). Methods ranging from mild/moderate to high shear forces include mortar and pestle (Kawaguchi et al., 2018; Saharan et al., 2008), stainless steel ball mill (Bor et al., 2018; Saharan et al., 2008) and mechanofusion (Bungert et al., 2021). Several commercial mechanofusion devices are available (Nadimi & Ghadiri, 2021; Zhou et al., 2013) including the Hosokawa AMS Mechanofusion system (Bungert et al., 2021; Kumon et al., 2006). The mechanofusion technique is an example of a very high shear method, whereby high shear forces produced by high centrifugal and compression forces, cause the guest particles to fuse onto the surface of the host particles (Saharan et al., 2008; Zheng et al., 2019).

Aims of this chapter:

To investigate powder coating of gentamicin sulfate with magnesium stearate, and to incorporate the coated gentamicin sulfate particles into commercial bone cement to improve the drug release properties whilst maintaining mechanical properties.

Objectives of this chapter:

- To use different mixing methods to create homogenous magnesium stearate coated gentamicin sulfate blends.
- To characterise these powder blends using SEM, SEM-EDX and particle size analysis.
- To incorporate magnesium stearate coated gentamicin sulfate blends into bone cement.

- To characterise the drug release profiles, mechanical properties and antimicrobial efficacies of these bone cements, comparing them to those of Palacos R+G and LCP-CEMENT cements used in Chapter 3.

6.2 Methods

6.2.1 Materials

Acetonitrile ($\geq 99\%$), formic acid ($\geq 99\%$), phosphate buffered saline (10 \times concentrate), and magnesium stearate were purchased from Fisher Scientific (Fisher Scientific UK, Loughborough). Gentamicin sulfate (≥ 590 μg Gentamicin base per mg) was obtained from Sigma Aldrich (Sigma-Aldrich Ltd, Gillingham, UK). Sodium chloride, tryptone and tryptone soy broth were purchased from Fisher Scientific (Fisher Scientific UK, Loughborough, UK). Palacos cements R and R+G were provided by Heraeus (Heraeus Medical, Newbury, UK). *Staphylococcus aureus* (*S. aureus*, NCTC 10788) was used.

6.2.2 Cement preparation

Cements were prepared as per the method specified in Section 2.1.1.

6.2.3 Mixing techniques used for gentamicin sulfate and magnesium stearate

Gentamicin sulfate powder was coated with magnesium stearate using mixing methods of varying mechanical energy input. Conventional blending was performed using a hexagonal tumble mixer; furthermore, higher energy input methods such as mortar and pestle and ball mill were also used. The methods were based on those used in similar studies found in literature. Three different concentrations of magnesium stearate with respect to gentamicin sulfate were prepared for each of the different techniques (1% w/w, 5% w/w and 10% w/w). For each of the required concentrations, gentamicin sulfate and magnesium stearate were weighed out and then mixed together carefully by geometric dilution.

6.2.3.1 Hexagonal mixer

1 g of pre-mixed GS/MgSt (Section 6.2.3) was added to the hexagonal mixer and run for one hour at a setting of 50 rpm.

6.2.3.2 Pestle and mortar

1 g of each premixed concentration was added to the mortar. Each mixture was then ground vigorously using a pestle for 10 minutes.

6.2.3.3 Ball Mill

1 g of each premixed concentration was added to a 500 ml volume stainless steel ball mill, containing 363 steel balls of total weight 1.27 kg and a total volume of 167 ml. The ball mill was placed onto a mechanical roller for 5 hours on a setting of 60 rpm.

6.2.4 LC-MS

Gentamicin was assayed using LC-MS. The instrument and method were used as specified in Section 2.7.2.

6.2.5 Compressive strength

Compressive strength testing was performed using the method specified in Section 2.4.1.

6.2.6 Particle size analysis using laser diffraction

Particle size analyses by laser diffraction was performed on powder samples using a Malvern Mastersizer 2000 (Malvern Instruments Ltd, Worcestershire, UK). Samples were introduced with a spatula into the sample inlet and analysed using the Mastersizer software v5.6 (Malvern Instruments Ltd, Worcestershire, UK). Particle size distribution was expressed as the mass median diameter (D50) in microns (μm) and span. Span is a commonly used parameter used to describe size distribution data using laser diffraction, as it shows the width of the particle size distribution (Dyankova et al., 2016; Moghadam et al., 2019; Polakowski et al., 2014). Span was calculated using the standard percentile readings obtained from the analysis, as per the formula in the National Institute of Standards and Technology standard (NIST: SRM 114q Part II: Particle size distribution, 2006):

$$\text{Span} = \frac{D90 - D10}{D50}$$

Where, D10, D50 and D90 are the percentile values obtained from the particle size distribution. These values indicate particle sizes below which 10%, 50% and 90% of the distribution have a smaller particle size, respectively. The remaining percentage has a larger particle size. For example, at the mass median diameter (D50), 50% of particles in the sample have a smaller particle size and 50% have a larger particle size.

6.2.7 Contact angle measurement

Water contact angles were measured using the Attension contact angle analyser as specified in Section 2.3.

6.2.8 Antimicrobial Testing

Overnight cultures of *S. aureus* (NCTC 10788) were prepared as described in Section 2.9. All antimicrobial testing was carried out using the methods specified in Section 2.9. This includes sterilisation of glassware, media sterilisation, sample sterilisation; quantitative suspension tests, and analysis of biofilm formation.

6.2.9 Scanning electron microscopy

Scanning electron microscopy (SEM) was carried out using the method specified in Section 2.10.

6.2.10 Scanning electron microscope using Energy Dispersive X-ray Spectroscopy (SEM-EDX)

SEM-EDX was performed by using a TESCAN VEGA3 with energy dispersive X-ray microanalyser detector (EDX). An EDX beryllium window detector was used for the elemental analysis. The detector was calibrated using a copper elemental standard. For topography of particles, powder was dusted on to carbon conductive adhesive tape, attached to an SEM aluminium stub and carbon coated. Analysis was performed using IDFix EDS acquisition software (Point Electronic GmbH, Germany).

6.2.11 Statistical analysis

Statistical analysis was performed as described in Section 2.11.

6.3 Results

6.3.1 Scanning electron microscopy images of gentamicin and magnesium stearate powder blends

SEM images were taken of the gentamicin sulfate and magnesium stearate powder blends, as prepared by the different processing methods, in order to show particle size and to visualise the degree of contact between gentamicin sulfate and magnesium stearate particles. Figure 86 shows SEM images of A) gentamicin sulfate, B) magnesium stearate,

C) a preliminary mixture of magnesium stearate in gentamicin sulfate powder (25% w/w magnesium stearate in gentamicin sulfate), mixed for 10 seconds with a glass rod. This preliminary mixture was prepared to see if there is possible contact between both types of particle after mixing. Gentamicin sulfate particles are spherical and of particle size between 5 and 100 μm . Magnesium stearate particles are amorphous in shape and of particle size between approximately 5 and 30 μm . Particles of gentamicin are visually distinctive from particles of magnesium stearate. It can be seen from image C) that by mixing gentamicin sulfate and magnesium stearate using a glass rod, without much energy input for a short amount of time, causes the smaller magnesium stearate to adhere to the gentamicin particles. Image (D) shows a higher magnified image of gentamicin sulfate particles with magnesium stearate particles adhered to its surface. Furthermore, in all images, it can be seen that some magnesium stearate particles remain unattached to the gentamicin sulfate particles.

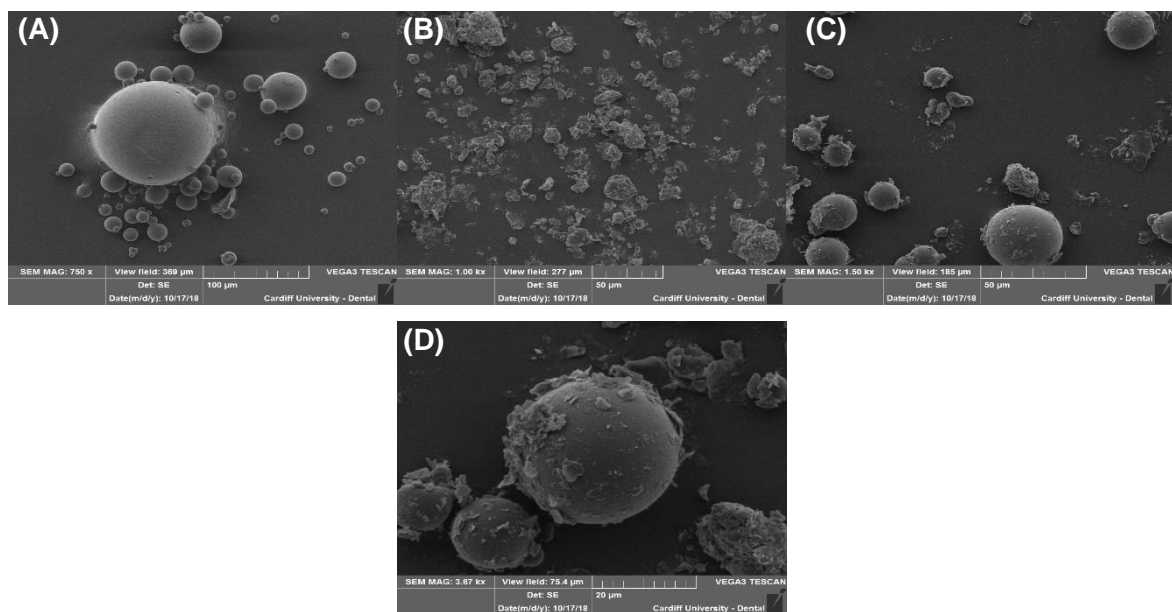


Figure 86: SEM images of (A) gentamicin sulfate, (B) magnesium stearate and (C) gentamicin sulfate and magnesium stearate 25% w/w preliminary mixture, (D) gentamicin sulfate and magnesium stearate 25% w/w mixture at a high magnification. Sample magnifications are between x1k and x3.7k.

Figure 87 shows SEM images of samples after hexagonal mixing. It can be seen that for all of the magnesium stearate concentrations, smaller particles of magnesium stearate are adhered to gentamicin sulfate particles. It is also observed that increasing the concentration

of magnesium stearate leads to an increase in the number of magnesium stearate particles surrounding the gentamicin sulfate particles.

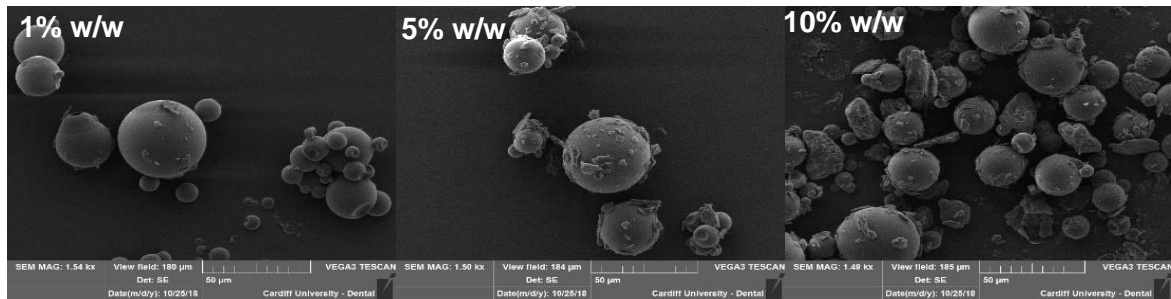


Figure 87: SEM images of gentamicin sulfate and magnesium stearate powder blends of concentration 1% w/w, 5% w/w and 10% w/w with respect to gentamicin sulfate, prepared by hexagonal mixing. Sample magnifications are 1.5k.

Figure 88 shows SEM images of samples after manually grinding using a mortar and pestle for 10 minutes. It can be seen that for all of the of magnesium stearate concentrations, smaller particles of magnesium stearate are adhered to the larger gentamicin sulfate particles. For all of the samples ground with mortar and pestle, it can be seen that some of the gentamicin sulfate particles have fragmented into smaller pieces, of varying particle size. By visual inspection, particle size ranges from around 10 µm to 50 µm for all the samples. The 1% w/w powder blend shows the least number of surface-adhered particles. At magnification of 1.5k it is not possible to differentiate between the 5% w/w and 10% w/w powder blends regarding the number of surrounding particles surrounding gentamicin sulfate particles.



Figure 88: SEM images of gentamicin sulfate and magnesium stearate powder blends of concentration 1% w/w, 5% w/w and 10% w/w with respect to gentamicin sulfate, prepared by manually grinding with a mortar and pestle. Sample magnifications are 1.5k.

Figure 89 shows SEM images of samples after being milled for 5 hours in a stainless-steel ball mill. It can be seen that the particle size has been greatly reduced, and it is not possible to distinguish between gentamicin sulfate and magnesium stearate particles. Even at 3.5k magnification, gentamicin sulfate and magnesium stearate cannot be distinguished.

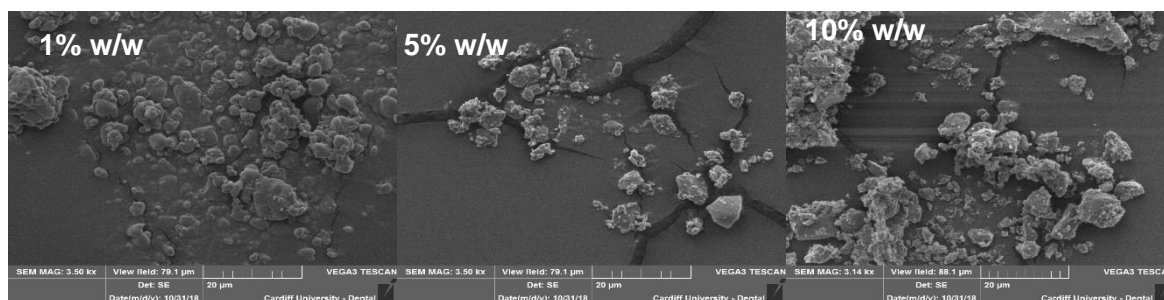


Figure 89: SEM images of gentamicin sulfate and magnesium stearate powder blends of concentration 1% w/w, 5% w/w and 10% w/w with respect to gentamicin sulfate, prepared by the ball mill technique. Sample magnifications are between x3k and x3.5k.

6.3.2 Particle size analysis using laser diffraction

Mean particle diameter was measured to characterise particle size differences by the different processing methods. The particle size was expressed as the mass median diameter (D50) in microns, which is the particle size at which 50% of the sample is smaller and 50% is larger (Pilcer et al., 2008). Results for particle size analysis are shown in Figure 90.

Gentamicin sulfate was found to have a mean diameter of $34.7 \pm 1.2 \mu\text{m}$, using the ball mill technique, significantly reducing the particle size to $3.4 \pm 0.1 \mu\text{m}$ ($p < 0.0001$). Magnesium stearate was found to have a diameter of $6.4 \pm 0.4 \mu\text{m}$. Comparing the mean values of samples from each technique, the ball mill had the largest effect on size ($3.2 \mu\text{m}$), followed by pestle and mortar ($18.7 \mu\text{m}$), and hexagonal mixing ($34.0 \mu\text{m}$). The high shear ball mill technique caused the largest effect on mean particle diameter. BM1, BM5 and BM10 were found to have mass median diameter, D50, of $3.1 \pm 0.1 \mu\text{m}$, $2.7 \pm 0.0 \mu\text{m}$ and $3.9 \pm 0.1 \mu\text{m}$ respectively. PM1, PM5 AND PM10 were found to have average particle diameters of $16.6 \pm 0.4 \mu\text{m}$, $18.2 \pm 0.4 \mu\text{m}$ and $21.1 \pm 0.3 \mu\text{m}$ respectively. HEX1, HEX5 and HEX10 were found to have average particle diameters of $33.8 \pm 0.9 \mu\text{m}$, $36.1 \pm 0.2 \mu\text{m}$ and $32.3 \pm 1.6 \mu\text{m}$ respectively. BM1, BM5 and BM10 samples were all significantly reduced compared to unprocessed gentamicin sulfate (all samples were $p < 0.0001$), and they did not show any significant difference in particle diameter with one another ($p > 0.05$). Compared to unprocessed gentamicin sulfate, only HEX10 was significantly different ($p = 0.0320$); HEX5 and HEX10 samples did not show a significant difference in particle diameter with respect to HEX1 ($p = 0.0546$ and $p = 0.5194$ respectively), although they were significantly different to

each other ($p < 0.0001$). PM1, PM5 and PM10 samples were all significantly reduced compared to unprocessed gentamicin sulfate (all samples were $p < 0.0001$), PM1 was significantly lower than PM5 ($p = 0.4732$), however, both PM1 and PM5 were significantly lower than PM10 ($p = < 0.0001$ and $p = 0.0063$ respectively). Figure 91 shows the distributions of the particle size analyses. Span is used to show the width of the particle size distribution; a high span value indicates a broad particle size distribution and low span value indicates a narrow particle size distribution. Whilst span is not an absolute method, whereby there are no reference values to compare any given value to, it is a useful tool for comparing particle size distribution. Span values for all samples, except for the 10% mixture processed by the ball-mill technique, were between 2 and 3; however, there is no inference that can be made from these span values, other than that the span values are generally similar to one another, therefore it can be assumed that they have similar particle size distribution widths. The 10% mixture processed by the ball-mill technique had a span of 5, indicating a larger distribution width.

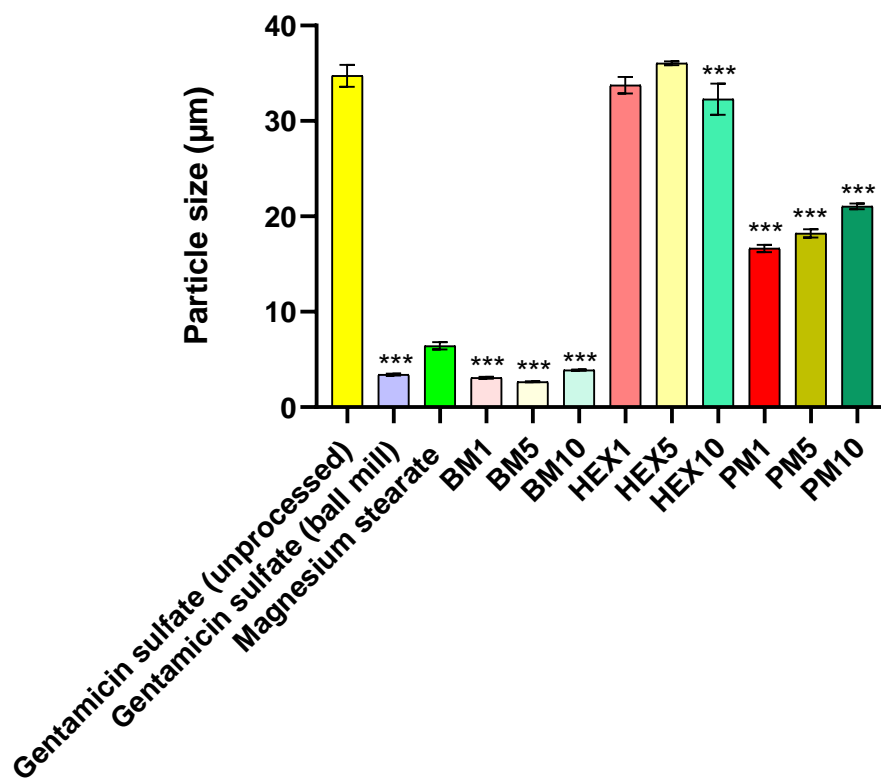


Figure 90: Particle size, D50, measurements (µm) for unprocessed gentamicin sulfate, gentamicin sulfate (ball milled), magnesium stearate, BM, HEX and PM mixtures. BM (ball mill), HEX (hexagonal mixer) and PM (pestle and mortar) indicate particles produced from these mixing methods; 1, 5, and 10 indicate the percentage weight of magnesium stearate added to gentamicin sulfate, prior to mixing. Data is presented as mean ± standard deviation (n=3). Asterisks indicate the level of significance with respect to unprocessed gentamicin sulfate (* $p < 0.05$, ** $p < 0.01$, * $p < 0.001$).**

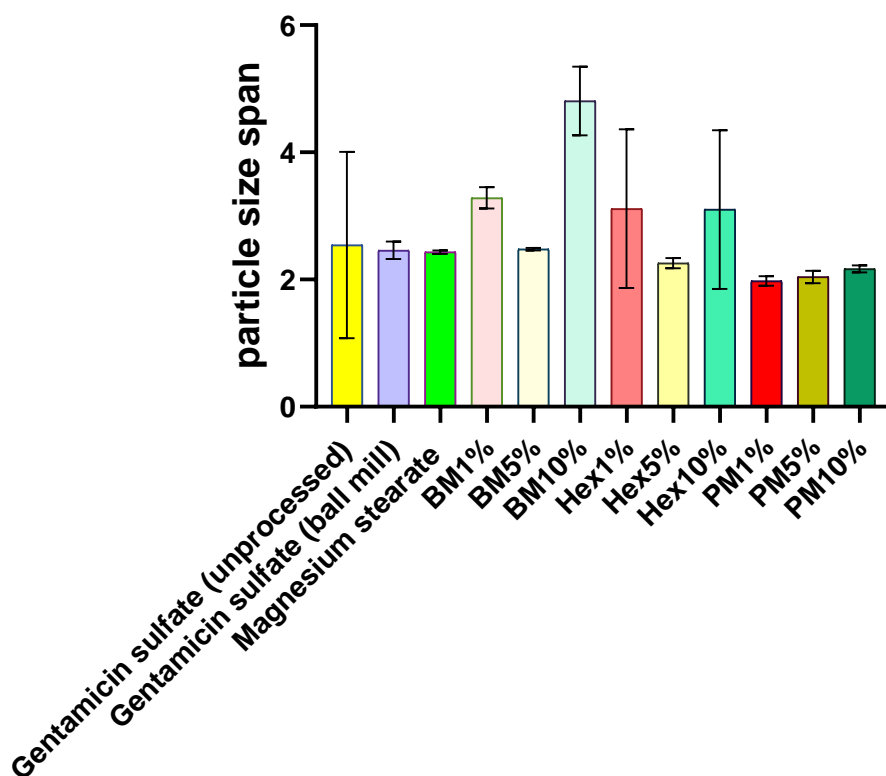


Figure 91: Span (no units) showing width of distribution calculated from particle distribution data for unprocessed gentamicin sulfate, gentamicin sulfate (ball milled), magnesium stearate, BM, HEX and PM mixtures. BM (ball mill), HEX (hexagonal mixer) and PM (pestle and mortar) indicate particles produced from these mixing methods; 1, 5, and 10 indicate the percentage weight of magnesium stearate added to gentamicin sulfate, prior to mixing. Data is presented as mean \pm standard deviation ($n=3$).

6.3.3 Scanning electron microscope using Energy Dispersive X-ray Spectroscopy (SEM-EDX) to characterise gentamicin and magnesium stearate blend

Energy Dispersive X-Ray Analysis (EDX) was used to detect elemental magnesium from magnesium stearate used in all of the sample preparations. EDX is mostly used in qualitative analysis for element identification. It is also used for semi-quantitative analysis of elements on solid surfaces, where the results give an indication of the elemental composition (Newbury & Ritchie, 2013). However with the use of elemental standards and method optimisation, precisions of 95% can be achieved (Newbury & Ritchie, 2013; Scimeca et al., 2018). By pinpointing large areas, which are scans of the surface of the entire SEM image,

and specific particles of the gentamicin sulfate/magnesium stearates blends, it can be seen whether magnesium stearate is present in those areas and present on particular particles, by detecting elemental magnesium. This can provide information on both the degree of coating upon the gentamicin sulfate surface i.e., whether magnesium stearate is actually present on a given particle, and also it could give information on the distribution of coated gentamicin sulfate throughout the powder blends. Analysis was conducted over several large areas and specific particles of each powder sample. Control samples of gentamicin sulfate (Figure 92) and magnesium stearate (Figure 93) were scanned for interfering peaks; no interfering peaks were found. Gentamicin sulfate showed a strong sulfur peak and magnesium stearate showed a strong magnesium peak. Both compounds showed background peaks for carbon and oxygen.

Gentamicin sulfate

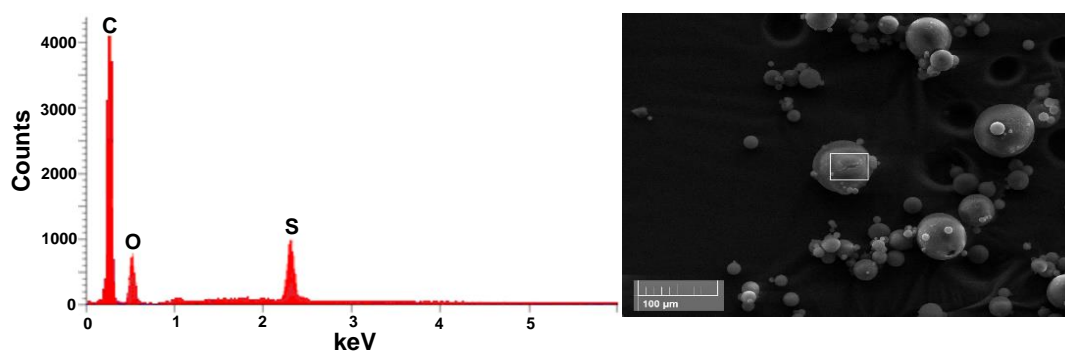


Figure 92: Energy-dispersive EDX spectra for gentamicin sulfate, showing detection of elemental carbon, oxygen and sulfur; magnification is shown at x550.

Magnesium stearate

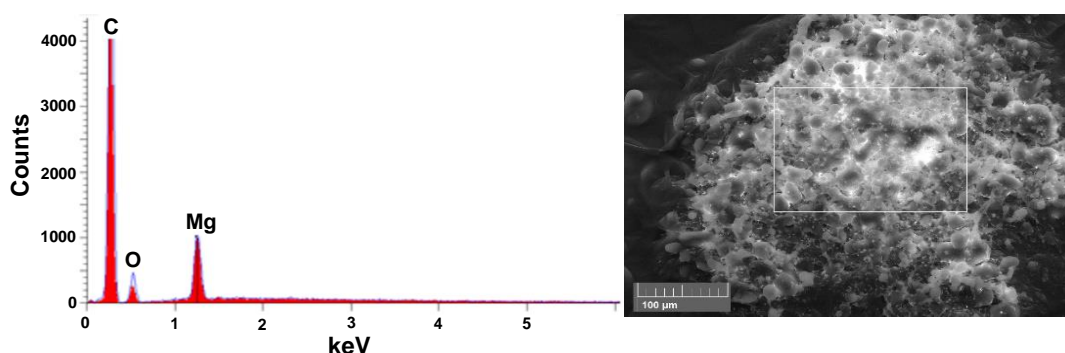
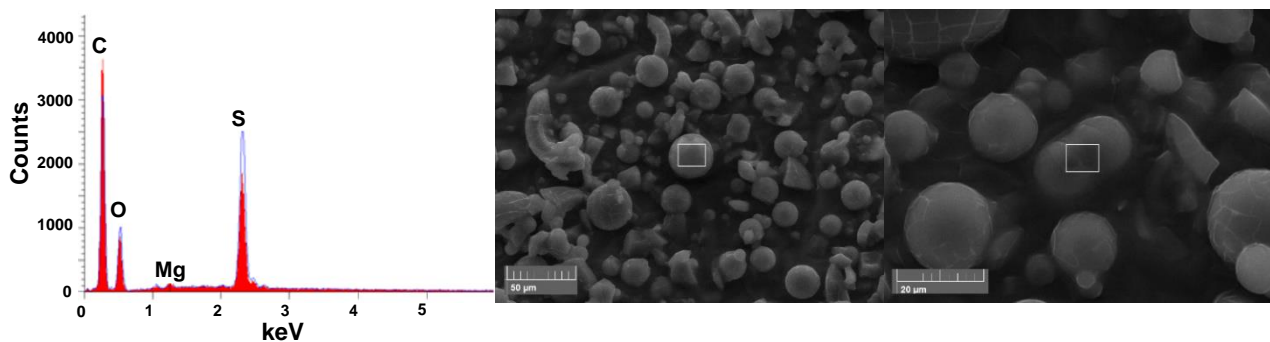


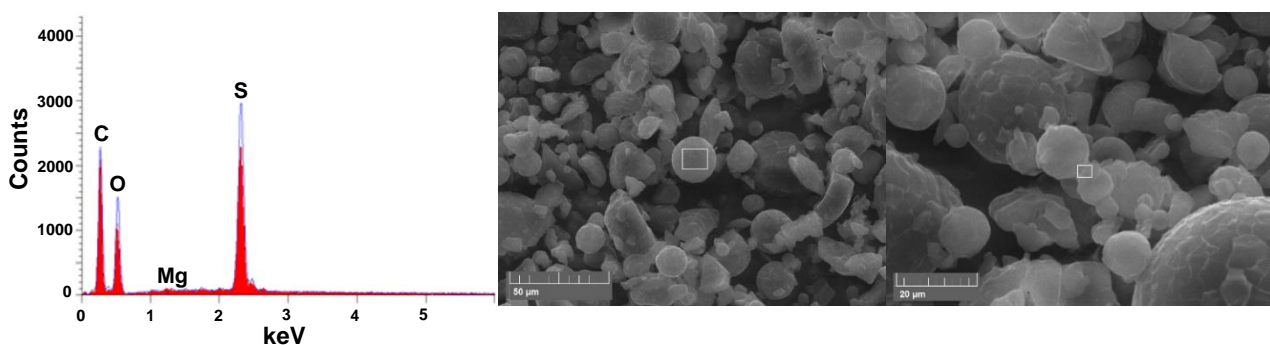
Figure 93: Energy-dispersive EDX spectra magnesium stearate, showing detection of elemental carbon, oxygen and sulfur; magnification is shown at x550.

Figure 94 shows the results of SEM-EDX analysis for a 1 of the gentamicin sulfate and magnesium stearate powder blends produced by different methods. Several points of the powder blends were tested for elemental composition to see if magnesium could be detected. It was not possible to detect elemental magnesium from any of the ball mill samples nor the pestle and mortar samples over several points of analysis; moreover, having pinpointed several points on all the 1% w/w powder blends, it was not possible to detect magnesium on those samples of smaller magnesium stearate concentration. However, magnesium was detected at several points for the hexagonal mixer processed, 5% and 10%, powder samples. It is also worth noting that strong sulfur peaks emanating from gentamicin sulfate were detected for all of the gentamicin sulfate and magnesium stearate powder blends (Figure 94). A large area of a Palacos R cement disc surface was also scanned to see if any interfering peaks arise from it (Figure 95), following the finding that strong sulfur peaks arise from gentamicin sulfate. Elemental silicon, zirconium and calcium were detected, but not sulfur. Zirconium is likely to be from the radiopacifier (ZrO_2).

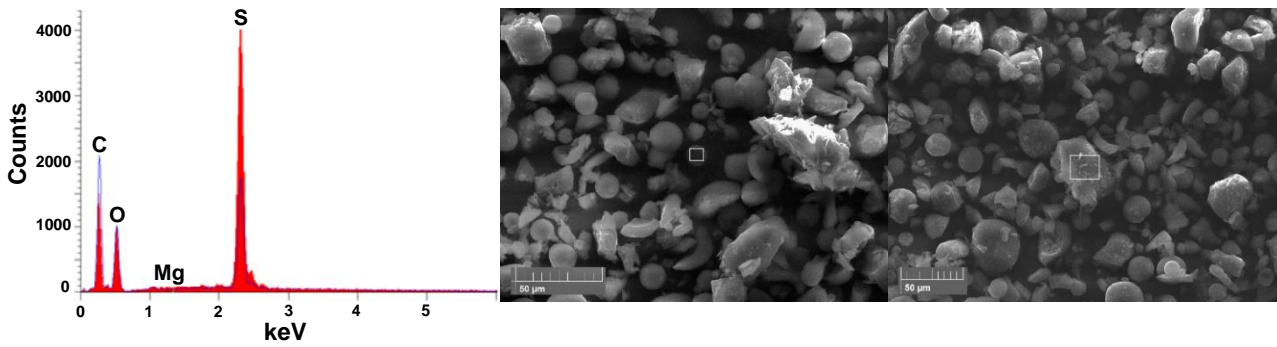
Pestle and mortar 10% w/w blend



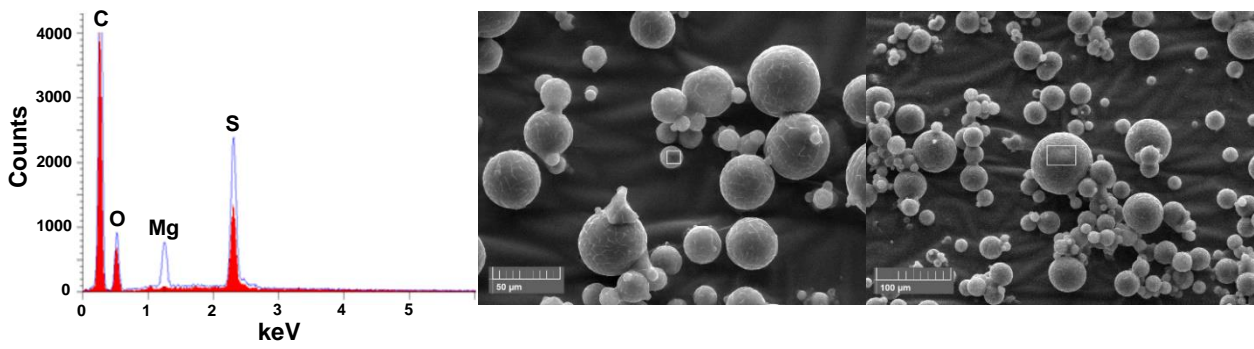
Pestle and mortar 5% w/w blend



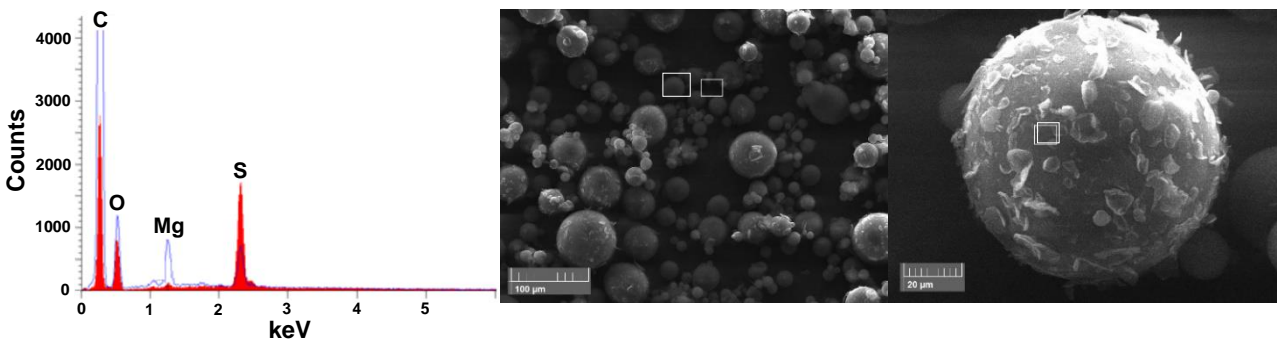
Pestle and mortar 1% w/w blend



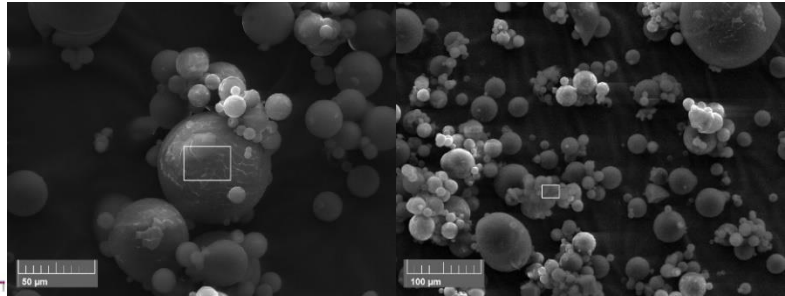
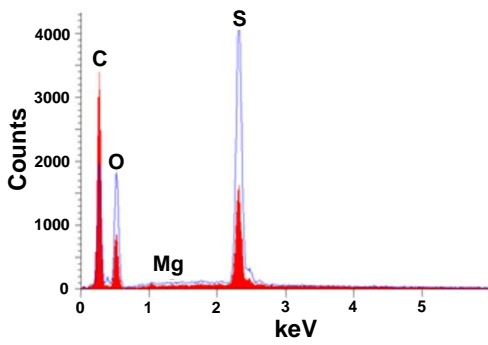
Hexagonal mixing 10% w/w blend



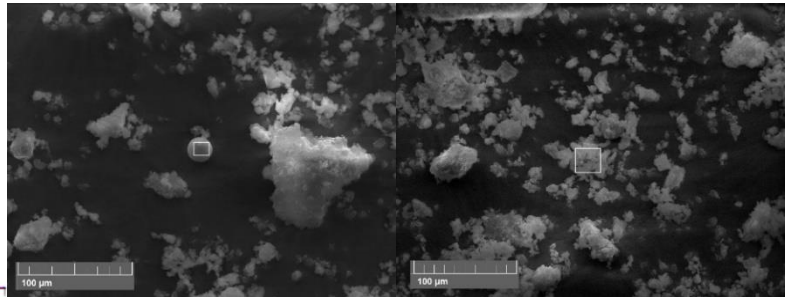
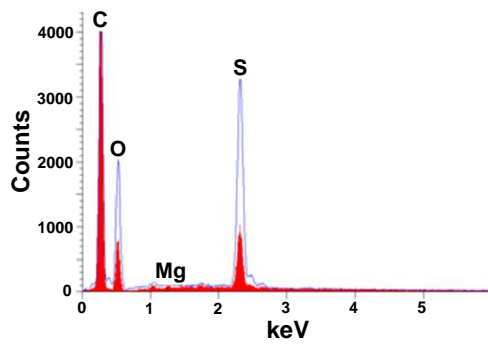
Hexagonal mixing 5% w/w blend



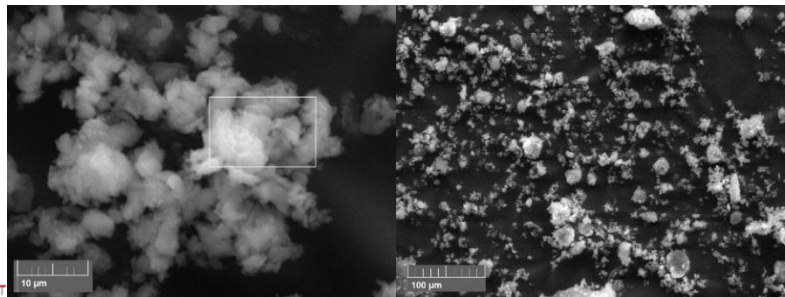
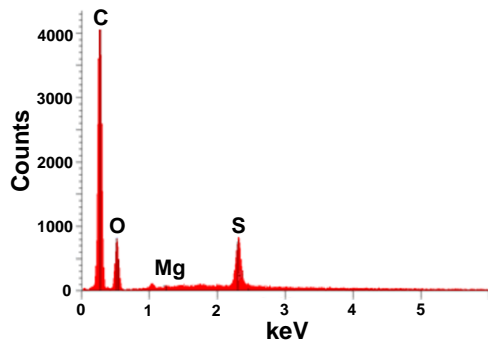
Hexagonal mixing 1% w/w blend



Ball mill 10% w/w blend



Ball mill 5% w/w blend



Ball mill 1% w/w blend

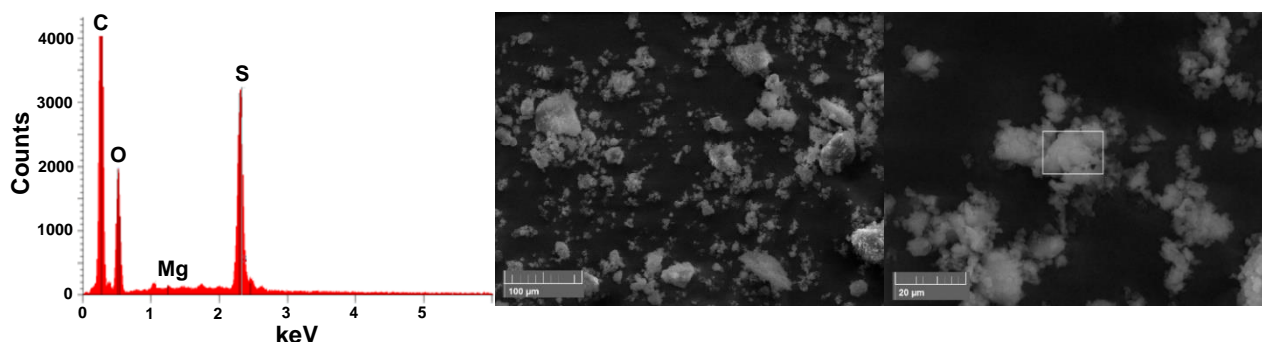


Figure 94: Energy-dispersive EDX spectra for gentamicin sulfate and magnesium stearate blends prepared by ball mill technique, hexagonal mixing and mortar and pestle. The red peaks denote the point of interest on the left-hand SEM image, and blue peaks denote the point of interest on the right-hand image; magnification is shown at x550.

Palacos R

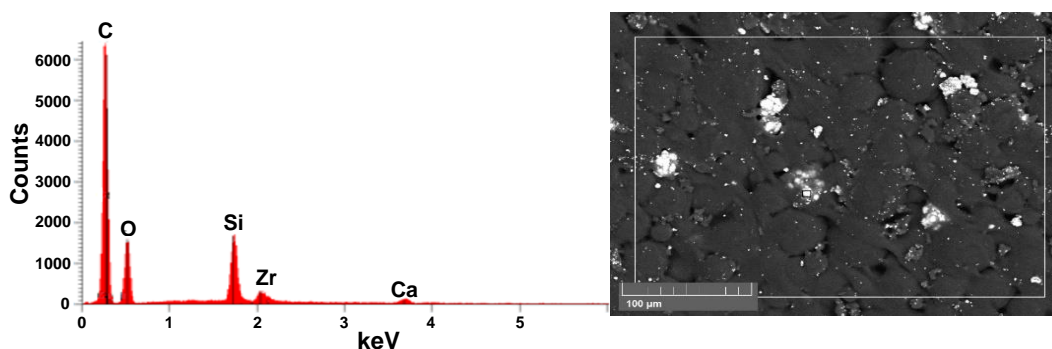


Figure 95: Energy-dispersive EDX spectra for Palacos R bone cement showing detection of elemental silicon, zirconium and calcium; magnification is shown at x550.

6.3.4 Compressive strength

The compressive strengths for Palacos R, Palacos R+G, BM1, BM5, BM10, HEX1, HEX5, HEX10, PM1, PM5 and PM10 cements are shown in Figure 96. All of the cements tested showed compressive strengths above the ISO 5833 minimum requirement of 70 MPa. HEX1 showed the highest compressive strength (85.3 ± 2.1 MPa). There was no significant difference in compressive strength between any of the cements tested ($p > 0.05$) showing that none of the magnesium stearate containing cements showed any significant decrease with regards the Palacos R or Palacos R+G cements.

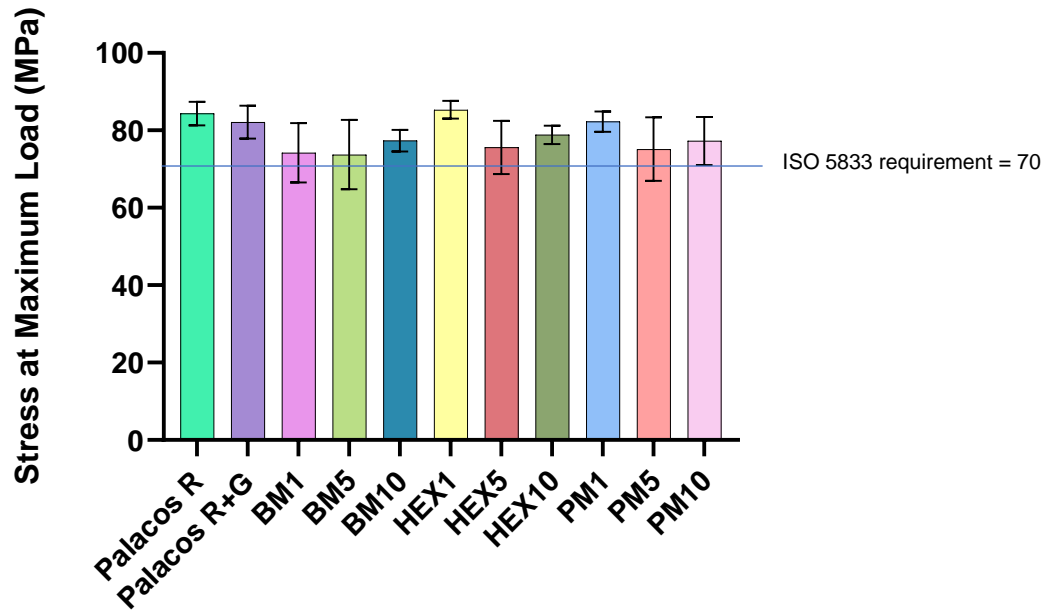


Figure 96: Compressive strength results for Palacos R and Palacos R+G, BM1, BM5, BM10, HEX1, HEX5, HEX10, PM1, PM5 and PM10. Data is presented as mean \pm standard deviation (n=5). There was no significant difference between any of the sample groups tested.

6.3.5 Contact angles for cement discs

The contact angles for Palacos R, Palacos R+G, BM1, BM5, BM10, HEX1, HEX5, HEX10, PM1, PM5 and PM10 cements are shown in Figure 97. Palacos R cements had a contact angle of $116 \pm 0.8^\circ$ and Palacos R+G cements had the lowest contact angle of $98 \pm 0.8^\circ$. The different formulations of bone cement prepared had contact angles ranging from 105° to 123° , PM1 had the lowest contact angle $99 \pm 2.9^\circ$. HEX5 had the highest contact angle of all the cements tested $116 \pm 0.8^\circ$. Compared to Palacos R+G, HEX5 ($p=0.0001$), PM5 ($p=0.0337$) and PM10 ($p=0.00280$) cements showed significant increases in contact angle ($p<0.05$). Compared to Palacos R, only PM1 showed a significant reduction in contact angle ($p=0.0074$).

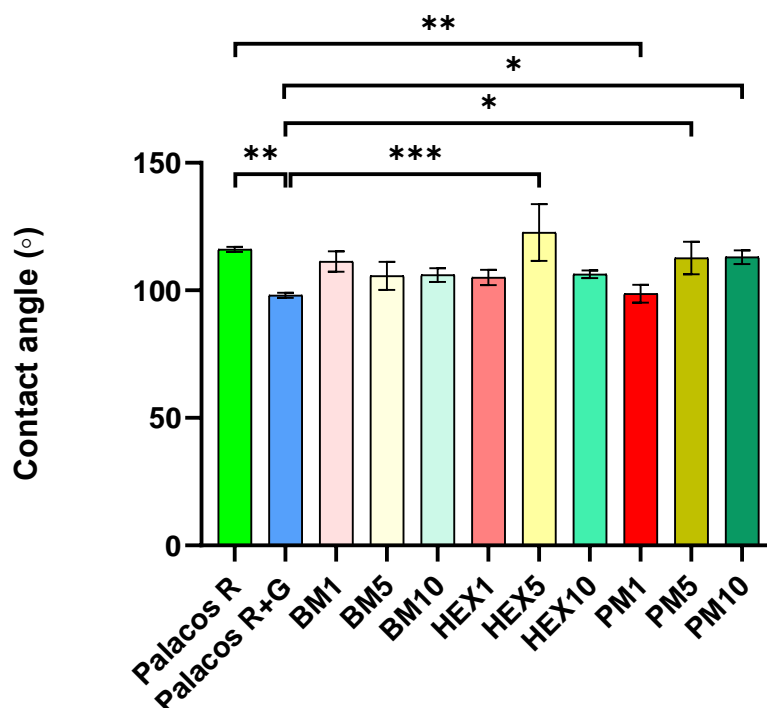


Figure 97: Contact angles for Palacos R and Palacos R+G, BM1, BM5, BM10, HEX1, HEX5, HEX10, PM1, PM5 and PM10 cements. Data is presented as mean \pm standard deviation ($n=3$). Asterisks indicate the level of significance (* $p<0.05$, ** $p<0.01$, * $p<0.001$).**

6.3.6 Antibiotic release from the different cement formulations of Palacos R containing magnesium stearate powder coated gentamicin sulfate

The cumulative mass quantities of release of antibiotic from Palacos R+G and all of the powder coated gentamicin sulfate cement discs (BM1, BM5, BM10, HEX1, HEX5, HEX10, PM1, PM5 and PM10) are shown in Figures 98 and 99. The results show that after 624 hours (4 weeks) a much greater total mass amount of gentamicin has been released from the Palacos R+G cement discs compared to the magnesium stearate cement discs. Burst release was observed for all the samples followed by low levels of gentamicin release. Palacos R+G released a mass quantity of $537.3 \pm 4.4 \mu\text{g}$ of gentamicin at 6 hours, and a total cumulative mass amount of $1176.3 \pm 10.4 \mu\text{g}$ of gentamicin content at 624 hours (4 weeks). The magnesium stearate cements all released gentamicin at a slower rate than Palacos R+G. All of the magnesium stearate sample discs released between $414.5 \pm 7.5 \mu\text{g}$ and $447.7 \pm 20.7 \mu\text{g}$ of gentamicin at 6 hours, and a between $827.0 \pm 10.0 \mu\text{g}$ and $919.0 \pm 12.1 \mu\text{g}$ of gentamicin released at 624 hours. At every time point, Palacos R+G

released significantly higher mass quantities of gentamicin than each of the magnesium stearate cement discs ($p < 0.05$). There was no significant difference in gentamicin mass quantity released between any of the magnesium stearate discs, at any of the time points, up until and including 624 hours ($p > 0.05$). Table 14 shows the difference in cumulative mass quantities of gentamicin release between 6 hours and 624 hours. Palacos R+G shows a difference in gentamicin mass quantity released of 639.0 μg of gentamicin between 6 hours and 624 hours, whereas all of the magnesium stearate cements show cumulative mass quantities of gentamicin release between 412.5 μg to 480.7 μg , over the same time period.

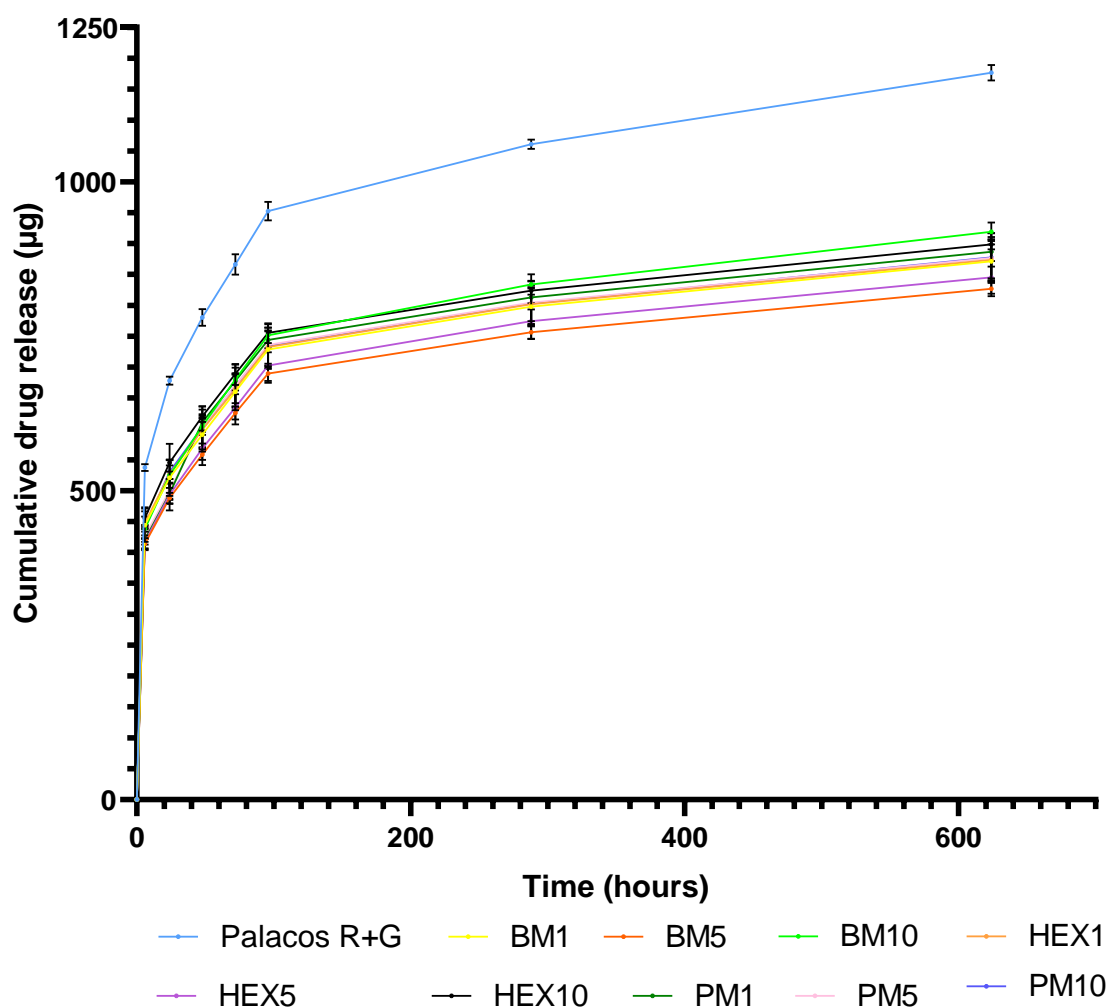


Figure 98: Cumulative drug release of GS (μg) from Palacos R+G, BM1, BM5, BM10, HEX1, HEX5, HEX10, PM1, PM5 and PM10 cement discs all stored in PBS solution (pH 7.4, 37 °C) from time point 0 to 624 hours. (n=3).

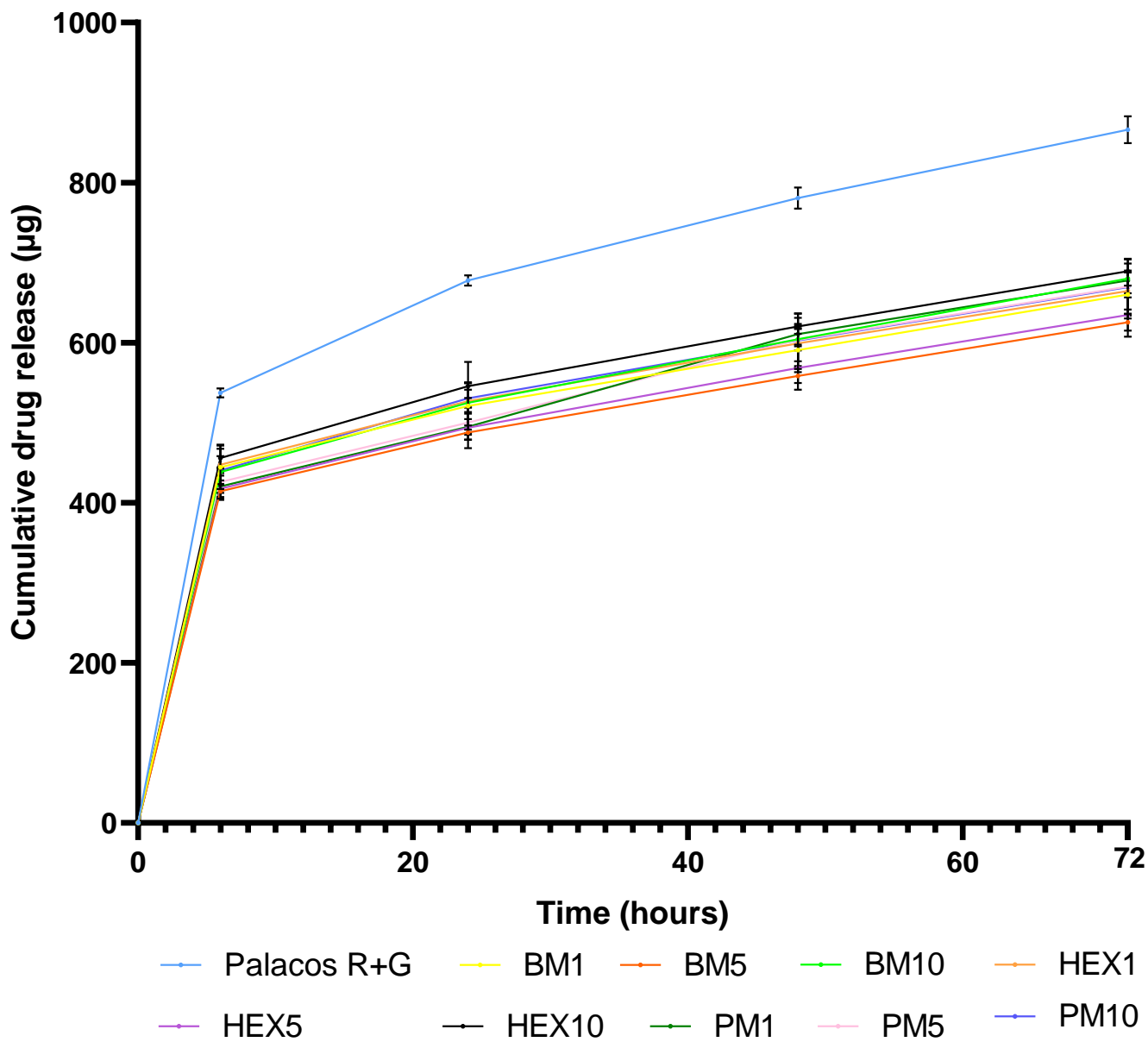


Figure 99: Cumulative drug release of GS (µg) from Palacos R+G, BM1, BM5, BM10, HEX1, HEX5, HEX10, PM1, PM5 and PM10 cement discs all stored in PBS solution (pH 7.4, 37 °C) from time point 0 to 72 hours. (n=3).

Table 14: Difference in mass quantity of gentamicin released (μg), between 6 hours and 624 hours, for each sample (Palacos R+G, all HEX, BM and PM cements).

| Sample | Drug release at 6 hours (μg) | Drug release at 624 hours (μg) | Difference in drug release mass quantity (6 to 624 hours) (μg) |
|-------------|---|---|---|
| Palacos R+G | 537.3 \pm 4.4 | 1176.3 \pm 10.4 | 639.0 |
| BM1 | 444.3 \pm 22.1 | 870.9 \pm 22.8 | 426.6 |
| BM5 | 414.5 \pm 7.5 | 827.0 \pm 10.0 | 412.5 |
| BM10 | 438.4 \pm 3.6 | 919.0 \pm 12.1 | 480.7 |
| HEX1 | 447.7 \pm 20.7 | 873.8 \pm 27.0 | 426.1 |
| HEX5 | 417.4 \pm 8.6 | 845.3 \pm 21.8 | 427.9 |
| HEX10 | 455.9 \pm 9.4 | 898.4 \pm 6.7 | 442.5 |
| PM1 | 420.6 \pm 13.8 | 886.6 \pm 19.5 | 466.0 |
| PM5 | 426.0 \pm 11.1 | 876.4 \pm 33.3 | 450.4 |
| PM10 | 440.3 \pm 14.7 | 877.5 \pm 31.8 | 437.2 |

6.3.7 Antimicrobial testing

Antimicrobial efficacy was assessed by using a quantitative suspension test. Cement discs were incubated for 4 hours, at 37 °C in a suspension of *S. aureus*. After 48 hours, cement discs were vortexed with glass beads to dislodge any microbial biofilm attachment which may have formed on the discs.

6.3.7.1 Quantitative suspension test

The sample discs were tested using an antimicrobial quantitative suspension test in order to determine antimicrobial efficacy. Results from the test are shown in Figure 100. All formulations tested led to a reduction of growth of *S. aureus*. The starting bacteria count was 1×10^6 colony forming units per mL (CFU/ml). All of the formulations tested, showed a similar efficacy to Palacos R+G ranging from 1.0×10^5 CFU/ml to 1.3×10^5 CFU/ml. Palacos R showed a result of 2.2×10^5 CFU/ml. Only Palacos R was significantly different to Palacos R+G ($p=0.0016$). The magnesium stearate containing cements showed no significant

difference with regards to reduction in colony forming units; moreover, all of the magnesium stearate cements were not significantly different to Palacos R+G ($p>0.05$).

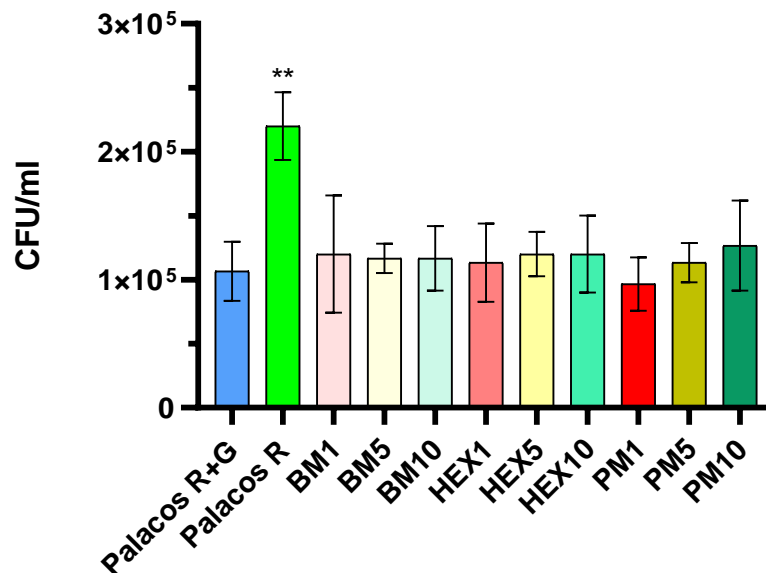


Figure 100: Colony forming units (CFU) for Palacos R and Palacos R and Palacos R+G, BM1, BM5, BM10, HEX1, HEX5, HEX10, PM1, PM5 and PM10. Data is presented as mean ± standard deviation (n=3). Asterisks indicate the level of significance with respect to Palacos R+G (* $p<0.05$, ** $p<0.01$, * $p<0.001$).**

6.3.7.2 Analysis of biofilm formation

The cement discs stored in inoculum were removed after 48 hours, vortexed with glass beads and sonicated to dislodge any biofilm formed around the cement discs. Any dislodged *S. aureus* biofilm was allowed to regrow on plates. For all cement discs tested, no colony forming units were observed after incubation of the agar plate for 18 hours (0 CFU/ml for all samples), meaning that *S. aureus* was not detected.

6.3.8 Sample weight loss after storage in PBS

Sample discs were stored in PBS solution (pH 7.4, 37 °C) for one week and then dried in order to characterise the total sample weight loss. Results from the antimicrobial quantitative suspension test are shown in Figure 101. The total weight loss is expressed as a percentage of the initial cement disc weight prior to storage in PBS. Palacos R had the lowest weight

loss of all the samples tested, 0.2 ± 0.0 %. Palacos R+G had a weight loss of 1.1 ± 0.1 %. All of the magnesium stearate cements showed a weight loss ranging from 0.5 % to 1.1%. Of the magnesium stearate cements, HEX5 had the lowest weight loss (0.5 ± 0.1 %) and BM1 had the highest weight loss (1.1 ± 0.1 %). All cements showed a significant decrease in weight compared to Palacos R ($p < 0.05$), except for HEX5 which showed no significant difference ($p = 0.1751$). Palacos R ($p < 0.0001$), BM5 ($p = 0.02810$), HEX5 ($p < 0.0001$), HEX10 ($p = 0.0041$) and PM10 ($p = 0.0119$) all showed a significant reduction in weight loss compared to Palacos R+G ($p < 0.05$).

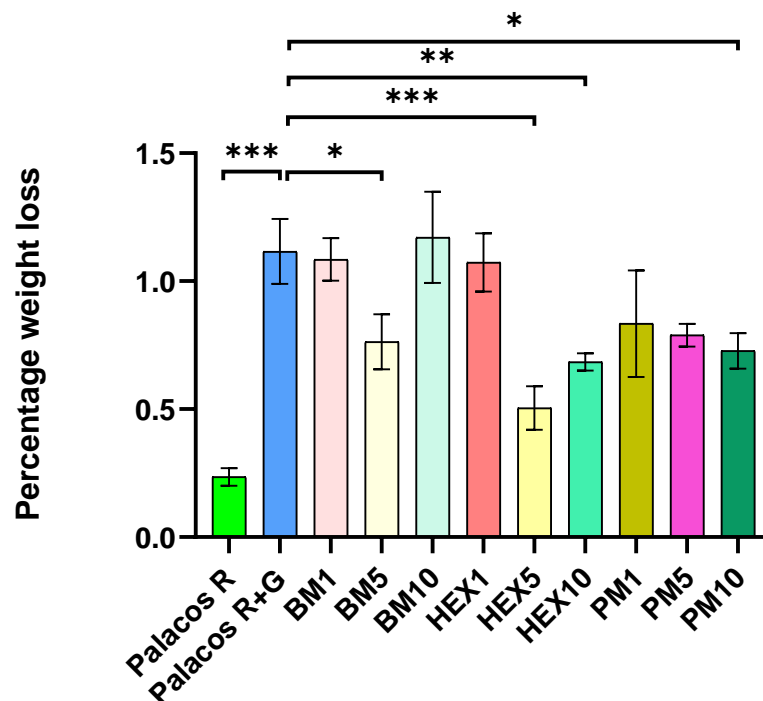


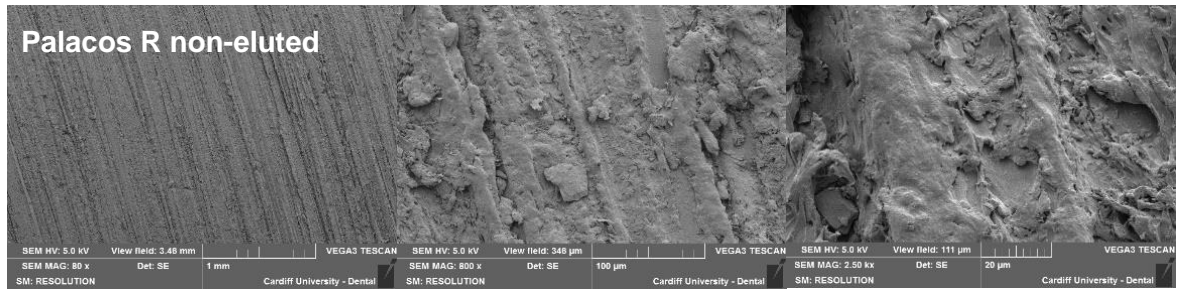
Figure 101: Percentage weight loss for commercial cements Palacos R and Palacos R+G and BM1, BM5, BM10, HEX1, HEX5, HEX10, PM1, PM5 and PM10 cements all stored in PBS solution (pH 7.4, 37 °C) for one week and dried. Data is presented as mean ± standard deviation (n=3). Asterisks indicate the level of significance with respect to Palacos R+G (* $p < 0.05$, ** $p < 0.01$, * $p < 0.001$).**

6.3.10 SEM images of cement disc surface

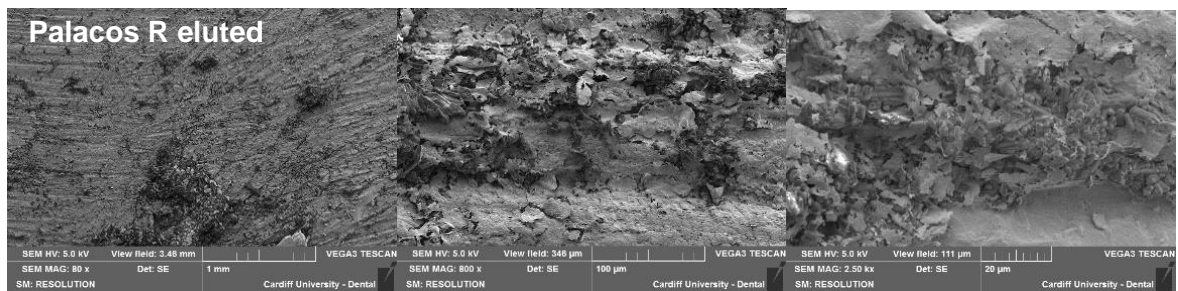
SEM was used to characterise all of the cement disc formulations' surface morphology after manufacture; moreover, the discs were also analysed to see the difference in surface morphology before and after incubation in PBS for one week. Figure 102 shows SEM images, at magnifications of 80, 800 and 2.5k, of Palacos R and Palacos R+G, BM1, BM5, BM10, HEX1, HEX5, HEX10, PM1, PM5 and PM10, freshly prepared (non-eluted) and after

an incubation period in PBS at 37 °C for one week (eluted). Palacos R+G, HEX5, HEX10, BM5, BM10, PM5 and PM10 cement discs all showed some degree of formation of round particles in their structure. Palacos R, BM1, HEX1 and PM1 cements did not show any rounded structures after their manufacture. Similar to the observation in Chapter 5, showing lesser-fused PMMA particles in cements containing magnesium stearate (10 and 25% w/w), BM5, BM10 and PM10 had formed all contained lesser-fused PMMA particles on the surface. HEX5 and HEX10 contained round fused PMMA particles after incubation, although they were not observed prior to incubation. Fused PMMA particles, lesser-fused particles and pores are indicated on the images using orange, yellow and blue arrows respectively.

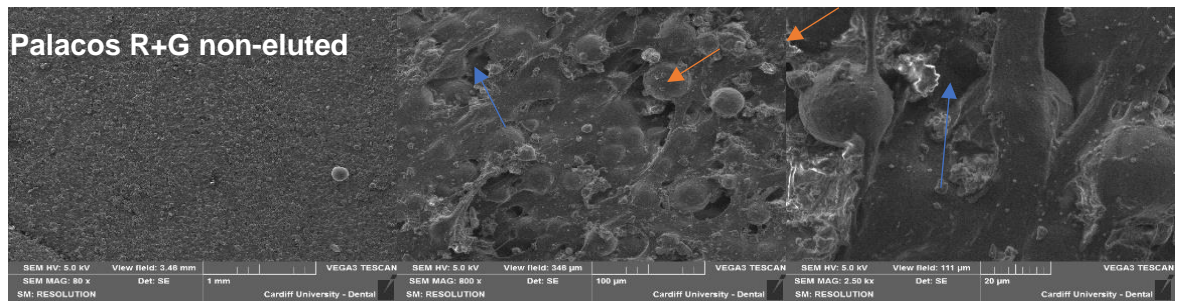
(A)



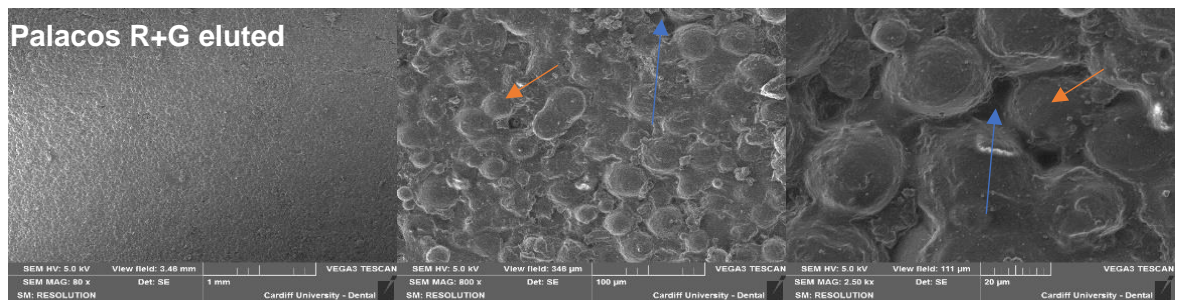
(B)



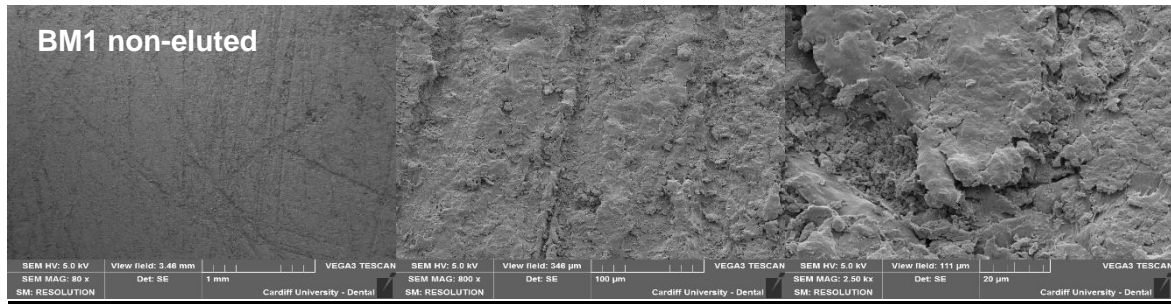
(A)



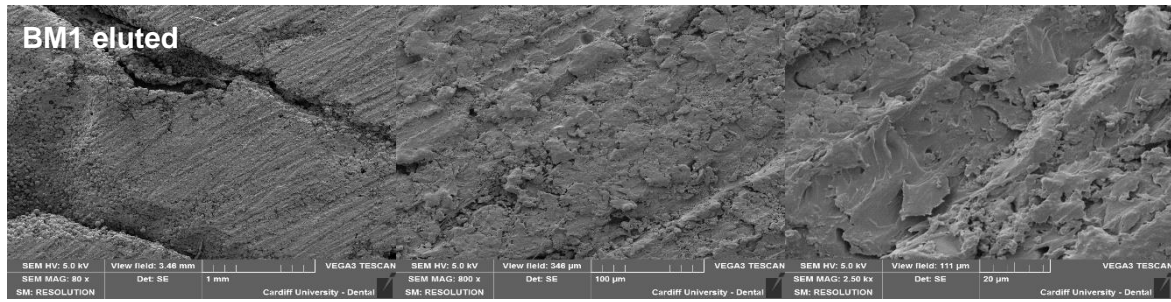
(B)



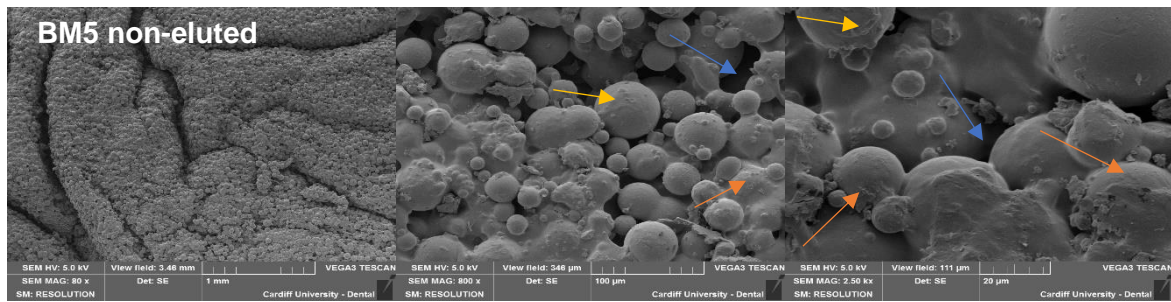
(A)



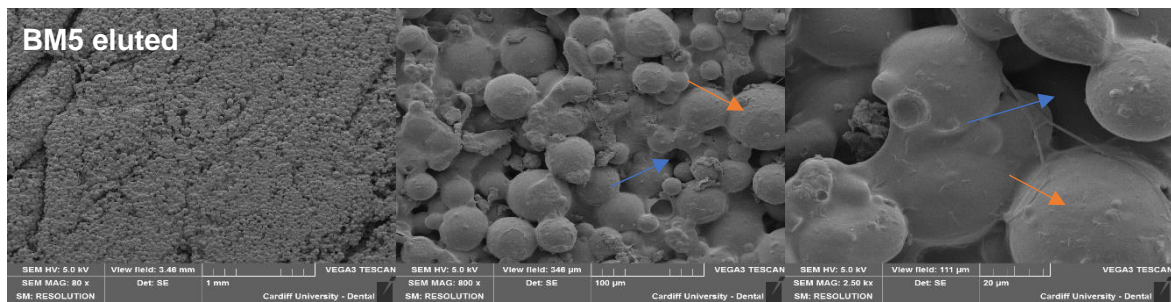
(B)



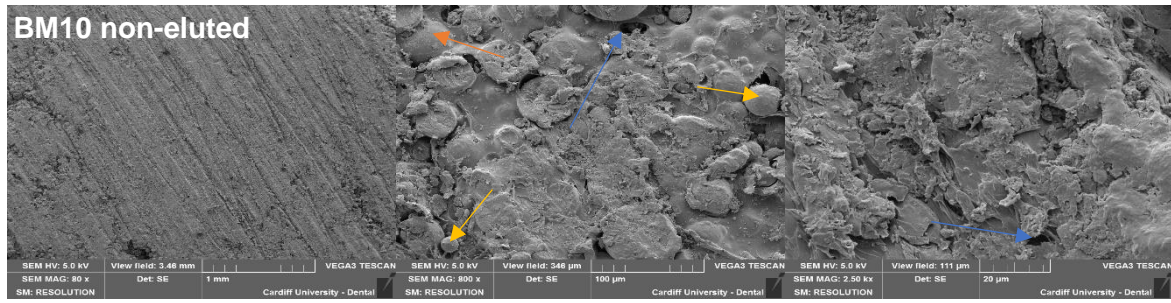
(A)



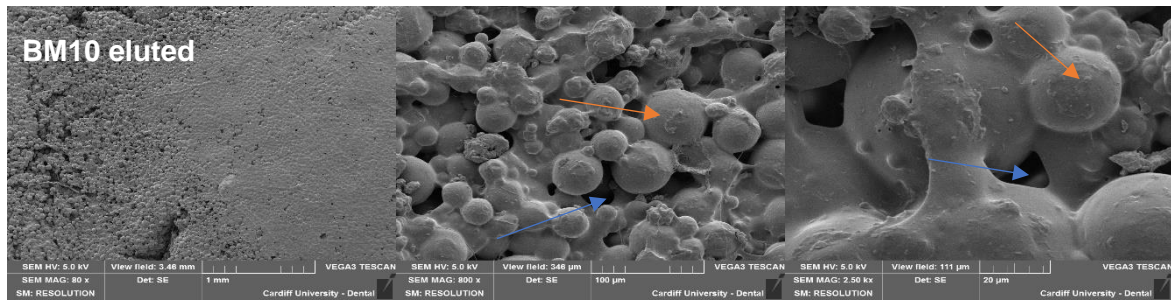
(B)



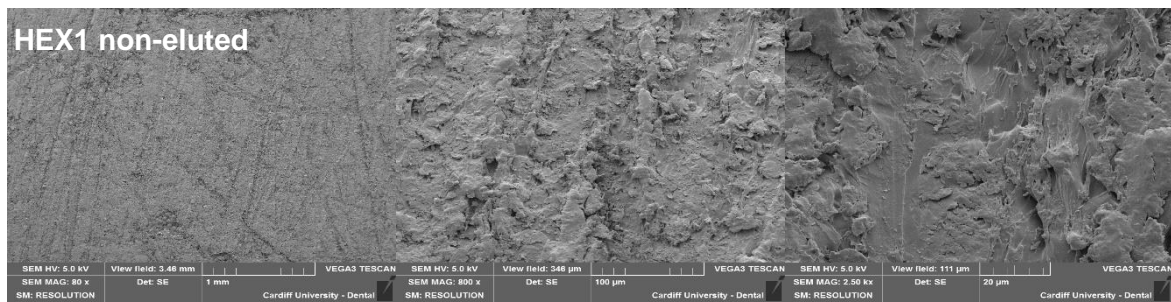
(A)



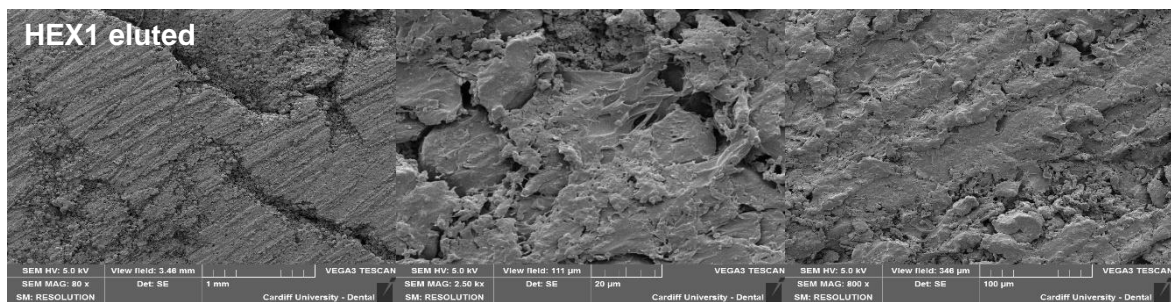
(B)



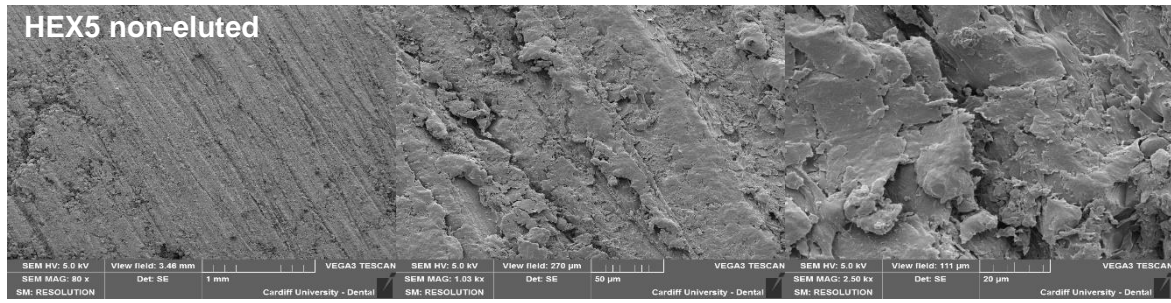
(A)



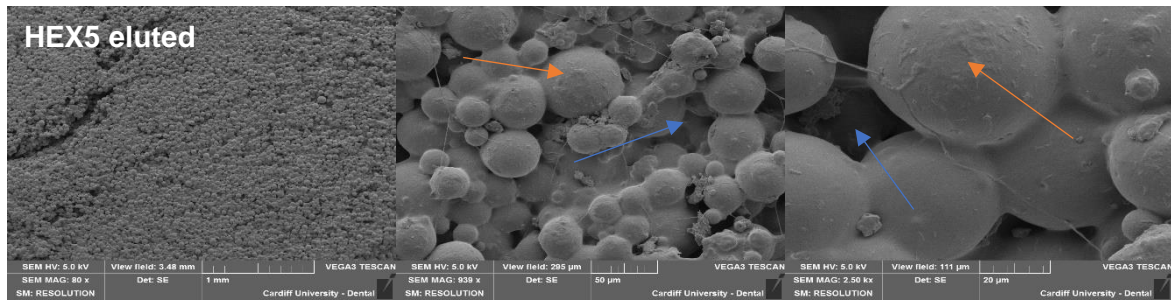
(B)



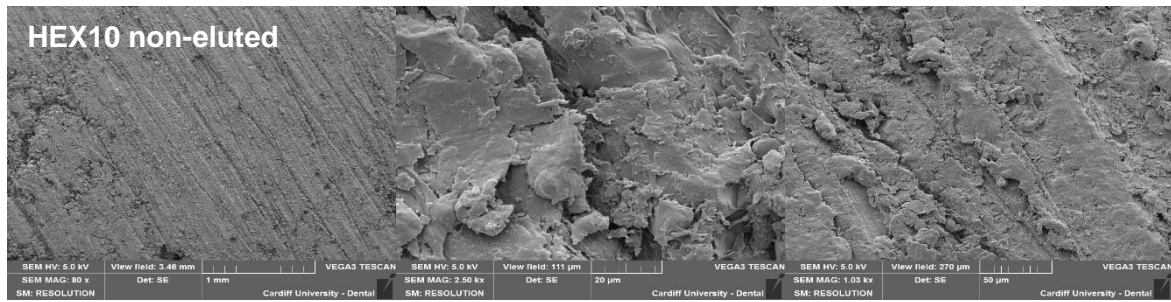
(A)



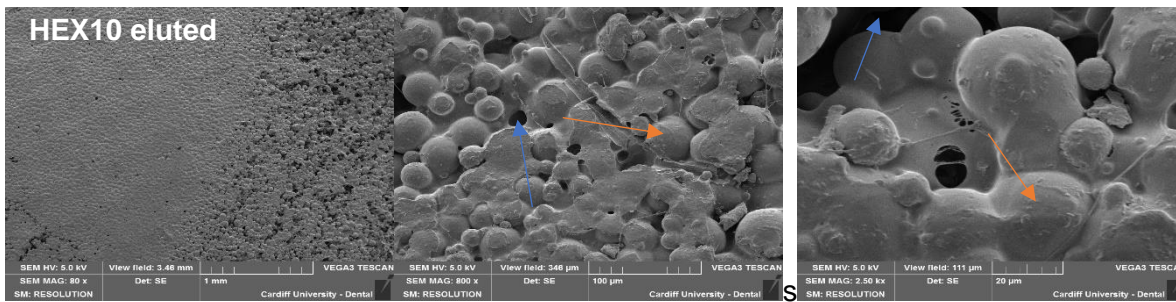
(B)



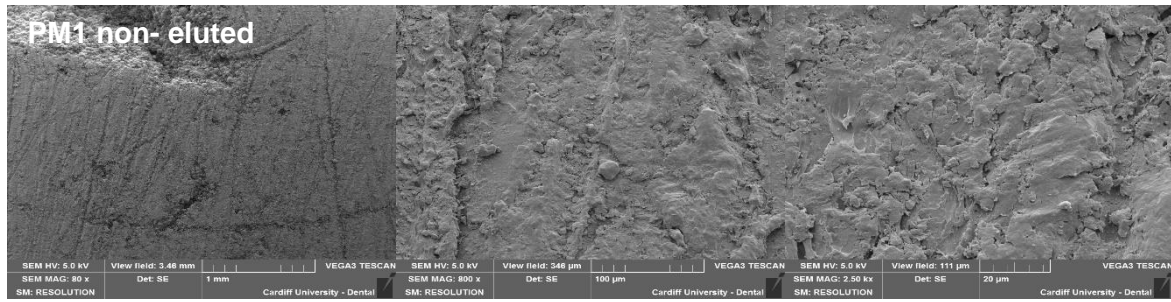
(A)



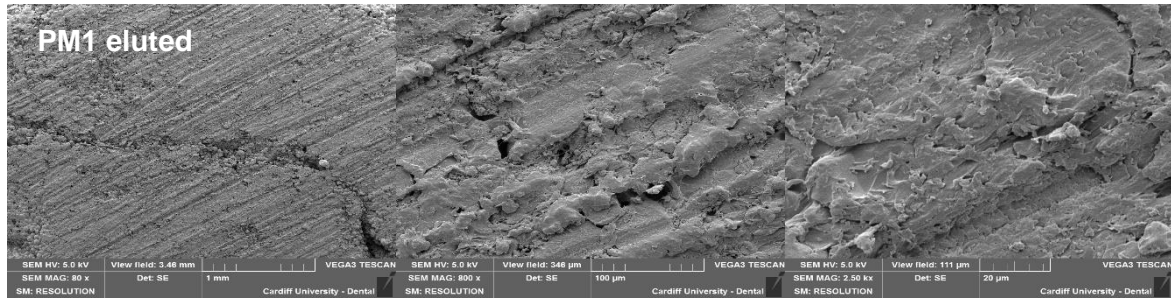
(B)



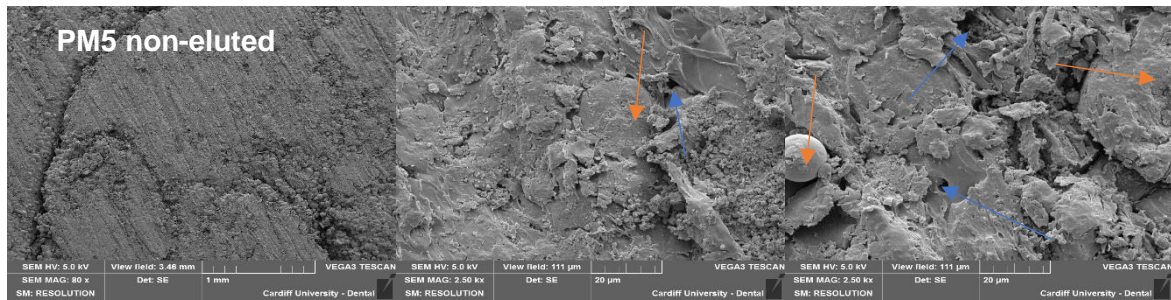
(A)



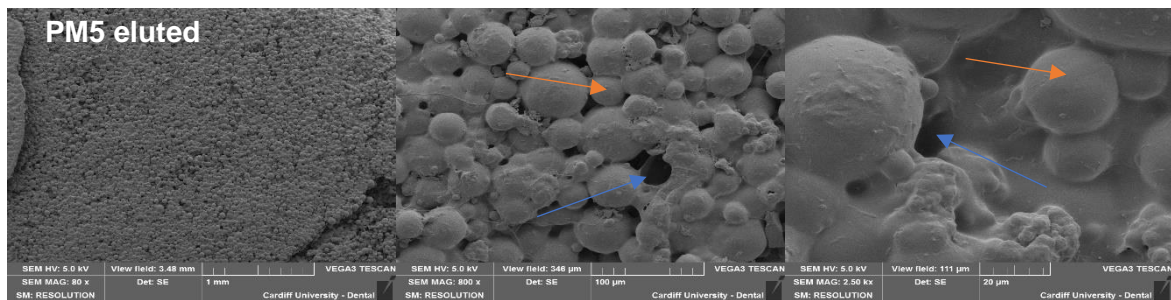
(B)



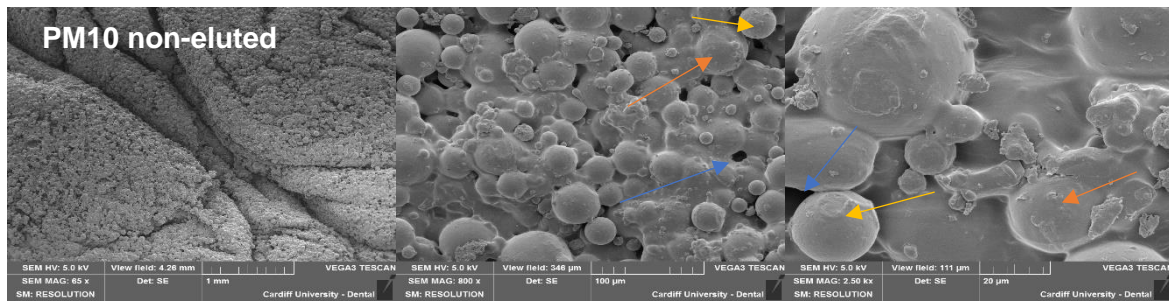
(A)



(B)



(A)



(B)

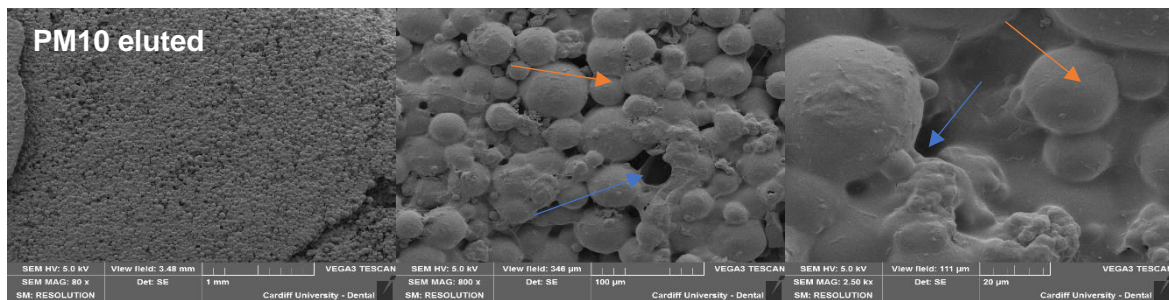


Figure 102: SEM surface images for Palacos R and Palacos R+G, BM1, BM5, BM10, HEX1, HEX5, HEX10, PM1, PM5 and PM10 cements (A) before and (B) after incubation in PBS for one week at 37 °C; sample magnifications are x80, x800 and x2.5k respectively. Arrows indicate PMMA particles (orange), lesser-fused particles (yellow) and pores (blue).

6.4 Discussion

In Chapter 5, it was observed that bone cements containing magnesium stearate released antibiotic at a slower, more controlled rate, than those that did not contain magnesium stearate. In this chapter it was proposed that combining magnesium stearate and gentamicin sulfate to produce hybrid surface-coated antimicrobial particles could improve drug release characteristics, without compromising mechanical properties, as very small quantities of magnesium stearate would need to be added to the overall bone cement formulation. Since magnesium stearate has been successfully coated on to hydrophilic particles in pharmaceutical formulations (Bungert et al., 2021; Zhou et al., 2013), it was thought that this principle could be applied to gentamicin sulfate. The aims of this chapter were therefore to investigate powder coating of gentamicin sulfate using magnesium stearate, and to incorporate these particles into commercial bone cement, to improve drug release properties, whilst maintaining mechanical properties of the cement. To address the first aim, gentamicin sulfate was dry powder coated with magnesium stearate, using methods of differing shear force, including conventional low-shear mixing such as a rotational hexagonal

mixer, and higher-shear mixing methods using a mortar and pestle and ball mill. Characterisation of the efficacy of the coating was performed using SEM to visualise the particles, and to assess the extent of the particle coating; SEM-EDX was used to detect magnesium stearate particles surrounding gentamicin particles within the powder blends. The second aim was addressed by incorporating these powder blends into bone cement to characterise drug release and mechanical properties. Several factors regarding the material properties and mechanical processing have been established for optimal dry powder coating (Alyami et al., 2017; Dahmash & Mohammed, 2015; Kawaguchi et al., 2018; Zhou et al., 2010). Powder properties, for optimal dry powder coating, include reducing host particle size, avoiding irregular particle shape (Alyami et al., 2017), a narrow size distribution (Dahmash & Mohammed, 2015), particle hardness (Kawaguchi et al., 2018), partial attraction between components (Saharan et al., 2008). Processing properties, for optimal dry powder coating, include mixing time, mass amount of the components used (Alyami et al., 2017; Dahmash & Mohammed, 2015; Saharan et al., 2008).

SEM images were taken of the two separate starting materials (gentamicin sulfate and magnesium stearate). Visualising guest particle numbers and surface area coverage can be a suitable way to evaluate dry coating efficacy (Zheng et al., 2020). SEM images were taken of a preliminary mixture, containing magnesium stearate (25% w/w) in gentamicin sulfate, mixed for just 10 seconds by gently stirring with a glass rod; this was prepared to see if there is inherent interparticle attraction between the two compounds, prior to subjecting them to the various processing methods, as this would be favourable for successful dry powder coating (Alyami et al., 2017; Dahmash & Mohammed, 2015; Saharan et al., 2008). It was seen that with very little processing time and energy, the smaller magnesium stearate particles adhered to larger gentamicin sulfate particles, producing a partial coating, indicating that there is some level of interparticle attraction, meaning that with further processing time and energy, dry powder coating of gentamicin by magnesium stearate could possibly be achieved by mixing the two compounds directly. It could also be seen that the gentamicin sulfate particles were generally larger than the magnesium stearate particles used, which is also a favourable property of the dry powder coating system (Alyami et al., 2017; Dahmash & Mohammed, 2015; Saharan et al., 2008). Gentamicin particles were within a size range of 5 μm to 100 μm , whereas magnesium stearate particles were within a size range of 5 μm to 30 μm . For the mixtures produced by hexagonal mixing, images of gentamicin sulfate surrounded by magnesium stearate were similar to that of the preliminary mixture, insofar as they showed that magnesium stearate had adhered to the larger gentamicin sulfate particles, producing a partial coating. Furthermore, it was seen that increasing concentration of magnesium stearate caused for a larger number of particles to adhere and surround the

gentamicin sulfate particles. In similar studies using low shear mixing methods, similar to the hexagonal mixer, to powder coat magnesium stearate on to various particles, it has been shown that discrete, partial coatings can be obtained. In one study that used various low to high shear mixing methods to powder coat lactose, it was shown that by using the low shear method, only a partial coating was possible (Zhou et al., 2013). Magnesium stearate particles had adhered to the lactose surface but had not formed a continuous film around the host particle. Moreover, it was shown that this partial coating had not been sufficient to alter the functionality of the host particles (Zhou et al., 2013). In another study which sought to coat ibuprofen particles with magnesium stearate, similar results were obtained with a low shear mixing method, whereby partial coating was achieved and no change in functionality was observed (Qu et al., 2015). During the powder coating process, sufficient energy is required to break up cohesive agglomerates of the guest and host materials, to distribute guest particles around the host particles, and providing energy for particle collisions and hence adsorption on to the guest particles (Dahmash & Mohammed, 2015); moreover, it is thought that conventional low-shear methods will not provide sufficient energy to achieve this (Alonso et al., 1989; Zhou et al., 2013).

For all powder samples ground by mortar and pestle, particle size had been visibly reduced and many larger gentamicin sulfate particles became fragmented. It could be seen that a partial coating of discrete magnesium stearate particles had formed around the gentamicin sulfate. It was not possible to visualise any coating around the gentamicin sulfate for the ball mill method. For the powder that was ball milled, the particles were broken up into very small pieces and the magnesium stearate could not be distinguished from gentamicin sulfate by visual inspection alone. It can be seen that the gentamicin sulfate particles are larger than their surrounding magnesium stearate particles in the hexagonal mixer and mortar and pestle samples. The host particle is always larger than the guest particle size (Dahmash & Mohammed, 2015; Honda et al., 1994; Saharan et al., 2008; Zheng et al., 2020). If the host particle size is of orders of magnitude bigger than the guest particle size, particle size will have very little effect on dry particle coating (Zheng et al., 2020). However, for optimal coatings where the order of magnitude between guest and host particle size is similar for example where the host and guest particle sizes are less than one order magnitude, as is the case in this study, particle size should be investigated and optimised (Zheng et al., 2020). In fact, ratios of guest and host particle sizes for various compounds have been documented (Honda et al., 1994). It is thought that even though theoretically larger host particles would have more energy to collide with guest particles, that there is a threshold at which if the particle is too large it will tend to bounce off the host particle (Zheng et al., 2020). Using different particle sizes of magnesium stearate and gentamicin sulfate, with the same

processing methods as used in this study, would provide information on the effects of particle size of the two compounds on surface-coating using both low and mild-shear mixing methods.

Particle size analysis by laser diffraction was performed to confirm the mean particle diameters of the compounds and compound mixtures. The overall D50 particle size for the hexagonal mixing mixture of gentamicin sulfate and magnesium stearate had remained around the same as the average diameter of gentamicin sulfate. Since the mixing method was a low shear process, it could be seen by SEM that none of the particles were fractured and that they were partially coated with much smaller magnesium stearate particles. The average size of the powders produced by mortar and pestle had been decreased from the original gentamicin sulfate particle size of 35 μm for all of the mixed samples, i.e., at 1%, 5% and 10% relative concentration of magnesium stearate to gentamicin sulfate. The average particle diameter ranged from 16 μm to 21 μm and increased with increasing concentration of magnesium stearate. The average particle size for the 10% mixture was significantly higher than the 1% and 5% mixtures by mortar and pestle, suggesting the possibility that magnesium stearate has adhered to the surface of gentamicin sulfate particles resulting in an increase in particle size, and that this occurs in a proportionate manner with increasing mass amount of magnesium stearate. Although it is not possible to quantify the energy imparted by the pestle and mortar process, it is still considered as an energetic comminution process which is capable of inducing chemical reactions, phase transitions and plastic deformation of materials (Fernandez-Bertran, 1999; Šepelák et al., 2012). Pestle and mortar is used when higher energetic processes are required for shorter amounts of time (Fernandez-Bertran, 1999), moreover, pestle and mortar in the context of dry powder coating has been described as a high impact force (Kawaguchi et al., 2018); this would explain the fragmenting of the gentamicin sulfate particles, as well as a partial coating by smaller particles of magnesium stearate which was observed by SEM. The average size of the particles produced by the ball-mill technique was greatly decreased from the original gentamicin sulfate particle size of 35 μm for all of the different concentrations; the average particle diameter ranged from 3 μm to 4 μm . In any milling process, mechanical energy imparts stress to particles, causing strain and deformation; when sufficient strain is caused to the point of failure, cracks form and propagate through the particles, causing breakage (Seibert et al., 2019). If sufficient force is applied rapidly to a particle surface, directed towards its centre, then fragmentation can occur (Seibert et al., 2019). This appears to be the case with gentamicin sulfate. Hexagonal mixing provided continuous low-impact force over a time period of one hour, which was not sufficient to fragment the particles, whereas pestle and mortar provided a much higher-shear for a shorter time-period, which was able to

fragment the particles; moreover, the ball mill method provided a consistently high shear, for a longer period of time, causing a greater degree of fragmentation.

EDX was used to detect elemental magnesium from magnesium stearate used in all of the sample preparations. By pinpointing particles of interest of the gentamicin sulfate/magnesium stearate blends, it could be confirmed as to whether a given particle contains magnesium stearate or not. Control samples of magnesium stearate and gentamicin sulfate gave strong magnesium and sulfur peaks respectively. It was only possible to detect strong magnesium peaks on particles of interest from the 5% w/w and 10% w/w magnesium stearate samples mixed with the hexagonal mixer. This could be due to the fact that the gentamicin sulfate and magnesium stearate particles remained similar with the low shear mixing method, and hence discrete magnesium stearate particles remained attached to gentamicin sulfate particles, giving rise to stronger magnesium readings. As the 1% w/w magnesium stearate powder contained less elemental magnesium, it may have been below the limit of detection. Magnesium stearate contains approximately 4-5% of elemental magnesium (Hobbs et al., 2017). The powdered samples contain 1% w/w, 5% w/w and 10% w/w magnesium stearate; therefore they contain 0.05% w/w, 0.25% w/w and 0.5% w/w of elemental magnesium. For detection of an element by EDX, the element must be present in quantities above its detection limit (Wassilkowska et al., 2014). EDX detectors have detection limits of approximately 0.1 – 0.3% w/w depending on several factors, including the element of interest itself, sample matrix and detector used for analysis. The SEM images of the 1% w/w powder samples produced by hexagonal mixing also show that the magnesium stearate particles are distributed to a lesser degree onto the gentamicin sulfate particles, than for the 5% w/w and 10% w/w samples, reducing the probability of detecting magnesium. The higher shear mixing methods increased the particle size and decreased the surface area of the gentamicin particles. This may have resulted in an increased dispersion of magnesium stearate throughout the gentamicin powder. A more dispersed sample may have resulted in much smaller particles of magnesium stearate or even a thin coating of magnesium stearate, meaning that the mass amount of elemental magnesium may have been too low for detection by the EDX detector.

In addition to the sustained release by magnesium stearate observed in chapter 5, magnesium stearate was chosen as a coating material in this study due to several of its properties. Kawaguchi et al. (2018) lists several key material properties required for optimal dry powder coating. The guest particle should be much smaller than the host particle (Kawaguchi et al., 2018); in this case the magnesium stearate particles are much smaller than the gentamicin sulfate particles, irrespective of the milling process used.

Magnesium stearate is a soft material (Cheng et al., 2008) and ideally there should be a difference in modulus between the guest and host particles (Kawaguchi et al., 2018; Zheng et al., 2020), ideally the guest particle should be soft and the host should be hard (Kawaguchi et al., 2018) as the guest particle will undergo deformation and coalescence, during the particle coating process, eventually forming a continuous layer around the host particle (Kawaguchi et al., 2018). There should be a partial attraction between the guest and host particles (Kawaguchi et al., 2018), which was observed by SEM for the preliminary mixture using very low energy input to mix the compounds together. Furthermore, magnesium stearate has been used to successfully coat other particles such as lactose particles which are also hydrophilic like gentamicin sulfate.

Using SEM-EDX, it was observed that gentamicin sulfate gave rise to strong sulfur peaks. This was observed on the gentamicin sulfate control sample and for all of the analyses performed at gentamicin particle points of interest. Palacos R, without gentamicin sulfate was scanned and it was found that no interfering peaks were observed. This is very useful information for studies relating to the incorporation of gentamicin sulfate into bone cements, as the extent of homogenous dispersion of gentamicin sulfate could possibly be investigated on cured and powder samples, by confirming the presence of elemental sulfur over test samples. It is recommended to further investigate this method to assess sample homogeneity. If this method is successful in demonstrating the degree of dispersion and homogeneity of the gentamicin sulfate/bone cement powder mixtures, it could be used to assess whether the incorporation of the various powder coated gentamicin sulfate samples produced in this chapter contain a homogenous dispersed gentamicin sulfate.

Compressive testing was performed on the modified bone cement samples, to provide an indication of whether they have maintained their mechanical properties. All of the cements produced from the magnesium stearate and gentamicin sulfate blends showed compressive strengths that were above the ISO 5833 requirement of 70 MPa, and all were comparable with the commercial bone cement samples, Palacos R and Palacos R+G. This suggests that the low quantities of magnesium stearate used in the blends, had not affected the mechanical properties. Whilst it is recommended that further mechanical tests according to ISO 5833 should be performed, for bending strength and bending modulus, it is possible that as proposed initially, the gentamicin sulfate/magnesium stearate functionalised particles were well dispersed, reducing agglomerations, therefore not adversely affecting the mechanical properties. In particular, agglomerations have been shown to cause weakness in the bone cement (Dunne et al., 2008).

Characterising antibiotic release is critical for bone cements, as infection prophylaxis is the secondary purpose of antibiotic-loaded bone cements (Schwarz et al., 2021). The aim is to extend the antibiotic release for as long a time as possible, so that clinically significant mass amounts of gentamicin are released over longer time points. As previously mentioned, commercial antibiotic loaded bone cement is characterised by antibiotic release occurring as a burst release, with most drug released in the first hours of application (Moojen et al., 2008; Neut et al., 2010). Gentamicin release from the modified bone cement discs was measured over a time-period of 624 hours (4 weeks), using LC-MS. Results for magnesium stearate bone cements were compared to the commercial product, Palacos R+G, as commercial antibiotic loaded bone cement is the most commonly used material in orthopaedic surgery and is currently considered to be the gold standard for drug delivery (Karaglani et al., 2020; Singh et al., 2019). Palacos R+G released the highest mass amount of gentamicin sulfate of all the cement discs tested. At each time point, Palacos R+G released significantly higher mass quantities of gentamicin sulfate; all of the magnesium stearate cement discs released lower mass quantities of gentamicin than Palacos R+G. However, they all released similar mass amounts of gentamicin to each other, and at each time point there was no significant difference in gentamicin release between any of the magnesium stearate discs. In total, at 624 hours (4 weeks), the magnesium stearate cement discs released between 827 µg and 919 µg of gentamicin, whereas Palacos R+G released 1176 µg of gentamicin. Burst release was observed for all the samples, followed by low levels of gentamicin release. It was shown that for all the magnesium stearate cement discs, the difference in mass quantity of gentamicin release between 6 hours and 624 hours (4 weeks) was similar, between 413 µg and 481 µg; whereas the difference in mass release Palacos R+G was 639 µg. Since Palacos R+G released a higher quantity of drug at every time point, this demonstrates that the incorporation of magnesium stearate into the cement formulation, even at very low mass quantities, had retarded the rate of release of the drug, causing for significantly lower mass quantities to be released at each time point compared to Palacos R+G. It is possible that as theorised, that the attachment of magnesium stearate on to the gentamicin sulfate particles, has indeed altered the particle functionality by anchoring itself to PMMA molecules due to its hydrophobic character, thus causing for an improved dispersion within the bone cement matrix, with less surface agglomerations, and therefore causing for a more gradual drug release profile. Moreover, magnesium stearate, a hydrophobic compound, is known to have drug dissolution retarding properties, effectively able to repel water from various formulations and cause drug dissolution slow down (Li & Wu, 2014; Qu et al., 2015). This could mean that magnesium stearate attachment to gentamicin sulfate, has prevented water from effectively coming into contact with the gentamicin sulfate, therefore, slowing down drug release. It has been shown in various studies that coating drug particles with magnesium stearate has

caused significant retardation of dissolution rate (J. Li & Wu, 2014). All of the antibiotic loaded cement samples investigated, throughout this thesis, whether hydrophilic or hydrophobic in character, have shown show a burst release profile, releasing antibiotic in a biphasic manner; in effect releasing a large proportion of incorporated antibiotic within the first hours (Cyphert et al., 2018; Mori et al., 2011). This is a phenomenon that cannot be avoided, as it has been shown that drug release from PMMA bone cement is primarily a surface phenomenon (Letchmanan et al., 2017; van Belt et al., 2000), most antibiotic is released at the outset upon contact between dissolution medium and the PMMA surface. A drawback of this characteristic burst-release profile is the consequent and continual drug release at low concentrations (Cyphert et al., 2018), even releasing at sub-inhibitory concentrations after the first week (Moojen et al., 2008). Release of aminoglycosides at sub-inhibitory amounts induce biofilm formation (Xiong et al., 2014) and can also cause for antibiotic resistance to occur (ter Boo et al., 2015). An ideal bone cement should release antibiotic at levels above the MIC for at least 1 -2 months, to prevent acute orthopaedic infections, whilst maintaining its mechanical properties (Cyphert et al., 2018). This study was performed over 4 weeks. In order to assess the full drug release profile of these formulations, a longer time-period is required.

Contact angle characterises the wettability of a surface, which is the ability of a liquid to adhere on to a surface. Generally low contact angles denote good contact between water and solid whereas high contact angles denote the surface's ability to repel water (Huhtamäki et al., 2018). One may expect the water contact angles on magnesium stearate cements to be generally higher than the commercial cements, due to the hydrophobic character of magnesium stearate. However, most of the magnesium stearate cements did not show a significant increase in contact angle compared to Palacos R+G. As mentioned earlier, it is possible that that the attachment of magnesium stearate on to the gentamicin sulfate particles facilitated changes to their dispersion within the bone cement matrix, resulting in no or little surface agglomerations, meaning that if indeed the dispersion of gentamicin sulfate has been improved, the amount of gentamicin sulfate would be uniform, which would mean that upon contact with the test droplet, a lower concentration of gentamicin in water would be created. Effectively, upon initial contact with the water droplet in this test, less gentamicin sulfate will have been dissolved into it, either from within the cement or from the surface, therefore causing for a higher contact angle. Diaz-Pena *et al.* (2002) proposed that the reason for initial release of gentamicin in water was due to an immediate dissolution of surface components (Gálvez-López et al., 2014) Contact angles for cement discs may be due to gentamicin release during the droplet stage of the analysis, whereby the droplet contains differing mass amounts of gentamicin, depending on what sample it is placed on,

therefore affecting the contact angle (Kubiak et al., 2011). One way to investigate this phenomenon would perhaps be to analyse contact angle for a droplet on a given disc, over a period of time; measuring the contact angle at regular time points. This would give an indication of whether the contact angle for cement discs is a result of the overall surface hydrophobicity or if it is a result of drug releasing into the droplet, affecting the composition of the water.

The quantitative suspension test was performed to determine the antimicrobial efficacy of the modified cement discs with regards to *S. aureus*. All of the formulations tested reduced the bacteria count, showing a similar efficacy to Palacos R+G. None of the magnesium stearate cements showed any significant difference to each other or to Palacos R+G, with regards to reduction in bacteria counts. No biofilm formation was detected on any of the cements after 48 hours, indicating that biofilm formation may have been prevented by the various cement formulations. However, although the *S. aureus* strain used in this experiment (NCTC 10788) is known to produce biofilms (Gwynne et al., 2021), the experiment should be conducted by using a control disc made from a material where biofilm growth is known to occur e.g. glass (Marques et al., 2007; Shukla & Rao, 2017). Although gentamicin release, using LC-MS was measured at 6 hours, and not 4 hours which was the time point employed in this test, the magnesium stearate disc cements had released on average 0.09 mg/ml and Palacos R+G released 0.11 mg/ml by that time point. This is above the minimum inhibitory concentration (MIC) required to inhibit *S. aureus*. In a study by Figueroa *et al.* (2008) it was shown that the MIC of gentamicin sulfate required to inhibit bacteria growth of *S. aureus* was 0.0125 mg/ml (Figueroa et al., 2008). This experiment showed that the cement formulations were all capable of releasing sufficient antibiotic in order to inhibit bacteria growth of *S. aureus* at 4 hours; and there is further indication that consequent biofilm formation at 48 hours may have been prevented, although this would need to be confirmed by further testing.

Sample discs were stored in PBS (pH 7.4, 37 °C) for one week and then dried in order to characterise the total sample weight loss. Weight loss can give information of mass quantities of drug-release, as well as loss of excipients. Palacos R showed the lowest weight loss of 0.2% and Palacos R+G showed a weight loss of 1.1%. All of the magnesium stearate discs had weight losses of between 0.5% and 1.1%; no obvious trend was observed. The weight losses suggest that Palacos R+G had the highest degree of water penetration compared to all the other samples, as it had the highest weight loss. In Chapter 5, it was observed that cement discs with a higher weight loss, released more drug than cement discs with lower weight loss; moreover, it was also shown in Chapter 5, by SEM imaging that for

some cement discs, with much higher weight losses, pores were formed after incubation. No noticeable changes to the magnesium stearate discs surfaces were observed in Chapter 5, as they did not release as much drug as the other lactose supplemented discs. In this chapter, SEM images were taken of control cement discs and cement discs that were allowed to elute, by incubation in PBS (pH 7.4, 37 °C) for one week. Of the freshly prepared, non-eluted, samples made from particle coated gentamicin sulfate that were imaged, not all surfaces showed pores/air pockets and round fused particles, as can be seen in Palacos R+G or the lactose and magnesium stearate supplemented cements, prepared in Chapter 5. No round particles or pores and air pockets could be seen in any of the samples produced containing magnesium stearate 1% w/w in gentamicin sulfate, before or after incubation. Although only selected areas of the cement discs were imaged, it is assumed that 1% w/w of magnesium stearate in gentamicin sulfate, does not affect the polymerisation process of PMMA/MMA, regardless of the blending process used. Cement discs prepared using 5% and 10% w/w of magnesium stearate in gentamicin sulfate, by different mixing methods, gave varying results. HEX5, PM5, HEX10 and BM10 did not show the same degree of pores or round particles in the cement sample prior to incubation, although it was seen that after incubation these were present. In fact, from the images taken, only BM10 and PM5 showed a high degree of the round particles formed prior to incubation. It is unclear why these discs contained round particles and pores after incubation, but none prior; although it could suggest that the degree of incomplete polymerisation due to unreacted MMA (Vallo, 2000), did not extend throughout the entire PMMA sample, and that further investigation by imaging more areas of the same discs could show whether some parts of the cement are polymerised fully, as with Palacos R, and other parts show incomplete polymerisation.

6.5 Conclusions

Gentamicin sulfate was dry powder coated with magnesium stearate using mixing methods of different shear. It was thought that a functionalised, hybrid particle could impart some of magnesium stearate's hydrophobic properties on to gentamicin sulfate, allowing it to disperse more fully within the hydrophobic PMMA cement matrix, as well demonstrating slow drug release, which is a known property of magnesium stearate when used as an excipient. Mixes prepared using a conventional rotary mixer or a mortar and pestle, resulted in a partial magnesium stearate coating around gentamicin sulfate particles; however, this was not confirmed for the powder produced by the ball-mill technique, as it could not be observed by SEM. EDX spectroscopy could only confirm the presence of magnesium stearate on

gentamicin sulfate particles for the 5% and 10% mixtures processed by the rotary mixer, this is possibly due to elemental magnesium being below threshold quantities at each test point for all other samples. All of the cements produced from the magnesium stearate and gentamicin sulfate blend showed compressive strengths that were above the standard ISO 5833 requirement and comparable with the commercial bone cements, Palacos R and Palacos R+G, suggesting that the low quantities of magnesium stearate used had not affected the mechanical properties of the bone cement. *In vitro* release studies in PBS showed that all of the magnesium stearate cements released gentamicin at a slower rate than the commercial cement, Palacos R+G. Although all of the magnesium stearate cements showed a burst release profile in the first hours; they released significantly less gentamicin mass quantities than Palacos R+G at each time point. All of the magnesium stearate supplemented cement discs decreased *S. aureus* bacteria counts, comparable with the commercial cement, Palacos R+G. LC-MS data showed that with clinically significant levels of gentamicin were released at the 6-hour time point.

In conclusion, a novel method for controlling drug-release has been applied to antibiotic bone cements. The combination of gentamicin sulfate and magnesium stearate caused a slower drug-release than the commercial cement. Compressive strength was unaffected by incorporation of the magnesium stearate. It is recommended that the dry powder coating of gentamicin sulfate and its incorporation into PMMA bone cement is further investigated, to achieve optimal drug-release over a longer time frame, whilst still maintaining its mechanical properties.

Chapter 7

7 Conclusions and future work

7.1 Conclusions

From the time when bone cement was first used in orthopaedic surgery in the 1950s until now, there have been very few improvements to it. Moreover, there are ongoing concerns regarding antibiotic loaded bone cements, as used in total joint replacements. Failure due to post-surgical infections is still a leading cause of joint failure, and with an ageing population, this problem is set increase. Despite its drawbacks, antibiotic loaded PMMA bone cement is still considered to be the clinical gold standard for local antibiotic prophylaxis and prevention of infection. There have been many studies aimed at improving antibiotic delivery from commercial bone cements. The actual issue with antibiotic loaded bone cements is the release kinetics. All bone cements are characterised by an initial burst in the first hours, upon contact with water, which is followed by a slow release of antibiotics at sub-inhibitory concentrations. The problem is also not helped by the fact that antibiotic drugs do not disperse well within the bone cement matrix, causing surface agglomerations that add to the burst release. This drug-release profile means that the antibiotic loaded bone cement is unable to provide a long-term release of antibiotics for prophylaxis, as it is known that microorganisms of low virulence can cause delayed onset of infection; furthermore, sub-inhibitory antibiotic release can cause antibiotic resistance to occur. The emergence and spread of multidrug resistant bacteria are a growing global health problem. Therefore, there is a need to improve the antibiotic release kinetics from bone cement.

The main purpose of this research programme was to optimise and enhance a current liposomal delivery system. It was necessary to understand the properties of antibiotic loaded bone cement in terms of the drug-release profile and its mechanical properties, to improve on the already existing drug-release system. Moreover, it was necessary to determine the repeatability and robustness of the liposomal delivery system to ascertain whether a

liposomal formulation is a viable choice for potential commercial use. The results for the liposomal formulation were comparable with that of the previous study, including the drug release mass amounts. The current liposomal delivery system released less drug mass amount compared to the commercial antibiotic loaded cement; however, it released a higher percentage of its relative incorporated mass amount of gentamicin (31%), compared to the commercial antibiotic loaded bone cement, Palacos R+G (18%). Moreover, despite the mean compressive strength of liposomal cement being slightly lower than in the previous study, the mechanical properties were overall consistent with that study, showing that incorporation of liposomes did not cause for a significant reduction in mechanical strength.

Liposomes containing gentamicin sulfate were reproduced from the original method and incorporated into bone cement. The cements were stored in PBS and allowed to release antibiotic over a time period of 4.5 months. An LC-MS assay method was developed to analyse gentamicin, so that potentially low concentrations could be detected and measured, as LC-MS is a more sensitive technique than the standard colorimetric derivatisation method currently used. The encapsulation efficiency of the liposomes was determined to be 15% meaning that not all the drug was encapsulated by the liposomes. The addition of Pluronic components alone were shown to affect drug release depending on their hydrophobic/hydrophilic character.

Liposomal cement was stored in PBS, and at various time points, the eluent was analysed using the Stewart assay for detection of phospholipids to indicate liposomal or phospholipid release. However, no lipid content was measured using this UV-Vis method. Consequently, fluorescent labelled liposomes were prepared using fluorescent labelled phospholipids and incorporated into bone cement. Cement discs containing fluorescent labelled liposomes were stored in PBS and the eluent was collected at various time points for analysis using newly developed and validated fluorospectroscopic methods. Using fluorescence spectroscopy, it was not possible to determine any fluorescent lipid content, despite both methods' low limits of detection. It was therefore inferred, that given the measurable quantities of gentamicin in the eluent and the absence of phospholipids, liposomes or phospholipids alone do not take part in the drug release mechanism. However, despite phospholipids not being released, they may have a role in the dispersion of gentamicin within the PMMA matrix, as a higher percentage release was observed for the liposomal cement compared to Palacos R+G.

Liposomes containing gentamicin sulfate were successfully freeze-dried alongside sucrose, a cryopreservant, and incorporated into bone cements. It was found that following freeze-

drying the liposomes did not maintain their size, as they increased from 200 nm to 6000 nm, possibly due to liposome fusion. It was observed that gentamicin itself had degraded by approximately 50% in each vial. There is published literature showing that interaction with other sugars such as glucose, is possible, so it is thought that the cryopreservant may have caused gentamicin to degrade. Moreover, drug-release from bone cement containing freeze-dried liposomes released minimal gentamicin, which may have been due to further interaction with the cryopreservant in solution. Even though the mass quantities of gentamicin released were minimal, and below MIC for *S. aureus*, cements produced from freeze-dried liposomes had the largest effect on bacteria reduction. It was not clear as to why the bone cements containing freeze-dried liposomes were the most efficient at reducing bacteria counts, especially as the mass quantities of sucrose were below known MIC levels. It is possible that larger pores formed due to channelling by sucrose, allows more MMA, which was shown to reduce bacteria counts, to exit the cement, although this has not been formally investigated in this study. Different stages of the liposome manufacturing process were investigated and found to be the cause of phospholipid loss at each of those individual stages. The first stage of loss was found to be during the liposome extrusion process: residual phospholipid was observed on the polycarbonate filters, and a total loss of around one sixth of phospholipid content was measured using the Stewart assay. Second, during the ultracentrifugation process, following the method used to produce the liposomal formulation, 75% of the initial phospholipid content added to the tubes was retained by supernatant liquid. Although increasing the length of ultracentrifugation improved the yield, it was very time-consuming. Using a faster rotor improved the liposomes yield, however, this was a very lengthy task to do, as much time was required to obtain the correct conditions for the centrifuge. Given that the ultracentrifugation process is inefficient, and the freeze-dried product did not perform as expected. It was therefore decided to not pursue this formulation. Further understanding of drug release by the bone cements was investigated.

Mechanisms of release from bone cement were investigated by incorporating large mass amounts of hydrophilic and hydrophobic excipients. Lactose and magnesium stearate, which are commonly used pharmaceutical excipients were incorporated into commercial antibiotic loaded bone cement. Cements containing lactose and magnesium stearate experienced a significant reduction in their mechanical properties, and the higher loaded cements failed as per the standard requirements of ISO 5833. Bone cement containing no gentamicin sulfate or any excipients, experienced a very negligible weight loss upon storage in PBS for one week (0.2%), indicating that minimal contents are released. Palacos R+G showed an increase in weight loss (1.2%), which may be due to channels created by gentamicin sulfate and its further release. A loss of 1.2% indicated that a small percentage of incorporated

gentamicin sulfate was released from the cement after one week. Cements containing large mass quantities of magnesium stearate showed weight losses that were similar to Palacos R+G and had weight losses similar to each other, indicating that magnesium stearate slows down drug release and itself is not significantly released. Lactose incorporated bone cement showed the highest weight losses, increasing in weight loss with increasing lactose mass content. MicroCt was performed on post-incubation samples, and although porosity was not visually shown in the reconstructed images, it was calculated that the cements incorporated with larger mass amounts of lactose, contained a higher total porosity than Palacos R+G. Drug release was measured, and it was shown that the lactose incorporated bone cement discs released the largest mass amounts of gentamicin. However, compared to Palacos R+G, the magnesium stearate cement discs released comparable mass quantities of gentamicin and had a more controlled release profile.

Given the magnesium stearate effect on retardation of drug release; moreover, that magnesium stearate causes a more controlled drug release profile, it was thought that using dry powder coating technology by combining the drug release retardant properties of magnesium stearate to gentamicin sulfate, an optimal drug release profile could be achieved. In particular, as minimal mass quantities of magnesium stearate would be incorporated, the mechanical properties of the bone cement could possibly be maintained. Dry powder coating was performed using gentamicin sulfate as the host particle and magnesium stearate as the guest particle. Methods using different shear forces were used: conventional rotary mixing, pestle and mortar, and ball milling. Using SEM, it was seen that using a conventional rotary mixer and pestle and mortar, resulted in a partial magnesium stearate coating around gentamicin sulfate particles. However, this could not be confirmed for the ball mill particles which were much smaller than the other samples, making it impossible to differentiate between gentamicin sulfate and magnesium stearate. EDX was used to detect magnesium stearate, however, this method did not confirm the presence of magnesium stearate on mixtures with lower percentage concentrations of magnesium stearate. EDX could not be applied to the ball mill or the pestle and mortar samples which contained finer particles. It was shown, however, that EDX could detect gentamicin sulfate, by giving strong peaks for sulfur. Drug release from all of the cement discs produced from powder coated gentamicin had good compressive strengths which were comparable with commercial cement; however, they released significantly less gentamicin mass amounts than the commercial cement at each time point.

7.2 Future work

The work carried out in this study has sought to investigate several aspects of drug formulations and analytical methods and has therefore contributed to the existing body of knowledge.

Although the freeze-dried formulation was shown to be ineffective for drug release from bone cement, understanding the reasons for the degradation of gentamicin sulfate is important, for future work, where freeze drying of gentamicin sulfate may be required. A series of experiments should be performed on common cryopreservants including sucrose to characterise the possible degradation of gentamicin. Sucrose and gentamicin sulfate should be mixed together, both dry and in solution, to characterise the effect on the latter's potency. Moreover, the conditions due to the freeze-drying process should be simulated to characterise loss in gentamicin potency at each stage. This will provide an indication of the effect of sucrose and other cryopreservants on the potency of gentamicin.

The extent of penetration due to water should be further investigated using MicroCT. In this study, the experiment was based on that fact that pmma contains an incorporated radiopacifier (zirconium dioxide) in commercial bone cement. Although, some basic detail of the discs were visualised like shape and defects, intricate detail such as pores, channels and voids within the discs were not visualised. Alternate methods obtained in literature show that a possibly better way to do this experiment would be to use an iodine staining method (Boyde et al., 2014), by exposing the discs to iodine vapour (a contrasting agent) which can enter channels and pores, and will therefore be able to show clear porosity visually. This will provide very important information as to mechanism of release of different cement systems, showing the extent of porosity and channelling due to water penetration.

EDX analysis showed that strong sulfur peaks were consistently obtained from gentamicin sulfate. This method could be used to show uniformity of mixing of gentamicin sulfate in PMMA. Moreover, this could be shown in powder and in cured bone cement. Moreover, Newbury & Ritchie (2013) describes the possibility of using EDX as a fully quantitative method (Newbury & Ritchie, 2013), which could allow quantification of gentamicin sulfate. Being able to characterise gentamicin sulfate within bone cement would be very useful as it could show the dispersion of gentamicin within the formulations. Optimising a quantification, as described by Newbury & Ritchie (2013), could also be used to assay gentamicin in formulations prior to drug elution such as the freeze-dried bone cements, in order to quantify

and characterise gentamicin in the cured cements containing freeze-dried formulation, since only trace amounts were detected by LC-MS.

The results of the dry particle coating showed that a partial discrete coating around gentamicin sulfate particles was obtained with the conventional tumble mixing method and pestle and mortar methods, as observed by SEM. It was not possible to confirm whether the particles produced by ball mill, were particle coated. This should be investigated further by trying to detect magnesium on gentamicin particles. This could be done by improving the sensitivity of the EDX method used by optimising the electron accelerating voltage and/or by using a more sensitive windowless detector, capable of collecting low-energy x-rays (Burgess et al., 2017).

Powder coating of gentamicin sulfate with magnesium stearate should be further investigated, as it was shown that a very small mass quantity of magnesium stearate was able to slow down, significantly, the release of gentamicin sulfate, whilst maintaining compressive strength. The drug release experiment should be continued for a longer time, possible over several months, as the rate of release has not been confirmed beyond one month. Full mechanical testing as per ISO 5833 should also be performed, as only compressive strength was assessed. Investigation into the ball mill method in this study should also be investigated, by varying parameters such as particle sizes of the host and guest particles prior to mixing, mass amounts of guest and host compounds, time and rotation speed which are known to affect powder coating. Other guest particles should be investigated based on physico-chemical properties.

The adhesive forces acting between gentamicin sulfate and a given host compound can be measured and compared using atomic force microscopy (AFM). Similarly, vancomycin was coated on to AFM tips to assess forces between itself and a target surface (Grzeszczuk et al., 2020). Furthermore, due to time constraints in this study, the stability of the coating was not investigated, stability should be characterised at different time points, to see if magnesium stearate or if any given guest particles remain adhered to gentamicin sulfate particles. After having investigated the optimal dry powder coating formulation, high impact devices should be investigated to coat guest particles more effectively on to the gentamicin sulfate particles. Patented technologies such as Mechanofusion or hybridiser which exert high shear forces could be used for this. However, due to the high force impact from these techniques, causing much excess heat, the potential degradation of gentamicin sulfate should also be assessed. The hybrid particles should be characterised to ascertain the degree of coating and their stability. Should dry-powder coating prove to be effective and

successful, the incorporation of dry powder coated gentamicin sulfate into PMMA bone cement should further be assessed for homogeneity of mixing, mechanical properties, antimicrobial efficacy and for gentamicin release.

References

- 2016 13th Annual Report National Joint Registry for England, Wales, Northern Ireland and the Isle of Man. (2016). [http://www.njrreports.org.uk/Portals/0/PDFdownloads/NJR 13th Annual Report 2016.pdf](http://www.njrreports.org.uk/Portals/0/PDFdownloads/NJR_13th_Annual_Report_2016.pdf)
- Abed, N., & Couvreur, P. (2014). International Journal of Antimicrobial Agents Nanocarriers for antibiotics : A promising solution to treat intracellular bacterial infections. *International Journal of Antimicrobial Agents*, 43(6), 485–496. <https://doi.org/10.1016/j.ijantimicag.2014.02.009>
- Aboofazeli, R. (2010). Carbon nanotubes: a promising approach for drug delivery. *Iranian Journal of Pharmaceutical Research : IJPR*, 9(1), 1–3. <http://www.pubmedcentral.nih.gov/articlerender.fcgi?artid=3869555&tool=pmcentrez&rendertype=abstract>
- Abu-Amer, Y., Darwech, I., & Clohisy, J. C. (2007). Aseptic loosening of total joint replacements: Mechanisms underlying osteolysis and potential therapies. *Arthritis Research and Therapy*, 9(SUPPL.1), 1–7. <https://doi.org/10.1186/ar2170>
- Adhikari, U., Goliaei, A., Tsereteli, L., & Berkowitz, M. L. (2016). Properties of poloxamer molecules and poloxamer micelles dissolved in water and next to lipid bilayers: Results from computer simulations. *Journal of Physical Chemistry B*, 120(26), 5823–5830. <https://doi.org/10.1021/acs.jpccb.5b11448>
- Akbarzadeh, A., Rezaei-sadabady, R., Davaran, S., Joo, S. W., & Zarghami, N. (2013). Liposome : classification , preparation , and applications. *Nanoscale Research Letters*, 8(1), 1. <https://doi.org/10.1186/1556-276X-8-102>
- Akiyama, H., Yamasaki, O., Kanzaki, H., & Tada, J. (1998). *Effects of sucrose and silver on*. 629–634.
- Akram, M., Yu, H., Wang, L., Khalid, H., Abbasi, N. M., Zain-ul-Abdin, Chen, Y., Ren, F., & Saleem, M. (2016). Sustained release of hydrophilic drug from polyphosphazenes/poly(methyl methacrylate) based microspheres and their degradation study. *Materials Science and Engineering C*, 58, 169–179. <https://doi.org/10.1016/j.msec.2015.08.010>
- Al-Orf, S. M. (2011). Effect of oxidized phosphatidylcholine on biomarkers of oxidative stress in rats. *Indian Journal of Clinical Biochemistry*, 26(2), 154–160. <https://doi.org/10.1007/s12291-010-0064-4>
- Al Thaher, Y., Perni, S., & Prokopovich, P. (2016). Nano-carrier based drug delivery systems for sustained antimicrobial agent release from orthopaedic cementous material. *Advances in Colloid and Interface Science*, December 2016, 0–1.

<https://doi.org/10.1016/j.cis.2017.04.017>

- Ali, B. H., Al Za'abi, M., Blunden, G., & Nemmar, A. (2011). Experimental Gentamicin Nephrotoxicity and Agents that Modify it: A Mini-Review of Recent Research. *Basic and Clinical Pharmacology and Toxicology*, 109(4), 225–232. <https://doi.org/10.1111/j.1742-7843.2011.00728.x>
- Ali, U., Karim, K. J. B. A., & Buang, N. A. (2015). A Review of the Properties and Applications of Poly (Methyl Methacrylate) (PMMA). *Polymer Reviews*, 55(4), 678–705. <https://doi.org/10.1080/15583724.2015.1031377>
- Alice Brochu, Gregory A. Evans, and W. M. R. (2014). Mechanical and cytotoxicity testing of acrylic bone cement embedded with microencapsulated 2-octyl cyanoacrylate. *J Biomed Mater Res B Appl Biomater*, 102, 181–189. <https://doi.org/10.1016/j.earlhumdev.2006.05.022>
- Allison, K. R., Brynildsen, M. P., & Collins, J. J. (2011). Metabolite-enabled eradication of bacterial persisters by aminoglycosides. *Nature*, 473(7346), 216–220. <https://doi.org/10.1038/nature10069>
- Alonso, M., Satoh, M., & Miyanami, K. (1988). Powder coating in a rotary mixer with rocking motion. *Powder Technology*, 56(2), 135–141. [https://doi.org/10.1016/0032-5910\(88\)80007-X](https://doi.org/10.1016/0032-5910(88)80007-X)
- Alonso, M., Satoh, M., & Miyanami, K. (1989). Mechanism of the combined coating-mechanofusion processing of powders. *Powder Technology*, 59(1), 45–52. [https://doi.org/10.1016/0032-5910\(89\)80094-4](https://doi.org/10.1016/0032-5910(89)80094-4)
- Alyami, H., Dahmash, E., Bowen, J., & Mohammed, A. R. (2017). An investigation into the effects of excipient particle size, blending techniques & processing parameters on the homogeneity & content uniformity of a blend containing low-dose model drug. *PLoS ONE*, 12(6), 1–19. <https://doi.org/10.1371/journal.pone.0178772>
- Amaro, F., Morón, Á., Díaz, S., Martín-González, A., & Gutiérrez, J. C. (2021). Metallic nanoparticles—friends or foes in the battle against antibiotic-resistant bacteria? *Microorganisms*, 9(2), 1–11. <https://doi.org/10.3390/microorganisms9020364>
- Anagnostakos, K., & Kelm, J. (2009). Enhancement of antibiotic elution from acrylic bone cement. *Journal of Biomedical Materials Research - Part B Applied Biomaterials*, 90 B(1), 467–475. <https://doi.org/10.1002/jbm.b.31281>
- Andrews, J. (2001). Determination of MIC. *Journal of Antimicrobial Chemotherapy*, 48(1), 5–16.
- Ansteinsson, V., Kopperud, H. B., Morisbak, E., & Samuelsen, J. T. (2013). Cell toxicity of methacrylate monomers-The role of glutathione adduct formation. *Journal of Biomedical Materials Research - Part A*, 101(12), 3504–3510. <https://doi.org/10.1002/jbm.a.34652>

- Antonakou, E. V., & Achilias, D. S. (2013). Recent advances in polycarbonate recycling: A review of degradation methods and their mechanisms. *Waste and Biomass Valorization*, 4(1), 9–21. <https://doi.org/10.1007/s12649-012-9159-x>
- Anyakudo, F., Adams, E., & Van Schepdael, A. (2020). Analysis of amikacin, gentamicin and tobramycin by thin layer chromatography-flame ionization detection. *Microchemical Journal*, 157(March). <https://doi.org/10.1016/j.microc.2020.105032>
- Apel, P. Y., Blonskaya, I. V., Dmitriev, S. N., Orelovitch, O. L., & Sartowska, B. (2006). Structure of polycarbonate track-etch membranes: Origin of the “paradoxical” pore shape. *Journal of Membrane Science*, 282(1–2), 393–400. <https://doi.org/10.1016/j.memsci.2006.05.045>
- Arciola, C. R., Campoccia, D., & Montanaro, L. (2018). Implant infections: Adhesion, biofilm formation and immune evasion. *Nature Reviews Microbiology*, 16(7), 397–409. <https://doi.org/10.1038/s41579-018-0019-y>
- Ariyasu, A., Hattori, Y., & Otsuka, M. (2016). Delay effect of magnesium stearate on tablet dissolution in acidic medium. *International Journal of Pharmaceutics*, 511(2), 757–764. <https://doi.org/10.1016/j.ijpharm.2016.07.034>
- Arthritis of the Knee-OrthoInfo - AAOS*. (2012). <http://orthoinfo.aaos.org/topic.cfm?topic=a00212>
- Ashraf, H., Najafi, F., Heidari, S., Mohammadian, M., & Zadsirjan, S. (2017). Physical properties and chemical characterization of two experimental epoxy resin root canal sealers. *Iranian Endodontic Journal*, 12(2), 149–156. <https://doi.org/10.7508/iej.2017.02.005>
- Ateeq, R., Veikko, U., & Daniel, L. (2018). Mini review on emerging methods of preparation of liposome and its application as Liposome drug delivery systems. *Open Journal of Pharmacology and Pharmacotherapeutics*, 3(1), 005–021. <https://doi.org/10.17352/ojpp.000007>
- Avanti Polar Lipids.18:1-06:0 NBD PC. [online] Available at: <https://avantilipids.com/product/810132> [Accessed 10 Dec. 2020]. (n.d.). <https://avantilipids.com/product/810132>. <https://avantilipids.com/product/810132>
- Ayre et al. 2016. Liposomal drug delivery system for bone cements. US9895466.
- Ayre, W. N., Birchall, J. C., Evans, S. L., & Denyer, S. P. (2015). *A novel liposomal drug delivery system for PMMA bone cements*. 1510–1524. <https://doi.org/10.1002/jbm.b.33488>
- Ayre, W. N., Denyer, S. P., & Evans, S. L. (2014). Ageing and moisture uptake in polymethyl methacrylate (PMMA) bone cements. *Journal of the Mechanical Behavior of Biomedical Materials*, 32, 76–88. <https://doi.org/10.1016/j.jmbbm.2013.12.010>
- Bager, C. L., Karsdal, M., Bihlet, A., Thudium, C., Byrjalsen, I., & Bay-Jensen, A. C. (2019).

- Incidence of total hip and total knee replacements from the prospective epidemiologic risk factor study: Considerations for event driven clinical trial design. *BMC Musculoskeletal Disorders*, 20(1), 1–6. <https://doi.org/10.1186/s12891-019-2680-3>
- Baker, A., & Greenham, L. (1988). Release of gentamicin from acrylic bone cement. Elution and diffusion studies. *The Journal of Bone and Joint Surgery. American Volume*, 70(10), 1551–1557.
- Bangham, A. D., Standish, M. M., & Watkins, J. C. (1965). Diffusion of univalent ions across the lamellae of swollen phospholipids. *Journal of Molecular Biology*, 13(1), 238–252. [https://doi.org/10.1016/S0022-2836\(65\)80093-6](https://doi.org/10.1016/S0022-2836(65)80093-6)
- Barbosa, A. I., Barreto, A. S., & Reis, N. M. (2019). Transparent, Hydrophobic Fluorinated Ethylene Propylene Offers Rapid, Robust, and Irreversible Passive Adsorption of Diagnostic Antibodies for Sensitive Optical Biosensing. *ACS Applied Bio Materials*, 2(7), 2780–2790. <https://doi.org/10.1021/acsabm.9b00214>
- Battocchio, C., Meneghini, C., Fratoddi, I., Venditti, I., Russo, M. V., Aquilanti, G., Maurizio, C., Bondino, F., Matassa, R., Rossi, M., Mobilio, S., & Polzonetti, G. (2012). *Silver Nanoparticles Stabilized with Thiols : A Close Look at the Local Chemistry and Chemical Structure*.
- Bayliss, L. E., Culliford, D., Monk, A. P., Glyn-Jones, S., Prieto-Alhambra, D., Judge, A., Cooper, C., Carr, A. J., Arden, N. K., Beard, D. J., & Price, A. J. (2017). The effect of patient age at intervention on risk of implant revision after total replacement of the hip or knee: a population-based cohort study. *The Lancet*, 389(10077), 1424–1430. [https://doi.org/10.1016/S0140-6736\(17\)30059-4](https://doi.org/10.1016/S0140-6736(17)30059-4)
- Belisle et al. 2015. Colloidal Coomassie stain. US9034652B2., 2 0 (2015).
- Bergmann, G., Graichen, F., & Rohlmann, A. (1993). Hip joint loading during walking and running, measured in two patients. *Journal of Biomechanics*, 26(8), 969–990. [https://doi.org/10.1016/0021-9290\(93\)90058-M](https://doi.org/10.1016/0021-9290(93)90058-M)
- Bernard, L., Legout, L., Zürcher-Pfund, L., Stern, R., Rohner, P., Peter, R., Assal, M., Lew, D., Hoffmeyer, P., & Uçkay, I. (2010). Six weeks of antibiotic treatment is sufficient following surgery for septic arthroplasty. *Journal of Infection*, 61(2), 125–132. <https://doi.org/10.1016/j.jinf.2010.05.005>
- Bharti, C., Gulati, N., Nagaich, U., & Pal, A. (2015). Mesoporous silica nanoparticles in target drug delivery system: A review. *International Journal of Pharmaceutical Investigation*, 5(3), 124. <https://doi.org/10.4103/2230-973X.160844>
- Bhattacharya, S., Pal, K., Jain, S., Chatterjee, S. S., & Konar, J. (2016). Surgical site infection by methicillin resistant staphylococcus aureus– On decline? *Journal of Clinical and Diagnostic Research*, 10(9), DC32–DC36. <https://doi.org/10.7860/JCDR/2016/21664.8587>

- Bianco, A., Kostarelos, K., & Prato, M. (2005). Applications of carbon nanotubes in drug delivery. *Current Opinion in Chemical Biology*, 9(6), 674–679.
<https://doi.org/10.1016/j.cbpa.2005.10.005>
- Bistolfi, A., Massazza, G., Vern, E., Mass, A., Deledda, D., Ferraris, S., Miola, M., Galetto, F., & Crova, M. (2011). *Antibiotic-Loaded Cement in Orthopedic Surgery : A Review. 2011*. <https://doi.org/10.5402/2011/290851>
- Blanco-Príeto, M. J., Lecaroz, C., Renedo, M. J., Kunkova, J., & Gamazo, C. (2002). In vitro evaluation of gentamicin released from microparticles. *International Journal of Pharmaceutics*, 242(1–2), 203–206. [https://doi.org/10.1016/S0378-5173\(02\)00158-8](https://doi.org/10.1016/S0378-5173(02)00158-8)
- Bligh, E.G. and Dyer, W. J. (1959). Canadian Journal of Biochemistry and Physiology. *Canadian Journal of Biochemistry and Physiology*, 37(8).
- Bor, A., Jargalsaikhan, B., Lee, J., & Choi, H. (2018). Surface coating copper powder with carbon nanotubes using traditional and stirred ball mills under various experimental conditions. *Particuology*, 40, 177–182. <https://doi.org/10.1016/j.partic.2017.10.011>
- Bottaro, Larsen, B. (2008). 基因的改变 NIH Public Access. *Bone*, 23(1), 1–7.
<https://doi.org/10.1002/art.34453.Osteoarthritis>
- Boyde, A., Mccorkell, F. A., Taylor, G. K., Bomphrey, R. J., & Doube, M. (2014). Iodine vapor staining for atomic number contrast in backscattered electron and X-ray imaging. *Microscopy Research and Technique*, 77(12), 1044–1051.
<https://doi.org/10.1002/jemt.22435>
- BOZIC, K. J., KATZ, P., CISTERNAS, M., ONO, L., RIES, M. D., & SHOWSTACK, J. (2005). Hospital Resource Utilization for Primary and Revision Total Hip Arthroplasty. *The Journal of Bone and Joint Surgery-American Volume*, 87(3), 570–576.
<https://doi.org/10.2106/00004623-200503000-00014>
- Bozzuto, G. (2015). *Liposomes as nanomedical devices*. 975–999.
- British Pharmacopoeia*. (2017). <https://www.pharmacopoeia.com/>
- British Pharmacopoeia. (2021). Gentamicin Sulfate. *British Pharmacopoeia*, 403–405.
<https://doi.org/10.1016/b978-0-323-70957-6.00236-3>
- British Standards Institution. (2015). Chemical disinfectants and antiseptics - Quantitative suspension test for the evaluation of bactericidal activity in the medical area - Test method and requirements (phase 2, step 1). *European Committee for Standardization*, 3(1).
[http://www.cen.eu/cen/Sectors/TechnicalCommitteesWorkshops/CENTechnicalCommittees/Pages/Standards.aspx?param=6197&title=Chemical disinfectants and antiseptics](http://www.cen.eu/cen/Sectors/TechnicalCommitteesWorkshops/CENTechnicalCommittees/Pages/Standards.aspx?param=6197&title=Chemical%20disinfectants%20and%20antiseptics)
- Bruker-microCT. (2012). Morphometric parameters measured by Skyscan™ CT - analyser software . In *Reference Manual*. <http://bruker-microct.com/next/CTAn03.pdf>

- Buchholz HW, E. H. (1970). Depot effects of various antibiotics mixed with Palacos resins. *Chirurg*, 41(11), 511–515.
- Bumpass, D. B., & Nunley, R. M. (2012). Assessing the value of a total joint replacement. *Current Reviews in Musculoskeletal Medicine*, 5(4), 274–282.
<https://doi.org/10.1007/s12178-012-9139-6>
- Bungert, N., Kobler, M., & Scherließ, R. (2021). In-depth comparison of dry particle coating processes used in dpi particle engineering. *Pharmaceutics*, 13(4).
<https://doi.org/10.3390/pharmaceutics13040580>
- Burgess, S., Sagar, J., Holland, J., Li, X., & Bauer, F. (2017). Ultra-Low kV EDS – A New Approach to Improved Spatial Resolution, Surface Sensitivity, and Light Element Compositional Imaging and Analysis in the SEM. *Microscopy Today*, 25(2), 20–29.
<https://doi.org/10.1017/s1551929517000013>
- Burri, L., Hoem, N., Banni, S., & Berge, K. (2012). Marine Omega-3 phospholipids: Metabolism and biological activities. *International Journal of Molecular Sciences*, 13(11), 15401–15419. <https://doi.org/10.3390/ijms131115401>
- Capello, C., Fischer, U., & Hungerbühler, K. (2007). What is a green solvent? A comprehensive framework for the environmental assessment of solvents. *Green Chemistry*, 9(9), 927–993. <https://doi.org/10.1039/b617536h>
- Castañeda-Reyes, E. D., Perea-Flores, M. de J., Davila-Ortiz, G., Lee, Y., & de Mejia, E. G. (2020). Development, characterization and use of liposomes as amphipathic transporters of bioactive compounds for melanoma treatment and reduction of skin inflammation: A review. *International Journal of Nanomedicine*, 15, 7627–7650.
<https://doi.org/10.2147/IJN.S263516>
- Chang, J. S., & Haddad, F. S. (2020). Long-term survivorship of hip and knee arthroplasty. *Bone and Joint Journal*, 102 B(4), 401–402. <https://doi.org/10.1302/0301-620X.102B4.BJJ-2020-0183>
- Charles, J., & Stewart, M. (1980). *Colorimetric Determination of Phospholipids Ferriothiocyanate*. 14.
- Chen, A.F. and Parvizi, J. (2014). Antibiotic-loaded bone cement and periprosthetic joint infection. *Journal of Long-Term Effects of Medical Implants*, 24, 2–3.
<http://www.dl.begellhouse.com/journals/1bef42082d7a0fdf,0134a0a71af442c9,787108b078050b67.html>
- Chen, C., Han, D., Cai, C., & Tang, X. (2010). An overview of liposome lyophilization and its future potential. *Journal of Controlled Release*, 142(3), 299–311.
<https://doi.org/10.1016/j.jconrel.2009.10.024>
- Chen, L., Tang, Y., Zhao, K., Zha, X., Wei, M., Tan, Q., & Wu, Z. (2021). Sequential release of double drug (graded distribution) loaded gelatin microspheres/PMMA bone cement.

- Journal of Materials Chemistry B*, 9(2), 508–522. <https://doi.org/10.1039/d0tb01452d>
- Chen, W., Duša, F., Witos, J., Ruokonen, S. K., & Wiedmer, S. K. (2018). Determination of the Main Phase Transition Temperature of Phospholipids by Nanoplasmonic Sensing. *Scientific Reports*, 8(1), 1–11. <https://doi.org/10.1038/s41598-018-33107-5>
- Cheng, W. T., Wang, S. L., & Lin, S. Y. (2008). Effect of moisture content on solid-state interaction at the interface between magnesium stearate and captopril. *Applied Surface Science*, 255(5 PART 2), 2782–2786. <https://doi.org/10.1016/j.apsusc.2008.08.009>
- Chopra, B. K. (2015). Joint replacement surgery in the armed forces medical services, India: The journey so far and looking ahead. *Medical Journal Armed Forces India*, 71(1), 5–10. <https://doi.org/10.1016/j.mjafi.2014.12.012>
- Cioffi, M., Hoffmann, A. C., & Janssen, L. P. B. M. (2001). Reducing the gel effect in free radical polymerization. *Chemical Engineering Science*, 56(3), 911–915. [https://doi.org/10.1016/S0009-2509\(00\)00305-5](https://doi.org/10.1016/S0009-2509(00)00305-5)
- Clarot, I., Chaimbault, P., Hasdenteufel, F., Netter, P., & Nicolas, A. (2004). Determination of gentamicin sulfate and related compounds by high-performance liquid chromatography with evaporative light scattering detection. *Journal of Chromatography A*, 1031(1–2), 281–287. <https://doi.org/10.1016/j.chroma.2003.12.032>
- Cobo, J., & Del Pozo, J. (2011). Diagnosis and management of prosthetic joint infection. *Perioperative Management of Patients with Rheumatic Disease*, 9(9), 261–269. https://doi.org/10.1007/978-1-4614-2203-7_22
- Conaghan, P. G., Porcheret, M., Kingsbury, S. R., Gammon, A., Soni, A., Hurley, M., Rayman, M. P., Barlow, J., Hull, R. G., Cumming, J., Llewelyn, K., Moscogiuri, F., Lyons, J., & Birrell, F. (2015). Impact and therapy of osteoarthritis: the Arthritis Care OA Nation 2012 survey. *Clinical Rheumatology*, 34(9), 1581–1588. <https://doi.org/10.1007/s10067-014-2692-1>
- Cook, R., Davidson, P., & Martin, R. (2019). More than 80% of total knee replacements can last for 25 years. *The BMJ*, 367(December), 2017–2018. <https://doi.org/10.1136/bmj.l5680>
- Costanzo, S., Di Sarno, A., D'Apuzzo, M., Avallone, P. R., Raccone, E., Bellissimo, A., Auriemma, F., Grizzuti, N., & Pasquino, R. (2021). Rheology and morphology of Pluronic F68 in water. *Physics of Fluids*, 33(4). <https://doi.org/10.1063/5.0049722>
- Coulman, S. A., Anstey, A., Gateley, C., Morrissey, A., McLoughlin, P., Allender, C., & Birchall, J. C. (2009). Microneedle mediated delivery of nanoparticles into human skin. *International Journal of Pharmaceutics*, 366(1–2), 190–200. <https://doi.org/10.1016/j.ijpharm.2008.08.040>
- Cunningham, B., McLaren, A. C., Pauken, C., & McLemore, R. (2012). Liposomal formulation increases local delivery of amphotericin from bone cement: A pilot study

- infection. *Clinical Orthopaedics and Related Research*, 470(10), 2671–2676.
<https://doi.org/10.1007/s11999-012-2317-4>
- Cyphert, E. L., Learn, G. D., Hurley, S. K., Lu, C. yi, & von Recum, H. A. (2018). An Additive to PMMA Bone Cement Enables Postimplantation Drug Refilling, Broadens Range of Compatible Antibiotics, and Prolongs Antimicrobial Therapy. *Advanced Healthcare Materials*, 1800812, 1–13. <https://doi.org/10.1002/adhm.201800812>
- Dahmash, E. Z., & Mohammed, A. R. (2015). Functionalised particles using dry powder coating in pharmaceutical drug delivery: Promises and challenges. *Expert Opinion on Drug Delivery*, 12(12), 1867–1879. <https://doi.org/10.1517/17425247.2015.1071351>
- Dakin, H., Gray, A., Fitzpatrick, R., MacLennan, G., & Murray, D. (2012). Rationing of total knee replacement: A cost-effectiveness analysis on a large trial data set. *BMJ Open*, 2(1), 1–9. <https://doi.org/10.1136/bmjopen-2011-000332>
- Das, U. N. (2015). Sucrose, fructose, glucose, and their link to metabolic syndrome and cancer. *Nutrition*, 31(1), 249–257. <https://doi.org/10.1016/j.nut.2014.05.015>
- Davidson, D. J., Spratt, D., & Liddle, A. D. (2019). Implant materials and prosthetic joint infection: The battle with the biofilm. *EFORT Open Reviews*, 4(11), 633–639. <https://doi.org/10.1302/2058-5241.4.180095>
- Delaey, J., Dubruel, P., & Van Vlierberghe, S. (2020). Shape-Memory Polymers for Biomedical Applications. *Advanced Functional Materials*, 30(44), 1–23. <https://doi.org/10.1002/adfm.201909047>
- Diez-Pena, E., Frutos, G., Frutos, P., Manuel, J., & Rienda, B. (2002). *Gentamicin Sulphate Release from a Modified Commercial Acrylic Surgical Radiopaque Bone Cement . I . Influence of the Gentamicin Concentration on the Release Process Mechanism*. 50(September), 1201–1208.
- Dorati, R., DeTrizio, A., Spalla, M., Migliavacca, R., Pagani, L., Pisani, S., Chiesa, E., Conti, B., Modena, T., & Genta, I. (2018). Gentamicin Sulfate PEG-PLGA/PLGA-H nanoparticles: Screening design and antimicrobial effect evaluation toward clinic bacterial isolates. *Nanomaterials*, 8(1). <https://doi.org/10.3390/nano8010037>
- Drescher, S., & van Hoogevest, P. (2020). The phospholipid research center: Current research in phospholipids and their use in drug delivery. *Pharmaceutics*, 12(12), 1–36. <https://doi.org/10.3390/pharmaceutics12121235>
- Du, Y., He, W., Xia, Q., Zhou, W., Yao, C., & Li, X. (2019). Thioether Phosphatidylcholine Liposomes: A Novel ROS-Responsive Platform for Drug Delivery. *ACS Applied Materials and Interfaces*, 11(41), 37411–37420. <https://doi.org/10.1021/acsami.9b08901>
- Dunne N.J, Buchanan F, Hill K, Newe C, Tunney M, Brady A, & Walker G. (2008). In vitro testing of chitosan in gentamicin-loaded bone cement: No antimicrobial effect and

- reduced mechanical performance. *Acta Orthopaedica*, 79(6), 851–860.
<https://doi.org/10.1080/17453670810016957>
- Dunne N.J, Hill J, Mcafee P, Todd K, Kirkpatrick R, Tunney M, & Patrick S. (2007). In vitro study of the efficacy of acrylic bone cement loaded with supplementary amounts of gentamicin: Effect on mechanical properties, antibiotic release, and biofilm formation. *Acta Orthopaedica*, 78(6), 774–785. <https://doi.org/10.1080/17453670710014545>
- Dunne N.J, Hill J, Mcafee P, Todd K, Kirkpatrick R, Tunney M, & Patrick S. (2009a). *In vitro study of the efficacy of acrylic bone cement loaded with supplementary amounts of gentamicin : Effect on mechanical properties , antibiotic release , and biofilm formation In vitro study of the efficacy of acrylic bone cement loaded with suppleme.* 3674(February 2017). <https://doi.org/10.1080/17453670710014545>
- Dunne N.J, Hill J, Mcafee P, Todd K, Kirkpatrick R, Tunney M, & Patrick S. (2009b). *In vitro testing of chitosan in gentamicin-loaded bone cement No antimicrobial effect and reduced mechanical performance.* 911796915.
<https://doi.org/10.1080/17453670810016957>
- Dunne N.J, Hill J, Mcafee P, Todd K, Kirkpatrick R, Tunney M, & S, P. (2008). *Incorporation of large amounts of gentamicin sulphate into acrylic bone cement : effect on handling and mechanical properties , antibiotic release , and biofilm formation.* 222, 355–365.
<https://doi.org/10.1243/09544119JEIM355>
- Dunne N.J, & Orr J.F. (2001). Influence of mixing techniques on the physical properties of acrylic bone cement. *Biomaterials*, 22(13), 1819–1826. [https://doi.org/10.1016/S0142-9612\(00\)00363-X](https://doi.org/10.1016/S0142-9612(00)00363-X)
- Dyankova, S., Doneva, M., Todorov, Y., & Terziyska, M. (2016). Determination of particle size distribution and analysis of a natural food supplement on pectin base. *IOSR Journal Of Pharmacy Wwww.iosrphr.Org*, 6(5), 1–08.
- El-Fallal, A. A., Shams, M., & Abouelatta, O. B. (2009). Effect of roughness, porosity and wettability on release of gentamicin-loaded glass ionomer bone cement. *Egyptian Dental Journal*, 55(1.3), 625–637.
- El-Nesr, O. H., Yahiya, S. A., & El-Gazayerly, O. N. (2010). Effect of formulation design and freeze-drying on properties of fluconazole multilamellar liposomes. *Saudi Pharmaceutical Journal*, 18(4), 217–224. <https://doi.org/10.1016/j.jsps.2010.07.003>
- Evans, J. T., Evans, J. P., Walker, R. W., Blom, A. W., Whitehouse, M. R., & Sayers, A. (2019). How long does a hip replacement last? A systematic review and meta-analysis of case series and national registry reports with more than 15 years of follow-up. *Lancet (London, England)*, 393(10172), 647–654. [https://doi.org/10.1016/S0140-6736\(18\)31665-9](https://doi.org/10.1016/S0140-6736(18)31665-9)
- Farouk, F., Azzazy, H. M. E., & Niessen, W. M. A. (2015). Challenges in the determination of

- aminoglycoside antibiotics, a review. *Analytica Chimica Acta*, 890, 21–43.
<https://doi.org/10.1016/j.aca.2015.06.038>
- Fernandez-Bertran, J. (1999). *Mechanochemistry: an overview* *. 71(4), 581–586.
- Fernández-Ramos, J. M., García-Campaña, A. M., Alés-Barrero, F., & Bosque-Sendra, J. M. (2006). Determination of gentamicin in pharmaceutical formulations using peroxyoxalate chemiluminescent detection in flow-injection analysis. *Talanta*, 69(3), 763–768. <https://doi.org/10.1016/j.talanta.2005.11.008>
- NIST: SRM 114q Part II: Particle size distribution, (2006).
- Figuroa V, L., Ceballos R, G., Díaz Cedillo, F., López R, M. D. C., Escalante Magaña, R. M., & García Fuentes, L. V. (2008). Evaluation and characterization of antimicrobial properties of pregnenolone-derivatives on *Staphylococcus aureus*, *Klebsiella pneumoniae* and *Escherichia coli*. *Revista Latinoamericana de Microbiología*, 50(1–2), 13–18.
- Forough Reyhani, M., Hosseinian Ahangarnezhad, S., Ghasemi, N., & Salem Milani, A. (2021). Effects of various liquid-to-powder ratios on the compressive strength of calcium enriched mixture: Original research. *Journal of Dental Research, Dental Clinics, Dental Prospects*, 15(2), 129–132. <https://doi.org/10.34172/joddd.2021.022>
- Franzé, S., Selmin, F., Samaritani, E., Minghetti, P., & Cilurzo, F. (2018). Lyophilization of liposomal formulations: Still necessary, still challenging. *Pharmaceutics*, 10(3). <https://doi.org/10.3390/pharmaceutics10030139>
- Friesen, W. J., Johnson, B., Sierra, J., Zhuo, J., Vazirani, P., Xue, X., Tomizawa, Y., Baiazitov, R., Morrill, C., Ren, H., Babu, S., Moon, Y. C., Branstrom, A., Mollin, A., Hedrick, J., Sheedy, J., Elfring, G., Weetall, M., Colacino, J. M., ... Peltz, S. W. (2018). The minor gentamicin complex component, X2, is a potent premature stop codon readthrough molecule with therapeutic potential. *PLoS ONE*, 13(10), 1–18. <https://doi.org/10.1371/journal.pone.0206158>
- Fry, D. W., White, J. C., & Goldman, I. D. (1978). Rapid separation of low molecular weight solutes from liposomes without dilution. *Analytical Biochemistry*, 90(2), 809–815. [https://doi.org/10.1016/0003-2697\(78\)90172-0](https://doi.org/10.1016/0003-2697(78)90172-0)
- Fsadni, C., & Peter, F. (2013). Prosthetic joint infections. *Surgical Clinics of North America*, 94(6), 1265–1281. <https://doi.org/10.1016/j.suc.2014.08.009>
- Gálvez-López, R., Peña-Monje, A., Antelo-Lorenzo, R., Guardia-Olmedo, J., Moliz, J., Hernández-Quero, J., & Parra-Ruiz, J. (2014). Elution kinetics, antimicrobial activity, and mechanical properties of 11 different antibiotic loaded acrylic bone cement. *Diagnostic Microbiology and Infectious Disease*, 78(1), 70–74. <https://doi.org/10.1016/j.diagmicrobio.2013.09.014>
- Gamble, J. F., Chiu, W. S., Gray, V., Toale, H., Tobby, M., & Wu, Y. (2010). Investigation

- into the degree of variability in the solid-state properties of common pharmaceutical excipients-anhydrous lactose. *AAPS PharmSciTech*, 11(4), 1552–1557.
<https://doi.org/10.1208/s12249-010-9527-4>
- Gatoo, M. A., Naseem, S., Arfat, M. Y., Mahmood Dar, A., Qasim, K., & Zubair, S. (2014). Physicochemical properties of nanomaterials: Implication in associated toxic manifestations. *BioMed Research International*, 2014.
<https://doi.org/10.1155/2014/498420>
- Gentilini, E., Denamiel, G., Llorente, P., Godaly, S., Rebuelto, M., & DeGregorio, O. (2000). Antimicrobial susceptibility of Staphylococcus aureus isolated from bovine mastitis in Argentina. *Journal of Dairy Science*, 83(6), 1224–1227.
[https://doi.org/10.3168/jds.S0022-0302\(00\)74988-5](https://doi.org/10.3168/jds.S0022-0302(00)74988-5)
- Ghadi, A., Mahjoub, S., Tabandeh, F., & Talebnia, F. (2014). Synthesis and optimization of chitosan nanoparticles: Potential applications in nanomedicine and biomedical engineering. *Caspian Journal of Internal Medicine*, 5(3), 156–161.
- Ghorbani, B., Ghorbani, M., Abedi, M., & Tayebi, M. (2016). *Effect of Antibiotics Overuse in Animal Food and its Link with Public Health Risk*. 1(2), 46–50.
- Glyn-Jones, S., Palmer, A. J. R., Agricola, R., Price, A. J., Vincent, T. L., Weinans, H., & Carr, A. J. (2015). Osteoarthritis. *The Lancet*, 386(9991), 376–387.
[https://doi.org/10.1016/S0140-6736\(14\)60802-3](https://doi.org/10.1016/S0140-6736(14)60802-3)
- Gönen, M., Egbuchunam, T. O., Balköse, D., Inal, F., & Ülkü, S. (2015). Preparation and characterization of magnesium stearate, cobalt stearate, and copper stearate and their effects on poly(vinyl chloride) dehydrochlorination. *Journal of Vinyl and Additive Technology*, 21(4), 235–244. <https://doi.org/10.1002/vnl.21384>
- Gosavi, S. S., Gosavi, S. Y., & Alla, R. K. (2010). Local and systemic effects of unpolymerised monomers. *Dental Research Journal*, 7(2), 82–87.
<http://www.ncbi.nlm.nih.gov/pubmed/22013462>
<http://www.pubmedcentral.nih.gov/articlerender.fcgi?artid=PMC3177373>
- Goss, B., Lutton, C., Weinrauch, P., Jabur, M., Gillett, G., & Crawford, R. (2007). Elution and Mechanical Properties of Antifungal Bone Cement. *Journal of Arthroplasty*, 22(6), 902–908. <https://doi.org/10.1016/j.arth.2006.09.013>
- Graham, A. E., Speicher, E., & Williamson, B. (1997). Analysis of gentamicin sulfate and a study of its degradation in dextrose solution. *Journal of Pharmaceutical and Biomedical Analysis*, 15(4), 537–543. [https://doi.org/10.1016/S0731-7085\(96\)01852-3](https://doi.org/10.1016/S0731-7085(96)01852-3)
- Grebe, S. K. G., & Singh, R. J. (2011). LC-MS/MS in the clinical laboratory - Where to from here? *Clinical Biochemist Reviews*, 32(1), 5–31.
- Grzeszczuk, Z., Rosillo, A., Owens, Ó., & Bhattacharjee, S. (2020). Atomic Force Microscopy (AFM) As a Surface Mapping Tool in Microorganisms Resistant Toward

- Antimicrobials: A Mini-Review. *Frontiers in Pharmacology*, 11(October), 1–8.
<https://doi.org/10.3389/fphar.2020.517165>
- Guo, Y., Song, G., Sun, M., Wang, J., & Wang, Y. (2020). Prevalence and Therapies of Antibiotic-Resistance in *Staphylococcus aureus*. *Frontiers in Cellular and Infection Microbiology*, 10(March), 1–11. <https://doi.org/10.3389/fcimb.2020.00107>
- Gustke, K. (2017). Cementless TKA: The preferred method for young, active, and heavy patients. *Seminars in Arthroplasty*, 28(2), 58–61.
<https://doi.org/10.1053/j.sart.2017.07.001>
- Gwynne, L., Williams, G. T., Yan, K. C., Patenall, B. L., Gardiner, J. E., He, X. P., Maillard, J. Y., James, T. D., Sedgwick, A. C., & Jenkins, A. T. A. (2021). TCF-ALP: A fluorescent probe for the selective detection of: *Staphylococcus* bacteria and application in “smart” wound dressings. *Biomaterials Science*, 9(12), 4433–4439.
<https://doi.org/10.1039/d0bm01918f>
- Hakemi-Vala, M., Rafati, H., Aliahmadi, A., & Ardalan, A. (2017). Nanoemulsions: A Novel Antimicrobial Delivery System. In *Nano- and Microscale Drug Delivery Systems: Design and Fabrication*. Elsevier Inc. <https://doi.org/10.1016/B978-0-323-52727-9.00013-3>
- Halwani, M., Mugabe, C., Azghani, A. O., Lafrenie, R. M., Kumar, A., & Omri, A. (2007). Bactericidal efficacy of liposomal aminoglycosides against *Burkholderia cenocepacia*. *Journal of Antimicrobial Chemotherapy*, 60(4), 760–769.
<https://doi.org/10.1093/jac/dkm289>
- Hansen, L. J. J., Daoussi, R., Vervaet, C., Remon, J. P., & De Beer, T. R. M. (2015). Freeze-drying of live virus vaccines: A review. *Vaccine*, 33(42), 5507–5519.
<https://doi.org/10.1016/j.vaccine.2015.08.085>
- Heraeus. (2018). *Palacos R+G information sheet*.
https://www.heraeus.com/media/media/hme/doc_hme/products_us/PALACOS_RG_pro_IFU_US.pdf
- Hasandoost, L., Rodriguez, O., Alhalawani, A., Zalzal, P., Schemitsch, E. H., Waldman, S. D., Papini, M., & Towler, M. R. (2020). The role of poly(methyl methacrylate) in management of bone loss and infection in revision total knee arthroplasty: A review. *Journal of Functional Biomaterials*, 11(2), 1–18. <https://doi.org/10.3390/jfb11020025>
- Hayward, R. S., Harding, J., Molloy, R., Land, L., Longcroft-Neal, K., Moore, D., & Ross, J. D. C. (2018). Adverse effects of a single dose of gentamicin in adults: a systematic review. *British Journal of Clinical Pharmacology*, 84(2), 223–238.
<https://doi.org/10.1111/bcp.13439>
- Hendriks, J. G. E., Van Horn, J. R., Van Der Mei, H. C., & Busscher, H. J. (2004). Backgrounds of antibiotic-loaded bone cement and prosthesis-related infection. *Biomaterials*, 25(3), 545–556. [https://doi.org/10.1016/S0142-9612\(03\)00554-4](https://doi.org/10.1016/S0142-9612(03)00554-4)

- Hinarejos, P., Guirro, P., Puig-Verdie, L., Torres-Claramunt, R., Leal-Blanquet, J., Sanchez-Soler, J., & Monllau, J. C. (2015). Use of antibiotic-loaded cement in total knee arthroplasty. *World Journal of Orthopaedics*, *6*(11), 877–885. <https://doi.org/10.5312/wjo.v6.i11.877>
- Hiremath, P., & Agrahari, V. (2019). Influence of Wet Granulation Process Parameters on Wet Granulation Process Performance: Material Attributes and Their Impact on Magnesium Stearate. In *Encyclopedia of Pharmacy Practice and Clinical Pharmacy*.
- Hobbs, C. A., Saigo, K., Koyanagi, M., & Hayashi, S. (2017). Magnesium stearate, a widely-used food additive, exhibits a lack of in vitro and in vivo genotoxic potential. *Toxicology Reports*, *4*(October), 554–559. <https://doi.org/10.1016/j.toxrep.2017.10.003>
- Honda, H., Kimura, M., Honda, F., Matsuno, T., & Koishi, M. (1994). Preparation of monolayer particle coated powder by the dry impact blending process utilizing mechanochemical treatment. *Colloids and Surfaces A: Physicochemical and Engineering Aspects*, *82*(2), 117–128. [https://doi.org/10.1016/0927-7757\(93\)02620-T](https://doi.org/10.1016/0927-7757(93)02620-T)
- Hope, P. G., Kristinsson, K. G., Norman, P., & Elson, R. A. (1989). Deep infection of cemented total hip arthroplasties caused by coagulase-negative staphylococci. *Journal of Bone and Joint Surgery - Series B*, *71*(5), 851–855. <https://doi.org/10.1302/0301-620x.71b5.2584258>
- Horváth, T., Hanák, L., Hegyi, P., Butt, E., Solymár, M., Szűcs, Á., Varga, O., Thien, B. Q., Szakács, Z., Csonka, E., & Hartmann, P. (2020). Hydroxyapatite-coated implants provide better fixation in total knee arthroplasty. A meta-analysis of randomized controlled trials. *PLoS ONE*, *15*(5), 1–13. <https://doi.org/10.1371/journal.pone.0232378>
- Huhtamäki, T., Tian, X., Korhonen, J. T., & Ras, R. H. A. (2018). Surface-wetting characterization using contact-angle measurements. *Nature Protocols*, *13*(7), 1521–1538. <https://doi.org/10.1038/s41596-018-0003-z>
- ICH. (2005). VALIDATION OF ANALYTICAL PROCEDURES: TEXT AND METHODOLOGY Q2(R1). In *Quality guidelines*. <https://doi.org/10.1002/9781118532331.ch23>
- Igbinaduwa, P. O., Kabari, K. M., & Chikwue, T. C. (2019). *Nigerian Journal of Pharmaceutical and Applied Science Research*, *8* (2): 55-61 May 2019 (ISSN 1485-8059 Available at www.nijophasr.com *Nigerian Journal of Pharmaceutical and Applied Science Research*, *8* (2): 55-61 May 2019 (ISSN 1485-8059 Available . 8(May), 55–61.
- Isalomboto Nkanga, C., Murhimalika Bapolisi, A., Ikemefuna Okafor, N., & Werner Maçedo Krause, R. (2019). General Perception of Liposomes: Formation, Manufacturing and Applications. In *Liposomes - Advances and Perspectives*. <https://doi.org/10.5772/intechopen.84255>
- ISO 5833, 5833 Iso 1 (2002).

- Isoherranen, N., Lavy, E., & Soback, S. (2000). *Pharmacokinetics of Gentamicin C1, C1a, and C2 in Beagles after a Single Intravenous Dose*. *44*(6), 1443–1447.
- Jaafar-Maalej, C., Diab, R., Andrieu, V., Elaissari, A., & Fessi, H. (2010). Ethanol injection method for hydrophilic and lipophilic drug-loaded liposome preparation. *Journal of Liposome Research*, *20*(3), 228–243. <https://doi.org/10.3109/08982100903347923>
- Jafari, S. (2015). Application of Hydroxyapatite Nanoparticle in the Drug Delivery Systems. *Journal of Molecular Pharmaceutics & Organic Process Research*, *03*(01), 1–2. <https://doi.org/10.4172/2329-9053.1000e118>
- Jafari, S. M., Coyle, C., Mortazavi, S. M. J., Sharkey, P. F., & Parvizi, J. (2010). Revision hip arthroplasty: Infection is the most common cause of failure. *Clinical Orthopaedics and Related Research*, *468*(8), 2046–2051. <https://doi.org/10.1007/s11999-010-1251-6>
- Jensen, S. K. (2008). Improved Bligh and Dyer extraction procedure. *Lipid Technology*, *20*(12), 280–281. <https://doi.org/10.1002/lite.200800074>
- Jiranek, W. A., Hanssen, A. D., & Greenwald, A. S. (2006). Current concepts review: Antibiotic-loaded bone cement for infection prophylaxis in total joint replacement. *Journal of Bone and Joint Surgery - Series A*, *88*(11), 2487–2500. <https://doi.org/10.2106/JBJS.E.01126>
- Johnson, J. M., & Conforti, F. D. (2003). *J.M. Johnson, F.D. Conforti, in Encyclopedia of Food Sciences and Nutrition (Second Edition), 2003*.
- Jórárt, I., Sovány, T., Pintye-Hódi, K., & Kása, P. (2012). Study of the behaviour of magnesium stearate with different specific surface areas on the surface of particles during mixing. *Journal of Adhesion Science and Technology*, *26*(24), 2737–2744. <https://doi.org/10.1080/01694243.2012.701481>
- Jones, M. D., & Buckle, C. L. (2020). How does aseptic loosening occur and how can we prevent it? *Orthopaedics and Trauma*, *34*(3), 146–152. <https://doi.org/10.1016/j.mporth.2020.03.008>
- Joseph, A., & Rustum, A. (2010). Development and validation of a RP-HPLC method for the determination of gentamicin sulfate and its related substances in a pharmaceutical cream using a short pentafluorophenyl column and a Charged Aerosol Detector. *Journal of Pharmaceutical and Biomedical Analysis*, *51*(3), 521–531. <https://doi.org/10.1016/j.jpba.2009.09.002>
- Kalhapure, R. S., Suleman, N., Mocktar, C., Seedat, N., & Govender, T. (2015). Nanoengineered drug delivery systems for enhancing antibiotic therapy. *Journal of Pharmaceutical Sciences*, *104*(3), 872–905. <https://doi.org/10.1002/jps.24298>
- Kamble, R., Ghag, M., Gaikwad, S., & Panda, B. K. (2012). Review article halloysite nanotubes and applications : A review. *Journal of Advanced Scientific Research*, *3*(2), 25–29.

- Kampf, G. (2016). Acquired resistance to chlorhexidine – is it time to establish an ‘antiseptic stewardship’ initiative? *Journal of Hospital Infection*, 94(3), 213–227.
<https://doi.org/10.1016/j.jhin.2016.08.018>
- Karaglani, M., Tzitzikou, E., Tottas, S., Kougioumtzis, I., Arvanitidis, K., Kolios, G., Chatzaki, E., & Drosos, G. I. (2020). Gentamycin elution from polymethylmethacrylate and bone graft substitute: Comparison between commercially available and home-made preparations. *Journal of Orthopaedics*, 19(November 2019), 9–13.
<https://doi.org/10.1016/j.jor.2019.11.034>
- Karpiński, R., Szabelski, J., & Maksymiuk, J. (2019). Effect of physiological fluids contamination on selected mechanical properties of acrylate bone cement. *Materials*, 12(23). <https://doi.org/10.3390/ma122333963>
- Katti, K. S. (2004). Biomaterials in total joint replacement. *Colloids and Surfaces B: Biointerfaces*, 39(3), 133–142. <https://doi.org/10.1016/j.colsurfb.2003.12.002>
- Kaur, D. C., & Chate, S. S. (2015). Study of antibiotic resistance pattern in methicillin resistant staphylococcus aureus with special reference to newer antibiotic. *Journal of Global Infectious Diseases*, 7(2), 78–84. <https://doi.org/10.4103/0974-777X.157245>
- Kawaguchi, T., Nakamura, H., & Watano, S. (2018). Dry coating of electrode particle with model particle of sulfide solid electrolytes for all-solid-state secondary battery. *Powder Technology*, 323, 581–587. <https://doi.org/10.1016/j.powtec.2016.03.055>
- Kelner, D. N., Apostol, I., Miller, K. J., & Ratto, J. (2009). Comparison of different approaches for evaluation of the detection and quantitation limits of a purity method: A case study using a capillary isoelectrofocusing method for a monoclonal antibody. *Analytical Biochemistry*, 385(1), 101–106. <https://doi.org/10.1016/j.ab.2008.09.053>
- Keqi Tang, et al. (2011). 基因的改变 NIH Public Access. *Bone*, 23(1), 1–7.
<https://doi.org/10.1161/CIRCULATIONAHA.110.956839>
- Khan, M., Osman, K., Green, G., & Haddad, F. S. (2016). The epidemiology of failure in total knee arthroplasty: avoiding your next revision. *The Bone & Joint Journal*, 98-B(1), 105–112. <https://doi.org/10.1302/0301-620X.98B1.36293>
- Kim, R. S., & LaBella, F. S. (1987). Comparison of analytical methods for monitoring autoxidation profiles of authentic lipids. *Journal of Lipid Research*, 28(9), 1110–1117.
[https://doi.org/10.1016/s0022-2275\(20\)38624-7](https://doi.org/10.1016/s0022-2275(20)38624-7)
- King, A., & Phillips, J. R. A. (2016). Total hip and knee replacement surgery. *Surgery (Oxford)*, 34(9), 468–474. <https://doi.org/10.1016/j.mpsur.2016.06.005>
- Kitajima, H., & Ogawa, T. (2021). *Prolonged Post-Polymerization Biocompatibility of Bone Cement*.
- Kowalska-Krochmal, B., & Dudek-Wicher, R. (2021). The minimum inhibitory concentration

- of antibiotics: Methods, interpretation, clinical relevance. *Pathogens*, 10(2), 1–21.
<https://doi.org/10.3390/pathogens10020165>
- krishna sailaja, A., Amareshwar, P., & Chakravarty, P. (2010). Chitosan nanoparticles as a drug delivery system. *Rjpbcs*, 1(January 2010).
- Krupka, T. M., & Exner, A. A. (2011). Structural parameters governing activity of Pluronic triblock copolymers in hyperthermia cancer therapy. *International Journal of Hyperthermia*, 27(7), 663–671. <https://doi.org/10.3109/02656736.2011.599828>
- Kubiak, K. J., Wilson, M. C. T., Mathia, T. G., & Carval, P. (2011). Wettability versus roughness of engineering surfaces. *Wear*, 271(3–4), 523–528.
<https://doi.org/10.1016/j.wear.2010.03.029>
- Kubica, P., Wasik, A., Kot-Wasik, A., & Namieśnik, J. (2014). An evaluation of sucrose as a possible contaminant in e-liquids for electronic cigarettes by hydrophilic interaction liquid chromatography-tandem mass spectrometry. *Analytical and Bioanalytical Chemistry*, 406(13), 3013–3018. <https://doi.org/10.1007/s00216-014-7690-2>
- Kumar, A., & Dixit, C. K. (2017). Methods for characterization of nanoparticles. In *Advances in Nanomedicine for the Delivery of Therapeutic Nucleic Acids* (pp. 44–58).
<https://doi.org/10.1016/B978-0-08-100557-6.00003-1>
- Kumon, M., Suzuki, M., Kusai, A., Yonemochi, E., & Terada, K. (2006). Novel approach to DPI carrier lactose with mechanofusion process with additives and evaluation by IGC. *Chemical and Pharmaceutical Bulletin*, 54(11), 1508–1514.
<https://doi.org/10.1248/cpb.54.1508>
- Kunz, C., Schuldt-Lieb, S., & Gieseler, H. (2019). Freeze-Drying From Organic Co-Solvent Systems, Part 2: Process Modifications to Reduce Residual Solvent Levels and Improve Product Quality Attributes. *Journal of Pharmaceutical Sciences*, 108(1), 399–415. <https://doi.org/10.1016/j.xphs.2018.07.002>
- Kurtz, S. M., Ong, K. L., Lau, E., Bozic, K. J., Berry, D., & Parvizi, J. (2010). Prosthetic joint infection risk after TKA in the medicare population. *Clinical Orthopaedics and Related Research*, 468(1), 52–56. <https://doi.org/10.1007/s11999-009-1013-5>
- Lakowicz, J. R., & Lakowicz, J. R. (1983). Effects of Solvents on Fluorescence Emission Spectra. *Principles of Fluorescence Spectroscopy*, 187–215.
https://doi.org/10.1007/978-1-4615-7658-7_7
- Laouini, A., Jaafar-Maalej, C., Limayem-Blouza, I., Sfar, S., Charcosset, C., & Fessi, H. (2012). Preparation, Characterization and Applications of Liposomes: State of the Art. *Journal of Colloid Science and Biotechnology*, 1(2), 147–168.
<https://doi.org/10.1166/jcsb.2012.1020>
- Latorre, R., & Baez-nieto, D. (2013). Encyclopedia of Biophysics. In *Encyclopedia of Biophysics*. <https://doi.org/10.1007/978-3-642-16712-6>

- Le, A. T., Tam, L. T., Tam, P. D., Huy, P. T., Huy, T. Q., Van Hieu, N., Kudrinskiy, A. A., & Krutyakov, Y. A. (2010). Synthesis of oleic acid-stabilized silver nanoparticles and analysis of their antibacterial activity. *Materials Science and Engineering C*, 30(6), 910–916. <https://doi.org/10.1016/j.msec.2010.04.009>
- Lecároz, C., Campanero, M. A., Gamazo, C., & Blanco-Prieto, M. J. (2006). Determination of gentamicin in different matrices by a new sensitive high-performance liquid chromatography-mass spectrometric method. *Journal of Antimicrobial Chemotherapy*, 58(3), 557–563. <https://doi.org/10.1093/jac/dkl258>
- Lee, A. S., De Lencastre, H., Garau, J., Kluytmans, J., Malhotra-Kumar, S., Peschel, A., & Harbarth, S. (2018). Methicillin-resistant *Staphylococcus aureus*. *Nature Reviews Disease Primers*, 4(May), 1–23. <https://doi.org/10.1038/nrdp.2018.33>
- Lee, C. (2017). IJN-130722-pmma-denture-base-material-enhancement---a-review-of-fiber-. In *International Journal of Nanomedicine* (Vol. 12). <https://www.ncbi.nlm.nih.gov/pmc/articles/PMC5440038/pdf/ijn-12-3801.pdf>
- Letchmanan, K., Shen, S. C., Ng, W. K., Kingshuk, P., Shi, Z., Wang, W., & Tan, R. B. H. (2017). Mechanical properties and antibiotic release characteristics of poly(methyl methacrylate)-based bone cement formulated with mesoporous silica nanoparticles. *Journal of the Mechanical Behavior of Biomedical Materials*, 72(May), 163–170. <https://doi.org/10.1016/j.jmbbm.2017.05.003>
- Lewis, G. (2015). Not all approved antibiotic-loaded PMMA bone cement brands are the same: ranking using the utility materials selection concept. *Journal of Materials Science: Materials in Medicine*, 26(1), 1–9. <https://doi.org/10.1007/s10856-015-5388-4>
- Lewis, G., & Janna, S. (2006). Estimation of the optimum loading of an antibiotic powder in an acrylic bone cement: Gentamicin sulfate in SmartSet HV. *Acta Orthopaedica*, 77(4), 622–627. <https://doi.org/10.1080/17453670610012700>
- Li, G., Yin, J., Gao, J., Cheng, T. S., Pavlos, N. J., Zhang, C., & Zheng, M. H. (2013). *OA Insight into risk factors and microstructural changes.pdf*. <http://arthritis-research.com/content/15/6/223>
- Li, J., & Wu, Y. (2014). Lubricants in pharmaceutical solid dosage forms. *Lubricants*, 2(1), 21–43. <https://doi.org/10.3390/lubricants2010021>
- Linke, S., Thürmer, A., Bienger, K., Kleber, C., Bellova, P., Lützner, J., & Stiehler, M. (2022). Microbiological pathogen analysis in native versus periprosthetic joint infections: a retrospective study. *Journal of Orthopaedic Surgery and Research*, 17(1), 1–7. <https://doi.org/10.1186/s13018-021-02850-3>
- Lora-Tamayo, J., Murillo, O., Iribarren, J. A., Soriano, A., Sánchez-Somolinos, M., Baraia-Etxaburu, J. M., Rico, A., Palomino, J., Rodríguez-Pardo, D., Horcajada, J. P., Benito, N., Bahamonde, A., Granados, A., Del Toro, M. D., Cobo, J., Riera, M., Ramos, A.,

- Jover-Sáenz, A., & Ariza, J. (2013). A large multicenter study of methicillin-susceptible and methicillin-resistant staphylococcus aureus prosthetic joint infections managed with implant retention. *Clinical Infectious Diseases*, *56*(2), 182–194.
<https://doi.org/10.1093/cid/cis746>
- Lowry, G. V., Hill, R. J., Harper, S., Rawle, A. F., Hendren, C. O., Klaessig, F., Nobbmann, U., Sayre, P., & Rumble, J. (2016). Guidance to improve the scientific value of zeta-potential measurements in nanoEHS. *Environmental Science: Nano*, *3*(5), 953–965.
<https://doi.org/10.1039/c6en00136j>
- Łukaszewska-Kuska, M., Krawczyk, P., Martyła, A., Hędzerek, W., & Dorocka-Bobkowska, B. (2018). Hydroxyapatite coating on titanium endosseous implants for improved osseointegration: Physical and chemical considerations. *Advances in Clinical and Experimental Medicine*, *27*(8), 1055–1059. <https://doi.org/10.17219/acem/69084>
- Lutz, M. J., Pincus, P. F., Whitehouse, S. L., & Halliday, B. R. (2009). The Effect of Cement Gun and Cement Syringe Use on the Tibial Cement Mantle in Total Knee Arthroplasty. *Journal of Arthroplasty*, *24*(3), 461–467. <https://doi.org/10.1016/j.arth.2007.10.028>
- Maherani, B., Arab-Tehrany, E., R. Mozafari, M., Gaiani, C., & Linder, M. (2011). Liposomes: A Review of Manufacturing Techniques and Targeting Strategies. *Current Nanoscience*, *7*(3), 436–452. <https://doi.org/10.2174/157341311795542453>
- Maradit Kremers, H., Larson, D. R., Crowson, C. S., Kremers, W. K., Washington, R. E., Steiner, C. A., Jiranek, W. A., & Berry, D. J. (2015). Prevalence of Total Hip and Knee Replacement in the United States. *The Journal of Bone and Joint Surgery-American Volume*, *97*(17), 1386–1397. <https://doi.org/10.2106/JBJS.N.01141>
- Marmur, A., Volpe, C. Della, Siboni, S., Amirfazli, A., & Drelich, J. W. (2017). Contact angles and wettability: Towards common and accurate terminology. *Surface Innovations*, *5*(1), 3–8. <https://doi.org/10.1680/jsuin.17.00002>
- Marques, S. C., Rezende, J. D. G. O. S., Alves, L. A. D. F., Silva, B. C., Alves, E., De Abreu, L. R., & Piccoli, R. H. (2007). Formation of biofilms by Staphylococcus aureus on stainless steel and glass surfaces and its resistance to some selected chemical sanitizers. *Brazilian Journal of Microbiology*, *38*(3), 538–543.
<https://doi.org/10.1590/S1517-83822007000300029>
- Martínez-Moreno, J., Mura, C., Merino, V., Nácher, A., Climente, M., & Merino-Sanjuán, M. (2015). Study of the Influence of Bone Cement Type and Mixing Method on the Bioactivity and the Elution Kinetics of Ciprofloxacin. *Journal of Arthroplasty*, *30*(7), 1243–1249. <https://doi.org/10.1016/j.arth.2015.02.016>
- Matthijssen, X. M. E., Akdemir, G., Markusse, I. M., Stijnen, T., Riyazi, N., Han, K. H., Bijkerk, C., Kerstens, P. J. S. M., Lems, W. F., Huizinga, T. W. J., & Allaart, C. F. (2016). Age affects joint space narrowing in patients with early active rheumatoid

- arthritis. *RMD Open*, 2(2), 1–9. <https://doi.org/10.1136/rmdopen-2016-000338>
- McConoughey, S. J., Howlin, R., Granger, J. F., Manring, M. M., & Jason, H. (2014).
Corrigendum: Biofilms in periprosthetic orthopedic infections (Future Microbiology
(2014) 9:8 (987-1007)). *Future Microbiology*, 9(10), 987–1007.
<https://doi.org/10.2217/fmb.14.64>
- McConoughey, S. J., Howlin, R. P., Wiseman, J., Stoodley, P., & Calhoun, J. H. (2015).
Comparing PMMA and calcium sulfate as carriers for the local delivery of antibiotics to
infected surgical sites. *Journal of Biomedical Materials Research - Part B Applied
Biomaterials*, 103(4), 870–877. <https://doi.org/10.1002/jbm.b.33247>
- Meftah, R., Van Stappen, J., Berger, S., Jacquus, G., Lalue, J. Y., Guering, P. H., Van
Hoorebeke, L., & Cnudde, V. (2019). X-ray computed tomography for characterization
of expanded polystyrene (EPS) foam. *Materials*, 12(12).
<https://doi.org/10.3390/ma12121944>
- Mehmood, A., Ghafar, H., Yaqoob, S., Gohar, U. F., & Ahmad, B. (2017). Mesoporous Silica
Nanoparticles: A Review. *Journal of Developing Drugs*, 06(02).
<https://doi.org/10.4172/2329-6631.1000174>
- Mertz, L. (2013). What Is Biocompatibility? *Ieee Pulse*, July, 14–15.
- Meure, L. A., Foster, N. R., & Dehghani, F. (2008). Conventional and dense gas techniques
for the production of liposomes: A review. *AAPS PharmSciTech*, 9(3), 798–809.
<https://doi.org/10.1208/s12249-008-9097-x>
- Miola, M., Bistolfi, A., Valsania, M. C., Bianco, C., Fucale, G., & Verné, E. (2013). Antibiotic-
loaded acrylic bone cements: An in vitro study on the release mechanism and its
efficacy. *Materials Science and Engineering C*, 33(5), 3025–3032.
<https://doi.org/10.1016/j.msec.2013.03.032>
- Mizzi, L., Maniscalco, D., Gaspari, S., Chatzitzika, C., Gatt, R., & Valdramidis, V. P. (2020).
Assessing the individual microbial inhibitory capacity of different sugars against
pathogens commonly found in food systems. *Letters in Applied Microbiology*, 71(3),
251–258. <https://doi.org/10.1111/lam.13306>
- Moghadam, H., Zakeri, M., & Samimi, A. (2019). *J | P | S | T*. 5, 71–76.
<https://doi.org/10.22104/JPST.2019.3455.1144>
- Monzón, R. A., Coury, J. G., Disse, G. D., & Lum, Z. C. (2019). Bone Cement in Total Hip
and Knee Arthroplasty. *JBJS Reviews*, 7(12), 1–7.
<https://doi.org/10.2106/JBJS.RVW.19.00031>
- Morais, J. M., Papadimitrakopoulos, F., & Burgess, D. J. (2010). Biomaterials/Tissue
Interactions: Possible Solutions to Overcome Foreign Body Response. *The AAPS
Journal*, 12(2), 188–196. <https://doi.org/10.1208/s12248-010-9175-3>
- Mori, R., Nakai, T., Enomoto, K., Uchio, Y., & Yoshino, K. (2011). Increased antibiotic

- release from a bone cement containing bacterial cellulose. *Clinical Orthopaedics and Related Research*, 469(2), 600–606. <https://doi.org/10.1007/s11999-010-1626-8>
- Moss, D. M., & Siccardi, M. (2014). Optimizing nanomedicine pharmacokinetics using physiologically based pharmacokinetics modelling. *British Journal of Pharmacology*, 171(17), 3963–3979. <https://doi.org/10.1111/bph.12604>
- Mottola, C., Matias, C. S., Mendes, J. J., Melo-Cristino, J., Tavares, L., Cavaco-Silva, P., & Oliveira, M. (2016). Susceptibility patterns of *Staphylococcus aureus* biofilms in diabetic foot infections. *BMC Microbiology*, 16(1), 1–9. <https://doi.org/10.1186/s12866-016-0737-0>
- Mullins, N. D., Deadman, B. J., Moynihan, H. A., McCarthy, F. O., Lawrence, S. E., Thompson, J., & Maguire, A. R. (2016). The impact of storage conditions upon gentamicin coated antimicrobial implants. *Journal of Pharmaceutical Analysis*, 6(6), 374–381. <https://doi.org/10.1016/j.jpha.2016.05.002>
- Nadimi, S., & Ghadiri, M. (2021). Stress and input energy analyses of shearing a particle bed under a centrifugal field. *Powder Technology*, 394, 575–583. <https://doi.org/10.1016/j.powtec.2021.08.086>
- Naveed, S., Shah, S. N., Qamar, F., Waheed, N., & Nazeer, S. (2014). Simple Uv Spectrophotometric Assay of New Formulation Gentamycin. *Journal of Applied Pharmacy*, 6(4), 408–410.
- Naveed, S., Waheed, N., Nazeer, S., & Qamar, F. (2014). Degradation study of gentamicin by UV spectroscopy. *American Journal of Chemistry and Applications*, 1(4), 36–39.
- Neuprez, A., Neuprez, A. H., Kaux, J. F., Kurth, W., Daniel, C., Thirion, T., Huskin, J. P., Gillet, P., Bruyère, O., & Reginster, J. Y. (2020). Total joint replacement improves pain, functional quality of life, and health utilities in patients with late-stage knee and hip osteoarthritis for up to 5 years. *Clinical Rheumatology*, 39(3), 861–871. <https://doi.org/10.1007/s10067-019-04811-y>
- Neut, D., Kluin, O. S., Thompson, J., Van Der Mei, H. C., & Busscher, H. J. (2010). Gentamicin release from commercially-available gentamicin-loaded PMMA bone cements in a prosthesis-related interfacial gap model and their antibacterial efficacy. *BMC Musculoskeletal Disorders*, 11, 1–9. <https://doi.org/10.1186/1471-2474-11-258>
- New, R. R. C. (2003). Liposomes: a practical approach. In *Science*.
- Newburg, D., & Neubauer, S. (1995). Carbohydrates in Milks: Analysis, Quantities, and Significance. *Handbook of Milk Composition*, 273–349. <https://doi.org/10.1016/b978-012384430-9/50015-9>
- Newbury, D. E., & Ritchie, N. W. M. (2013). Is scanning electron microscopy/energy dispersive X-ray spectrometry (SEM/EDS) quantitative? *Scanning*, 35(3), 141–168. <https://doi.org/10.1002/sca.21041>

- NicDaéid, N. (2019). Forensic sciences | Systematic drug identification. In *Encyclopedia of Analytical Science* (Vol. 4, Issue June 2019, pp. 75–80). Elsevier.
<https://doi.org/10.1016/B978-0-12-409547-2.14457-9>
- Nireesha, G., Divya, L., Sowmya, C., Venkateshan, N., Niranjan Babu, M., & Lavakumar, V. (2013). Lyophilization/Freeze Drying -An Review. *Ijntps*, 3(4), 87–98.
- O'Donnell, V. B. (2011). Mass spectrometry analysis of oxidized phosphatidylcholine and phosphatidylethanolamine. *Biochimica et Biophysica Acta - Molecular and Cell Biology of Lipids*, 1811(11), 818–826. <https://doi.org/10.1016/j.bbalip.2011.07.018>
- Oh, E. J., Oh, S. H., Lee, I. S., Kwon, O. S., & Lee, J. H. (2016). Antibiotic-eluting hydrophilized PMMA bone cement with prolonged bactericidal effect for the treatment of osteomyelitis. *Journal of Biomaterials Applications*, 30(10), 1534–1544.
<https://doi.org/10.1177/0885328216629823>
- Okolo, C. (2019). *The pharmaceutical excipient , magnesium stearate , depresses lymphocyte counts in vivo , but does not lower humora ...*
- Oliveira, W. F., Silva, P. M. S., Silva, R. C. S., Silva, G. M. M., Machado, G., Coelho, L. C. B. B., & Correia, M. T. S. (2017). Staphylococcus aureus and Staphylococcus epidermidis infections on implants. *Journal of Hospital Infection*, 98(2), 111–117.
<https://doi.org/10.1016/j.jhin.2017.11.008>
- Omri, A. (2008). *Liposomes as a carrier for gentamicin delivery : Development and evaluation of the physicochemical properties*. 359, 254–263.
<https://doi.org/10.1016/j.ijpharm.2008.03.035>
- Onggo, J., Onggo, J., Phan, K., & Wilson, C. (2020). Comparison of infection in cemented, cementless and hybrid primary total knee arthroplasty: a network meta-analysis and systematic review of randomized clinical trials. *ANZ Journal of Surgery*, 90(7–8), 1289–1298. <https://doi.org/10.1111/ans.16078>
- Palacios-Morillo, A., Alcázar, Á., De Pablos, F., & Jurado, J. M. (2013). Differentiation of tea varieties using UV-Vis spectra and pattern recognition techniques. *Spectrochimica Acta - Part A: Molecular and Biomolecular Spectroscopy*, 103, 79–83.
<https://doi.org/10.1016/j.saa.2012.10.052>
- Panáček, A., Kvítek, L., Smékalová, M., Večeřová, R., Kolář, M., Röderová, M., Dyčka, F., Šebela, M., Pruček, R., Tomanec, O., & Zbořil, R. (2018). Bacterial resistance to silver nanoparticles and how to overcome it. *Nature Nanotechnology*, 13(1), 65–71.
<https://doi.org/10.1038/s41565-017-0013-y>
- Parvizi, J., Fassihi, S. C., & Enayatollahi, M. A. (2016). Diagnosis of Periprosthetic Joint Infection Following Hip and Knee Arthroplasty. *Orthopedic Clinics of North America*, 47(3), 505–515. <https://doi.org/10.1016/j.ocl.2016.03.001>
- Patel, A., Pavlou, G., Mújica-Mota, R. E., & Toms, A. D. (2015). The epidemiology of revision

- total knee and hip arthroplasty in England and Wales: A comparative analysis with projections for the United States. a study using the national joint registry dataset. *Bone and Joint Journal*, 97-B(8), 1076–1081. <https://doi.org/10.1302/0301-620X.97B8.35170>
- Patel, Patel, & Patel. (2009). Poloxamers: A pharmaceutical excipients with therapeutic behaviors. *International Journal of PharmTech Research*, 1(2), 299–303.
- Pereira, D., Peleteiro, B., Araújo, J., Branco, J., Santos, R. A., & Ramos, E. (2011). The effect of osteoarthritis definition on prevalence and incidence estimates: A systematic review. *Osteoarthritis and Cartilage*, 19(11), 1270–1285. <https://doi.org/10.1016/j.joca.2011.08.009>
- Petersson, I. F., & Jacobsson, L. T. H. (2002). Osteoarthritis of the peripheral joints. *Best Practice and Research: Clinical Rheumatology*, 16(5), 741–760. <https://doi.org/10.1053/berh.2002.0266>
- Pilcer, G., Vanderbist, F., & Amighi, K. (2008). Correlations between cascade impactor analysis and laser diffraction techniques for the determination of the particle size of aerosolised powder formulations. *International Journal of Pharmaceutics*, 358(1–2), 75–81. <https://doi.org/10.1016/j.ijpharm.2008.02.014>
- Pinto, I. C., Cerqueira-Coutinho, C., De Freitas, Z. M. F., Dos Santos, E. P., Do Carmo, F. A., & Ricci Junior, E. (2017). Development and validation of an analytical method using high performance liquid chromatography (HPLC) to determine ethyl butylacetylaminopropionate in topical repellent formulations. *Brazilian Journal of Pharmaceutical Sciences*, 53(2), 1–8. <https://doi.org/10.1590/s2175-97902017000216033>
- Polakowski, C., Sochan, A., Bieganowski, A., Ryzak, M., Földényi, R., & Tóth, J. (2014). Influence of the sand particle shape on particle size distribution measured by laser diffraction method. *International Agrophysics*, 28(2), 195–200. <https://doi.org/10.2478/intag-20014-0008>
- Pradeep, N., & Sreekumar, A. V. (2012). An in vitro investigation into the cytotoxicity of methyl methacrylate monomer. *Journal of Contemporary Dental Practice*, 13(6), 838–841. <https://doi.org/10.5005/jp-journals-10024-1239>
- Prasad, A. K., Tan, J. H. S., Hanna, S. A., Dawson-Bowling, S., & Bedair, H. S. (2020). Cemented vs. cementless fixation in primary total knee arthroplasty: a systematic review and meta-analysis. *EFORT Open Reviews*, 5(11), 793–798. <https://doi.org/10.1302/2058-5241.5.200030>
- Prior, S., Gamazo, C., Irache, J. M., Merkle, H. P., & Gander, B. (2000). Gentamicin encapsulation in PLA/PLGA microspheres in view of treating Brucella infections. *International Journal of Pharmaceutics*, 196(1), 115–125. [https://doi.org/10.1016/S0378-5173\(99\)00448-2](https://doi.org/10.1016/S0378-5173(99)00448-2)

- Prokopovich, P., K??brick, M., Brousseau, E., & Perni, S. (2015). Potent antimicrobial activity of bone cement encapsulating silver nanoparticles capped with oleic acid. In *Journal of Biomedical Materials Research - Part B Applied Biomaterials*.
<https://doi.org/10.1002/jbm.b.33196>
- Pugmire, B. S., Lim, R., & Avery, L. L. (2015). Review of ingested and aspirated foreign bodies in children and their clinical significance for radiologists. *Radiographics*, *35*(5), 1528–1538. <https://doi.org/10.1148/rg.2015140287>
- Qu, L., Zhou, Q. T., Gengenbach, T., Denman, J. A., Stewart, P. J., Hapgood, K. P., Gamlen, M., & Morton, D. A. V. (2015). Investigation of the potential for direct compaction of a fine ibuprofen powder dry-coated with magnesium stearate. *Drug Development and Industrial Pharmacy*, *41*(5), 825–837.
<https://doi.org/10.3109/03639045.2014.908901>
- R.H. Burdon, P.H. van Knippenberg, P. T. S. (1988). *Methods of Cell Separation* (Issue 18).
- Raddi, S. (2017). *Desinfectant Bone And Dental Filler Materials Comprising Liposomes*.
- Raikos, V., Neacsu, M., Morrice, P., & Duthie, G. (2015). Anti- and pro-oxidative effect of fresh and freeze-dried vegetables during storage of mayonnaise. *Journal of Food Science and Technology*, *52*(12), 7914–7923. <https://doi.org/10.1007/s13197-015-1897-x>
- Ranjan, R., Kumar, M., & Ali, M. (2017). Bone cement. *Journal of Hand Surgery*, *36*(6), 1086–1088. <https://doi.org/10.1016/j.jhsa.2011.01.041>
- Rashid, I., Daraghme, N., Al-Remawi, M., Leharne, S. A., Chowdhry, B. Z., & Badwan, A. (2010). Characterization of the impact of magnesium stearate lubrication on the tableting properties of chitin-Mg silicate as a superdisintegrating binder when compared to Avicel® 200. *Powder Technology*, *203*(3), 609–619.
<https://doi.org/10.1016/j.powtec.2010.06.028>
- Ratner, B. D. (2011). The biocompatibility manifesto: Biocompatibility for the twenty-first century. *Journal of Cardiovascular Translational Research*, *4*(5), 523–527.
<https://doi.org/10.1007/s12265-011-9287-x>
- Refai, H., Hassan, D., & Abdelmonem, R. (2017). Development and characterization of polymer-coated liposomes for vaginal delivery of sildenafil citrate. *Drug Delivery*, *24*(1), 278–288. <https://doi.org/10.1080/10717544.2016.1247925>
- Reffuveille, F., Josse, J., Vallé, Q., Mongaret, C., & Gangloff, S. C. (2017). Staphylococcus aureus Biofilms and their Impact on the Medical Field. *The Rise of Virulence and Antibiotic Resistance in Staphylococcus Aureus*. <https://doi.org/10.5772/66380>
- Roberts, J., Bingham, J., McLaren, A. C., & McLemore, R. (2015). Liposomal Formulation Decreases Toxicity of Amphotericin B In Vitro and In Vivo. *Clinical Orthopaedics and Related Research*, *473*(7), 2262–2269. <https://doi.org/10.1007/s11999-015-4232-y>

- Ross Hallett, F. (1994). Particle size analysis by dynamic light scattering. *Food Research International*, 27(2), 195–198. [https://doi.org/10.1016/0963-9969\(94\)90162-7](https://doi.org/10.1016/0963-9969(94)90162-7)
- Roy, A., Dutta, R., Kundu, N., Banik, D., & Sarkar, N. (2016). A Comparative Study of the Influence of Sugars Sucrose, Trehalose, and Maltose on the Hydration and Diffusion of DMPC Lipid Bilayer at Complete Hydration: Investigation of Structural and Spectroscopic Aspect of Lipid-Sugar Interaction. *Langmuir*, 32(20), 5124–5134. <https://doi.org/10.1021/acs.langmuir.6b01115>
- Rutherford, T. (2012). *Population ageing: statistics*. <http://webcache.googleusercontent.com/search?q=cache:HbXYZWfJFioJ:researchbriefings.parliament.uk/ResearchBriefing/Summary/SN03228+&cd=2&hl=en&ct=clnk&gl=uk>
- S. Dukhin, & Labib, M. (2012). Theory of effective drug release from medical implants based on the Higuchi model and physico-chemical hydrodynamics. *Colloids Surf A Physicochem Eng*, 409, 10–20. <https://doi.org/10.1016/j.colsurfa.2012.04.040>
- Saharan, V., Kukkar, V., Kataria, M., Kharb, V., & Choudhury, P. (2008). Ordered mixing: mechanism, process and applications in pharmaceutical formulations. *Asian J Pharm Sci*, 3(6), 240–259.
- Sampath, S. S., & Robinson, D. H. (1990). Comparison of new and existing spectrophotometric methods for the analysis of tobramycin and other aminoglycosides. *Journal of Pharmaceutical Sciences*, 79(5), 428–431. <https://doi.org/10.1002/jps.2600790514>
- Sanarova, E., Lantsova, A., Oborotova, N., Orlova, O., Polozkova, A., Dmitrieva, M., & Nikolaeva, N. (2019). *Liposome Drug Delivery*. 11(3), 1148–1155.
- Sánchez-Lozada, L. G., Mu, W., Roncal, C., Sautin, Y. Y., Abdelmalek, M., Reungjui, S., Le, M., Nakagawa, T., Lan, H. Y., Yu, X., & Johnson, R. J. (2010). Comparison of free fructose and glucose to sucrose in the ability to cause fatty liver. *European Journal of Nutrition*, 49(1), 1–9. <https://doi.org/10.1007/s00394-009-0042-x>
- Sato, A., Serris, E., Grosseau, P., Thomas, G., Galet, L., Chamayou, A., & Baron, M. (2013). Experiment and simulation of dry particle coating. *Chemical Engineering Science*, 86, 164–172. <https://doi.org/10.1016/j.ces.2012.07.037>
- Schwalm, R. (2007). The UV Curing Process. In *UV Coatings* (pp. 19–61). <https://doi.org/10.1016/b978-044452979-4/50002-0>
- Schwarz, E. M., McLaren, A. C., Sculco, T. P., Brause, B., Bostrom, M., Kates, S. L., Parvizi, J., Alt, V., Arnold, W. V., Carli, A., Chen, A. F., Choe, H., Coraça-Huber, D. C., Cross, M., Ghert, M., Hickok, N., Jennings, J. A., Joshi, M., Metsemakers, W. J., ... Wenke, J. C. (2021). Adjuvant antibiotic-loaded bone cement: Concerns with current use and research to make it work. *Journal of Orthopaedic Research*, 39(2), 227–239. <https://doi.org/10.1002/jor.24616>

- Scimeca, M., Bischetti, S., Lamsira, H. K., Bonfiglio, R., & Bonanno, E. (2018). Energy dispersive X-ray (EDX) microanalysis: A powerful tool in biomedical research and diagnosis. *European Journal of Histochemistry*, 62(1), 89–99. <https://doi.org/10.4081/ejh.2018.2841>
- Seibert, K. D., Collins, P. C., Luciani, C. V., & Fisher, E. S. (2019). Milling operations in the pharmaceutical industry. *Chemical Engineering in the Pharmaceutical Industry*, 861–879. <https://doi.org/10.1002/9781119600800.ch38>
- Sek, L., Boyd, B. J., Charman, W. N., & Porter, C. J. H. (2010). Examination of the impact of a range of Pluronic surfactants on the in-vitro solubilisation behaviour and oral bioavailability of lipidic formulations of atovaquone†. *Journal of Pharmacy and Pharmacology*, 58(6), 809–820. <https://doi.org/10.1211/jpp.58.6.0011>
- Šepelák, V., Bégin-Colin, S., & Le Caër, G. (2012). Transformations in oxides induced by high-energy ball-milling. *Dalton Transactions*, 41(39), 11927–11948. <https://doi.org/10.1039/c2dt30349c>
- Sercombe, L., Veerati, T., Moheimani, F., Wu, S. Y., Sood, A. K., & Hua, S. (2015). Advances and challenges of liposome assisted drug delivery. *Frontiers in Pharmacology*, 6(DEC), 1–13. <https://doi.org/10.3389/fphar.2015.00286>
- Serris, E., Sato, A., Chamayou, A., Galet, L., Baron, M., Grosseau, P., & Thomas, G. (2013). Dry coating in a high shear mixer: Comparison of experimental results with DEM analysis of particle motions. *AIP Conference Proceedings*, 1542(June 2013), 779–782. <https://doi.org/10.1063/1.4812047>
- Seyyed Hosseinzadeh, H. R., Emami, M., Lahiji, F., Sina, A., Masoudi, A., & Emami, S. (2013). The Acrylic Bone Cement in Arthroplasty. In *Arthroplasty - Update*. <https://doi.org/10.5772/53252>
- Shen, S. C., Ng, W. K., Dong, Y. C., Ng, J., & Tan, R. B. H. (2016). Nanostructured material formulated acrylic bone cements with enhanced drug release. *Materials Science and Engineering C*, 58, 233–241. <https://doi.org/10.1016/j.msec.2015.08.011>
- Shi, Z., Neoh, K. G., Kang, E. T., & Wang, W. (2006). Antibacterial and mechanical properties of bone cement impregnated with chitosan nanoparticles. *Biomaterials*, 27(11), 2440–2449. <https://doi.org/10.1016/j.biomaterials.2005.11.036>
- Shinsako, K., Okui, Y., Matsuda, Y., Kunimasa, J., & Otsuka, M. (2008). Effects of bead size and polymerization in PMMA bone cement on vancomycin release. *Bio-Medical Materials and Engineering*, 18(6), 377–385. <https://doi.org/10.3233/BME-2008-0554>
- Shiramizu, K., Lovric, V., Leung, A., & Walsh, W. R. (2008). How do porosity-inducing techniques affect antibiotic elution from bone cement? An in vitro comparison between hydrogen peroxide and a mechanical mixer. *Journal of Orthopaedics and Traumatology*, 9(1), 17–22. <https://doi.org/10.1007/s10195-008-0099-y>

- Shukla. (2011). FREEZE DRYING PROCESS: A REVIEW Soham Shukla* Department of Pharmaceutical Technology, B. S. Patel Pharmacy College, Saffrony Institute of Technology, Near Saffrony Holiday Resort, Ahmedabad-Mehsana Highway, At & Post Linch-384435, Mahesana, Gujarat, Indi. *International Journal of Pharmaceutical Sciences and Research*, 2(12), 3061–3068. <https://ijpsr.com/bft-article/freeze-drying-process-a-review/?view=fulltext>
- Shukla, S., & Rao, S. (2017). Staphylococcus aureus biofilm removal by targeting biofilm-associated extracellular proteins. *Journal of Dental Education*, 146, 1–8. <https://doi.org/10.4103/ijmr.IJMR>
- Sierra Villar, A. M., Calpena Campmany, A. C., Bellowa, L. H., Trenchs, M. A., & Naveros, B. C. (2013). Validated spectrofluorometric method for determination of gemfibrozil in self nanoemulsifying drug delivery systems (SNEDDS). *Spectrochimica Acta - Part A: Molecular and Biomolecular Spectroscopy*, 113, 22–27. <https://doi.org/10.1016/j.saa.2013.04.092>
- Simonzadeh, N., & Ronsen, B. (2012). An isocratic HPLC method for the determination of sorbitol and glycerol in pharmaceutical formulations. *Journal of Chromatographic Science*, 50(7), 644–647. <https://doi.org/10.1093/chromsci/bms044>
- Singh, V. A., Wei, C. C., Haseeb, A., Shanmugam, R., & Ju, C. S. (2019). JectOS® versus PMMA vancomycin-loaded cement: The biomechanical and antimicrobial properties. *Journal of Orthopaedic Surgery*, 27(1), 1–6. <https://doi.org/10.1177/2309499018822247>
- Slane, J., Vivanco, J., Rose, W., Ploeg, H. L., & Squire, M. (2015). Mechanical, material, and antimicrobial properties of acrylic bone cement impregnated with silver nanoparticles. *Materials Science and Engineering C*, 48, 188–196. <https://doi.org/10.1016/j.msec.2014.11.068>
- Sombié, B. C., Yameogo, B. G. J., Semdé, R., Amighi, K., & Goole, J. (2014). *Stability Study in Accelerated Conditions of Based Gel Used in the Treatment of Chronic Osteomyelitis*.
- Stapleton, P., & Taylor, P. W. (2002). Methicillin Resistance in Staphylococcus aureus. *Pet-to-Man Travelling Staphylococci: A World in Progress*, 85(Pt 1), 225–235. <https://doi.org/10.1016/B978-0-12-813547-1.00017-0>
- Sternberg, K. (2009). Current requirements for polymeric biomaterials in otolaryngology. *GMS Current Topics in Otorhinolaryngology, Head and Neck Surgery*, 8, Doc11. <https://doi.org/10.3205/cto000063>
- Stravinskas, M., Nilsson, M., Horstmann, P., Petersen, M. M., Tarasevicius, S., & Lidgren, L. (2018). Antibiotic Containing Bone Substitute in Major Hip Surgery: A Long Term Gentamicin Elution Study. *Journal of Bone and Joint Infection*, 3(2), 68–72. <https://doi.org/10.7150/jbji.23901>

- Sudha, B. S., Sridhar, B. K., & Srinatha, A. (2010). Modulation of tramadol release from a hydrophobic matrix: Implications of formulations and processing variables. *AAPS PharmSciTech*, 11(1), 433–440. <https://doi.org/10.1208/s12249-010-9400-5>
- Swartz, M. (2010). HPLC detectors: A brief review. *Journal of Liquid Chromatography and Related Technologies*, 33(9–12), 1130–1150. <https://doi.org/10.1080/10826076.2010.484356>
- Syamchand, S. S., & Sony, G. (2015). Multifunctional hydroxyapatite nanoparticles for drug delivery and multimodal molecular imaging. *Microchimica Acta*, 182(9–10), 1567–1589. <https://doi.org/10.1007/s00604-015-1504-x>
- Szoka, F., & Papahadjopoulos, D. (1978). Procedure for preparation of liposomes with large internal aqueous space and high capture by reverse-phase evaporation. *Proceedings of the National Academy of Sciences of the United States of America*, 75(9), 4194–4198. <https://doi.org/10.1073/pnas.75.9.4194>
- Tai, C.-L., & Hsieh, P.-H. (2013). Gentamicin in bone cement: A potentially more effective prophylactic measure of infection in joint arthroplasty. *Bone & Joint Research*, 2(10), 220–226. <https://doi.org/10.1302/2046-3758.210.2000188>
- Tande, A. J., & Patel, R. (2014). Prosthetic joint infection. *Clinical Microbiology Reviews*, 27(2), 302–345. <https://doi.org/10.1128/CMR.00111-13>
- ter Boo, G. J. A., Grijpma, D. W., Moriarty, T. F., Richards, R. G., & Eglin, D. (2015). Antimicrobial delivery systems for local infection prophylaxis in orthopedic- and trauma surgery. *Biomaterials*, 52(1), 113–125. <https://doi.org/10.1016/j.biomaterials.2015.02.020>
- Trucillo, P., Campardelli, R., & Reverchon, E. (2020). Liposomes: From bangham to supercritical fluids. *Processes*, 8(9), 1–15. <https://doi.org/10.3390/pr8091022>
- Tsang, S. T. J., Gwynne, P. J., Gallagher, M. P., & Simpson, A. H. R. W. (2018). The biofilm eradication activity of acetic acid in the management of periprosthetic joint infection. *Bone and Joint Research*, 7(8), 517–523. <https://doi.org/10.1302/2046-3758.78.BJR-2018-0045.R1>
- Uhumwangho, M. U., Okor, R. S., Eichie, F. E., Azu, H., & Onyebuchi, A. E. (2007). Incorporation of Certain Hydrophobic Excipients in the Core of Melt Granules of Paracetamol and the Effect on Drug Release Profiles. *Tropical Journal of Pharmaceutical Research*, 6(3), 767–771. <https://doi.org/10.4314/tjpr.v6i3.14657>
- USP. (2020). *United States Pharmacopeia*.
- Vaishya, R., Chauhan, M., & Vaish, A. (2013). Bone cement. *Journal of Clinical Orthopaedics and Trauma*, 4(4), 157–163. <https://doi.org/10.1016/j.jcot.2013.11.005>
- Valentin, E., Bottomley, A. L., Chilambi, G. S., Harry, E. J., Amal, R., Sotiriou, G. A., Rice, S. A., & Gunawan, C. (2020). Heritable nanosilver resistance in priority pathogen: A

- unique genetic adaptation and comparison with ionic silver and antibiotics. *Nanoscale*, 12(4), 2384–2392. <https://doi.org/10.1039/c9nr08424j>
- Vallo, C. I. (2000). Residual monomer content in bone cements based on poly(methyl methacrylate). *Polymer International*, 49(8), 831–838. [https://doi.org/10.1002/1097-0126\(200008\)49:8<831::AID-PI462>3.0.CO;2-3](https://doi.org/10.1002/1097-0126(200008)49:8<831::AID-PI462>3.0.CO;2-3)
- van Belt, H., Neut, D., Uges, D. R. A., Schenk, W., van Horn, J. R., van der Mei, H. C., & Busscher, H. . (2000). Surface roughness, porosity and wettability of gentamicin-loaded bone cements and their antibiotic release. *Biomaterials*, 1981–1987. [https://doi.org/10.1016/0030-4220\(93\)90268-9](https://doi.org/10.1016/0030-4220(93)90268-9)
- Van de Belt, H., Neut, D., Schenk, W., Van Horn, J. R., Van der Mei, H. C., & Busscher, H. J. (2001). Infection of orthopedic implants and the use of antibiotic-loaded bone cements. *Acta Orthopaedica Scandinavica*, 72(6), 557–571. <https://doi.org/10.1080/000164701317268978>
- van Hoogevest, P., & Wendel, A. (2014). The use of natural and synthetic phospholipids as pharmaceutical excipients. *European Journal of Lipid Science and Technology*, 116(9), 1088–1107. <https://doi.org/10.1002/ejlt.201400219>
- Vanhegan, I. S., Malik, A. K., Jayakumar, P., Ul Islam, S., & Haddad, F. S. (2012). A financial analysis of revision hip Arthroplasty. *Journal of Bone and Joint Surgery - Series B*, 94 B(5), 619–623. <https://doi.org/10.1302/0301-620X.94B5.27073>
- Vert et al. (2012). Terminology for biorelated polymers and applications (IUPAC Recommendations 2012). *Pure Appl. Chem.*, 84(2), 377–410. <https://doi.org/10.1351/PAC-REC-10-12-04>
- Vestergaard, M., Frees, D., & Ingmer, H. (2019). Antibiotic resistance and the MRSA problem. *Gram-Positive Pathogens*, 747–765. <https://doi.org/10.1128/9781683670131.ch47>
- Virto, M. R., Frutos, P., Torrado, S., & Frutos, G. (2003). *Gentamicin release from modified acrylic bone cements with lactose and hydroxypropylmethylcellulose*. 24, 79–87.
- Wang, G., Liu, S. J., Ueng, S. W. N., & Chan, E. C. (2004). The release of cefazolin and gentamicin from biodegradable PLA/PGA beads. *International Journal of Pharmaceutics*, 273(1–2), 203–212. <https://doi.org/10.1016/j.ijpharm.2004.01.010>
- Wang, J. S. (2005). The benefit of vacuum mixing. In *The Well-Cemented Total Hip Arthroplasty: Theory and Practice*. Springer International Publishing. https://doi.org/10.1007/3-540-28924-0_12
- Wang, J., Wen, H., & Desai, D. (2010). Lubrication in tablet formulations. *European Journal of Pharmaceutics and Biopharmaceutics*, 75(1), 1–15. <https://doi.org/10.1016/j.ejpb.2010.01.007>
- Wang, L., Shi, X., Zhao, Q., Sun, A., Li, D., & Zhao, J. (2019). Determination of lipophilic

- marine toxins in fresh and processed shellfish using modified QuEChERS and ultra-high-performance liquid chromatography–tandem mass spectrometry. *Food Chemistry*, 272(July 2017), 427–433. <https://doi.org/10.1016/j.foodchem.2018.08.071>
- Wassilkowska, A., CZAPLICKA, A., ZIELINA, M., & BIELSKI, A. (2014). An analysis of the elemental composition of micro-samples using EDS technique. *Technical Transactions*, 2014(Chemia Zeszyt 1-Ch (18) 2014), 133–148. <https://doi.org/10.4467/2353737XCT.14.283.3371>
- Watson, J., Greenough, E. B., Leet, J. E., Ford, M. J., Drexler, D. M., Belcastro, J. V., Herbst, J. J., Chatterjee, M., & Banks, M. (2009). Extraction, identification, and functional characterization of a bioactive substance from automated compound-handling plastic tips. *Journal of Biomolecular Screening*, 14(5), 566–572. <https://doi.org/10.1177/1087057109336594>
- Wear, K. A. (2020). Mechanisms of Interaction of Ultrasound with Cancellous Bone: A Review. *IEEE Transactions on Ultrasonics, Ferroelectrics, and Frequency Control*, 67(3), 454–482. <https://doi.org/10.1109/TUFFC.2019.2947755>
- Webb, J. C., Gbejuade, H., Lovering, A., & Spencer, R. (2013). Characterisation of in vivo release of gentamicin from polymethyl methacrylate cement using a novel method. *International Orthopaedics*, 37(10), 2031–2036. <https://doi.org/10.1007/s00264-013-1914-5>
- Webb, J. C. J., & Spencer, R. F. (2007). The role of polymethylmethacrylate bone cement in modern orthopaedic surgery. *Journal of Bone and Joint Surgery - British Volume*, 89-B(7), 851–857. <https://doi.org/10.1302/0301-620X.89B7.19148>
- Weber, M., Renkawitz, T., Voellner, F., Craiovan, B., Greimel, F., Worlicek, M., Grifka, J., & Benditz, A. (2018). Revision Surgery in Total Joint Replacement Is Cost-Intensive. *BioMed Research International*, 2018. <https://doi.org/10.1155/2018/8987104>
- Wei, W., Abdullayev, E., Hollister, A., Mills, D., & Lvov, Y. M. (2012). Clay nanotube/poly(methyl methacrylate) bone cement composites with sustained antibiotic release. *Macromolecular Materials and Engineering*, 297(7), 645–653. <https://doi.org/10.1002/mame.201100309>
- Weinstein, E. A., Li, H., Lawson, J. A., Rokach, J., FitzGerald, G. A., & Axelsen, P. H. (2000). Prothrombinase acceleration by oxidatively damaged phospholipids. *Journal of Biological Chemistry*, 275(30), 22925–22930. <https://doi.org/10.1074/jbc.M002438200>
- Whitehouse, M. R. and Evans, S. L. (2010). Bone Cement. *International Journal of Nano and Biomaterials*, 3(1), 4–19.
- Whitehouse, M. R., & Evans, S. L. (2010). *Bone cement: an overview*. 3(1), 4–19.
- Wilczewska, A. Z., Niemirowicz, K., Markiewicz, K. H., & Car, H. (2012). Nanoparticles as drug delivery systems. *Pharmacological Reports*, 64(5), 1020–1037.

- [https://doi.org/10.1016/S1734-1140\(12\)70901-5](https://doi.org/10.1016/S1734-1140(12)70901-5)
- Wilson, M., & Maggs, J. (2018). Symposium - Hindfoot and Ankle Trauma. *Indian*, 52(may), 161–169. <https://doi.org/10.4103/ortho.IJOrtho>
- Wixson, R. L. (1992). Do we need to vacuum mix or centrifuge cement? *Clinical Orthopaedics and Related Research*, 285, 84–90. <http://europepmc.org/abstract/MED/1446459>
- Wong, A. L. A., Xiang, X., Ong, P. S., Mitchell, E. Q. Y., Syn, N., Wee, I., Kumar, A. P., Yong, W. P., Sethi, G., Goh, B. C., Ho, P. C. L., & Wang, L. (2018). A review on liquid chromatography-tandem mass spectrometry methods for rapid quantification of oncology drugs. *Pharmaceutics*, 10(4). <https://doi.org/10.3390/pharmaceutics10040221>
- Wong, K. K. Y., & Liu, X. (2010). Silver nanoparticles - The real “silver bullet” in clinical medicine? *MedChemComm*, 1(2), 125–131. <https://doi.org/10.1039/c0md00069h>
- World Health Organisation. (2017). *WHO | Antibiotic resistance*. WHO; World Health Organization. <http://www.who.int/mediacentre/factsheets/antibiotic-resistance/en/>
- World Health Organization. (2018). 濟無No Title No Title No Title. In *Critically Important Antimicrobials for Human Medicine* (Vol. 1).
- World Health Organization. (2019). World Health Organization Model List of Essential Medicines. In *World Health Organization Model List of Essential Medicines* (Vol. 21).
- Wu, K. (2016). *Antibiotic-loaded Bone Cement Abstract*. 188–195.
- www.orthoped.org. (2017). *What is a total knee prosthesis | Orthoped*. www.orthoped.org/what-is-total-knee-prosthesis.html
- Yuan, P., Tan, D., & Annabi-Bergaya, F. (2015). Properties and applications of halloysite nanotubes: Recent research advances and future prospects. *Applied Clay Science*, 112–113, 75–93. <https://doi.org/10.1016/j.clay.2015.05.001>
- Zakaria, L., Wong, T. W., Anuar, N. K., Naharudin, I., Tripathy, M., Sheshala, R., & Hussain, Z. (2019). Enhancing sustained drug release property of chitosan in spheroids through crosslinking reaction and coacervation. *Powder Technology*, 354, 815–821. <https://doi.org/10.1016/j.powtec.2019.07.006>
- Zheng, J., Huang, C., & Wang, S. (2018). Challenging pharmaceutical analyses by gas chromatography with vacuum ultraviolet detection. *Journal of Chromatography A*, 1567, 185–190. <https://doi.org/10.1016/j.chroma.2018.06.064>
- Zheng, K., Kunnath, K., Ling, Z., Chen, L., & Davé, R. N. (2020). Influence of guest and host particle sizes on dry coating effectiveness: When not to use high mixing intensity. *Powder Technology*, 366, 150–163. <https://doi.org/10.1016/j.powtec.2020.02.059>
- Zheng, L., Wei, C., Garayt, M. D. L., MacInnis, J., & Obrovac, M. N. (2019). Spherically Smooth Cathode Particles by Mechanofusion Processing. *Journal of The*

- Electrochemical Society*, 166(13), A2924–A2927. <https://doi.org/10.1149/2.0681913jes>
- Zhou, Q., Armstrong, B., Larson, I., Stewart, P. J., & Morton, D. A. V. (2010). Effect of host particle size on the modification of powder flow behaviours for lactose monohydrate following dry coating. *Dairy Science and Technology*, 90(2–3), 237–251. <https://doi.org/10.1051/dst/2009046>
- Zhou, Q., Qu, L., Gengenbach, T., Larson, I., Stewart, P. J., & Morton, D. A. V. (2013). Effect of surface coating with magnesium stearate via mechanical dry powder coating approach on the aerosol performance of micronized drug powders from dry powder inhalers. *AAPS PharmSciTech*, 14(1), 38–44. <https://doi.org/10.1208/s12249-012-9895-z>
- Zhou, Y., Ji, Y., & Cao, Z. (2020). Recent advances in optical detection of aminoglycosides. *Applied Sciences (Switzerland)*, 10(18). <https://doi.org/10.3390/APP10186579>
- Zimmerli, W. (2014). Clinical presentation and treatment of orthopaedic implant-associated infection. *Journal of Internal Medicine*, 276(2), 111–119. <https://doi.org/10.1111/joim.12233>
- Zimmerli, Werner, Trampuz, A., & Ochsner, P. E. (2004). *Prosthetic-Joint Infections*. 1645–1654.